INSTITUTE OF FOOD, NUTRITION & HUMAN HEALTH
COLLEGE OF SCIENCES
UNIVERSITY OF MASSEY
PALMERSTON NORTH, NEW ZEALAND

# FOULING OF STAINLESS STEEL SURFACES BY HEATED WHOLE MILK

A thesis presented in partial fulfilment
of the requirements for the degree
of Doctor of Philosophy
in Food Technology

**Truong Ho Tuan**

**2001**

# *SUMMARY*

The formation of fouling deposits in heat treatment equipment such as pasteurisers and evaporators used in milk processing plants reduces heat transfer and is a source of economic loss as a result of more frequent shut-down of the equipment for cleaning. Measurement of the kinetics and mechanisms of such fouling will enable an improved understanding of the design and operation of heat treatment equipment and allow improved control of fouling.

The present study was carried out to investigate the fouling behaviour of heated whole milk on to non-heated stainless steel surfaces and to determine the effects of mass flow rate and flow disturbance on the fouling of these surfaces.

A pilot-scale fouling rig was designed and built to mimic the heat treatment methods and conditions that are currently used in large-scale processing plants. Whole milk was first heated from about 6 to 75 °C in a plate heat exchanger and then heat treated to 95 °C via a direct steam injection (DSI) heater. Custom built tubular and sudden expansion fouling test sections of different sizes were placed at different locations downstream of the DSI heater. These test sections were easily disassembled to access the fouling layers. Milk flow in these test sections was in the range of 80-120 kg/h and Reynolds numbers ranged between 2500 and 3800.

A system to monitor fouling at different locations on the internal surfaces of the fouling test sections was developed. This included the use of a calibrated sensor to measure the local heat flux and temperature at the outer surfaces of the test section. The fouling rate was calculated and expressed as the rate of decrease of the internal heat transfer

coefficient during the deposit growth, normalised using the internal heat transfer coefficient determined at the start of a run. A plot of the fouling rate versus run time exhibited a delay period during which the normalised internal heat transfer coefficient was either constant (*i.e.* the ratio = 1) or slightly increased (*i.e.* the ratio > 1) followed by a decrease period during which it gradually decreased (*i.e.* the ratio < 1). The decrease period started when the deposit thickness reached about 0.5 mm, at which stage the sensor began to respond to the changes in the heat flux and surface temperature.

To investigate the effects of local flow disturbance on the fouling behaviour of whole milk heated to 95°C, three tubular sudden expansion geometries, ratios of upstream-to-downstream diameter of 0.2, 0.43 and 0.74, were used. Fouling in the area beyond the step of the expansion coincided with the recirculation flow zone characterised by the rapid change of the fluid shear rates, as shown by the results of the computational fluid dynamics (CFD) modelling. The local fouling rate in this zone increased when the fluid velocity was increased and when the ratio of upstream-to-downstream diameter was decreased (*i.e.* the step height was increased). These results indicate that flow disturbance, which in turn causes the fluid velocity to change its direction and/or magnitude, can induce fouling.

Fully denatured and aggregated β-lactoglobulin or the casein proteins were found to play a minor role in the fouling of whole milk heated to 95°C in the fouling rig. It is therefore hypothesised that, during heating, the native β-lactoglobulin unfolds to form an 'active species' and this 'species' is responsible for the fouling of non-heated surfaces. The concentration of the 'active species' formed during heating is directly related to the concentration of residual native β-lactoglobulin. The local fouling rate in various areas downstream of the DSI heater, which was found to relate to the local concentration of residual native β-lactoglobulin confirms this hypothesis.

Relationships between local and average fouling rates to account for the effects of flow

geometry were determined.

Fouling by heated milk fluids in the downstream areas of the DSI heater in industrial-scale milk evaporators was monitored with heat flux sensors. The fouling behaviour matched very well the pattern obtained in the fouling rig although the milk was heated to a higher temperature, *i.e.* 105 °C, at a higher flow rate, *i.e.* Reynolds number > $10^5$, and the processing run time of up to 24 hrs was considerably longer than in the pilot-plant runs.

The rate and extent of fouling in large-scale plant were found to vary with the types of milk product, such as skim milk, whole milk, modified skim milk and modified whole milk, and with treatment temperatures. Local equipment geometry in the section downstream of the DSI, such as flow disturbed by an orifice, was also found to have a strong effect on local fouling.

Recommendations for improving the design and operation of the DSI heater to reduce fouling of unheated surfaces by whole milk heated 95 °C are suggested.

# FRONTISPIECES

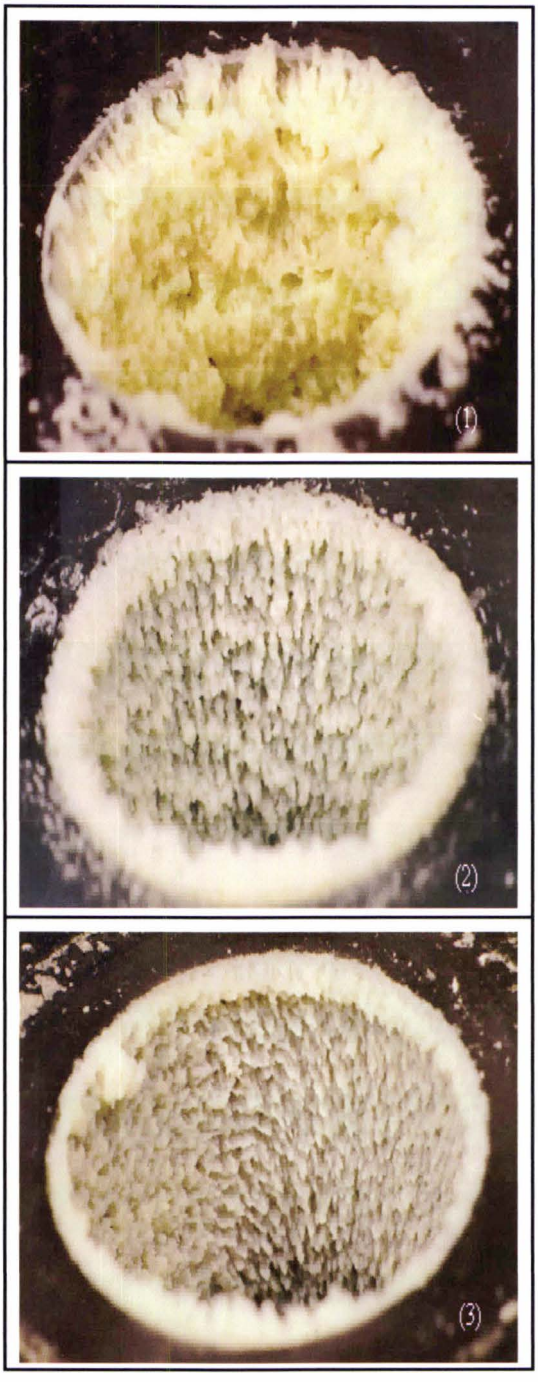


Photographs (3 x enlargement) of deposits formed inside tubular fouling test pieces: (1) placed near the direct steam injection (DSI) heater; (2) placed further downstream from the DSI heater; (3) placed farthest from the DSI heater.

# ACKNOWLEDGEMENTS

There have been a large number of people who have had input directly and indirectly and without whom it would have been impossible to carry out this research.

Firstly, I would like to sincerely thank my chief supervisor, Professor Ken Kirkpatrick, for his guidance, useful advice, discussions, encouragement and support throughout this research.

I also thank my co-supervisor, Dr Skelte Anema, from the New Zealand Dairy Research Institute (NZDRI), for his useful advice, discussions and support. In particular, for his help in understanding the wonders of the chemistry of milk proteins.

I also gratefully acknowledge the support of my employer, the NZDRI, who granted me the study leave. In particular, Mr Mike Donkin, Section Manager, for his support. The financial support for this project from the New Zealand Dairy Board (NZDB) is also gratefully acknowledged.

Other people who deserve my thanks are:

Dr Tuoc Trinh (from Massey University) for his initial ideas and suggestions on the research on fouling and his co-supervision during the first two years of the study.

From the NZDRI:

Dr David Newstead for his initial idea on the fouling measurement method.

Dr Jim Barnett, Dr Tony Mackereth, Dr Robert Norris and Mr Mike Rockell (from the NZDB) for their initial support in getting this project approved.

Ron Aird for his interest in this research, encouragement and for many challenging suggestions and stimulating discussions.

Steve Flint (former PhD student) for his useful suggestions and discussions and help. His friendship and many cups of coffee also helped to lessen the stress and to make this study enjoyable.

Roger Keedwell and Tony Foskett for setting up the data logging equipment. Their technical assistance during the initial trials in commercial plants is also appreciated.

Pat Janssen for the development of the data logging computer software.

Andrew Fletcher for his suggestions and help with the Computational Fluid Dynamics (CFD) Modelling.

Mrs Philippa Smith and Ms Lorraine Tremain for their assistance on the literature on-line search.

Staff from the NZDRI Protein, Powder and Environment Technology Group for their help in the pilot plant. Especially Shane Harvey for organising the milk supply and Mrs Giao Truong and Paul Mason for carrying out the analysis of milk fat globule sizes.

Staff from the NZDRI Analytical and Site Operation Groups for their support. Especially Ian Horley for the design of the horizontal open fouling test section and Darryl McGregor and Alan Donald for carrying out many urgent requests on the maintenance and modification of the fouling rig equipment.

My fellow colleagues and friends, Richard Archer, Alan Baldwin, Richard Lloyd, Tony Mackereth, Clive Marsh, Paul Morris, Kevin Pearce, David Pearce, Peter Wiles for their interest and useful suggestions and discussions.

Mr Doug Hopcroft from the Horticulture and Food Research Institute, New Zealand Ltd, Palmerston North, for carrying out the scanning electron microscopy (SEM).

Dr Al Rowland and Ms Liz Nickless from the Institute of Molecular Bio Sciences and Magesh Srinivasan (former PhD student), from Massey University, for their help with

confocal laser scanning microscopy (CLSM).

Managers and staff from the Kiwi Co-Operative Dairies Limited, Hawera, especially Roger Usmar, Jim King, Jim Fryer and Philip O'Malley for their support and Anna Zanker and Hong Chen for their help during the validation and implementation of the fouling monitoring system in the milk powder plants.

My family, Giao, Anh-Thu and Vinh for their tolerance of my long days at the university and at the NZDRI.

Lastly, I wish to dedicate this thesis to my parents and to the memory of my younger brother, Second-Lieutenant Truong Ho Vy.

I sincerely thank God for everything.

# TABLE OF CONTENTS

# LIST OF PRESENTATIONS

This study has been presented in part at the following scientific conferences:

1. Truong, T. (1997). Design and development of a pilot-scale fouling rig for the study of fouling of unheated stainless steel surfaces by dairy fluids. *Chemeca '97 Conference*, Rotorua, September 1997.

2. Truong, T., Anema, S., Kirkpatrick, K. & Trinh, K. T. (1998). In-line measurement of fouling and CIP in milk powder plants. *Fouling and Cleaning in Food Processing '98 Conference*, Cambridge, April 1998.

3. Truong, T., Anema, S. & Kirkpatrick, K. (2000). A novel local fouling monitoring system. *Chemeca '2000 Conference*, Perth, July 2000.

# LIST OF FIGURES

**Chapter 5**

**Chapter 6**

# LIST OF TABLES

**Chapter 6**

# LIST OF APPENDICES

# NOMENCLATURE

**Roman**

| | |
|---|---|
| a | constant |
| A | heat transfer area ($m^2$) |
| b | constant |
| C | concentration (kg $m^{-3}$) |
| Cf | heat flux calibration factor |
| Cp | heat capacity (J $kg^{-1}$ $K^{-1}$) |
| D | pipe, hydraulic diameter (m) or diffusion coefficient ($m^2$ $s^{-1}$) |
| d | thickness or small pipe and orifice diameter (m) |
| E | activation energy (J $mol^{-1}$) |
| f | friction factor |
| h | convective heat transfer coefficient (W $m^{-2}$ $K^{-1}$) or step height (m) |
| H | enthalpy (kJ $kg^{-1}$) |
| $I_i$ | Normalised internal heat transfer coefficient |
| k | thermal conductivity (W $m^{-1}$ $K^{-1}$) |
| Kd | deposition coefficient (m $s^{-1}$) |
| L | length (m) |
| m | mass flow rate (kg $s^{-1}$) or weight (kg) |
| M | weight (kg) |
| n | number of sensor |
| N | mass transfer rate (kg $s^{-1}$) |
| P | pressure (Pa) |
| q | heat flux (W $m^{-2}$) |
| Q | heat transfer (W) |
| r | flow ratio |
| R | thermal resistance (m K $W^{-1}$) or universal gas constant (8.314 J $mol^{-1}$) |
| r | pipe radius (m) |
| t | reaction, elapsed, transit, fouling and run time (s) |

| | |
|---|---|
| T | temperature (°C) or absolute temperature (K) |
| Tf | heat flux sensor temperature correction factor |
| U | overall heat transfer coefficient (W $m^{-2}$ $K^{-1}$) |
| v | average velocity (m $s^{-1}$) |
| V | volumetric flow rate ($m^3$ $s^{-1}$) or voltage (mV) |
| W | weight (kg) |

**Greek**

| | |
|---|---|
| α | fouled fraction of hydraulic channel diameter |
| δ | thickness of boundary layer (m) |
| ε | turbulence energy dispersion (J $kg^{-1}s^{-1}$) |
| k | turbulence kinetic energy (J $kg^{-1}$) |
| μ | dynamic viscosity (kg $m^{-1}$ $s^{-1}$) |
| ρ | density (kg $m^{-3}$) |
| τ | shear stress (N $m^{-2}$) |

**Dimensionless Group**

| | |
|---|---|
| Re | Reynolds number = $dv\rho / \mu$ |

**Subscript**

| | |
|---|---|
| a | ambient properties |
| agg | aggregated |
| b | bulk properties |
| c | critical conditions |
| den | denatured |
| f | fouling deposit properties, liquid properties |
| hf | heat flux sensor properties |
| i | internal, inlet condition |
| LMTD | log mean temperature difference |
| m | milk, molecular properties |
| nat | native |
| o | outlet, initial condition |

| | |
|---|---|
| s | sealant properties |
| ss | stainless steel properties |
| t | total, turbulent conditions |
| v | vapour properties |
| w | wall conditions |
| wt | weight |

**Superscript**

| | |
|---|---|
| n | reaction order |

CHAPTER 1

# INTRODUCTION

CONTENTS

## 1.1 THE FOULING PROBLEM

The heat treatment of milk (*e.g.* thermisation, pasteurisation, ultra-high-temperature treatment (UHT)) is to make milk and milk products microbiologically safe for human consumption. Heat treatment is also applied to change the chemical and physical properties of milk in order to impart desirable properties in the finished products (*e.g.* milk powder solubility). Another purpose of heat treatment is to bring the temperature of milk to a level at which a subsequent processing step can be effectively carried out (*e.g.* separation, evaporation, drying).

Heat treatment can cause undesirable changes to milk which results in adverse effects in the manufacturing process and on product quality. An important practical problem resulting from heating of milk is the deposition of a layer of milk components on the surface of equipment. The formation of this fouling layer has a number of important consequences. In particular, it leads to reduced heat transfer and restricted product flow which requires shut-down of the equipment for cleaning. Each extra shut-down can result in up to 3 h in lost production. For example, if the production cycle of a milk evaporator is reduced from 30 to 20 h, due to fouling, the loss can be up to 4% of the production time. This phenomenon reduces the availability of the plant for production and increases production costs. Other extra production costs as a result of fouling include:

- Increase in energy costs due to decrease in heat transfer coefficient and an increase in pressure.

- Loss of product due to product remaining on the wall of heat treatment equipment and to plant shut-down and start-up procedures.

- Increase in cleaning costs such as energy, water, cleaning chemicals and effluent

treatment.

- Increase in maintenance costs due to off-line mechanical cleaning.

In addition to the effect on production costs, fouling affects the capital cost of heat treatment equipment. At the design stage, the heat transfer area is increased by a safety margin of 20-30%. Sometimes, for difficult a product, the allowance can be as high as 100%. An example is the arrangement of dual plate (or tubular) heat exchangers in the milk evaporator plant. A 'stand-by' heat exchanger is provided so that production is maintained when the first heat exchanger is shut down for cleaning.

The dairy industry is one of the main industries in New Zealand, with a total revenue of 7400 million NZ dollars in 1999 (New Zealand Dairy Board, 2000). The formation of milk deposit in heat treatment equipment is of concern in milk evaporator plants, in particular for whole milk powder production. For example, the total amount of whole milk powder production was 382 thousand tons in the 1998/99 dairying season (about 60% of total milk powders production), hence every 1% of production loss costs the dairy industry millions of dollars.

## 1.2 FOULING INVESTIGATIONS

Several researchers have studied fouling from different milk fluids under different process and operating conditions using a variety of types of processing equipment and materials of the equipment surface. Considerable understanding on the chemistry of fouling and the mechanism of deposition have been achieved. Recommendations on how to reduce and control fouling in heat treatment equipment have also been reported. The results of these studies can be found in several publications (Burton, 1968; Somerscales & Knudsen, 1981; Lund *et al.*, 1985; Kessler & Lund, 1989; Belmar-Beiny & Fryer, 1994; International Dairy Federation, 1997; University of Cambridge, 1998;

Somerscales & Knudsen, 1981; Lund *et al.*, 1985; Kessler & Lund, 1989; Belmar-Beiny & Fryer, 1994; International Dairy Federation, 1997; University of Cambridge, 1998; The Institution of Chemical Engineers, 1999).

Although literature on milk fouling is now extensive, limited progress has been made towards minimising fouling and in optimising the production cycle in industrial-scale processing plants. There is little information available to the designers and operators to enable prediction of the change in the performance of the heat treatment equipment as the fouling proceeds. This may be due to the difficulty in relating the research results to the operation of large-scale equipment because these investigations have been performed with closely defined and specific process and operating conditions. These controlled conditions do not always reflect the overall conditions of operation of a large-scale plant.

In order to operate heat treatment equipment that minimises the effects of fouling, it is necessary to identify the mechanism of formation, the rate and extent of deposition, the conditions that cause fouling and the factors that encourage fouling deposits within the equipment. In addition, the available information should allow for the design of equipment that minimises fouling and optimises the surface area of heat treatment equipment.

Different measurement methods, such as calculation of heat transfer coefficient and measurement of pressure drop, to monitor the rate and extent of fouling have been developed (*e.g.* Tissier & Lalande, 1986). In industrial practice, data on fouling are often obtained from the overall assessment of plant performance which gives average values of fouling over the total surface, rather than local values at a particular site in the equipment. In addition, methods for monitoring of fouling of non-heated surfaces, such as the holding tubes of the milk pasteurisers, are limited. Optimisation of the production

cycle in the large-scale plant therefore requires an in-line measurement system that can continuously monitor local fouling of plant items so that the point at which cleaning of the equipment is necessary can be determined. Subsequent optimisation of the operating conditions or development of new process conditions to reduce fouling could then follow.

## 1.3 OBJECTIVES OF THE PRESENT STUDY

The objectives of the present study are to

- obtain a better understanding of the fouling behaviour of heated milk fluids on non-heated surfaces, and

- identify factors that could be used to improve the design and operation of heat treatment equipment to reduce fouling.

The focus is to study the effect of mass flow rate and flow geometry on fouling of whole milk heated to 95°C via a DSI heater. Custom built stainless steel tubular sudden expansion fouling test sections are used in the experiments. To monitor fouling at various location in these test sections, a system which includes commercial sensors to measure wall heat flux is developed.

The approach is to conduct a series of experiments that mimic the heat treatment methods and conditions that are currently used in large-scale milk evaporator plants. A custom built fouling rig was developed for this purpose. Investigation of the fouling behaviour of heated milk fluids in large-scale milk evaporator plants then followed.

CHAPTER 2

# REVIEW OF LITERATURE

CONTENTS

## 2.1 INTRODUCTION

This chapter presents an overview of the fouling process and factors that affect the formation of deposits on heated surfaces of dairy process equipment. Measurement of fouling of heat treatment equipment with reference to dairy process equipment such as plate and tubular heat exchangers is also presented and discussed. The scope of this review is focussed on the heat treatment of the milk fluids below 110°C. Nevertheless, some literature and data on fouling by milk fluids treated above 110°C are also included for cross-reference and discussion.

## 2.2 FOULING IN DAIRY PROCESS EQUIPMENT

Milk is a complex and variable mixture of a large number of components. The major components in raw milk are water, milk fat (in the form of globules), proteins (casein and whey proteins), lactose and milk salts (often called minerals). Raw milk also contains trace elements, organic acids, gases, vitamins, non-protein nitrogenous compounds, bacteria and endogenous enzymes which originate from the mammary gland tissue and blood plasma. There are numerous different molecular species that are present in low concentrations many of which have not been identified or isolated. The typical composition of milk is listed in Table 2.1.

The caseins account for about 80% the total milk proteins and consist of four major proteins: $\alpha_{s1}$- (39%), $\alpha_{s2}$- (10%), β- (37%) and κ- (14%) caseins. Most of the casein and a large proportion of the calcium and phosphate are found in the form of colloidal aggregates called casein micelles. These micelles contain about 92% protein and 8% inorganic salts on a dry basis.

**Table 2.1** Composition of the main constituents of milk (Walstra & Jenness, 1984)

| Component | Composition (% w/w) | | |
|---|---|---|---|
| | **Average (Liquid Basis)** | **Range (Liquid Basis)** | **Average (Dry Basis)** |
| Water | 87.3 | 85.5 - 88.7 | 0 |
| Milkfat | 3.9 | 2.4 - 5.5 | 30.7 |
| Total protein | 3.3 | 2.3 - 4.4 | 26 |
| Casein | 2.6 | 1.7 - 3.5 | 20.5 |
| Whey protein | 0.5 | 0.4 - 0.6 | 3.9 |
| Non-protein-nitrogen | 0.2 | 0.1 - 0.3 | 1.6 |
| Lactose | 4.6 | 3.8 - 5.3 | 36 |
| Minerals | 0.65 | 0.5 - 0.8 | 5.1 |
| Citrate | 0.18 | 0.1 - 0.2 | 1.4 |
| Ca | 0.12 | 0.09 - 0.14 | 0.9 |
| $PO_4$ | 0.15 | 0.1 - 0.2 | 1.6 |
| Organic acids | 0.18 | 0.13 - 0.22 | 1.4 |
| Miscellaneous | 0.12 | not available | 0.8 |
| Solid-non-fat (SNF) | 8.8 | 6.6 - 10.5 | 69.3 |
| Total solids | 12.7 | 9 - 16 | 100 |

Whey proteins account for about 20% of the proteins and consist of β-lactoglobulin (β-lg), α-lactalbumin (α-lac), bovine serum albumin (BSA), immunoglobulins (Ig) and other minor proteins. β-Lag and α-lac are the major constituents of whey proteins and their contents in milk are about 9.8% w/w and 3.7% w/w of the total proteins, respectively (Walstra & Jenness, 1984).

Milk contains about 0.12% calcium and 0.07% inorganic phosphate. Other constituents of the milk salts are magnesium, sodium, potassium, chloride and citrate.

Common heating processes which are used in the milk processing industry include thermisation, pasteurisation, sterilisation, preheat treatment, evaporation and ultra-high-temperature (UHT) treatment. Their typical heating conditions and methods are listed in Table 2.2.

**Table 2.2** Common heating processes employed in the milk processing industry

| **Heat Treatment** | **Temperature (°C)** | **Duration (s)** | **Method of Heating** |
|---|---|---|---|
| Thermisation | 63 - 65 | 15 - 20 | Indirect |
| Pasteurisation | 72 or 85 | 15 or 1 | Indirect |
| Preheat treatment | 70 - 110 | 15 - 120 | Direct & Indirect |
| Evaporation | 45 - 75 | 30 - 120 | Indirect |
| Ultra-high-temperature (UHT) treatment | 130 - 145 | 1 - 30 | Direct & Indirect |

Heat treatments can cause numerous changes to the milk and can have many effects on the properties of the milk and products manufactured from milk. Comprehensive articles concerning the effects of thermal processing on the physico-chemical properties of the major milk components and their interactions have been published (Fox, 1995). Examples of changes that can occur in milk as the result of heat treatments are:

- loss of nutrients,
- destruction of micro-organisms,
- inactivation of enzymes,

- decrease in solubility of whey protein due to denaturation,
- transfer of some calcium and phosphate from solution to the colloidal form, and
- aggregation of casein micelles.

### 2.2.1 Chemistry of milk fouling

It has been confirmed that, on heating, whey protein denaturation and aggregation as well as the insolubilisation of calcium and phosphate are significant factors that affect fouling on heated surfaces. β-Lactoglobulin denaturation has been shown to correlate strongly with the rate of fouling deposition (Lalande *et al.*, 1985; Hege & Kessler, 1986; Hiddink *et al.*, 1986; Fryer, 1989; de Jong *et al.*, 1992; Jeurnink, 1995a). Although there is a strong link between denaturation of β-lactoglobulin and fouling, the reaction kinetics for the fouling reaction are complex. Upon heating, two types of reaction are reported to occur sequentially:

(I) molecular denaturation of β-lactoglobulin during which the protein partially unfolds and exposes the reactive sulfydryl group (-SH), and

(ii) molecular aggregation of β-lactoglobulin
- with itself,
- with other denatured whey proteins such as α-lactalbumin,
- with κ-casein and $\alpha_{S2}$-casein of casein micelles (Creamer *et al.*, 1978; Mulvihill & Donovan, 1987; Dalgleish, 1990; Jeurnink, 1992; Corredig & Dalgleish, 1996a & b),
- by interaction with the proteins of the milk fat globule membranes (Dalgleish & Banks, 1991; Dalgleish & Sharma, 1992; Houlihan *et al.*, 1992; Corredig & Dalgleish, 1996c).

- with solid surfaces (Jeurnink *et al.*, 1995)

How these interactions affect fouling or which one is the controlling reaction is unknown. Nevertheless, these results partly explain the presence in the fouling deposits of other milk proteins, such as caseins and milk fat, in addition to β-lactoglobulin.

Although α-lactalbumin also denatures and associates with other proteins upon heating, its contribution to the fouling process has been considered less important than β-lactoglobulin (Visser *et al.*, 1997). This is probably because α-lactalbumin does not have free SH group, *i.e.* it is less reactive, and its concentration in whey is about half that of β-lactoglobulin.

Increasing the concentration of β-lactoglobulin (such as by evaporation) increases fouling (Fryer *et al.*, 1992; Jeurnink 1995a). The structure of deposits becomes compact and firm and the deposits strongly adhere to the heated surfaces. The main constituents of the deposits are still proteins but the lactose content decreases and the mineral content increases (Schraml *et al.*, 1996).

The kinetics of milk salts deposition on the equipment surface is also complex. The presence of calcium phosphate in the fouling deposits could be due to the following:

(i) The formation of nuclei and crystal growth of precipitated calcium phosphate which is partly driven by the temperature difference between the milk fluids and the heating surfaces (Burton, 1968; Barton *et al.*, 1985).

(ii) The interactions between protein aggregates and precipitated calcium phosphates (Delsing & Hiddink, 1983).

(iii) The interactions between protein aggregates and colloidal calcium phosphates

from the casein micelles (van Dijk, 1990).

Inhibiting calcium phosphate precipitation, through stabilisation of phosphate and calcium levels, has been found to be effective in preventing fouling or stopping the growth of protein deposits (Delsing & Hiddink, 1983).

Jeurnink & de Kruif (1995) studied the effects of calcium concentration in milk in relation to heat stability and fouling. They found that in low-calcium milk (about 15% less calcium than normal milk), the casein micelles are swollen and a large part of the β- and κ-caseins are dissociated from the micelles. In high-calcium milk (about 19% more calcium than normal milk) the casein micelles have shrunk and become unstable. They concluded that changes in the calcium ion activity of the serum, that influence the colloidal stability of casein micelles, coupled with the aggregation of whey protein with the casein micelle surface, would cause an increase in the protein deposition onto heated surfaces.

#### 2.2.1.1 Composition of fouling layers

The protein and mineral content of fouling deposits can vary widely depending on the type of milk fluid, milk composition and heat treatment conditions and methods. According to Burton (1968), there are generally two types of fouling deposits that form on the heated surfaces at different milk treatment temperatures.

(a) Type A deposit is found at heating temperatures below 110°C and normally consists of a large proportion of proteins (50 - 60%) and a smaller proportion of minerals (20 - 30%). This deposit starts to form at about 75°C and is at a maximum in the range 90-110°C. This type of deposit is predominantly soft, white and spongy. If fouling occurs over a long period (*e.g.* 20 h) or the deposit is 'overcooked', the fouling layer can become brown and very much harder.

This type of deposit tends to restrict the areas of the flow passages in the heat treatment equipment and causes an increase in the operating pressure. The mineral content of type A deposit is mainly calcium and phosphate, probably in the form of tricalcium phosphate ($Ca_3 (PO_4)_2$) (Burton, 1968).

(b) Type B deposit or milk stone is found at heating temperatures above 110°C and normally has a high content of minerals (60 - 70%) and a lower protein content. This is a much harder and greyer deposit than type A and has more influence on heat transfer than on the pressure drop across the equipment.

Recently, de Jong *et al.* (1994) showed that the composition of fouling deposits in a steam infusion plant for heating skim milk to the temperatures of 100 - 170°C is similar to that of type A deposit, *i.e.* high protein and low mineral contents.

Lactose does not contribute to the fouling process unless it participates in the Maillard reaction at high temperature (Visser *et al.*, 1997). Fat has usually been thought to play a minor role in milk fouling (Burton, 1968; Visser *et al.*, 1997) but a wide range of fat contents of deposits (4-36%) has been reported in the literature (Table 2.3). Burton (1968) and Patil & Reuter (1986) also reported that high-fat fouling deposits (34%) can form after heating milk to 140°C by direct steam injection. Although there was no explanation for the large variation of fat content in the deposit, it is thought that the milk fat globules may become involved in the fouling process by the interaction of membrane proteins with denatured whey proteins (refer Section 2.2.1) (Corredig & Dalgleish, 1996c).

There is little difference in the concentration of proteins and minerals between deposits formed from whole milk and skim milk at a heating temperature of 100°C. The deposit formed from skim milk has a smoother surface than that formed from whole milk (Foster *et al.*, 1989).

Jeurnink & Brinkman (1994) investigated fouling and cleaning of a tubular heat exchanger and a four-effect evaporator after processing whole milk and whey. In this study, throughout a 20 h period, whole milk and whey were heated at 90°C (holding time 315 s) in the tubular heat exchanger and concentrated in the evaporator. A significant amount of fouling deposit (85%) was found in the evaporator and a much smaller amount of deposit (15%) was found in the tubular heat exchanger. Protein was the main component of the milk fouling deposits but those from heated whey and concentrated whey contained mainly calcium phosphate. Calcium citrate was also found in deposits from heated concentrated whey. Their results also confirm the findings of previous workers (Delsing & Hidding, 1983) who showed that deposits from whey solutions contain more mineral components than deposits from milk under the same range of treatment temperatures (*i.e.* up to 90°C).

Recently, Robbins *et al.* (1999) compared fouling from whey protein concentrate (WPC) and whole milk at high temperature (*i.e.* up to 140°C) in a plate heat exchanger. The authors found that, as the processing temperature increases, the deposits from milk changed to a mineral-based type (*i.e.* type B deposit). However, the WPC deposits continued to show protein-based fouling (*i.e.* type A deposit). The data in part explains the difficulty in extrapolating fouling models from whey protein to milk fouling, in particular, in the high treatment temperature region.

A summary of the composition of fouling deposits derived from selected literature is listed in Table 2.3.

A detailed analysis of composition of deposits that form during pasteurisation of whole milk (temperature range 75 - 90°C) shows that the protein fraction of the deposits comprises at least 50% β-lactoglobulin (Lalande *et al.*, 1985; Tissier *et al.*, 1984). Other components of the protein fraction of the deposits include casein, α-lactalbumin and immunoglobulin. It should be noted that β-lactoglobulin content in ordinary bovine

milk is about 0.3% (3% on dry basis) which in turn represents about 9.8% of the total protein content in milk (refer Table 2.1 in Section 2.2). Jeurnink *et al.* (1996) reported that only 0.14% of the denatured β-lg in pasteurised milk ends up in the deposit layer. Nevertheless, the high content of β-lactoglobulin in the deposits confirms its role in the fouling process.

**Table 2.3** Average composition of fouling deposits (% dry basis)

| Authors | Heating Temp(°C) | Plant / Location | Protein | Minerals | Fat |
|---|---|---|---|---|---|
| Indirect Heating of Whole Milk | | | | | |
| Lyster (1965) | 85 | Plate heat exchanger | 60 | 25 | 12 |
| Lalande *et al.* (1985) | 82 | Heating | 54 | 27 | 16 |
| | 82 | Holding | 59 | 10 | 25 |
| Jeurnink & Brinkman (1994) | 90 | Tubular heat exchanger | 33 | 12 | 36 |
| | 45-74 | Evaporator | 49 | 9 | 30 |
| Jeurnink *et al.* (1989) | 85 | Tubular heat exchanger | 61 | 23 | 14 |
| Indirect Heating of Skim Milk | | | | | |
| Delsing & Hiddink (1983) | 76 | Tubular heat exchanger | 78 | 17 | - |
| Jeurnink (1991, 1995b) | 80 | Fresh | 42 | 46 | - |
| | 80 | Aged | 69 | 22 | - |
| | 85 | Reconstituted | 73 | 11 | - |

### 2.2.1.2 Deposition and formation of fouling layers

A number of detailed examinations of the micro-structure of the fouling layer of milk and whey on heated stainless steel surfaces have been reported (Tissier *et al*., 1984; Lalande *et al.*, 1985; Daufin *et al*., 1987; Lalande *et al.*, 1989; Foster *et al*., 1989; Visser *et al.*, 1995; Schraml *et al.*, 1996; Robbins *et al.*, 1999). The results show that the formation of fouling deposits is not uniform throughout its thickness. The deposits have a compact sub-layer about 15 μm thick and a spongy and porous top-layer. The top-layer consists of small particles of 10 - 50 μm in size comprising aggregates of smaller protein particles of 0.2-2 μm in size. The particles are randomly linked by bridges and anchored to the sub-layer. Minerals, fat globules, casein micelles and micro-organisms can be enclosed within this structure. An example of the internal structure of a fouling layer is illustrated in Figure 2.1.

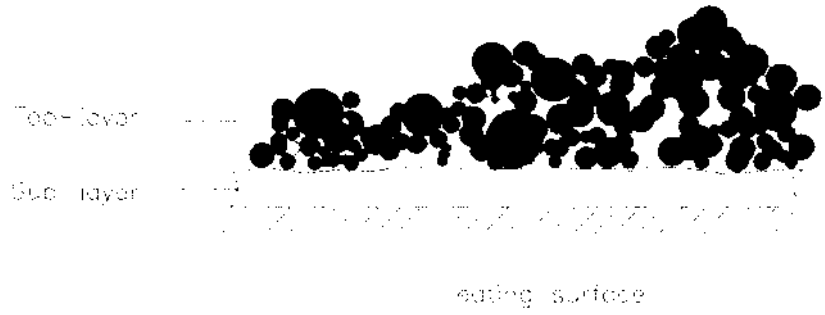


**Figure 2.1** Structure of fouling deposit from milk on heated surface (after Lalande *et al.*, 1989).

To date, it is not possible to conclude whether proteins or minerals are deposited first and contradictory results on the initial stages of fouling have been reported. Delsing & Hiddink (1983) and Daufin *et al.*, (1987) concluded that the presence of calcium

phosphate enhances the adsorption of whey proteins onto solid surfaces but the first layer mainly consists of protein. Foster & Green (1990) studied milk fouling at wall temperatures of 140°C and found that the distribution of minerals changed with the depth of the fouling layer. The authors suggested that minerals and protein layers are formed simultaneously but minerals can later diffuse through the deposit layer to the heated surfaces. On the contrary, Tissier & Lalande (1986) found a mineral-rich layer of 0.02 μm thick after one minute of heating and this layer increased to 12 μm after 5 minutes. Belmar-Beiny & Fryer (1993) found that, for a whey protein concentrate solution (WPC), whey proteins are the first species to absorb onto the surface to form an initial deposit layer within 4 s at 73°C. As fouling progresses, the protein aggregates, which range in size from 0.2 μm to 2 μm, adhere and grow on the initial layer and form bridges between them. Jeurnink *et al.* (1996) later confirmed this finding with whey protein isolate, pure β-lg and cheese whey at room temperature. These authors also found that further build up of protein layers on to this first proteinaceous layer does not take place unless both protein aggregates (*i.e.* at temperature above 72°C) and calcium ions are present in the bulk fluid.

### 2.2.2 Factors affecting fouling

Generally, increase in treatment temperature causes more deposition on heated surfaces (Foster *et al.*, 1989; Foster & Green, 1990). However, there are a number of other factors that can also affect milk fouling. These factors are either milk related or process related and they are discussed in the following sections.

#### 2.2.2.1 Seasonal variations

Raw milk, as a natural product, varies considerably in composition (refer to Table 2.1, page 30). These variations are caused by factors such as stage of lactation, breed and age of cow, environmental factors such as feeding, weather and farm management. It

has been reported that stage of lactation, feeding regime and breed of cow affect the amount of deposit formation during heat treatment (Burton, 1967 & 1968; Grandison, 1988).

#### 2.2.2.2 Acidity of milk

The natural pH of milk, measured at 20°C, is about 6.7 (Walstra & Jenness, 1984). Studies have shown that fouling deposition increases if milk pH is lowered (Gordon *et al.*, 1968; Hege & Kessler, 1986; Skudder *et al.*, 1986; Patil & Reuter, 1988; Foster *et al.*, 1989; Yoon & Lund, 1989).

Yoon & Lund (1989) reported that a small reduction in pH from 6.76 to 6.59 increases the fouling rate by a factor of 2.5. However, a larger reduction in pH, such as from 6.76 to 6.47 will increase the fouling rate 8 fold. The proportion of minerals in the fouling deposits decreases with decreasing pH whereas the proportion of protein increases (in the temperature range 85-115°C). The adhesion strength of the deposits also decreases with decreasing pH. Scanning electron micrographs (SEM) have shown that the appearance of the deposits change with pH. They are porous and thick at pH 6.4, become smoother at pH 6.5 and contain discrete bodies at pH 6.7.

The increase in protein deposition with decreasing pH, below the natural level, is due to increasing calcium activity. In addition, casein micelles become unstable to heating as milk acidity is increased and hence their reaction rates with the whey proteins, mainly with β-lactoglobulin, increase (Corredig & Dalgleish, 1996a & b).

#### 2.2.2.3 Age of milk

Jeurnink (1991) showed that an increase in acidity of milk by the action of bacteria also increases the amount of fouling deposits. The increase is caused by the action of

proteolytic enzymes, which are produced by psychrotrophic bacteria, species that can grow when milk is stored at temperatures between 4 and 30°C. The author concluded that, in aged milk, κ-casein is hydrolysed by proteolytic enzymes resulting in a decreased heat stability of the casein micelles, which will coagulate on heating and result in an increase in protein deposition. Recently, de Jong (1996) reported that after whole milk has been stored for 3 days at 5°C, each additional storage day will result in three-fold increase in fouling rate.

#### 2.2.2.4 Dissolved air and gases

Heating removes gases, including $CO_2$, and these losses, which depend on the pressure of the system during heating, can be reversible (Walstra & Jenness, 1984). However, gas or entrained air can form bubbles on the heating surface and this promotes fouling (Burton, 1968; Gordon *et al.*, 1968; Jeurnink, 1995b). Jeurnink (1995b) visually observed the influence of air bubbles, which originated from the presence of dissolved air, on the amount of deposit in a pilot-plant heat exchanger. He found that these bubbles were formed on the heating surface and acted as nuclei for the formation of fouling deposits. This result in part explains the effect of boiling liquid on fouling in the heat exchanger, especially in the evaporator. When the heated surface is not constantly wetted by the fluid, evaporation and/or gas separation occurs. Fouling could therefore take place under a multiple-phase condition, under which the chemical changes in the milk layer between the heated surface and the bubbles occur rapidly which results in more fouling. Calvo & Rafael (1995) found that degassing of milk prior to pasteurisation reduces the amount of deposit by 80%.

#### 2.2.2.5 Preheat treatment of milk

It has been established that a preheat treatment (often called forewarming) that causes denaturation and aggregation of whey protein, mainly β-lactoglobulin, will result in a

reduction in the formation of fouling deposits later in the downstream process (Kessler & Beyer, 1991). This method was proposed by Bell & Sanders (1944) to extend the run time of the UHT process. They recommended that the milk should be held at 74-95°C for 15-600 s to reduce deposition on the heat transfer surface. The effects of the preheating of milk fluids on the rate of deposit formation on the heating surface have since been studied and confirmed by a number of researchers (Burton, 1968; Hasting & de Goerderen, 1988; Mottar & Moermans, 1988; Foster *et al.*, 1989; Jeurnink *et al.*, 1989). De Jong *et al.* (1994) showed that by providing a holding section with a high volume to surface ratio, which is required for the conversion of native into aggregated β-lactoglobulin, fouling of a downstream heat exchanger is reduced by 50%.

#### 2.2.2.6 Effects of flow velocity and geometry on the fouling of heated surfaces

The effects of flow velocity and equipment geometry on the transportation process and fouling have been considered for the design and operation of heat treatment equipment. In industrial practice, it is common to maintain the flow rate, and hence the average flow velocity, of the fluid past the heated surface as high as possible to reduce the fouling rate (Gordon *et al.,* 1968; Hasting & de Goederen, 1988). Later, using experimental equipment, Belmar-Beiny *et al.* (1993) showed that both the amount and extent of fouling decreases with increasing flow rate in a tubular heat exchanger. The effect of flow velocity on fouling is thought to be two-fold:

(a) it reduces the concentration gradient of the reacting species, which is the driving force for mass transfer, between the fluid and the heating surface, and

(b) it increases the heat transfer rate but decreases the temperature gradient and hence minimises the fouling reactions at the heating surface. On the other hand, it will decrease the temperature of the surface and hence reduce fouling if the heat transfer flux through the surface is kept constant.

Dead spaces or stagnation areas (*i.e.* low shear areas), which are located at complex valve assemblies, branches in pipeline systems and connections to measurement devices, are often prone to fouling (Fryer & Slater, 1984).

Delplace & Leuliet (1995) studied the effects of different flow arrangements in the channels of the plate heat exchanger on fouling and found that herringbone plates cause less fouling than straight corrugated plates. They concluded that the reduced fouling deposition on the herringbone plates is probably due to the high mixing intensity in the flow channels that promote aggregate formation in the bulk fluid rather than on the surface of the plates.

A number of novel heat exchangers which can reduce fouling have also been studied, for example, pulsatile flow and fluidised bed heat exchangers (Bradley et al., 1989; Bradley & Fryer, 1992). Fouling can be reduced because these exchangers can induce high surface shear stresses and eddy mixing so that the fluid spends less time at the surface.

#### 2.2.2.7 Effects of surface material and finish

It is generally expected that the adsorption rate of protein during the initial stages of fouling depends significantly on the roughness of the heated surface. A rough surface can result in higher deposition than a smooth surface because of its large effective contact areas. Yoon & Lund (1994) studied the effects of different surface materials and finishes on the fouling rates of milk. They found that the fouling rates of electro-polished and standard stainless steel surfaces, titanium surfaces and Teflon coated surfaces are only marginally different. Their results confirm the earlier findings of Britten *et al.* (1988) who also studied the effects of surface roughness on the fouling rate of milk. Yoon & Lund (1994) suggested that the absence of a significant difference in the initial fouling rate found between these different surfaces finishes could be due to

the relative dimensions between the milk constituents and surface roughness. The average roughness (measured as the average depth of the cavities) of electro-polished and standard stainless steel surfaces, titanium surfaces and Teflon coated surfaces reported in their study are 0.08, 0.13, 0.19 and 0.6 μm respectively. Whereas the diameters of protein molecules and fat globules are in the range between 0.001 and 15 μm (Walstra & Jenness, 1984). Due to their large size range, milk constituents could exhibit multiple contact sites and hence be able to fill up the cavities of these surfaces at a similar rate.

Britten *et al.* (1988) also studied the effects surface material and finish on the adhesive strength between the deposits and the solid surface. They found that coating the stainless steel surface with Teflon or polymer reduces the adhesive strength between the deposits and the solid surface. They concluded that the polar binding potential (or surface energy) of the coated surfaces is the main factor influencing the strength of adhesion.

### 2.2.3 Mechanisms of fouling

Fouling of heat exchangers is a complicated process which involves chemical reactions and momentum, heat and mass transfer processes (Sandu & Lund, 1985; Changani *et al.*, 1997). The formation of fouling deposits by milk fluids can result from a combination the following processes:

(1) heat-induced reactions which convert some of the milk constituents into a form capable of being deposited on the surface,

(2) transportation of the milk constituents and/or fouling materials to the equipment surfaces or the heat transfer surfaces,

(3) attachment of the milk constituents and/or fouling materials to the surface, and

(4) formation of the deposit layer.

There are a number of hypotheses with regard to which one or more of these processes may be the controlling steps of the overall fouling process. In early work, it was considered that the fouling of a heat transfer surface mainly varies with surface temperatures and with activation energies of the β-lactoglobulin reactions (Lalande *et al.*, 1985; Gotham *et al.*, 1992; de Jong *et al.*, 1992). Belmar-Beiny & Fryer (1993) suggested that fouling is a two-step process starting with protein adsorption followed by deposition of protein aggregates. These authors considered that fouling is not only controlled by the surface reactions but is also affected by the bulk fluid temperature and velocity. Visser & Jeurnink (1997) in their review stated that fouling is caused by both whey protein aggregates and calcium phosphates that are formed in the bulk of the fluid being processed. Other researchers (Toyoda *et al.*, 1994; Georgiadis *et al.*, 1998) presented models in which they assumed that the deposition is proportional to the concentration of aggregated protein in the thermal boundary layer.

For the designer and operator, fouling is a transient process that affects the performance of the heat treatment equipment. The build-up of a fouling layer with time can take place in two different periods (Paterson & Fryer, 1988):

(1) a delay period which is often called the initial or induction period, corresponds to the time taken to condition the surface so that deposition can begin. The performance of the heat exchanger does not change significantly,

and

(2) a fouling period. This period starts when the deposit layer is sufficiently thick

to create a sustained decrease in the heat transfer.

During the fouling period, the fouling curve can exhibit a linear, a falling or an asymptotic character. A linear period is obtained with rapid deposition and the fouling rate varies linearly with time. A falling period occurs when the deposition rate decreases with time and if it reaches a constant value then the behaviour is described as asymptotic (Changani *et al.*, 1997). The possible changes of fouling with time are illustrated in Figure 2.2.

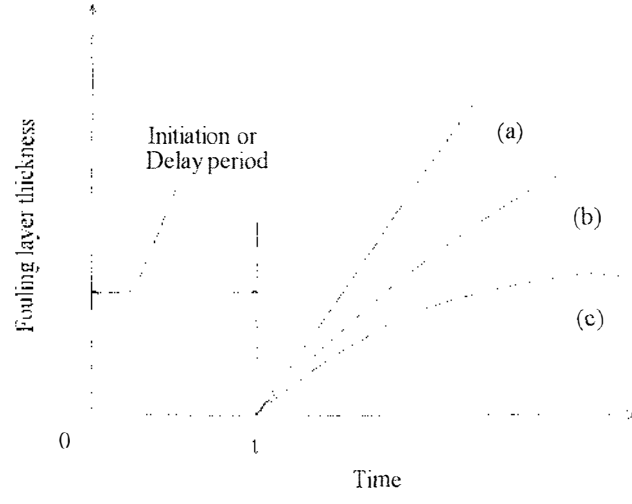


**Figure 2.2** Increase in thickness of fouling layer with time: (a) linear rate; (b) falling rate and (c) asymptotic rate.

### 2.2.4 Concluding remarks

The chemical changes to the milk and the major interactions between the milk constituents upon heating can modify and influence the fouling process. Denaturation and aggregation of whey proteins and the precipitation of milk salts are regarded as the key reactions that are important to milk fouling. Although extensive work has been carried out to characterise milk fouling, the mechanisms are complex and are not fully understood. In addition, several factors that can affect the heat-induced reactions in milk have been identified but the nature of the chemical reactions involved is not well defined.

Fundamental studies on milk fouling reactions are still required and before an analysis of the transport phenomena on fouling can be carried out, it is important to know:

(a) which milk constituents are involved in the fouling reactions and their reaction kinetics,

(b) how the changes in milk properties, especially under storage conditions, affect these reaction kinetics, and

(c) the concentration and the form in which the deposited materials are transported from the bulk fluid to the equipment surface.

Both protein and minerals may be involved in the early stages of fouling but their sequences, rates of adsorption and their strength of adhesion are not fully understood. If the events and the rates that occur during the initial stage of fouling can be identified, the heating surface could, perhaps, be modified and/or the process conditions could be optimised to minimise fouling.

Studies on the characteristics of the fouled surface *i.e.* the surface formed after the delay period, and how this can affect further adsorption and adhesion of milk components are also limited. Fundamental studies that involve heterogeneous reactions and processes in the deposits, especially when fouling occurs over a long period (*e.g.* 24 h) as is often observed in large scale processing plants, are needed.

Considerable work on the effect of different milk fluids and treatment temperatures on the composition and structure of the deposits have been reported, but studies on the effects of fluid dynamics of the treatment system, such as flow velocity and pressure, are limited. This could, in part, explain the difficulty in relating the fouling behaviour of the same type of fluid treated to the same conditions in different plants.

The transport processes that interact and influence the fouling process in the heat treatment equipment are also complex. In a multi-component mixture, heterogeneous reactions occur which cause difficulty in defining the reaction kinetics. In addition, if flow geometry, surface and flow conditions (*e.g.* turbulence) vary within the system, complicated transport equations must be solved to obtain the profiles of concentration, temperature and velocity over the surface. Consequently, the local conditions of the surface must be known in order to evaluate these transport properties.

The literature suggests the equipment should be designed and built to obtain an optimum combination of equipment size and surface temperature with minimum dead spaces or stagnation areas. It is also suggested that changing the configuration of the equipment could reduce fouling but further work is required.

In practice, there are several measures that can be applied to reduce fouling on heated surfaces during processing. They are:

(1) Avoid storage of unpasteurised milk for long periods (e.g. ≥48 h at 6 °C),

(2) Remove dissolved air from the milk fluid prior to heat treatment or maintain a system pressure well above the vapour pressure of the milk fluid at the treatment temperature,

(3) Modify the whey protein and calcium levels of the milk fluid,

(4) Preheat the milk fluid prior to heat treatment or modify the treatment conditions such as temperature and duration of treatment.

(5) Maintain a high velocity of the milk fluid past the heated surfaces.

However, (3) and (4) could be restricted in some product specifications.

## 2.3 MEASUREMENT OF FOULING

To design or select and operate heat treatment equipment that minimises the effects of fouling, information such as the characteristics of the deposits (*e.g.* chemical compositions and physical and mechanical properties), fouling kinetics and the extent of fouling resulting from a specific heat treatment duty must be available. These data can, generally, be obtained from laboratory or pilot-scale studies or by the use of data from large-scale processing plants.

The laboratory and pilot-scale studies are often carried out with simulated conditions that are likely to occur in the large-scale equipment, in particular, fluid flow velocity, surface temperature and material and duration of heat treatment. Although these conditions do not always reflect the overall conditions of the operation of a large-scale plant, laboratory and pilot-scale studies can provide valuable fouling data which can be useful in developing a fundamental understanding of the fouling mechanisms and the effects of heat treatment conditions on the fouling processes.

On the other hand, the data obtained on large-scale equipment are often scattered and not particularly useful for the development of a fouling model which can be applied for a range of process and operating conditions. This is partly due to the fact that individual plants are inadequately equipped with instruments, such as for the measurement of flow rate and temperature to permit reliable data on fouling to be collected for evaluation. It is also difficult to conduct tests or measurements in these plants because they are rarely operated smoothly for long periods.

Most of the studies on fouling discussed in the previous sections were based on laboratory and pilot-scale investigations. Different types of devices and different measurement methods have been developed and used in these studies according to the types of fouling being investigated. These devices and equipment can be classified into

groups according to the flow geometry such as wire, tube, sphere and plate or disc. The different methods used to obtain data on fouling can also be classified into two groups: direct or intrusive and indirect or non-intrusive measurement methods.

There are a number of different ways in which the milk fluids or the surface of the fouling test section can be heated. They include direct and indirect electric heating; hot water and hot oil heating (called sensible fluid heating); direct and indirect steam heating (called condensing vapour heating). Sensible fluid heating gives better thermal control than electric or condensing vapour heating and it is best suited for complex geometries.

Heating can be operated under constant heat flux or constant heating medium temperature. Under constant heat flux operation, the temperature of the solid surface increases as the fouling builds up but the bulk fluid is at a constant temperature. This type of operation is suitable for electric or sensible fluid heating and resembles the typical operating mode in large-scale processing plants. Operation at constant heating medium temperature can be achieved with condensing vapour or sensible fluid heating. The temperature of the fouled surface (*i.e.* solid surface) remains constant as the fouling layer increases and hence the temperature difference across the fouling layer also increases. This heating method is appropriate for investigations on the initial period of fouling or fouling behaviour due to surface reactions by which surface temperature is the controlling factor.

### 2.3.1 Devices and equipment

Burton (1966) used a platinum wire (0.15 mm diameter) which was directly heated by an electric current as a heating surface to study the rate of deposit formation from milk. Any change in the electrical resistance of the wire is a measure of its surface temperature which is affected by the fouling deposits. The author showed that this

laboratory method can reproduce the results of the effects of pH, seasonal variation and forewarming conditions on the deposit formation observed in a pilot-scale plate heat exchanger.

Fryer *et al.* (1985) used a heated radial flow chamber, in which fluid flowed out radially between two parallel discs, to study the effects of surface shear stress on fouling. The authors found that the expanding flows were unstable and fouling tended to form in streaks. Later, Fryer & Slater (1987) used a converging tapered tube, which has been shown to give stable flows to study the influence of fluid velocity on the formation of deposits at a wall held at a constant temperature. This device is a converging stainless steel tube, 40 cm in length, 19 mm inlet diameter and 12.7 mm outlet diameter. The flow area is continuously reduced along the tube length. The advantage of this device is that, for a given volumetric flowrate, the fluid velocity can be increased from inlet to outlet of the tube. Hence, the effects of a range of surface shear stresses on fouling can be investigated in a single experiment.

Common tubular devices which have been used for fouling studies are concentric tubes or double tubes (Delsing & Hiddink, 1983; Jeurnink, 1991; Schraml *et al.*, 1996). In these devices, hot water flows in the inner tube (*e.g.* 10 mm in diameter) and milk fluid flows in the annular space (*e.g.* 4 mm clearance) counter-current to the hot water. The inner tube is of stainless steel and the outer tube is of glass which allows for visual inspection of the deposits as they build-up. It is often considered that the flow condition in the annular space is different from that in the tube and hence it might affect the resulting data. In addition, only average deposition could be estimated because the temperatures of the heating fluid were measured only at the inlet and outlet of the tube.

Other tubular devices consist of a simple stainless steel tube (4.6 mm diameter and 9 cm in length) which is encased in an electrically heated brass block (Fryer & Slater, 1984) or a stainless steel tube (6 mm diameter and 25 cm long) inserted through an electric

water kettle, creating a simple heat exchanger (Belmar-Beiny & Fryer, 1992). The advantage of these devices is that a uniform heating temperature at the surface of the test section can be maintained during the experiments. Changes in the surface roughness due to deposition can be estimated from the measurement of pressure drop.

Different types of pilot-scale heat treatment equipment have been used successfully for fouling studies. They include tubular heat exchangers (Kastanas *et al.*, 1995), plate heat exchangers (Delplace & Leuliet, 1995) and direct steam injection and steam infusion units (de Jong, 1994).

### 2.3.2 Indirect fouling measurement methods

Indirect fouling measurement methods involve the removal of deposits from the fouled surface for visual inspection or microscopic examination, mass and/or thickness measurements and chemical analyses. Indirect measurements always require shut-down of the plant and hence they are more suitable for laboratory or pilot-scale studies. In addition, these fouling data alone will not adequately indicate how the deposits can affect the performance of the heat treatment system. However, they are essential in providing supplemental data that are important for understanding and analysing the fouling process.

Microscopic methods such as light microscopy (LM) and scanning electron microscopy (SEM) allow visual characterisation of the surface and structure of the deposits and its evolution with time. Samples are often sterilised or fixed with glutaraldehyde (0.5%) and osmic acid (1%) or with formaldehyde solution (4%), dried in open air or in an oven at 50 °C and then gold coated before the examination on SEM equipment. Transmission electron microscopy (TEM) can also be used to define internal structures and to locate protein, fat and mineral components within the deposits.

Fresh and ultra-thin sections of deposits (*i.e.* less than 1 μm thick) adhering onto the test surface can be analysed directly using infra-red spectroscopy (IRS) or X-ray photoelectron spectroscopy (XPS). Average composition of very small amounts of deposits, such as 0.5 mg, can also be determined by chemical microanalysis. The results of these techniques have been discussed in various reports (Tissier & Lalande, 1986; Daufin *et al.*, 1987)

Deposit mass measurement by direct weighing is the simplest method to monitor the extent of fouling in laboratory studies. It requires a micro-balance so that small changes in the deposit mass can be measured. Thin wall tube or test sections should also be used to increase the accuracy of the tare weight. The fouled section can be dried in an oven (e.g. 60 °C for 24 h) and then weighed to obtain the deposit dry weight. Daufin *et al.* (1987) reported an accuracy of ± 2.5 $\mu g.cm^{-2}$ of the weighing technique in their work.

### 2.3.3 Direct fouling measurement methods

#### 2.3.3.1 Heat transfer measurement

Heat transfer measurement involves the calculation of the decrease in either the local or overall heat transfer coefficient, U, of the heat transfer surface as the result of the accumulation of fouling deposits. The thermal resistance of the fouling layer, $R_f$, which is a measure of fouling deposition, is then estimated from the calculated value of U from the equation (Corrieu *et al.*, 1986):

$$R_f = \frac{1}{U(t)} - \frac{1}{U(0)} \qquad (2.1)$$

where U(0) and U(t) are the heat transfer coefficients calculated at start-up (*i.e.* clean condition) and at a time, t, thereafter.

For a uniform deposit layer, the deposit thickness, $d_f$, can be estimated from:

$$d_f = R_f k_f \tag{2.2}$$

where $k_f$ is the thermal conductivity of deposit.

However, it should be noted that, not only the deposit thickness changes with time during fouling, the thermal conductivity also varies and depends on the conditions (*e.g.* temperature and duration of heat treatment and deposit composition) that exist at the time of measurement. These values also change when the deposits are dried and removed for further examination. On the other hand, *in situ* measurements of the physical properties of the deposits are often difficult and time consuming. This partly explains the lack of information on the thermal conductivity of the deposits in the pertinent literature.

In practice, to monitor the extent of fouling as a function of time, the overall heat transfer coefficient, U, is calculated from an energy balance between the heating fluid and the product streams using the equation:

$$Q = U A \Delta T_{LMTD} \tag{2.3}$$

The value of fouling resistance, U, given by Equation 2.3 is therefore an overall value of thermal resistance of the heat exchanger (*i.e* both hot and cold sides) unless fouling on the heating or the hot side is negligible or its value is known. In addition, the calculation of the fouling resistance also includes the effects of the presence of the fouling layer on the hydrodynamics of the system. These effects will be further discussed in Chapters 4 and 5.

### 2.3.3.2 Pressure drop measurement

This method involves the calculation of the average thickness of the deposit from the measurement of the pressure drop across a flow channel. It is based on the theory that the build-up of fouling deposits on the surface of a flow channel will reduce its flow area and hence cause an increase in pressure necessary to maintain the fluid flow rate. For a given fluid flow rate, the relationship between the differential pressure and the hydraulic diameter of a flow channel is given by the following equation (Corrieu *et al.*, 1986):

$$\Delta P = \frac{2 f L \rho v^2}{D} = \frac{32 f L \rho V^2}{\pi^2 D^3} \qquad (2.4)$$

The extent of fouling in a flow channel can then be expressed by the ratio of the difference in the hydraulic diameter of clean and fouled channels and the initial hydraulic diameter as follows:

$$\alpha = \frac{D_o - D_f}{D_o} \qquad (2.5)$$

where the subscripts o and f denote the clean and fouled conditions, respectively.

The value of the fouled fraction of the hydraulic channel diameter, $\alpha$, will therefore be between 0 and 1, which represents a clean condition and a complete blockage condition of the flow channel, respectively. If the fouling deposits are distributed evenly on the fouled surface and if the change in the surface friction factor is assumed to be negligible, then $\alpha$ can be calculated from the values of the measured differential pressures using the following equation (Corrieu *et al.*, 1986):

$$\alpha = 1 - \left(\frac{\Delta P_o}{\Delta P_f}\right)^{\frac{1}{3}} \qquad (2.6)$$

Monitoring of fouling by pressure measurements is simple and well suited for narrow flow channel equipment such as plate heat exchangers. However, this technique could have a sensitivity limit for monitoring fouling in a tubular heat exchanger or in a holding tube. An increase in the thickness of the deposits in these apparatus results in a small reduction in the hydraulic diameter and therefore causes only a small increase in the pressure drop. In addition, the pressure drop is not an accurate indication of fouling because blockage can be local *i.e.* a high pressure drop could result although only a little overall deposit is formed. This method can not distinguish between local and average fouling phenomena.

### 2.3.4 Local fouling measurement

These measurement methods often give average values of overall fouling over the total surface, rather than local values at a particular area in the equipment. In particular, fouling resistance is estimated from heat transfer coefficient, U, which in turn is calculated from the bulk fluid temperatures taken from the inlet and outlet of the equipment. In complicated geometries such as plate heat exchangers, the local conditions such as temperature and velocity can vary over the heat transfer surface. This results in different rates of deposition at different locations on the heat transfer surface. The overall thermal resistance, $R_f$, is therefore not informative because it does not apply to specific locations and surface conditions. Significant errors can result when the local fouling areas are small relative to the total surface area. In addition, overall measurements cannot be applied for continuous monitoring of fouling of the surface which is not part of a flow channel or a heat transfer surface such as the surface of a steam infuser unit (de Jong *et al.*, 1994) or holding tubes.

Withers *et al.* (1994) have developed and tested an ultrasonic device to detect and monitor fouling during UHT processing in a pilot-scale plant. The sensor is mounted on the pipe and can detect deposit layers from 0.1 to 6 mm in thickness on the inside

surface. They have also reported that the same sensor can be used to detect the efficiency of the cleaning process. However, further testing of the prototype sensor at different process and operating conditions such as milk fluid composition, flow rate, system pressure are still required.

Other techniques which can be used for the detection of fouling include acoustic and optical methods. Their applications to measurement of local fouling in heat treatment equipment have been reviewed by Withers (1996). The vibration sensor in the acoustic technique was found to be suitable in plate heat exchangers. The optical sensor could be used anywhere in the processing system. However, the author suggested that further development of the techniques is still required before they can be applied in large-scale equipment. Recently, Tuladhar *et al.* (1999) developed a novel non-contacting proximity gauge, based on a siphoning effect, to measure the thickness of deposit in situ and in a liquid environment. Local layer thickness up to 1 mm can be measured with an accuracy of ±20 μm.

Jones *et al.* (1994) used a commercially available heat flux sensor to measure the heat flux (or heat transfer) during fouling from whey protein solutions of various concentrations. The degree of fouling was determined by the reduction in heat flux from an electrically heated copper block to the fluid due to an increase in fouling deposit thickness on the heating surface. They concluded that the sensor gives a clear indication of the rate and extent of the fouling process. It appears that the sensor is a suitable device for measuring the local build-up of fouling deposits from milk fluids and could be adapted to monitor fouling at different locations in the heat treatment equipment of large-scale processing plant.

The technique of measuring fouling using heat flux sensors was further developed in this study for monitoring of local fouling of non-heated surfaces by heated whole milk. The system developed for this purpose is reported in Chapter 4.

## 2.5 SUMMARY AND RECOMMENDATIONS

More quantitative data are needed on the fouling of milk fluid in heat treatment equipment. The information will permit an understanding of the design of heat transfer equipment, thus better selection of large-scale equipment and operating procedures can be made to minimise fouling and to optimise the production time.

A better overall understanding of the fouling process which concerns the details of the fundamental knowledge of several sub-processes are needed. These are

(i) the nature of the chemical reactions occurring in the body of the fluid and at the heat transfer surface,

(ii) characterisation of the boundary layer at the heat transfer surface at which heterogeneous reactions and the transport phenomena of the system can occur simultaneously,

(iii) adsorption and deposition phenomena of milk constituents, in particular proteins and milk salts, on surfaces, and

(iv) evolution of physical and mechanical properties of the deposits during fouling.

Most studies have been carried out on fouling associated with indirect heating systems. Only recently, studies on fouling from the direct treatment by steam infusion have been reported (de Jong, 1994). Data on deposit formation in downstream areas of a heater, such as in the holding sections, are limited. Although no more heat is exchanged, the chemical and physical properties of the milk fluid immediately downstream of a heater could still change which may cause deposition long after the heating step. This type of fouling could take place by a different mechanism from the direct fouling on the

surfaces of a heater. The lack of a suitable direct measurement method for fouling of non-heated surfaces could in part, explain the small number of reports on this fouling process.

The pertinent literature shows that there are some methods that are available to the equipment designers and plant operators to reduce or eliminate fouling. These methods are either product or process related. However, fouling in the large-scale processing plant can vary significantly from day to day, hence a robust and reliable monitoring system, which can be used for measuring its rate and extent, is needed. It is also important to know where the deposition occurs within the processing equipment and what the controlling processes are. This type of information is more useful than the overall data because it applies to specific locations and surface conditions such as temperature, concentration and velocity. Knowledge of fouling at different locations in heat treatment equipment will permit the development of overall operating procedures that minimise local fouling and optimise the time for which the plant can be operated before cleaning is needed.

CHAPTER 3

# THE FOULING RIG

CONTENTS

## .3.1 DESIGN CONSIDERATIONS

A pilot-scale fouling rig was designed and built to allow the effects of treatment temperature, mass flow rate and flow geometry on fouling of stainless steel surfaces by heated milk fluids to be evaluated. The design of the rig was mainly based on the heat treatment methods which are currently employed in large-scale milk powder plants.

In industrial practice, milk fluids are first heated in a heat exchanger to a temperature of 75- 85 °C, and then heat treated to higher temperatures (*e.g.* 95 - 110°C) via a direct steam injection (DSI) heater. Holding tubes of suitable dimensions are placed directly downstream of the DSI heater to give the required heat treatment time (or holding time) which is dependent on the final product specifications.

To investigate fouling of the holding tube surfaces, tubular test sections of different sizes and geometries would be placed in different locations downstream of the DSI heater. The arrangement of these test sections would allow the setting up, isolation and removal of test sections without interrupting the pumping and heating process.

The effect of fouling of large-scale processing plant usually becomes noticeable when the plant has operated for 12 h or longer. Using this test rig, the investigation of the progress of fouling might also require the same run time. In order to minimize milk fluid utilisation, a maximum product flow rate of 200 kg $h^{-1}$ was selected.

The equipment and process control instrumentation were to be skid-mounted for portability. Standard utilities such as electricity, steam, water and compressed air were connected to the rig via cables and flexible hoses. Data collected during the experiment were recorded using data logging equipment and were transferred to a computer for further processing.

A fouling monitoring system which was based on the measurement of changes in wall heat flux was developed to directly measure the growth and extent of fouling at various locations on the non-heated surfaces. The development of this measurement system is reported and discussed in Chapter 4.

## 3.2 DESCRIPTION OF INSTALLATION

### 3.2.1 The fouling rig

The fouling rig comprises of two balance tanks (50 L each) equipped with bottom feed lines and in-line filters (500 μm), a feed pump, a plate heat exchanger, a DSI heater, a loop of tubular fouling sections and a bypass loop in parallel, cooler units and instruments and controller devices. The product piping had a diameter of 19 mm (nominal). The holding tubes, with internal diameter between 10 and 23 mm, were fabricated in various lengths to allow for different holding times. The main material of the construction was annealed cold-rolled 304 stainless steel, with surface roughness, $R_a$, between 0.125 and 0.5 μm (International Dairy Federation, 1985).

Photographs of the fouling rig are shown in Figures 3.1 and 3.2. The process equipment and instrumentation diagram (PID) of the rig is shown in Figure 3.3. A list of components used in the construction is provided in Appendix 3.1 and the major plant items are described in detail below.

#### 3.2.1.1 The feed system

The feed pump was a positive-displacement, non-pulsating type and was equipped with a pressure relief valve for safety purposes. The total flow rate could be adjusted by altering the pump motor speed with a frequency converter. The maximum capacity of the pump was 200 kg $h^{-1}$ at 6 bar gauge system pressure, based on water at 20°C. A

manual diaphragm valve, which was installed downstream of the fouling test sections, was used to maintain a positive pressure in the pipe work system and to avoid boiling and separation of gases of the milk fluids at the treatment temperatures.

#### 3.2.1.2 The initial heating system

Initial heating of milk fluid was carried out using a two-pass, counter-current plate heat exchanger having a heat transfer area of 0.7 $m^2$ and a logarithmic mean temperature difference, at maximum heating duty for whole milk, of 13.8°C. This plate heat exchanger was selected because it could provide a temperature difference (between whole milk and hot water) of 1°C and hence would minimise milk deposition on the plate surfaces during the heat treatment. The heater could raise the whole milk temperatures from 4 to 85°C at a maximum flow rate of 150 kg $h^{-1}$.

The heating medium of the plate heat exchanger was recirculated hot water, generated and maintained at the required temperature by injecting steam into the hot water stream. Steam condensate was continuously removed from the recirculated hot water loop and discarded via a pressure relief valve. This method of producing hot water by the injection of steam is not thermally efficient. However, this method eliminates the need for an external primary hot water supply and hence improves the mobility of the fouling rig because steam is often the only thermal energy supply which is available in the pilot plant.

The hot water was recirculated to the heating side of the plate heat exchanger at 600 kg $h^{-1}$ and at a pressure of 0.7 bar by a centrifugal pump. The steam supply line to the hot water loop was equipped with a steam strainer to remove any foreign matter in the steam, a steam pressure reducing valve for adjusting the main supply steam pressure to the required level, and a pressure relief valve for safety.


**Figure 3.1** Photograph of the fouling rig: (a) feed pump; (b) control panel; (c) plate heat exchanger; (d) steam supply to the direct steam injection (DSI) heater.

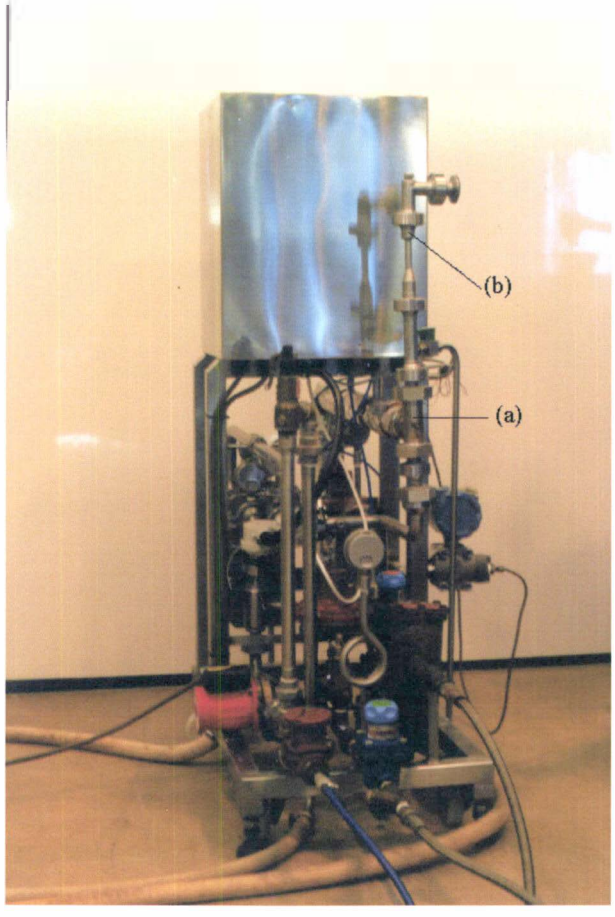


**Figure 3.2** Photograph of the fouling rig showing the back of the heat treatment unit: (a) DSI heater; (b) sudden expansion test piece.

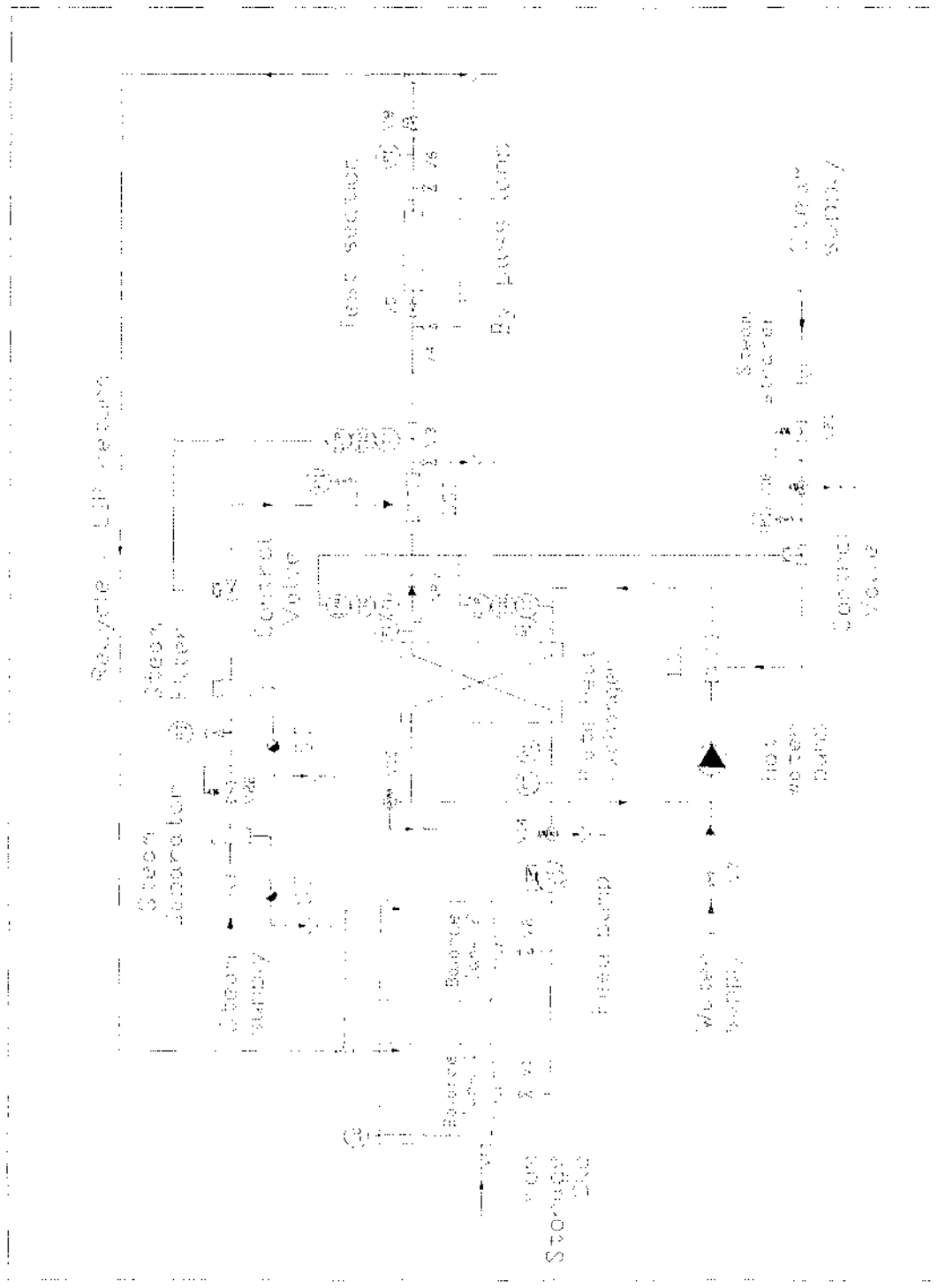

**Figure 3.3** Process and instrumentation diagram (PID) of the fouling rig.

**Notation for Figure 3.3**

| | |
|---|---|
| CIP | Cleaning-in-place |
| DSI | Direct steam injection device |
| FT | Flow rate transmitter |
| I/P | Integer/Pneumatic converter |
| LC | Level controller |
| NRV | Non return valve |
| PI | Pressure indicator |
| ST | Steam trap |
| TIC | Temperature indicator and controller |
| TT | Temperature transmitter |
| V1-7 | On-off valves |
| V8 | Back pressure valve |
| V14-16 | Pressure relief valves |
| V21-22 | Steam pressure reducing valves |

### 3.2.2 The direct-steam-injection (DSI) heater

The DSI heater is a device by which the final heating is carried out. Figure 3.4 shows a schematic drawing of the DSI heater installed within the fouling rig. Saturated high pressure steam was injected via a number of small radial nozzles (1- 2 mm in diameter) and was mixed with the milk fluid which was at a lower pressure in a flow channel having a constant cross-section area. Steam immediately condensed in the downstream diverging nozzle, giving up its latent heat of vaporisation and thus heating the milk.

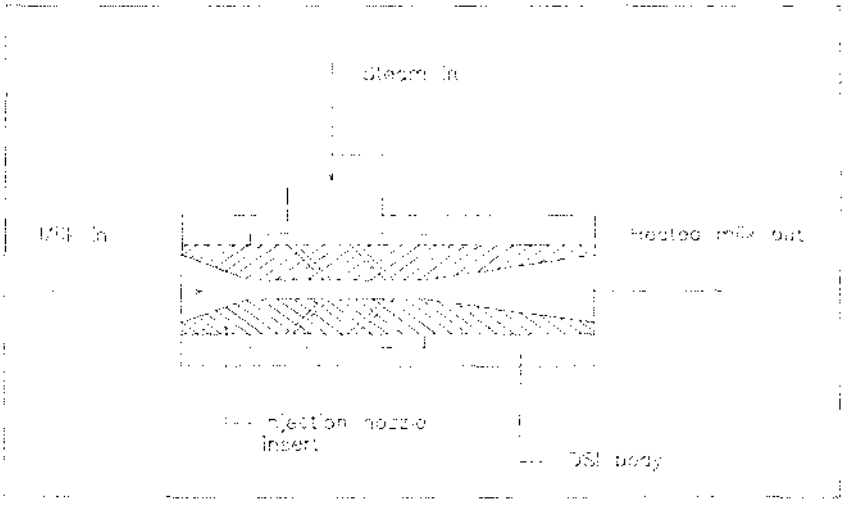


**Figure 3.4** Schematic drawing of the direct steam injection (DSI) heater.

The DSI body was designed to allow the nozzle insert to be easily removed and replaced. The nozzle insert was made of Teflon, which is a low thermal conductive plastic ($k = 0.45$ W m$^{-1}$ K$^{-1}$ at 100°C) compared with stainless steel ($k = 16$ W m$^{-1}$ K$^{-1}$ at 100°C). Milk was therefore separated from the steam until the moment of steam injection and was unlikely to be heated (indirectly) by the steam via the surfaces of the flow channel. The deposits are therefore less likely to build-up on these surfaces and

restrict the passage of the flow channel and hence affect the DSI performance.

The steam supply line to the DSI unit was equipped with a pressure reducing valve, a steam separator, a stainless steel steam filter and steam traps to remove any foreign matter and liquid condensate from the steam before mixing steam with the milk (refer to Figure 3.2). The steam pipes were made of 316 stainless steel to minimise corrosion and were insulated with 25 mm thick fibreglass ($k = 0.45$ W $m^{-1}$ $K^{-1}$ at 100°C) and lagged with thermal insulation tape. The details on the design of the DSI heater are given in Appendix 3.2.

### 3.2.3 The fouling test pieces

To investigate the effects of flow geometry on fouling, different test sections consisting of straight tubes of different lengths and diameters (between 14 and 23 mm inside diameter) and tubular sudden expansions of different step heights were fabricated. These test pieces were easily fitted to and removed from the rig using either Tri-clover® or RJT® fittings.

Figure 3.5 (a) shows a photograph of a tubular test piece. This test piece was made to allow inspection of the surface structures and measurement of the deposit thickness at the completion of the experimental run. The tube section was fabricated into two horizontal sections that can be fitted and held together. A rubber ring was embedded within their joining surfaces to provide sealing. The length of this test piece was 200 mm and its inside diameter was 23 mm. The test piece was hydraulically tested up to 6 bar gauge pressure before being used within the fouling rig. The mechanical design drawing of the test piece is given in Appendix 3.3.

Three different tubular sudden expansions (designated A, B and C) were used in this study. They all had the same large pipe diameter, D, of 23 mm but different small pipe

diameters, d, in order to give different step heights. The small diameter of A, B and C were 16.7, 10.3 and 4.6 mm respectively. Figure 3.5 (b) shows a photograph of tubular sudden expansion B and Figure 3.6 shows a schematic drawing of test pieces A, B and C. The details of the flow geometry of test pieces A, B and C will be discussed in Chapter 5.

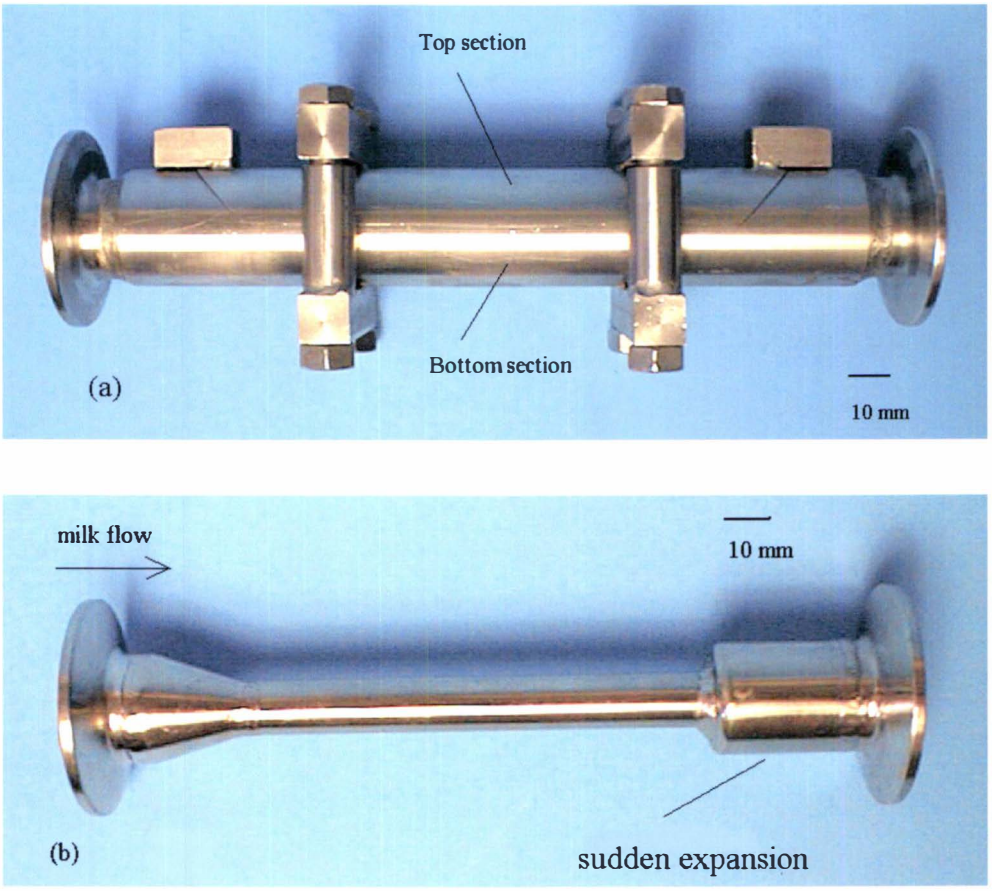


**Figure 3.5** Photographs of fouling test pieces: (a) horizontal open test piece; (b) tubular sudden expansion B (small/large diameter, d/D=0.43).

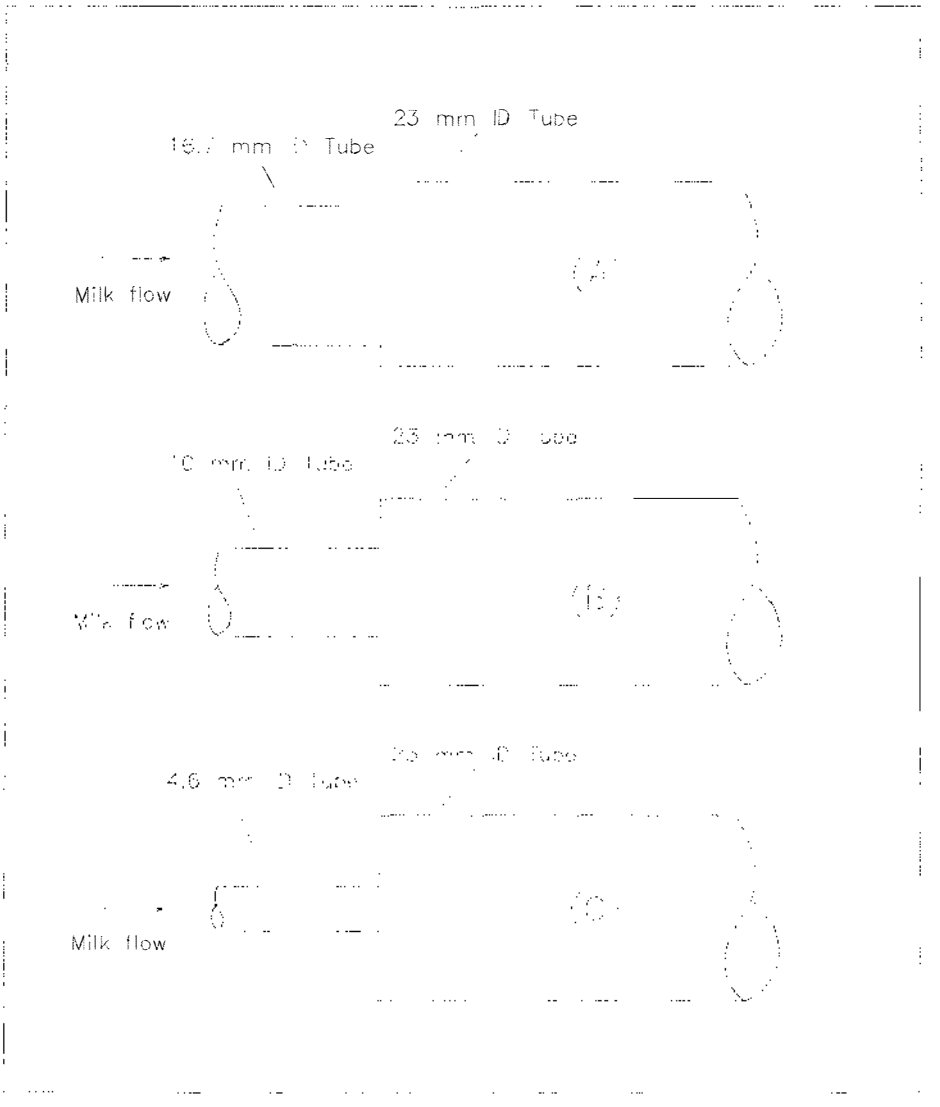


**Figure 3.6** Schematic drawings of tubular sudden expansions A, B and C.

## 3.3 INSTRUMENTATION AND DATA ACQUISITION

### 3.3.1 Flow rate measurement

The milk flow rate at the start and during each experimental run was checked by a stop watch and bucket method. The milk flow rate was also continuously measured by a turbine flow meter (Bailey Fischer & Porter, Model 10DX211-2A) installed in the pipe between the feed pump and the plate heat exchanger. The precision of the flow meter is $\pm 0.5$ $Lh^{-1}$.

### 3.3.2 Pressure measurement

The pressures of (1) the main steam supply and the steam supply to the DSI (*i.e.* before and after the steam control valve), (2) the hot water loop and (3) the milk fluids at the inlet and outlet of the plate heat exchanger and after the test section were measured by the Bourdon type pressure gauges (range 0- 4 and 0 - 10 bar). The precision of the gauge is $\pm 0.05$ bar. Provisions were also made for the installation of pressure transmitters (Rosemount, Smart Family) at these locations. This arrangement allowed these pressures to be continuously recorded by the data logging equipment, if required. The precision of the pressure transmitter is $\pm 0.001$ bar.

### 3.3.3 Temperature measurement and control

The temperatures of (1) the milk fluid leaving the plate heat exchanger, (b) the milk fluid leaving the DSI heater and (3) the hot water entering the plate heat exchanger were continuously measured with platinum resistance thermometers with transmitters. These temperatures were automatically controlled by the controllers which operated the pneumatic-actuator steam control valves. The sizes of these control valves (*i.e.* Cv numbers) were 1.25 and 0.5 for the hot water loop and the DSI heater respectively.

Calibration of all the temperature probes (initially and thereafter at every 6 months) was carried out according to ITS 90 (Nicholas & White, 1994) using a standard oil bath, a reference thermometer (RT200/026) and a calibrator (Fluke 702). The precision of the platinum resistance thermometer was ±0.1°C.

***Controlling the temperature of milk leaving the DSI heater***

At treatment temperatures above 70°C, the temperature probe was often coated with a layer of fouling deposits. A fouled temperature probe can give a reading of several degrees lower than a clean one, depending on the thickness and the thermal conductivity of the deposit layer (Cho & Choi, 1998). Consequently, the automatic temperature control system will respond wrongly in such a way that the milk fluid becomes overheated, which then causes more fouling on both the equipment and the probe.

To be less susceptible to fouling, a temperature probe should have a small sheath outside diameter (a standard probe has a sheath diameter of about 5 mm) and, preferably, should be able to be periodically cleaned without disturbing the temperature controller and the flow conditions.

A portable temperature probe for measuring the temperature of the milk fluid leaving the DSI heater was therefore developed and fabricated. It consisted of a platinum resistance thermometer, a temperature transmitter and a digital display. The sheath of the thermometer was 50 mm long and its outside diameter was only 1.5 mm. It had a sharp-tip and could be inserted into the pipe to measure the fluid temperature and then periodically retracted for cleaning via a sample extraction nozzle sealed with silicon rubber (called a Septum nozzle). A photograph of the sharp-tip temperature probe device is shown in Figure 3.7.

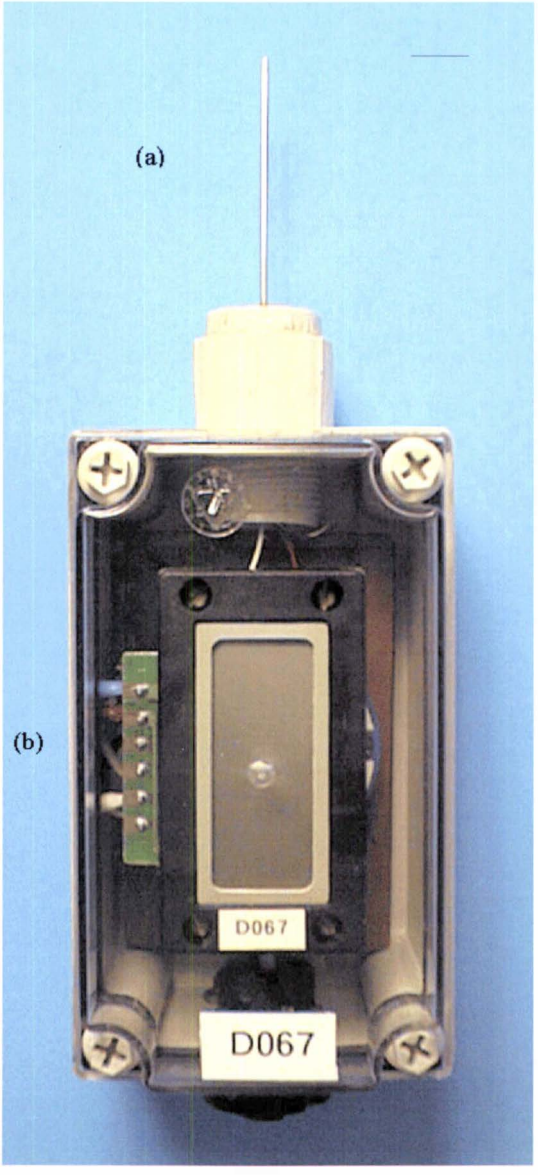


**Figure 3.7** Photograph of the temperature measurement device: (a) sharp-tip temperature probe and (b) temperature transmitter and digital display (bar = 10 mm).

### 3.3.4 Data logging equipment

The data logging equipment was a modular system which consisted of power supplies, input/output modules and a main processing unit (Opto 22, Huntington Beach, California), a communication converter, *i.e.* analogue to digital, (AC7B), a computer (Compaq Contura 5/20) with NZDRI prepared software and printer. Figure 3.8 shows the layout of the data logging equipment.

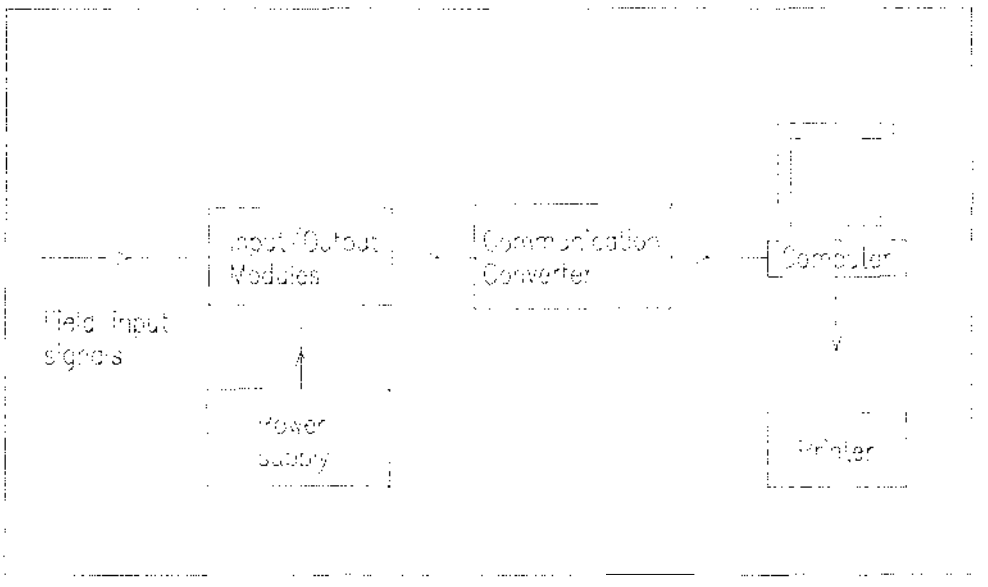


**Figure 3.8** Layout of the data logging equipment.

The data logging system was calibrated (initially and thereafter before each set of experiments) using a precision simulator (Memocal 81, ERO Electronics). The instrument was connected to each of the input modules of the data logging equipment and a range of simulated signals for the required measurements (such as temperature, pressure and flow rate) were generated. The built-in software of the data logging system calculated the off-set and the span values of the required measurement and automatically updated those values in the input terminal configurations.

### 3.3.5 Deposit thickness measurement

To measure the thickness of a soft and wet fouling layer on the surface of the test section at the completion of an experiment, a device which was based on the electrical conductivity technique (Bott, 1995) was developed. The instrument consisted of a test section support, a steel needle mounted on a micrometer (Mitutoyo, DMS60-25), a current meter (Fluke, 8060A) and a light indicator circuit. The light indicator circuit design was based on the electrical resistance of the wet deposit of 0.5 μ-Ohm with the supply voltage of 5 volts and the current of 10 μ-Amps. The precision of the micrometer was ±0.02 mm.

In operation, when a fouled test section was mounted on the device, it formed part of an electrical circuit of the instrument. The needle was advanced to the deposit surface until a connection was made, *i.e.* the current meter showed a reading and the indicator light was on. When the needle reached to the bottom of the deposit and touched the stainless steel surface, the current meter showed another reading. The difference in the two micrometer readings gave the effective deposit thickness.

Figure 3.9 shows a photograph of the deposit thickness measurement device.

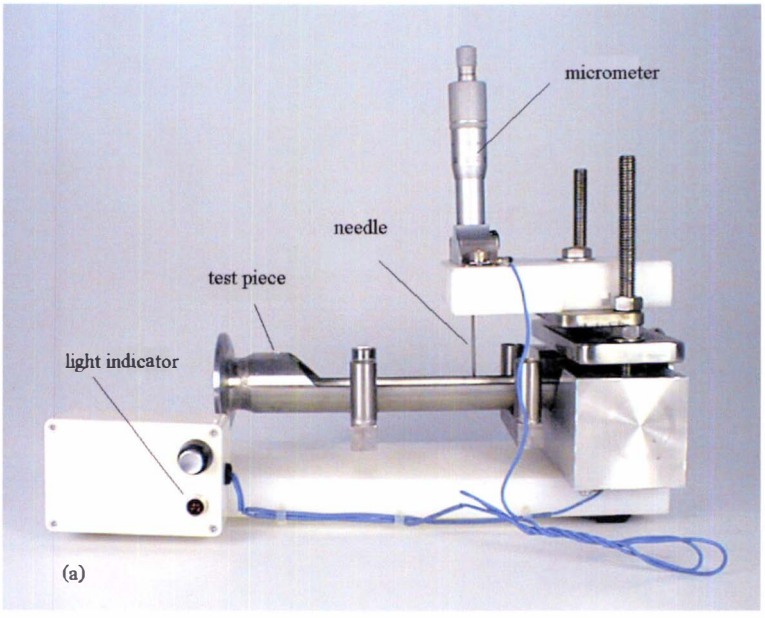


**Figure 3.9** Photograph of the instrument for measuring the thickness of fouling layers (current meter not shown).

## 3.4 OPERATING PROCEDURES

### 3.4.1 Start-up procedure

At start-up, a standard procedure was always followed:

- switch on the main power supply,

- open the isolating valves of steam, soft water and compressed air; if the steam had not been used earlier and the main line was not equipped with a steam trap, the drain valve was opened slowly to allow the steam condensates accumulated in the pipe to drain out without causing any water hammer,

- feed soft water to the first balance tank,

- switch on the feed pump and set the pump speed to the required flow rate,
- switch on the temperature controllers (of the plate heat exchanger and the DSI heater) and manually ramp up the controllers to the required set points, at the same time adjusting the back pressure valve to obtain 2 bar gauge system pressure, wait until the temperature readings appeared steady then switch the controllers to the automatic mode,

- from this step, either a cleaning or an experimental run could be started.

### 3.4.2 Experimental run procedure

To start an experimental run with milk:

- the standard cleaning procedure was completed,

- milk was transferred from storage silo to the second balance tank (as shown in Figure 3.2, the balance tank was equipped with an on-off level controller to prevent it from overflowing),

- the temperature controllers were reset and the system pressure was set to the required levels, then the plant was allowed to attain steady state conditions (regarding flow, pressure and temperature),

- the operation on milk was started by switching from the water balance tank to the product balance tank. The back pressure valve and the milk flow rate were adjusted if necessary and the process parameters such as flow rate, temperatures, pressures and heat flux data were recorded (via a data logger),

- other processing data, which were not recorded by the data logging equipment, were recorded to an operation logging sheet, every 30 minutes during the experiment,

- at the completion of the run, the data logging was stopped, the controller temperature setting was changed to zero and the fluid supply was switched from milk to water,

- when the temperature of water leaving the DSI was about 40°C, the feed pump was switched off, the back pressure valve was released and the drain valve (located downstream from the DSI) was opened,

- the fouling test sections were removed and the pipes were reconnected with key pieces in place of the fouling test sections,

- the rig was then ready for the cleaning step.

### 3.4.3 Cleaning procedures

After each experiment, the test sections were removed from the fouling rig. The test sections were then soaked and scrubbed manually with a 1% v/v caustic solution at 60°C, rinsed with soft water then soaked and cleaned with 1% v/v nitric acid solution and rinsed with soft water before being re-installed to the fouling rig. These test sections were cleaned again during the CIP of the rig.

A standard cleaning-in-place (CIP) procedure, as used in the dairy industry, was used for cleaning the fouling rig before and after each experiment. A two-stage clean, caustic solution followed by acid solution, was applied. A 1% v/v caustic solution was recirculated from the balance tank through the plant at 75°C for 30 min. The equipment was then rinsed with soft water at 75°C for 15 minutes at the completion of the caustic cycle, followed by a recirculation of 1% v/v nitric acid solution at 70°C for 30 min and then a rinse with warm soft water for another 15 minutes. The flow rate during cleaning was set at the maximum pump rate of 200 kg $h^{-1}$. At the completion of the cleaning, the rig was ready for the experimental run or for shut-down.

### 3.4.4 Shut-down procedure

To shut-down the fouling rig:

- the controller temperature settings were set to zero,

- when the temperature of the water leaving the DSI was about 20°C, the feed pump and the temperature controllers were switched off,

- all valves were closed, the main electrical supply was turned off and the drain valve was opened.

CHAPTER 4

# THE FOULING MONITORING EQUIPMENT

CONTENTS

## 4.1 INTRODUCTION

In this chapter, the equipment of the fouling monitoring system is described. The methodology used to estimate the heat transfer coefficient from measured heat flux and the problems encountered are discussed. Representative results obtained from fouling experiments together with the observations on the characteristics of the heat transfer coefficient-time and heat transfer coefficient-deposit thickness relationships are also reported and discussed.

## 4.2 SYSTEM DEVELOPMENT

### 4.2.1 System requirements

In the development of a fouling monitoring system, which can be used on different locations and sites under varying conditions, the following characteristics are desirable:

- The equipment should be of robust construction, non-intrusive and not cause disturbance to the routine operations of the processing plant.

- The system should be easily installed, replaced and serviced and requires the minimum of maintenance.

- The system should be capable of detecting the presence of fouling and the growth of the fouling layer during processing. The data should be reproducible.

### 4.2.2 Description of equipment

#### 4.2.2.1 Instrumentation

The monitoring system comprised of thin foil heat flux sensors (Micro-Foil Heat Flux Sensor, Rhopoint Ltd, Oxted, UK), programmable transmitters (Intech Instruments Auckland Ltd, NZ) and data logging equipment.

The function of the heat flux sensor is to directly measure heat transfer through a surface area. The sensor consists of a number of thermocouples in series on either side of a composite material of known thermal conductivity. When heat begins to flow through the material, it generates a differential in voltage which is proportional to the temperature differential between the material surfaces. The heat transfer rate (or heat flux) can therefore be directly read as a function of voltage. The sensitivity of the sensor depends on the number of thermocouple junctions and the thickness of the composite material.

Heat flux sensors have been used to determine plug closure in cryogenic pipe freezing (Tavner *et al.*, 1996), to measure the effective thermal resistance and conductivity of whey protein deposits (Davies *et al.*, 1997) and thermal conductivity of multilayered plastic containers (Tong & Sheen, 1992). Recently, Gillham *et al.* (1999) used a heat flux sensor to monitor the thermal resistance of a whey protein fouling layer during cleaning. Jones *et al.* (1994) used the sensor to measure the change in heat flux, which was caused by fouling, from an electrically heated block to a flow of milk protein solution. They found that the sensor gave clear indications of the rate and extent of fouling of milk protein heated over a range of products and process conditions such as concentration of whey protein, treatment temperature and Reynolds number.

In this study, the heat flux sensor was used to measure the change in heat flux due to

fouling of non-heated surfaces. The sensor was attached to the outer surface of a fouling test piece. The build-up of fouling deposits on the inner wall surfaces created an additional thermal resistance and caused a reduced heat flux or heat loss through the wall.

The main advantage of the heat flux sensor is that it can eliminate the need for installing a device on inner surfaces which, in some situations is neither desirable nor possible. The sensors are small in size (7x18 mm), thin (0.3 mm) and inexpensive (NZ$500 each). They can be attached to flat or curved surfaces and require no special wiring or reference junctions.

Because the output signal from the sensor is in micro-volts which can be affected by the resistance in lead wires and stray electrical noise (*e.g.* caused by the electrical motors in the plant), each sensor was provided with a transmitter to convert the micro-volt signal to an industry standard 4 to 20 mA current signal. Unlike voltage, current signals are immune to resistance in extension wires and stray electrical noise.

The signals from the sensors were fed to the data logging equipment (described in Section 3.3 of Chapter 3) where the current signals were converted back to micro-volt signals and recorded. Further calculations and analysis of the results were performed using the computer. A schematic layout of the monitoring equipment is given in Figure 4.1.

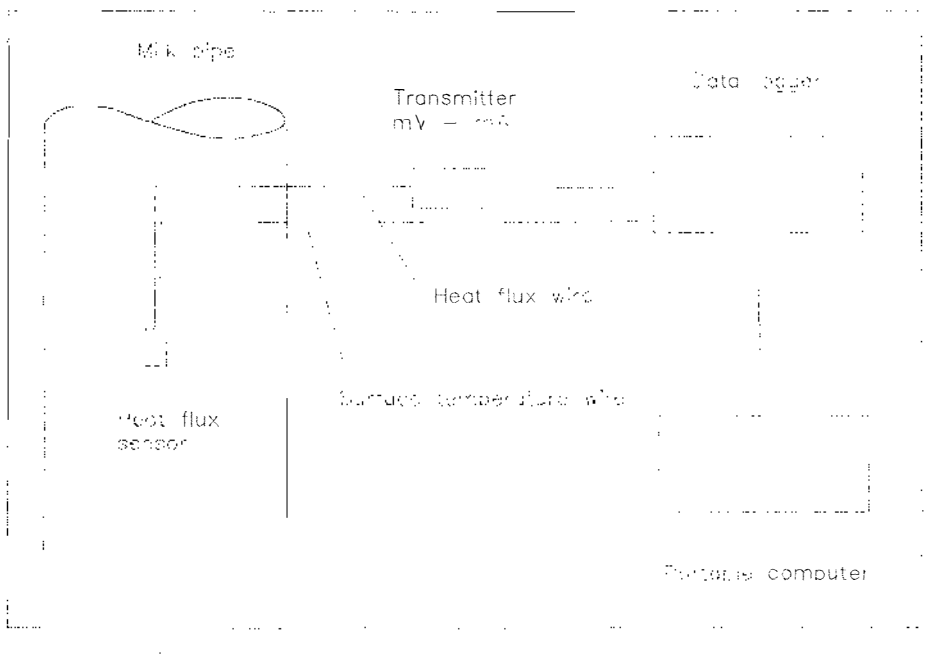


**Figure 4.1** Schematic layout of fouling monitoring equipment

#### 4.2.2.2 Heat flux sensor characteristics

Two different sized sensors were used in this work. The small sensors, size 5 mm x 10 mm and sensitivity of 0.317 μV/(W $m^{-2}$) were selected for monitoring of fouling of the small surface areas in the fouling rig. The large sensors, size 8 mm x 25 mm and sensitivity of 0.634 μV/(W $m^{-2}$) were selected for monitoring of fouling in the large-scale plant. Because the ambient temperature in the large scale plant was high, in particular in the evaporator and dryer plants (*i.e.* 50°C), and hence the temperature difference between the product and the surrounding air was small, a sensor with a higher sensitivity was required (Chapter 6). Both types of sensor have the same thermal resistance of 0.002 °C/(W $m^{-2}$), maximum heat flux of 113 kW $m^{-2}$ and response time of 0.4 s and both are 0.305 mm thick. These sensors were also equipped with additional thermocouples for surface temperature measurements. A photograph of the two sensors is shown in Figure 4.2.

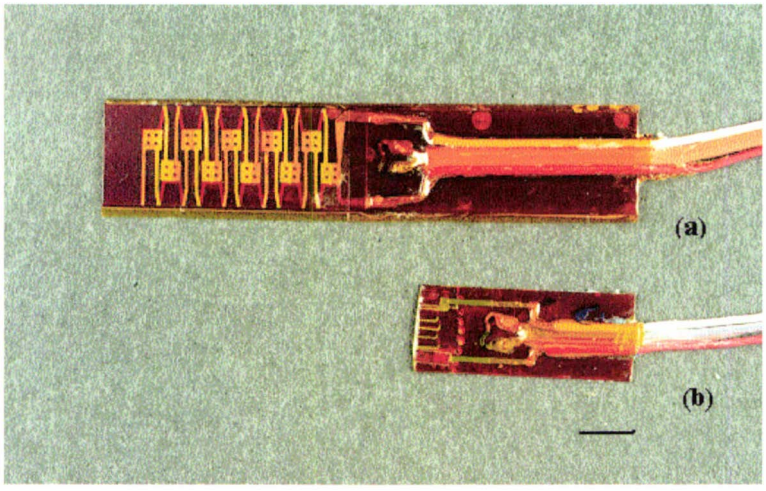


**Figure 4.2** Photograph of heat flux sensors: (a) used for monitoring of fouling in the large-scale plant; (b) used for monitoring of fouling in the fouling rig; (bar = 5 mm).

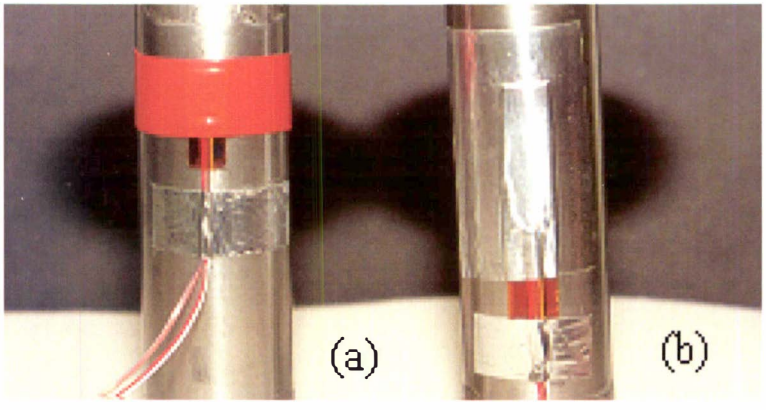


**Figure 4.3** Attachment of heat flux sensors using stretch tape (a) and self-adhesive tape (b).

Each heat flux sensor was supplied with a certificate containing the calibration factor, $CF_{hf}$, between the micro-voltage change and the heat flux rate together with a temperature correction graph, $Tf_{hf}$. The micro-volt signal, $V_{hf}$, from the sensor was therefore converted to heat flux using equation 4.1

$$q = V_{hf} ( CF_{hf} ) ( TF_{hf} ) \quad (4.1)$$

The calibration and temperature correction factors supplied by the manufacturer are listed in Appendix 4.1.

#### 4.2.2.3 Attachment of sensors

The sensors were applied to the surfaces of the fouling test pieces using silicon stretch tape (Minco Products, Inc., Minneapolis, USA). In the large-scale plant, self-adhesive tape, instead of stretch tape, was used to apply the sensors to the pipe surfaces. These methods allow rapid installing and removal of the sensors. An example of the attachment methods is shown in Figure 4.3.

In order to obtain good thermal contact and to eliminate any possible pockets of air between the pipe wall and the sensor, a thin and highly thermal conductivity paste (RS Components, Northants, UK) was applied to the surface of the sensor before each attachment. Both surfaces of the pipe and the sensor were also cleaned with acetone to remove any dirt and grease before the installation. The sensor was positioned lengthwise on the pipe and if the pipe was horizontal, it was always placed on the side walls. In these locations, the layers of air immediately next to the pipe walls are heated and tend to rise, which in turn cause a transfer heat from the pipe walls to the surrounded air by convection. The sensor was never placed in the top-centre of the pipe because the rising layers of hot air on each side of the pipe tends to separate and could form a zone of relatively stagnant and unheated air at the top of the pipe. This zone could hinder the heat transfer from the pipe wall to the surrounding air. The sensor was also never placed at the bottom of the pipe in case settling of large fouling particles occurred during the run. Care was always taken and the same method was always used when applying the sensor to the pipe surface to achieve uniformity and consistency between experimental runs.

## 4.3 METHODOLOGY

### 4.3.1 Theoretical consideration

A section of pipe through which milk flows at elevated temperatures will result in a heat transfer (or heat loss) from the fluid to the wall by convection, through the wall by conduction and to the surrounding air by natural convection. Fouling deposits increase the overall thermal resistance of the pipe wall and reduce the heat transfer. The overall heat transfer coefficient can be estimated from the measured heat flux (Jones *et al.*, 1994) using the equation:

$$q = \frac{Q}{A} = U ( T_b - T_a ) \qquad (4.2)$$

where $T_b$ and $T_a$ are the temperatures of the bulk milk fluid and the surrounding air respectively, A is the surface area, and U is the overall heat transfer coefficient which is defined as the inverse of the total heat transfer resistance, R.

Consider the heat transfer between the milk fluid and the surrounding air separated by the pipe wall as shown in Figure 4.4. The total heat transfer resistance, R, is made up of several components: the resistance contributed by the milk flowing inside the pipe, $R_m$, the resistance contributed by the fouling layer, $R_f$, the resistance contributed by the stainless steel wall, $R_{ss}$, the resistance contributed by the sensor, $R_{hf}$, and stretch tape, $R_s$, and the resistance contributed by the ambient air condition near the pipe wall, $R_a$. The overall heat transfer coefficient at a given time, t, is therefore represented by:

$$U(t) = \frac{1}{R(t)} = \frac{1}{R_m + R_f + R_{ss} + R_{hf} + R_s + R_a} \qquad (4.3)$$

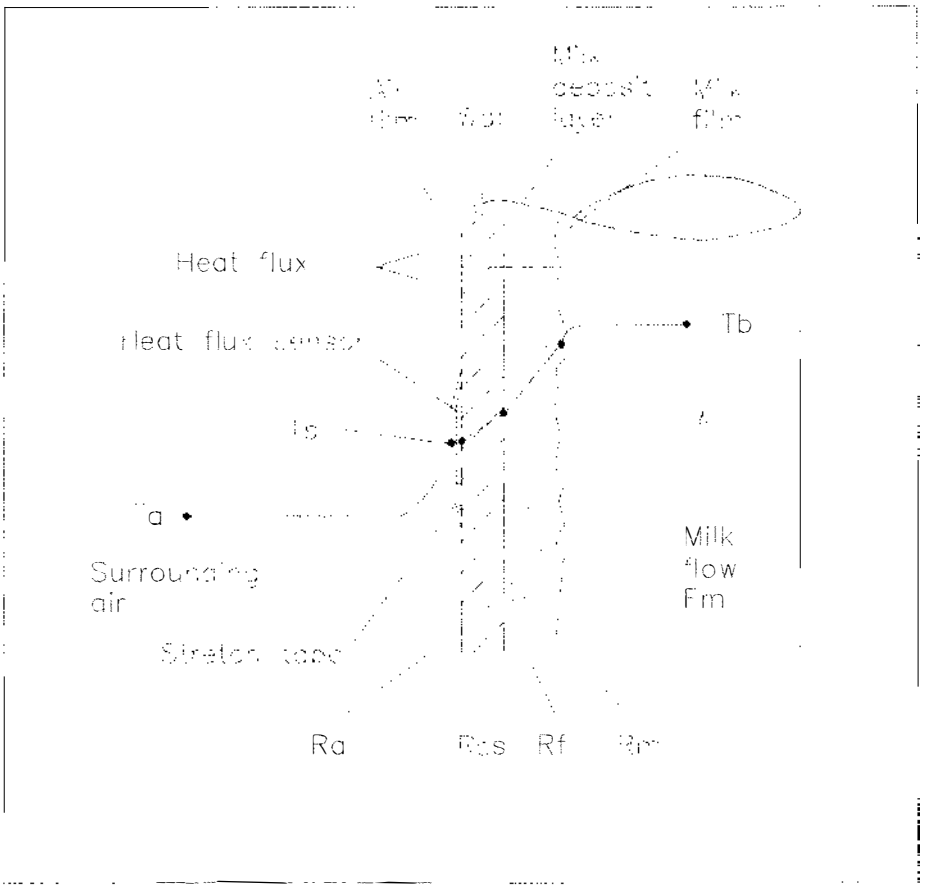


**Figure 4.4** Schematic drawing of section view of a fouled pipe showing heat flux, thermal resistance and temperature profiles across the pipe wall.

The sum of $R_m$, $R_{ss}$, $R_{inf}$ and $R_a$ can be approximated by the inverse of the initial heat transfer coefficient U(0) derived from the measured heat flux when the pipe is clean (*i.e.* at the start of the run). Therefore, the resistance of the fouling layer, $R_f$, at a given time can be estimated from the calculations of the overall heat transfer coefficient (Changani *et al.*, 1997) as:

$$R_f(t) = \frac{1}{U(t)} - \frac{1}{U(0)} \tag{4.4}$$

There are several assumptions involved in the use of equation 4.4. The most important is that the heat resistance outside the pipe, $R_a$, is constant throughout the run. This represents the ambient conditions near the pipe wall. However, in practice, it is almost impossible to guarantee that random variations in ambient conditions, such as air temperature and velocity, near the pipe wall do not occur, hence $R_a$ would vary during the run.

The effect of surrounding air conditions on the heat flux from a pipe can be eliminated if it is taken into account that, for steady state conditions, the temperature drop across the wall is proportional to the individual series resistances (Beek & Muttzall, 1975). Equation 4.2 can then be expressed as:

$$q = \frac{(T_b - T_a)}{\frac{1}{U}} = \frac{(T_b - T_s)}{\frac{1}{U_i}} = \frac{(T_s - T_a)}{\frac{1}{U_a}} \qquad (4.5)$$

If the flow rate and temperature of the milk are constant and both the heat flux, q, and the temperature, $T_s$, at the outer surfaces of the pipe are measured, then equation 4.6 allows the calculation of the internal heat transfer coefficient, $U_i$, independent of the external pipe wall conditions as:

$$U_i = \frac{q}{T_b - T_s} \qquad (4.6)$$

Equation 4.4 then becomes:

$$R_f(t) = \frac{1}{U_i(t)} - \frac{1}{U_i(0)} \qquad (4.7)$$

where $U_i(0) = 1/(R_m + R_{ss} + R_{hf})$ and $U_i(t) = 1/(R_m + R_f + R_{ss} + R_{hf})$ are the internal heat transfer coefficients derived from the heat fluxes measured at the start of the run and at

a time, t, during the run respectively.

By rearranging equation 4.7 the normalised internal heat transfer coefficient, $I_f$, which is a function of fouling deposit, is defined by:

$$I_f = \frac{U_i(t)}{U_i(0)} = \frac{1}{1 + R_f U_i (0)} \qquad (4.8)$$

Theoretically, $I_f$ values can range from 0 to 1. At the start of the run $R_f$ equals 0 and hence $I_f$ equals 1. When deposition sets in and the fouling layer is sufficiently thick to cause an effect on the heat transfer, $I_f$ will be less than 1.

The criteria for fouling assessment of a non-heated surface therefore can include:

(1) A relation between the $I_f$ value and the thickness of the fouling layer which determines its fouling condition.

(2) A change of $I_f$ values during processing time which measures the fouling rate.

(3) The mass flow rate and temperature of milk are steady.

(4) The reduction in cross-sectional area available to flow and the change in the roughness of the fouled surfaces as fouling progresses are negligible and hence $R_m$ and in turn $U_i(0)$ are assumed to remain constant during the run.

### 4.3.2 Validation

In this section, the changes in the normalised internal heat transfer coefficient, $I_f$, with run time were characterised. Methods of calculation of the fouling rate and fouling time are reported and discussed. The relationship between $I_f$ and local thickness of the fouling layer within the surface area covered by the heat flux sensor, determined at the completion of the run, is also reported and discussed.

#### 4.3.2.1 Experimental methods

Fouling experiments were carried out with whole milk heated to 85, 95 and 110°C. The milk, obtained from the Kiwi Co-operative Dairies Limited, Hawera, was pasteurized at 72°C for 15s, chilled and stored at 6°C for up to six days before the experiments. The stored milk was heated in the plate heat exchanger to 75°C and heat treated via the DSI heater. The milk was then passed through a number of fouling test pieces of different flow geometries, which were placed in series starting at about 0.5 m downstream from the DSI heater. The milk at exit was cooled to 22°C and discarded. The milk flow rates through the test sections were 80 and 120 kg $h^{-1}$ (Reynolds number of 2500 and 3800 at 95°C respectively). To measure the fouling rates in various locations in the fouling test pieces, up to three heat flux sensors were attached to each test piece. The duration of each experiment was also varied and was up to 10 h each. By using several test pieces and heat flux sensors and varying the duration of the experiment, a number of $I_f$ versus deposit thickness data were obtained in a single experiment. A summary of the run orders and experimental conditions is listed in Appendix 4.2. A total of 28 runs is listed including those reported in Chapter 5, as these data was also used validation purposes.

At the completion of each run, the heating system was turned off and the rig was allowed to cool down to about 40°C (at the DSI outlet). The feed pump was switched

off and the DSI heater and test pieces were removed from the rig and rinsed with distilled water to remove any remaining milk from the deposits. The fouling pattens and surface structures of the deposits were visually inspected and photographed. The thickness of the fouling layer was measured (Section 3.5.5). The deposits were also analysed for content of protein (as total nitrogen), fat and minerals (as dry ash) (AOAC International, 1990) and the results are listed in Appendix 4.3.

#### 4.3.2.2 Characteristics of fouling curves

Figure 4.5 shows an example of the comparative plots of heat flux and internal heat transfer coefficient, $U_i(t)$, versus run time taken from two different experimental runs (called runs A and B, referring to runs 4.8 and 4.12 in Appendix 4.2). The plots of heat flux profiles illustrate the difficulty encountered when the ambient conditions near the pipe wall varied either during the experiment or between runs. During these two runs, the ambient air temperatures in the room where the fouling rig was located increased about 5 °C between the start and finish of the experiment. During run B, the access doors were left open which created air currents into the room.

For runs A and B, the pattern of $U_i(t)$ versus run time were more comparable than the heat flux profiles. At the end of the experimental runs, the internal heat transfer coefficients, $U_i(t)$, of runs A and B were shown to reduce by roughly 15 and 7%, respectively, as the surface became fouled. Converting the heat flux to $U_i(t)$ was shown to reduce noise and fluctuations induced by the changing external environmental conditions.

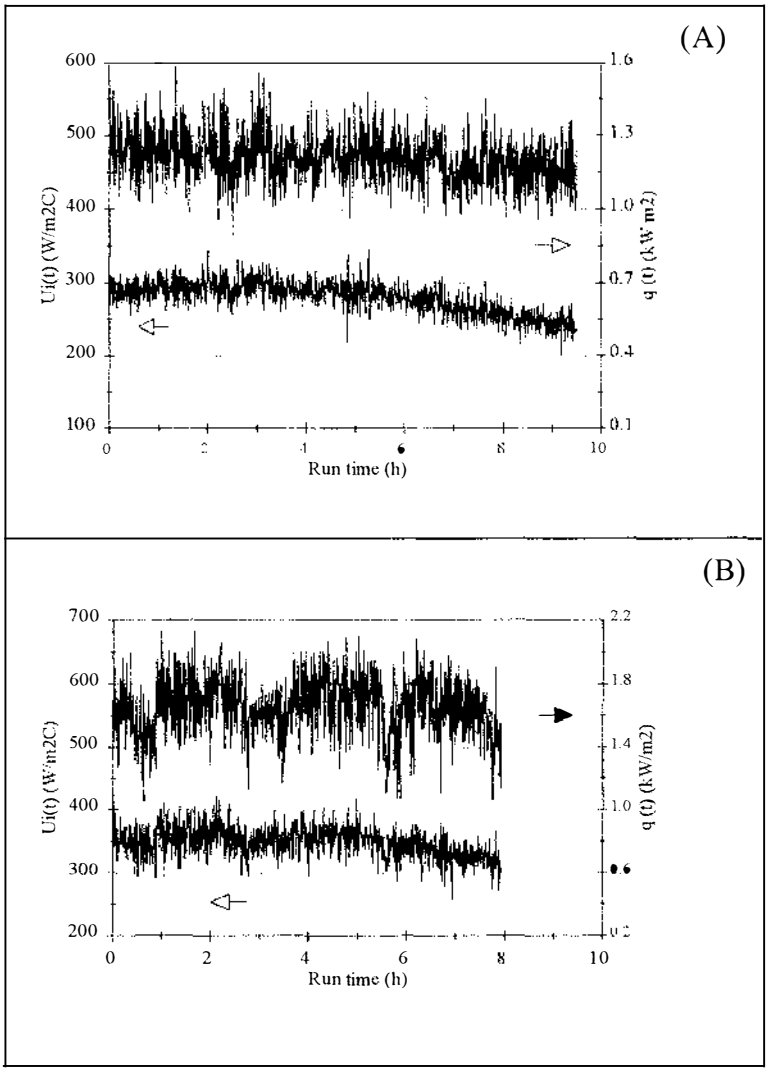


**Figure 4.5** Plots of heat flux (top line) and internal heat transfer coefficient (bottom line) versus run time for runs A and B.

To compare the fouling pattern between runs A and B, the internal heat transfer coefficient accumulated during each run was normalised against the initial heat transfer coefficient, $U_i(0)$ (*i.e.* Eq. 4.8). $U_i(0)$ was calculated using the average $U_i(t)$ over the first 0.5 h of each run (*i.e.* the average of the first 60 recorded heat flux data points). This period was selected to allow the fluctuation pattern of $I_f$ to be well established and hence the calculation of $U_i(0)$ could be reliable. In addition, during the first 0.5 h, the

fouling layer was not sufficiently thick to affect the heat flux and therefore the $U_i(t)$ remains constant. The comparative fouling curves of runs A and B are shown in Figure 4.6.

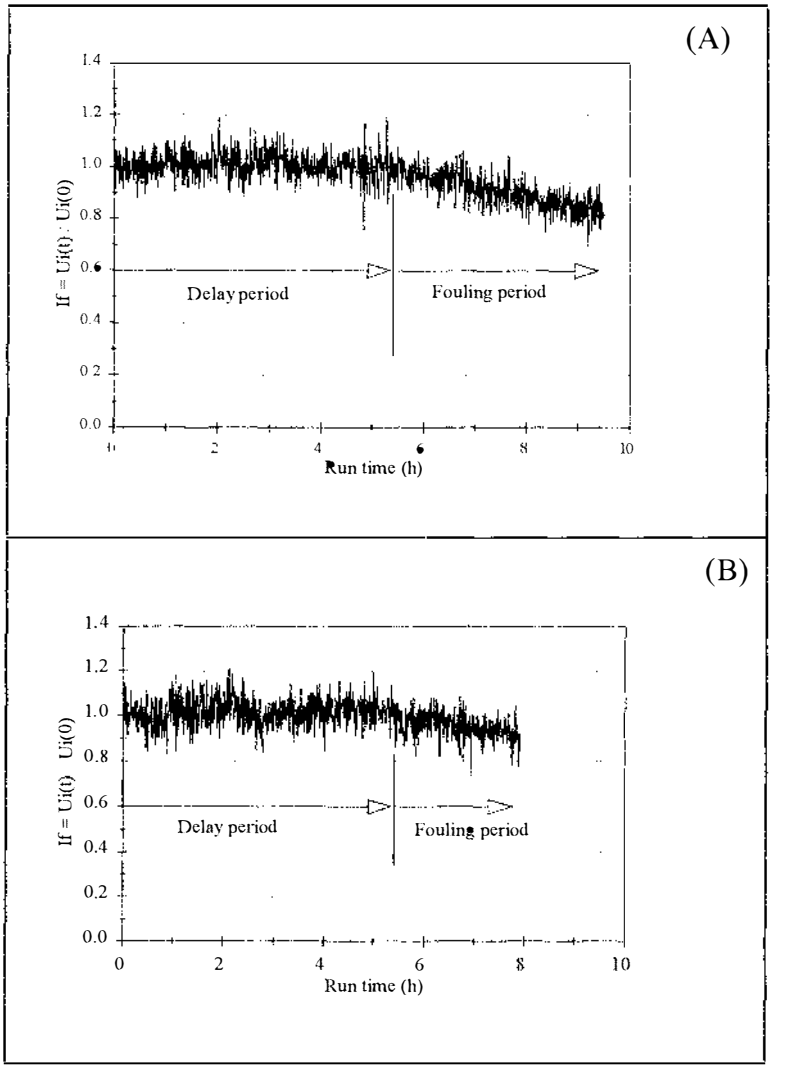


**Figure 4.6** Plots of normalised internal heat transfer coefficient versus run time showing a delay period and a fouling period for runs A and B.

Generally, the plots of normalised internal heat transfer coefficient, $I_f$, versus run time exhibited two periods:

(a) a delay period at the beginning of the run, during which there was no conclusive upward or downward trend, and

(b) a fouling period during which there was a sustained decrease in $I_f$ with run time.

$I_f$ values were generally found to decrease with run time after the delay period but the duration of the delay time, and hence the fouling time, varied between runs. Figure 4.7 (A) shows an example of a plot where a fouling period was not observed before the experiment was stopped (*e.g.* up to 10 h from start) because the milk supply was exhausted. In another run, the fouling curve exhibited a very short delay time after the start of the run (*e.g.* 0.5 h) (Figure 4.7 (B)). The cause of the differences in the duration of the delay time between runs is unknown. The delay time was not correlated with the treatment temperature, the milk flow rate conditions or the flow geometry (*i.e.* the different test pieces) used in the experiments. It is possible that the milk properties changed between runs and this affected the initial deposition (Visser & Jeurnink, 1997). Further study on the initial deposition of heated whole milk is warranted.

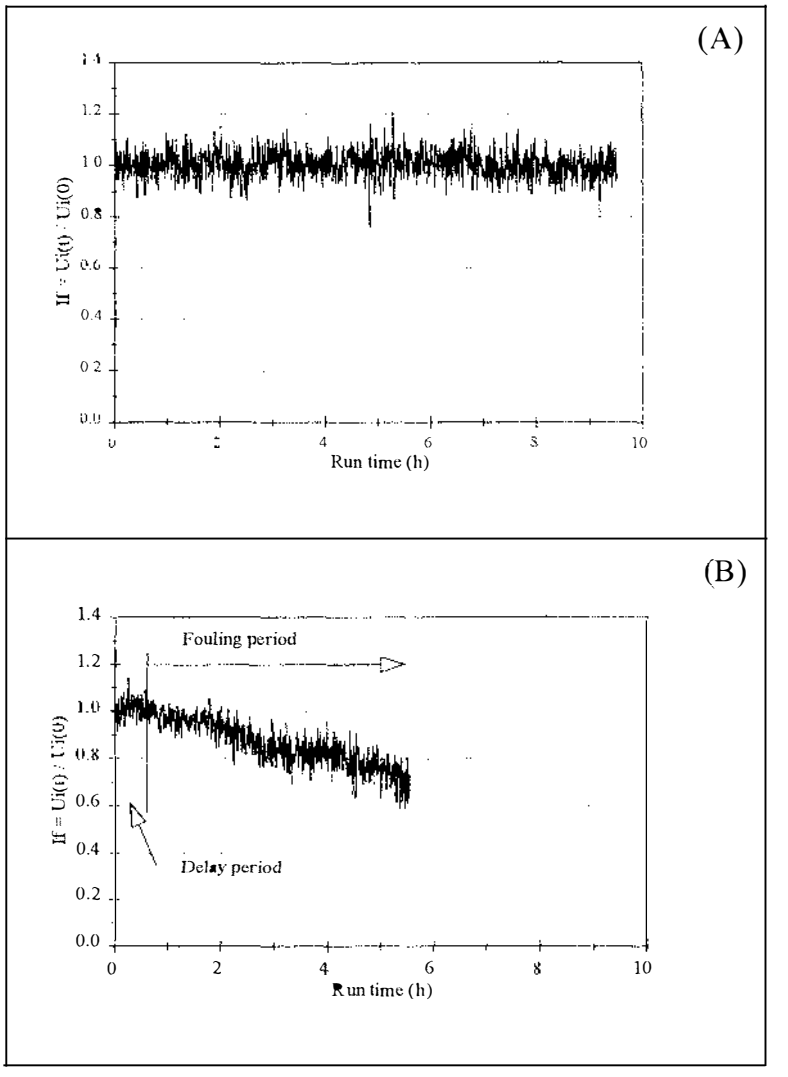


**Figure 4.7** Plots of normalised internal heat transfer coefficient versus run time showing: (A) no fouling period (run 4.8); (B) short delay period (run 5.9).

In some runs, there was an initial increase in $I_f$ followed by a sustained decrease in $I_f$ with run time. Figure 4.8 shows an example of this phenomenon. Delsing and Hiddink (1983) who studied fouling of skim milk in tubular heat exchanger also observed an increase in the overall heat transfer coefficient during the early stage of the run. Their calculated heat transfer coefficient values were recalculated as normalised heat transfer coefficients (Appendix 4.4) and the results are shown in Figure 4.9. Although the time

scales are different the general patterns for the change in $I_f$ with time are similar to that observed for milk fouling obtained in the present study.

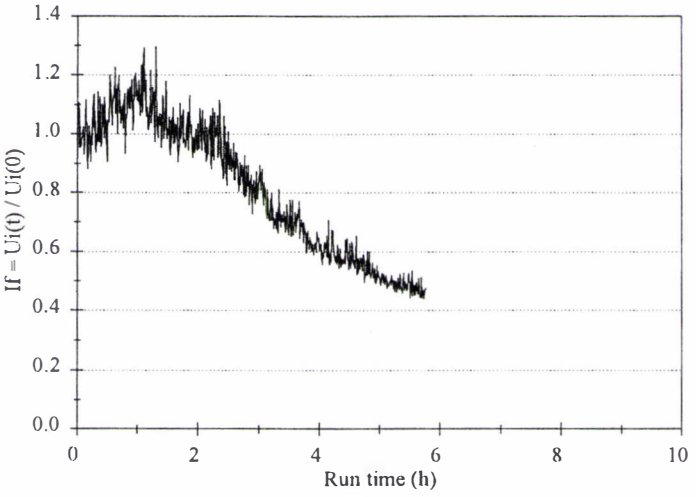


**Figure 4.8** Plot of normalised internal heat transfer coefficient versus run time showing an increase in $I_f$ (run 4.7)

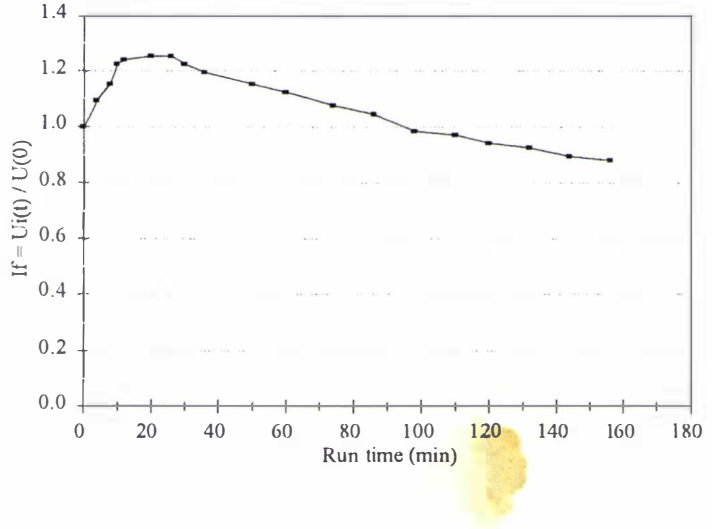


**Figure 4.9** Plot of normalised heat transfer coefficient of tubular heat exchanger versus run time (calculated from the data of Delsing & Hiddink, 1983).

Crittenden and Alderman (1992) investigated mechanisms by which fouling can increase heat transfer coefficients and suggested that this phenomenon could be attributed to the increasing roughness of the heat transfer surface by the deposits. They stated that, initially, the heat resistance of the earliest deposits was negligible but the increased roughness disturbed the viscous sub-layer and induced turbulence and hence an increased film heat transfer coefficient, $R_m$. As a result, the overall heat transfer coefficient, U(t), started to increase (*i.e.* $U(t)>U(0)$). As the deposit layer continues to grow, its thermal resistance increases and after some time eliminates the effect of roughness on heat transfer. After this, the overall heat transfer coefficient will start to decrease. How much the heat transfer coefficient could be increased depended on the number, size, shape and distribution of the roughness elements and the rate of growth of the peaks and the rate of filling up of the valleys.

In this study, the deposits observed during the early stage of fouling were found to consist of discrete particles of various sizes (*e.g.* 20-1000 μm in diameter) that randomly distributed over the solid surface (Figure 4.10 (b)). This deposit 'pattern' could cause disturbances to the viscous sub-layer and induce turbulence and hence cause $U_i(t)$ and in turn $I_f$ to increase. However, the reason why an increase in $I_f$ was only found in some runs, although the experimental conditions were unchanged, is unknown. As discussed in the previous section, it could be because the milk properties changed between runs and this affected the initial deposition (Visser & Jeurnink, 1997) and in turn the roughness of the pre-fouling layer.

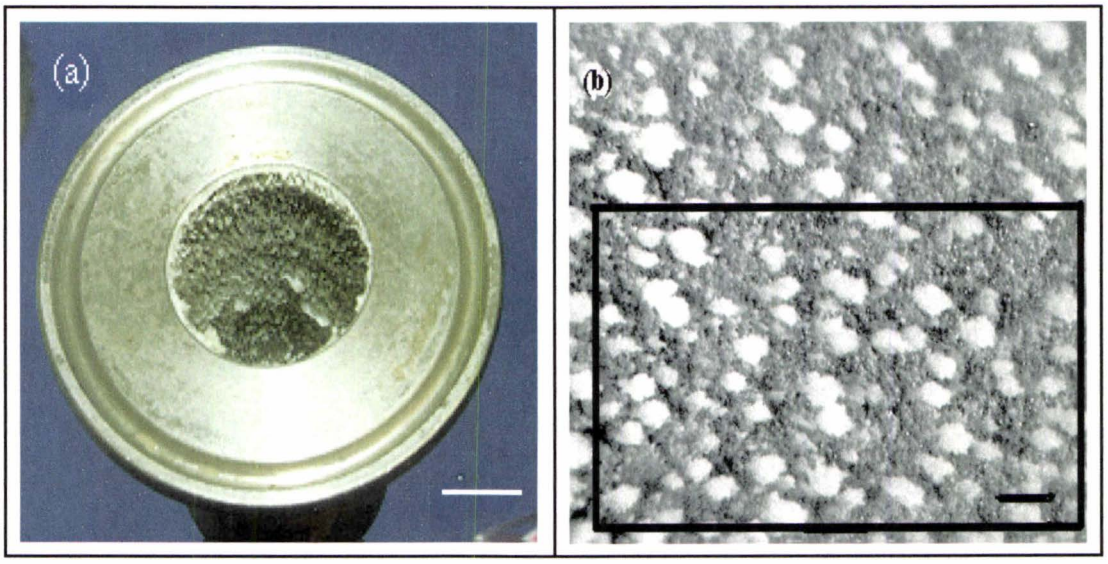


**Figure 4.10** Photographs of deposits: (a) inside the fouling test piece (bar = 8.5mm); (b) surface of fouling layer as viewed by light microscopy showing deposit particles of different sizes (box represents the footprint of heat flux sensor and bar = 0.6 mm).

Figure 4.8 also shows that the fluctuations in $I_f$ changed during the run. The fluctuations were initially large then gradually decreased as $I_f$ decreased with run time. This was probably caused by the effects of induced turbulence due to deposit roughness which resulted in random variations in the fluid velocity near the solid surfaces. Consequently, the film heat transfer coefficient or the film resistance, $R_m$, randomly varied with time. Initially, the deposit layer contained high peaks and deep valleys and hence the fluctuations were large. As the deposit layer continues to grow, the valleys fill up and the deposit surface becomes smooth and hence the fluctuations in $I_f$ will be reduced.

Another characteristic shown by the fouling curve in Figure 4.8 is that, at the beginning of the fouling period, $I_f$ decreased at a constant rate (*i.e.* exhibited a linear fouling rate) then it changed to a lower rate and appeared to tail away to an asymptotic level. This fouling pattern is similar to those observed by Paterson & Fryer (1988) who investigated

investigated fouling of reconstituted skim milk in tubular heat exchangers. They also found that the resistance to heat flow caused by fouling varied with time. The possible causes of the reduced rate of fouling observed in this study are:

(a) In the use of equation 4.8 to calculate the normalised heat transfer coefficient, $I_f$, it was assumed that the milk film resistance, $R_m$, remained constant throughout the run. However, as the thickness of the fouling layer increases it restricts the flow passage and causes the milk fluid velocity to increase. Consequently, it causes a decrease in the film resistance, $R_m$, (Beek & Muttzall (1975). If the increase in the thermal resistance of the fouling layer, $R_f$, remained constant during this period then the overall rate of change of the internal heat transfer coefficient, $U_i(t)$, would reduce.

(b) In addition to the reduction in the film resistance, $R_m$, increased fluid velocity could cause some of the newly formed deposits to detach from the fouling layer. Hence, the net deposition rate would be reduced and the fouling rate lowered.

#### 4.3.2.2 Calculations of the fouling rate

The fouling rate was determined by calculating the slope of the linear portion within the fouling period of the $I_f$ versus time curve. Two points on the curve were selected (as indicated in Figure 4.11) and the slope of the line was calculated using linear regression analysis assuming the curve was perfectly linear between these two points. The fitted $I_f$ line was represented by the linear equation:

$$y = a x + b \tag{4.8}$$

where a is the coefficient and b is the constant of the regression analysis results.

The fouling rate, defined as the rate of change of $I_f$ per second, was then calculated from:

$$\frac{dI_f}{dt} = \frac{\text{absolute (a)}}{3600} \tag{4.9}$$

An example of the calculation is illustrated in Figure 4.11 and the fouling rate was calculated at:

$$\frac{dI_f}{dt} = \frac{0.042}{3600} = 1.17 \times 10^{-5}\ s^{-1} \tag{4.10}$$

In other cases, where the $I_f$ - time curve exhibited a reduced fouling rate, as shown in Figure 4.12, the curve within the fouling period was divided into two linear portions. The slope of the first linear portion was calculated using the same procedure set out above and the result was then taken as the fouling rate for the whole run. The data of the second linear portion were not included because, as fouling progresses in extent during a run, the validity of the basic assumption that underlines normalisation (*i.e.* $U_i(t)/U_i(0)$) becomes increasingly stretched. Increase in the deposit thickness could cause a decrease in $R_m$ and an increase in fluid velocity and hence the initial internal heat transfer coefficient, $U_i(0)$, was no longer constant but reduced. Consequently, the relative change in $I_f$ with run time, such as in the second period, was reduced.

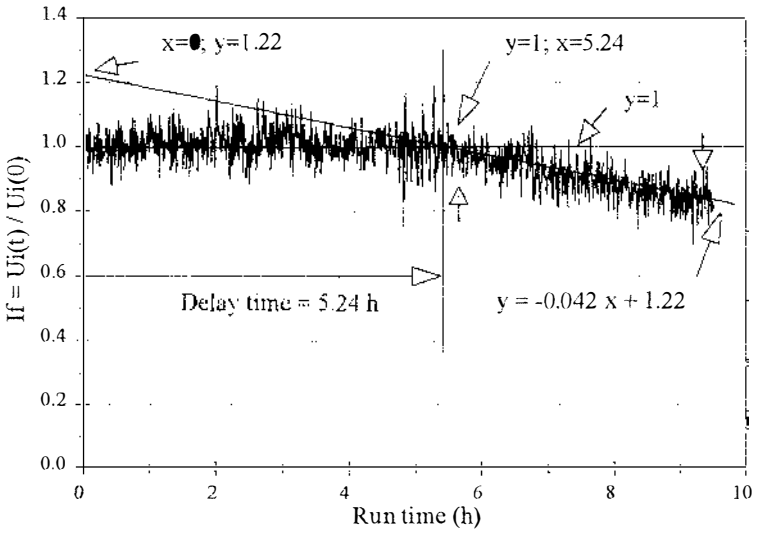


**Figure 11.4** Calculations of fouling rate and delay time from the plot of normalised internal heat transfer coefficient versus run time (run 4.8).

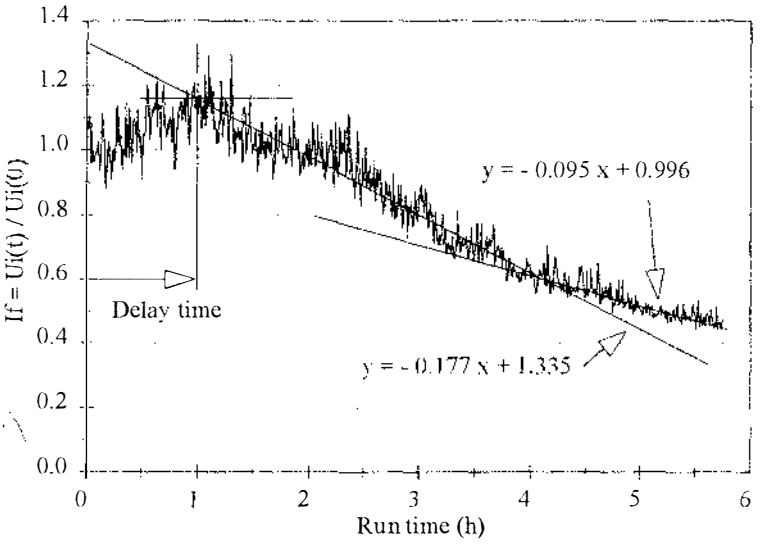


**Figure 4.12** Plot of normalised internal heat transfer coefficient versus run time showing the reduced fouling rate (at high fouling rate) (run 4.7).

#### 4.3.2.3 Calculation of the duration of the delay period

The delay period was defined as the duration between the run starting time and the time at which $I_f$ starts to continuously decline. The estimation was based on the results of the linear regression analysis of the $I_f$ data during the period at which $I_f$ decreased. The delay period was estimated to be the point where the fitted $I_f$ line (determined by equation 4.8) intercepted with the horizontal line calculated when y equals 1 (equation 4.11):

$$t_{I_f=1} = \frac{(1 - b)}{a} \tag{4.11}$$

The calculation method is illustrated in Figure 4.11 where a = - 0.042 and b = 1.22 and the delay time was estimated at:

$$t_{I_f=1} = \frac{(1 - b)}{a} = \frac{(1 - 1.22)}{-0.042} = 5.24 \text{ h} \tag{4.12}$$

This calculation method was not used in all runs. In the cases where there was an initial increase in $I_f$, the duration of the delay period was estimated directly from the plot of the fouling curve. The delay period was taken from the start of the run, through the period where $I_f$ was greater than 1 and to the time at which there was a sustained decline in $I_f$. An example of the method is illustrated in Figure 4.12. From this plot, the delay time was estimated at 1 h. The error of this estimation was about ± 15 minutes and it was considered this was not significant compared to the duration of the run.

#### 4.3.2.4 Relation between $I_f$ and fouling layer thickness

To relate the measured heat flux data to the fouling conditions inside the test pieces, both the calculated $I_f$ and the average thickness of the fouling layer were determined at the end of each experimental run.

The $I_f$ value at the end of the run was determined using the average of $I_f(t)$ which was accumulated during the last 0.5 h of a run (*i.e.* the average of 60 recorded heat flux data points). As mentioned in the previous section, this time interval was selected to allow the fluctuation pattern of $I_f$ to be consistent and hence the calculation of the average $I_f$ could be reproducible. However, in other cases where the run duration was short (*e.g.* less than 3h) and/or the fouling rate was high (*i.e.* the slope of the fouling curve was high), it was necessary to reduce this time interval to about 10 minutes. An example of the estimation of $I_f$ at the end of the run is illustrated in Figure 4.13.

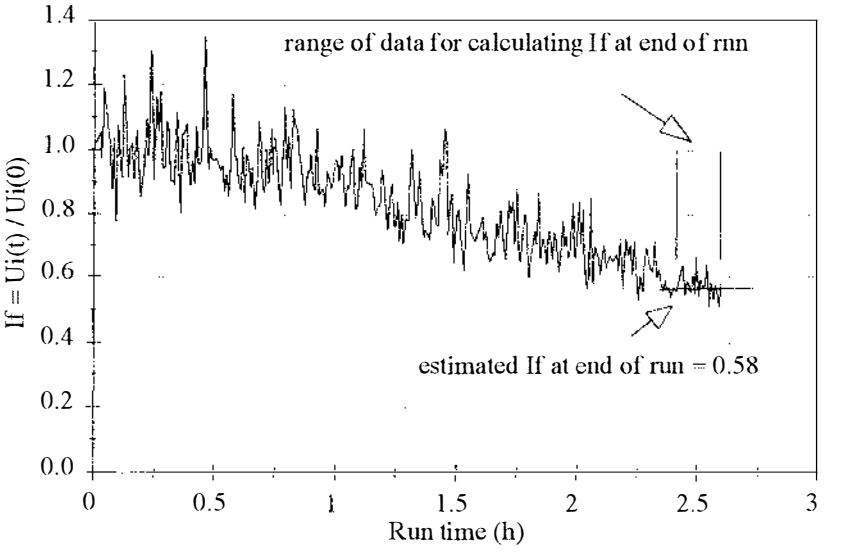


**Figure 4.13** Estimation of normalised internal heat transfer coefficient at end of run.

Two different methods were used for measuring the thickness of the fouling layer. The thickness of the fouling layer on the surface of a horizontal open test section (Figure 3.5) was directly measured using the apparatus described in Section 3.3.5. Before each measurement, the heat flux sensor was removed from the outer surface of the test piece and its area was marked (*i.e.* about 5 mm x 10 mm). The test piece was then mounted on the thickness apparatus and the measurement was performed as described in Section 3.3.5. Two measurements were made, each on the central line of the fouling layer that covered the marked area, in the axial direction, at 2.5 mm from the upstream edge and 5 mm apart. The result was taken as the average of the two measurements. A replicate measurement in each location was not feasible because after each advance, the needle disturbed the surface and created a cavity in the fouling layer.

To measure the thickness of the fouling layer inside tubular sections, the deposit layer that covered the heat flux sensor area was carefully scraped off using a small sharp plate. The thickness of the sample was then measured with a micrometer. Two measurements were also made, each 5 mm apart in the axial direction, on each sample and the average result was calculated from the two measurements. It was found very difficult to remove the soft and wet deposit layers from the test pieces and great care was always needed to ensure reasonably accurate and reproducible results.

Figure 4.14 shows the relation between $I_f$ and the average thickness of the fouling layer obtained from whole milk heated to 80 - 110°C. A summary of the results is listed in Appendix 4.3. The $I_f$ versus deposit thickness graph showed that wall heat flux strongly correlated with the level of fouling (*i.e.* deposit thickness) inside the test pieces. There was an amount of scatter of the data between $I_f$ and the average deposit thickness. The most likely causes of scatter of the data are thought to be:

(a) Different compactness of the deposit layer that could have dissimilar thermal conductivity.

(b) Different surface roughness of the fouling layer that could affect the total thermal resistance.

(c) Different fouling compositions and hence thermal resistances due to different treatment temperatures.

(d) Errors in handling the deposit samples and in measuring its thickness.

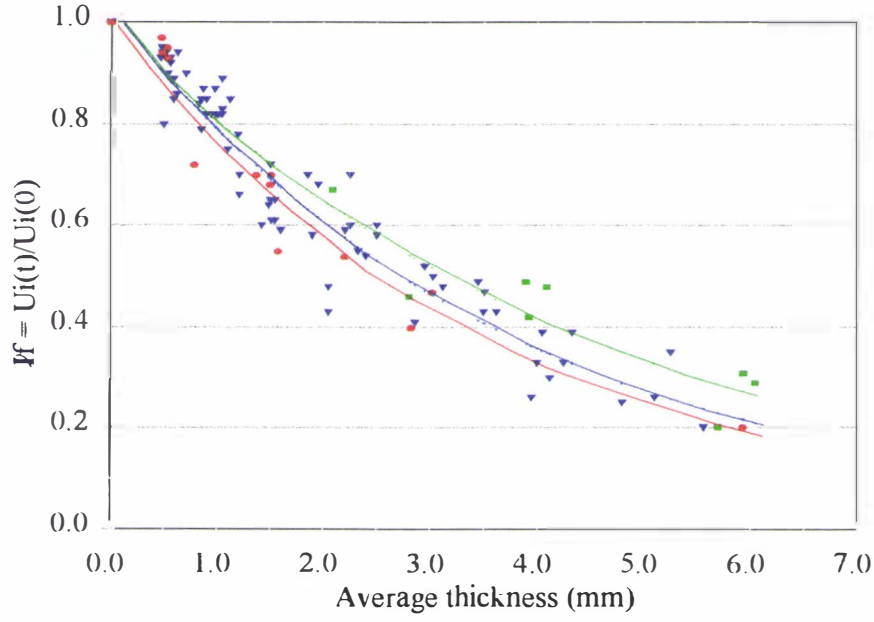


**Figure 4.14** Relation between the normalised internal heat transfer coefficient and the average deposit thickness, both measured at the end of runs of whole milk heated to 85 (green), 95 (blue) and 100° C (red).

The $I_f$ versus deposit thickness graph shows that the relationship between heat flux and deposit thickness was not linear. The possible cause of this non-linear relationship was thought to be similar to those that cause the reduced fouling rate, as was discussed in the section 4.3.2.2. An increase in the deposit thickness could cause a decrease in $R_m$ and an increase in fluid velocity and hence result in a small change in $U_i(t)$.

Consequently, the relative change in $1_f$ with deposit thickness, calculated at the end of the run, may be reduced.

Another characteristic of the $1_f$ - deposit thickness relationship observed in this study was that a change in $1_f$ was not found until the fouling layer was about 0.5 mm thick. It was thought that this relationship was not due to the sensitivity of the heat flux sensor but it was caused by the fouling behaviour of heated whole milk onto unheated surfaces under the conditions employed in this study. As mentioned in the previous section, the fouling layer observed during the early stage of fouling consisted of discrete particle sizes (*e.g.* 20-1000 μm in diameter/height) that randomly overlaid the solid surface (Figure 4.10 (b)). When fouling progressed, these particles probably became the preferred sites for further deposition and hence they grew in size. The solid surface area was still not fully covered with the deposits and therefore the heat flux from this area was not affected. As these particles continue to grow in size, the valleys surrounding them started to fill up. At a certain stage, they will form a continuous network of particles of a certain thickness over the entire solid surface and then began to cause a reduction in the heat flux. However, at this condition, measurement of deposit thickness was found difficult because the deposits were very soft and the data could not be reproduced due to the large variations in surface roughness (within the sensor footprint). An estimate on the average thickness can therefore be made.

Although the scatter of the data was large, the results also showed that $I_f$ - deposit thickness relationship was slightly affected by treatment temperatures in the range of 85 - 110°C. A higher treatment temperature resulted in a smaller $I_f$ value. It was thought that increasing treatment temperature could cause an increase in the compactness of the deposit layer which in turn increased its thermal resistance and hence lowered the $I_f$. The results highlight the possibility that $1_f$ - deposit thickness relationship could be limited due to a number of factors such as milk fluid type, treatment temperatures and specific hydrodynamic conditions which could affect the

deposit characteristics. Further work to determine the $I_f$ - deposit thickness relationships is warranted.

## 4.4 CONCLUDING REMARKS

A system based on heat flux measurement to monitor fouling of heated whole milk in various locations of non-heated surfaces has been successfully developed. The equipment is inexpensive, robust and requires minimal maintenance. Use of the normalised internal heat transfer coefficient is a convenient and successful method. The growth and extent of the fouling layer inside the test pieces during processing can be monitored with heat flux sensors. The characteristics of the response of the device are similar to those of other devices which have been reported in the literature by various researchers for measuring fouling of heated surfaces (*i.e.* heat exchangers). The present method also effectively correlated the fouling conditions (*i.e.* the thickness of the fouling layer) inside the test pieces.

CHAPTER 5

# FOULING OF NON-HEATED SURFACES

CONTENTS

## 5.1 INTRODUCTION

The major types of heat treatment equipment which are currently used in the dairy industry can be classified into two groups: indirect and direct heating systems. With indirect heating systems (such as plate heat exchangers and tubular heat exchangers), steam or hot water is employed as the heating medium and its thermal energy is transferred to the milk fluid via a heat exchanger wall. With direct heating system, the heating is performed by mixing steam directly with the milk fluid either in a direct steam injection heater or in a steam infusion vessel. The steam immediately condenses and gives up its latent heat of vaporisation and thus raises the temperature of the milk.

Direct heating is preferred in the New Zealand dairy industry, due to its rapid heating rates which result in higher quality product. For example, loss of vitamins, loss of flavour, and denaturation of the whey protein can be minimised due to short heating times whereas the effective destruction of bacteria is still achieved. Another advantage of the direct heating system includes its ability to process viscous or shear sensitive products such as concentrated milk, cheese and dessert foods that can not be satisfactorily heat treated in plate heat exchangers.

Even with direct heating, deposits of insoluble materials can form over time of operation. These are observed at two places: the distribution device where steam and milk are mixed, and downstream on the surfaces of the equipment even when these are not heated. Such downstream deposition has no direct effect on the thermal performance of the plant (de Jong, 1994). Deposition on non-heated surfaces has previously been observed in the holding and regeneration sections immediately after the heating sections of a plate heat exchanger (Jeurnink *et al.*, 1989; de Jong *et al.*, 1992; de Jong *et al.*, 1993) and the heating systems of ultra-high-temperature (UHT) equipment (Patil & Reuter, 1988).

It was observed during preliminary experiments (Chapter 3) that, when a tubular straight test piece was replaced with a tubular sudden expansion, the deposition rate increased significantly, even though all other conditions remained unchanged. This result suggests that, under fixed heat treatment conditions, flow disturbance can induce much higher rates of deposition on non-heated surfaces.

It was hypothesised that the process of deposition of heated milk fluid onto non-heated surfaces includes the following steps:

(1) Heat-induced reactions of components of the milk fluid occurs in the bulk fluid resulting in the formation of 'active species' that can later form fouling deposits.

(2) Mass transfer of the 'active species' from the bulk fluid to the viscous sub-layer adjacent to the solid surfaces takes place.

(3) 'Active species' deposit on to the solid surfaces.

(4) Detachment of deposit once formed from the solid surfaces does not take place to any material degree (*i.e.* the process is irreversible). This does not exclude mechanically induced detachment of fragments or lumps from the deposit but such events are probably random and infrequent.

In this chapter, the transport factors that affect the fouling process of heated whole milk onto non-heated surfaces are reported. The rate and the distribution of local fouling of heated whole milk in the sudden expansion of flow are examined. A computational fluid dynamics (CFD) program is used to characterise the local transport processes that relate to the local fouling rates. The variables investigated are Reynolds number and the height of the expansion step, h.

## 5.2 FOULING INDUCED BY SUDDEN EXPANSION OF FLOW

Immediately beyond the step of a sudden expansion there is a vortex region or corner recirculation zone (CRZ) of separated flow and streamlines ending in an area of zero longitudinal velocity and zero wall shear rate (Figure 5.1). This area is described as the stagnation or reattachment flow region. Further downstream from the reattachment region is the redeveloping flow region. Such disturbed patterns of flow often occur in the inlet and outlet connections of heat transfer equipment, at complex valve assemblies, at branches in pipeline systems and at connections to measurement devices.

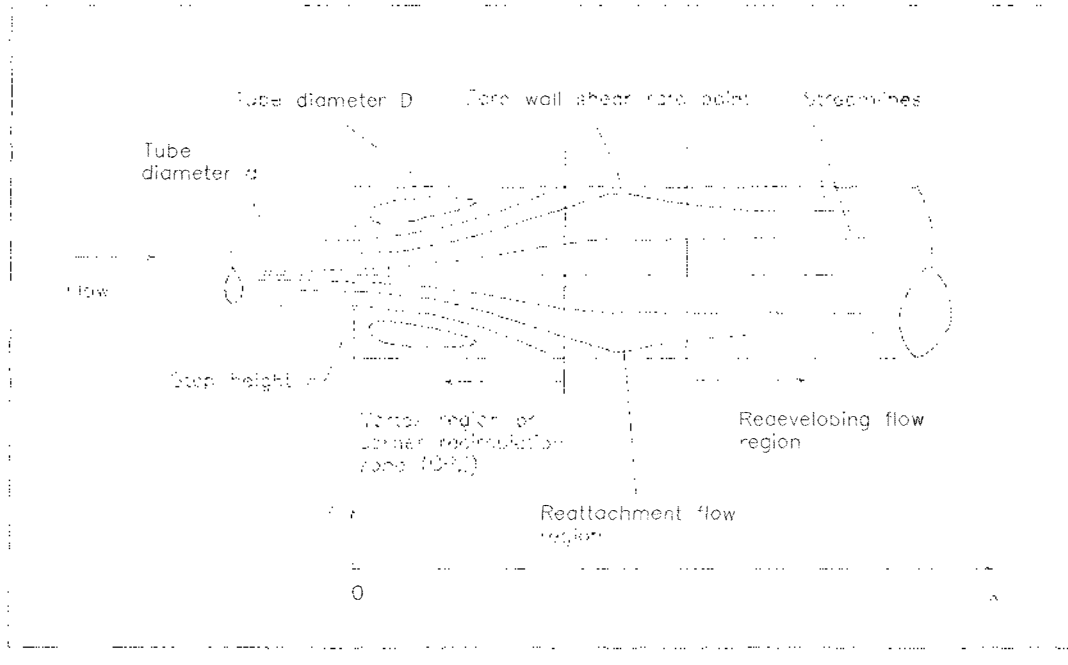


**Figure 5.1** Geometry of a tubular sudden expansion flow (after Fleuestein *et al.* 1975).

Flow downstream of a sudden expansion has been characterised by the occurrence of regions of high heat and mass transfer rates which are several times greater than those for fully developed pipe flow at the same Reynolds number (Zemanick & Dougal, 1970;

Runchal, 1971; Feuerstein *et al.*, 1975; Moon & Rudinger, 1977). These authors reported that the mass and heat transfer rates rise rapidly to a maximum in the reattachment region and then decay to their asymptotic values in the redeveloping flow region. The heat and mass transfer augmentation are attributed to increases in the level of turbulence or vortices which develop when flow separation occurs.

When mass transfer occurs through a fluid in motion, it is expected that dual processes of molecular and turbulent action will operate. The theory indicates that the mass transfer rate of a species, A, increases with increasing turbulence (Beek & Muttzal, 1975). At any point in the fluid, the relation between mass transfer and concentration gradient can be expressed as:

$$N_A = ( D_m + D_t ) \frac{dC_A}{dy} \qquad (5.1)$$

where subscripts m and t denote molecular and turbulent conditions

The mass transfer predominated by molecular diffusion process mainly occurs in the viscous sub-layer and its rate is inversely proportional to the thickness of the viscous sub-layer, $\delta_m$ (Beek & Muttzal, 1975). The diffusion rate of a species, A, in the viscous sub-layer is given by:

$$N_A = \frac{D_m}{\delta_m} ( C_{Ab} - C_{Ai} ) \qquad (5.2)$$

Corresponding to the equation for mass transfer under a concentration gradient, there will be a similar relation for momentum transfer under the influence of a velocity gradient. Consider the milk flows in the axis, x, of a pipe (Figure 5.1) and if it is taken that milk is a Newtonian fluid (Webb & Johnson, 1965), then the total shear stress on

the fluid at any distance from the wall can be expressed as:

$$\tau_t = ( \mu_m + \mu_t ) \frac{du}{dy} \qquad (5.3)$$

In the viscous sub-layer, only viscous forces are acting on the fluid and the molecular shear stress, $\tau_m$, is given by:

$$\tau_m = \mu_m \frac{du}{dy} \qquad (5.4)$$

Within the viscous sub-layer, the viscosity of the milk fluid, $\mu_m$, is constant and the fluid elements move along parallel streamlines. At the wall, flow velocity will be zero and there will be a constant velocity gradient, and hence constant shear rate, over the thickness of the sub-layer. On the other hand, when the milk fluid moves from the sub-layer interface toward the centre of the pipe into the turbulent region, the shear rate and the apparent viscosity, $\mu_m + \mu_t$, vary with the distance from the sub-layer interface.

It therefore follows that a disturbance such as the step of an expansion can induce fouling because of the turbulent augmentation after flow separation decreases the thickness of the viscous sub-layer and hence increases the mass transfer of 'active species' to the solid surface. In addition, the thickness of the viscous sub-layer can be estimated from a plot of apparent viscosity versus radial distance from the pipe wall. The thickness value can be taken at a point on the x axis where the apparent viscosity curve starts to depart from its constant value. An example of the apparent viscosity profile in the region adjacent to the wall is illustrated in Figure 5.2

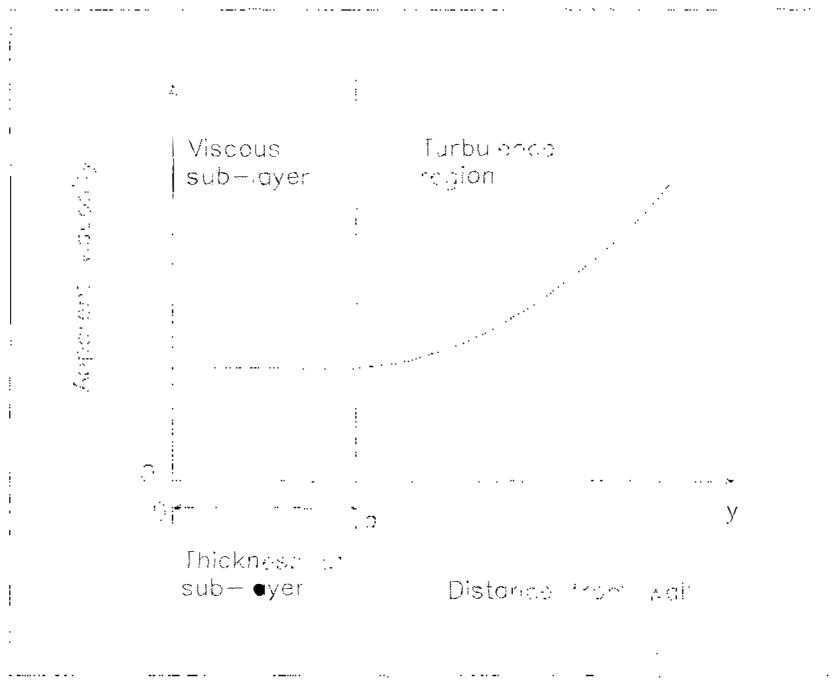


**Figure 5.2** Illustrative apparent viscosity profile in the region adjacent to the solid surfaces.

In the following sections, numerical calculations using computational fluid dynamics (CFD) to determine the thickness of the viscous sub-layer at different locations downstream of a sudden expansion are described. The fluid shear rate profiles at the solid surfaces are also determined in order to characterise the flow behaviour. Experiments are then carried out to relate the local fouling rate to the local thickness of the viscous sub-layer.

### 5.2.1 Computational fluid dynamics (CFD) modelling

CFD is a computer based numerical technique for the solution of the equations that govern the flow of fluids. It is a powerful tool for the prediction of, for example, fluid velocity, shear and pressure profiles inside a defined flow geometry where direct observations are difficult or impossible. The results of a CFD study can assist in

understanding the underlying dynamics of a processing operation and thus help in optimisation of the existing process and the design of new equipment. The origins of CFD can be found in the automotive, aerospace and nuclear industries. Recently, due to advances in computer hardware and software, this technique has been used in a variety of applications in the process industries (Hamil, 1996; Shanley, 1996).

#### 5.2.1.1 CFD model

A commercial CFD software package, CFX 4.2 (CFX International, AEA Technology, UK), was used to examine the flow behaviour in the area downstream of a tubular sudden expansion. The software package consists of a number of modules including grid generator, flow solver and post-processing modules. Simulated flow patterns and flow properties such as shear rate and apparent viscosity were generated using the software package and the data were exported to another computer for calculations of the sub-layer thickness and for further analysis.

***Grid generation***

The physical space of the tubular sudden expansion was divided into a large number of small cells. Each cell was connected to its neighbours to form a mesh for which the transport equations were calculated. A body-fitted grid that follows the geometrical form of the tubular expansion was generated. A non-uniform structured grid with a higher resolution or large number of small volumes near the wall of the expansion was selected in order to capture the details of the near-wall region (Figure 5.3). Although a higher resolution generally yielded more precise predictions, it took longer to compute. Trial runs with increasing resolution near the wall were therefore performed to obtain a solution which resulted in a sub-layer that contained a minimum of 5 cells.

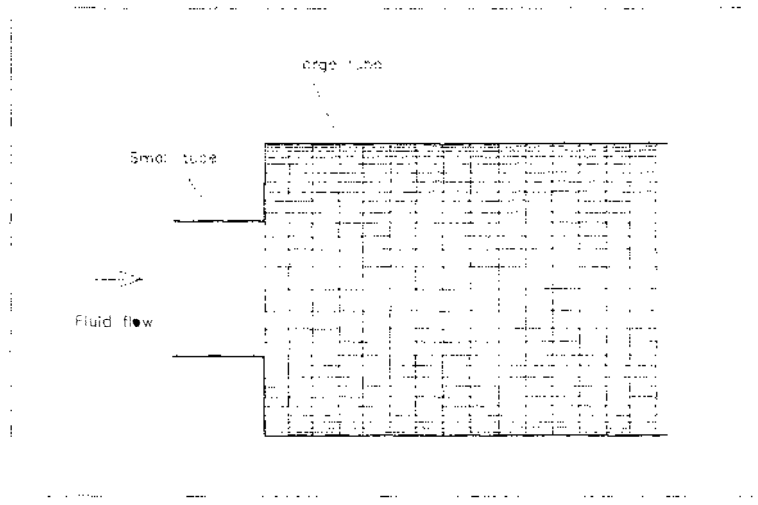


**Figure 5.3** An example of the numerical grid used for CFD simulation.

***Flow solving***

The numerical computations were made using the two-dimensional k-ϵ turbulence model supplied with the software package. This type of model had been successfully used by a number of workers to analyse flow behaviour and heat and mass transport downstream of tubular sudden expansions (Feuerstein, 1975; Moon & Rudinger, 1977; Chieng & Launder, 1980; Amano *et al.*, 1983). In the present study, a low-Reynolds-number form of the k-ϵ turbulence model was used because the Reynolds number of the milk flow in the sudden expansion test pieces, based on the large tube diameter, was in the range between 2500 and 3800 (Table 5.1). The equations of conservation governing mass, momentum and energy of flow were solved along with transport equations for kinetic energy, k, and energy dispersion, ϵ, to provide a solution, such as time-averaged velocities, for the bulk flow. The local value of the apparent viscosity was then derived from a specific relationship between k and ϵ.

### 5.2.1.2 Simulation

Three fouling test piece geometries A, B and C (Section 3.2.3) were numerically tested. Three flow rates 80, 100 and 120 kg $h^{-1}$ were employed in the simulations which resulted in a range of Reynolds number (for whole milk heated to 95°C) between 2500 and 3800 based on the large tube diameter. The geometric and flow parameters of the sudden expansions are set out in Table 5.1.

**Table 5.1** Geometric and flow parameters of test pieces A, B and C

| Test Piece | d (mm) | Reynolds Number, $Re_D$ | | | D (mm) | d/D ratio | h (mm) |
|---|---|---|---|---|---|---|---|
| | | 80 kg $h^{-1}$ | 100 kg $h^{-1}$ | 120 kg $h^{-1}$ | | | |
| A | 16.7 | 3500 | 4300 | 5200 | 23 | 0.74 | 3.2 |
| B | 10.3 | 5600 | 6300 | 8400 | 23 | 0.43 | 6.4 |
| C | 4.6 | 12700 | 15800 | 19000 | 23 | 0.20 | 9.2 |
| **Large tube** | **23** | **2500** | **3100** | **3800** | **23** | **1** | **0** |

To carry out a simulation, a grid of the sudden expansion was generated then the flow solver was run. Simulated flow patterns and flow properties such as shear rate and apparent viscosity were generated using the post-processing module and the data were exported to another computer for further analysis. The boundary conditions and assumptions used in the simulation were:

(1) Mass flow rate was constant.

(2) Flow was isothermal and incompressible.

(3) Fluid had a constant shear stress in the near-wall region for all solid boundaries.

(4) Flow met no-slip conditions at the wall, *i.e.* u = v = 0.

(5) Flows at the step and at the outlet were fully developed.

(6) Pipe wall was smooth.

(7) Step entrance had sharp edges.

#### 5.2.1.3 Simulation results

***Shear rate profiles***

Figure 5.4 shows plots of shear rate downstream of the sudden expansion with points of measurement at five different radial distances from the wall ranging from 0.1 to 1.5 mm. The results illustrated were calculated for test piece B using a milk flow rate of 120 kg $h^{-1}$. The shear rates in various locations exhibited the same general pattern: they started at a low level immediately at the step, increased rapidly to a maximum level then decreased rapidly to a minimum level and slowly increased again and eventually decayed to an asymptotic value in the location farthest from the step. From the graph, the length of the corner recirculation zone (CRZ) was defined as the distance between the step and the location at which the shear rate was lowest. Downstream from this location ws the redeveloping flow region. As can be seen from the graph, the CRZ and the redeveloping flow regions are characterised by rapid changes in the shear rates within the immediate wall vicinity. Between the CRZ and the redeveloping flow region is the area of lowest wall shear rate.

The changes in shear rates were found to gradually diminish at locations both farther

from the wall and from the redeveloping flow regions. This suggests that at these locations large-scale motions gradually predominate.

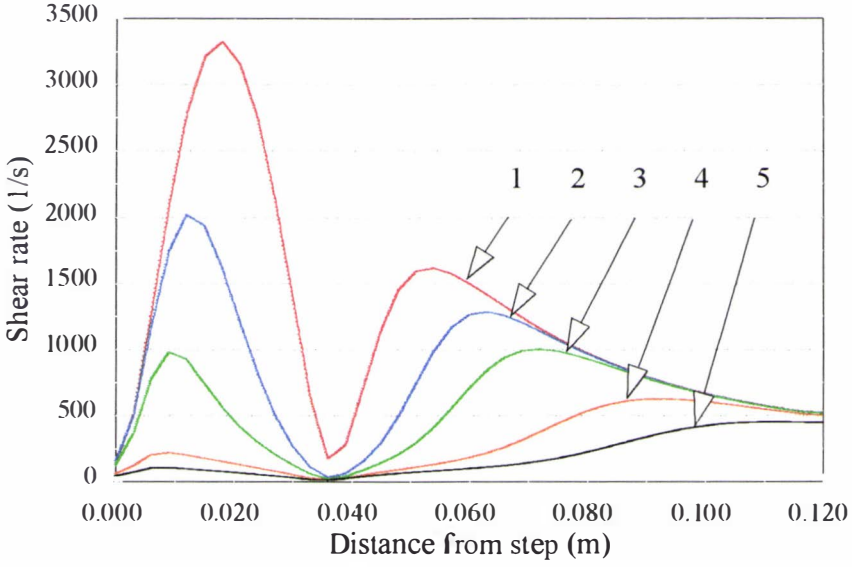


**Figure 5.4** CFD results for shear rate profiles downstream of test piece B geometry with milk flow of 120 kg $h^{-1}$ at various distance from wall: (1) 0.1 mm, (2) 0.3 mm, (3) 0.5 mm, (4) 1 mm and (5) 1.5 mm.

For comparison, the profiles of the shear rates at 0.3 mm from the wall in various locations downstream of test pieces A, B and C were determined. The results for flow rates of 80, 100 and 120 kg $h^{-1}$ were plotted and are shown in Figure 5.5. The shear rate data of test pieces B and C follow the general patterns as described above. In contrast, the shear rate profile of test piece A, which had the smallest step, started at a low level in the CRZ and increased to a much higher level in the redeveloping region and then slowly decreased. The results indicate that the change in the surface shear rate in the CRZ of a small step is relatively less than that in the subsequent redeveloping flow region. This implies that fouling in the CRZ should be less than that in the redeveloping flow region in test piece A geometry.

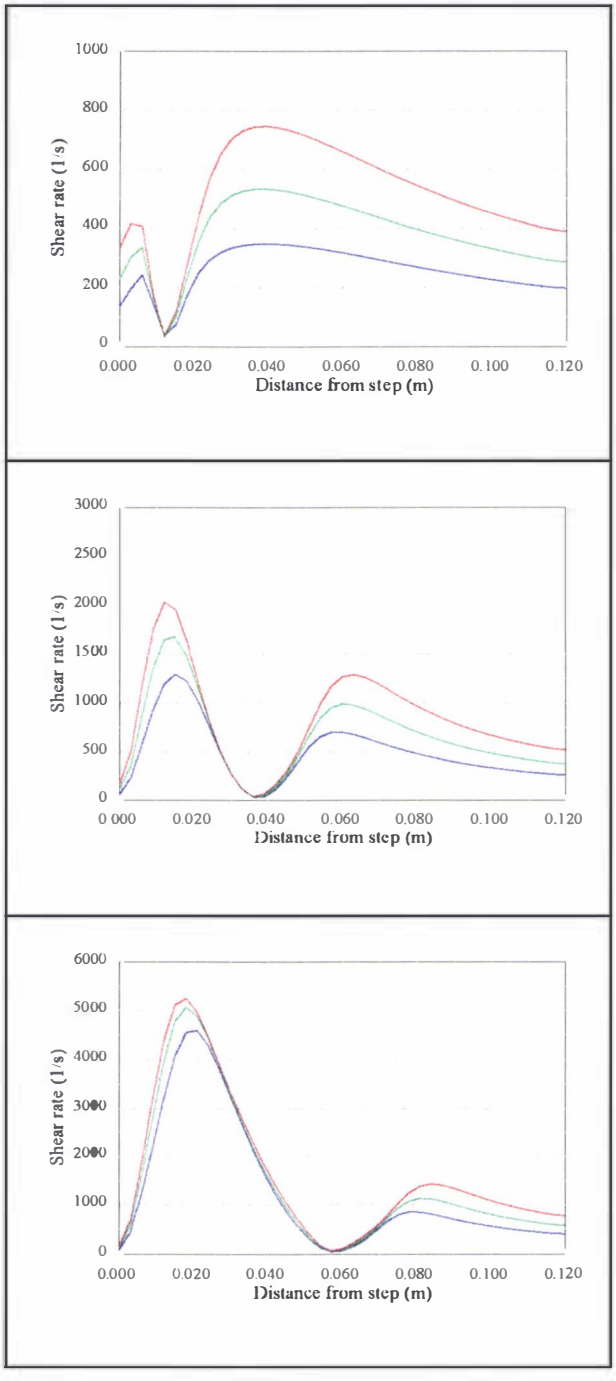


**Figure 5.5** CFD results for shear rate profiles obtained from 0.3 mm from the wall in various locations downstream of test pieces A (step height h=3.2 mm), B (h=6.4 mm) and C (h=9.2 mm) at flow rates (blue) 80 kg $h^{-1}$, (green) 100 kg $h^{-1}$ and (red) 120 kg $h^{-1}$.

The results also showed that increasing the step height and the milk flow rate both increased the shear rate profiles for all three test piece geometries. It is also seen from Figure 5.5 that the length of the CRZ significantly decreases with decreasing step height. The average lengths of the CRZ of test pieces A, B and C are 11, 39 and 59 mm respectively. However, unlike the effect of change in step height, flow rate in the range used had a small influence on the length of the CRZ. Increasing the flow rates from 80 to 120 kg $h^{-1}$ caused an increase the CRZ length of only about 2 mm. The effects of step height on the CRZ length are summarised in Table 5.2.

**Table 5.2** Effects of step height on the CRZ length

| Test Piece | d (mm) | D (mm) | d/D ratio | h (mm) | CRZ Length (mm) |
|---|---|---|---|---|---|
| | | | | | 80 - 120 kg $h^{-1}$ |
| A | 16.7 | 23 | 0.74 | 3.2 | 10 - 12 |
| B | 10.3 | 23 | 0.43 | 6.4 | 38 - 40 |
| C | 4.6 | 23 | 0.20 | 9.2 | 58 - 60 |

***Apparent viscosity profiles***

To estimate the thickness of the viscous sub-layer at different locations downstream of the step for test piece A, B and C geometries, the apparent viscosity at each location in these test pieces was plotted versus radial distance from the pipe wall. For illustration purposes, plots of apparent viscosity at various locations in test piece B geometry and for milk flow rate at 80 kg $h^{-1}$ are shown in Figure 5.6. The graph shows that the viscosity curves generally started at the same level of 0.0005 Pa $s^{-1}$, which was taken as the molecular viscosity of whole milk at 95 °C (Hall & Hendrick, 1966). The curves showed an initial region where the apparent viscosity remained constant with distance and a region where the viscosity increased with distance. The point at which the

apparent viscosity started to increase moved to a greater distance from the wall as the distance from the step height increased. The thickness of the viscous sub-layer was taken at a point where the curve started to depart from molecular viscosity (*e.g.* lines 1, 2, 4 and 5) or at an intercept of the viscosity curve with the horizontal line where the apparent viscosity equals the molecular viscosity (*e.g.* line 3).

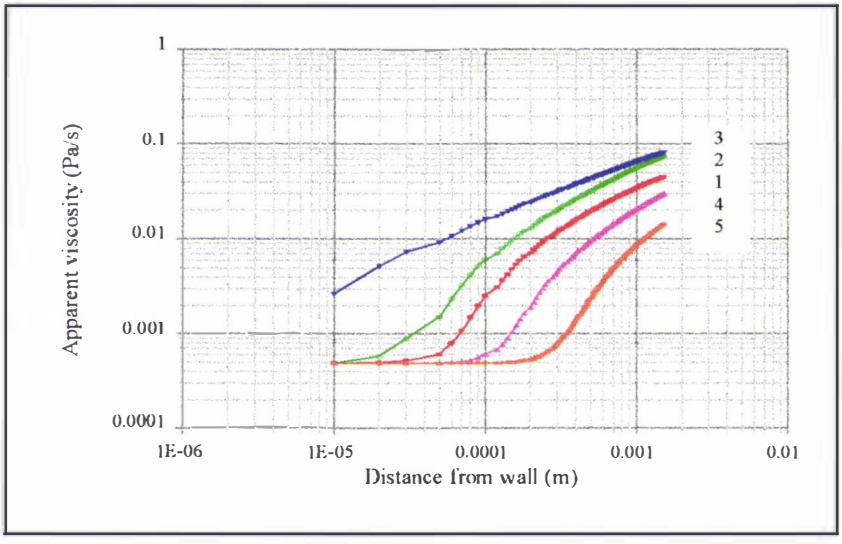


**Figure 5.6** CFD results of apparent viscosity profiles in the near wall region at various locations downstream of test piece B geometry (h=6.4 mm) and for milk flow of 80 kg/h: (line 1, red) x=10 mm; (line 2, green) x=20 mm; (line 3, blue) x=40 mm; (line 4, pink) x=80 mm; (line 5, light brown) x=120 mm.

To determine the effects of the step height and mass flow rate on the thickness of the sub-layer, the sub-layer thickness was plotted against the distance from the step for test pieces A, B and C and milk flow rates of 80, 100 and 120 kg $h^{-1}$. The results are summarised in Table 5.3 and are also shown in Figure 5.7. The thickness of the sub-

layer in various locations in test pieces B and C exhibited a very similar pattern: the sub-layer was thin in the locations near the step, reduced to a minimum thickness before rapidly increased to a higher level in locations further downstream from the step. The thickness of the sub-layer in test piece A was smallest in the location immediately behind the step and gradually increased in various locations downstream. Increasing the step height and the mass flow rate reduced the thickness of the sub-layer in all locations.

A comparison of the sub-layer thickness profiles (Figure 5.7) with the wall shear rate profiles (Figure 5.5) shows that the thinnest sub-layer was in the area between the CRZ and the redeveloping flow regions in which the wall shear rate was lowest (*i.e.* at x = 10, 40 and 60 mm in test piece A, B and C geometries respectively). The variation in the thickness of the sub-layers in the CRZ was small in relation to the rapid variation in the shear rates in this region. In contrast, the sub-layer thickness in the developing flow region distinctly increased in relation to the well-defined and continuously decreasing wall shear rates.

The results of the CFD model clearly demonstrate that flow disturbance behind the step of an expansion can vary the wall shear rate and the thickness of the viscous sub-layer at various locations downstream from the step. Consequently, the mass transfer rate at various locations downstream from the step could also expected to vary. The rate should be relatively high in the CRZ, increase to the highest level in the reattachment region and then gradually decrease in the redeveloping flow region.

**Table 5.3** Effect of step height and flow rate on the thickness of the viscous sub-layer

| **Location (mm)** | | **10** | **20** | **40** | **60** | **80** | **120** |
|---|---|---|---|---|---|---|---|
| **Flow rate** | **Test piece** | **Sub-layer thickness (μm)** | | | | | |
| 80 kg $h^{-1}$ | A | 5 | 17 | 60 | 120 | 180 | 250 |
| | B | 20 | 10 | 2 | 15 | 80 | 200 |
| | C | 10 | 20 | 7 | 2 | 20 | 100 |
| 100 kg $h^{-1}$ | A | 2 | 15 | 50 | 100 | 150 | 200 |
| | B | 10 | 10 | 2 | 10 | 70 | 170 |
| | C | 8 | 9 | 5 | 2 | 20 | 80 |
| 120 kg $h^{-1}$ | A | 2 | 12 | 40 | 70 | 100 | 150 |
| | B | 10 | 10 | 2 | 10 | 50 | 130 |
| | C | 7 | 9 | 5 | 2 | 17 | 70 |

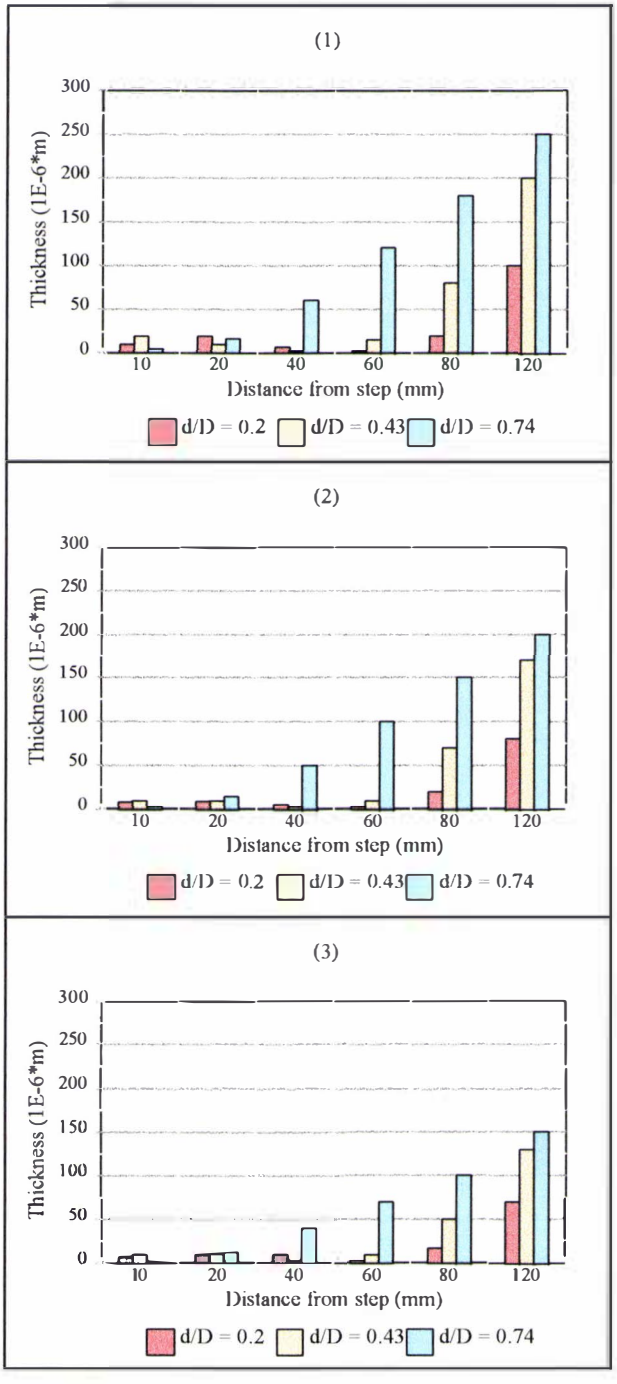


**Figure 5.7** CFD results for sub-layer thickness profiles in the near-wall region at various locations downstream of test piece A (blue), B (brown) and C (red) geometries and for milk flow rates of (1) 80 kg $h^{-1}$; (2) 100 kg $h^{-1}$ and (3) 120 kg $h^{-1}$.

### 5.2.2 Measurements of fouling

#### 5.2.2.1 Materials and methods

Fouling test piece B was used to measure the local fouling rates at different locations downstream of a sudden expansion. It had a d/D ratio of 0.43 (10/23 mm) and the axial length of the tube was 150 mm. A set of six heat flux sensors was attached to the outer surface of the expansion (Figure 5.8). The sensors were positioned at 10, 20, 40, 60, 80 and 120 mm from the step. When compared to the CFD shear rate profile, these locations span the CRZ and redeveloping flow regions (Figure 5.9).

The whole milk used for the experiments was obtained from the Kiwi Co-operative Dairies Limited, Hawera. The fresh milk was pasteurised at 75 °C for 15s, chilled and stored at 6 °C for up to 4 days before the experimental runs. The stored milk, at 6 °C, was preheated in the plate heat exchanger to 75 °C and then heat treated to 95 °C via the DSI heater of the fouling rig. Heated milk was then passed through test piece B which was placed 0.5 m downstream of the DSI heater. The heated milk was then cooled to 22 °C and discarded. A schematic drawing of the equipment set-up is shown in Figure 5.10.

Two different batches of whole milk were used and two runs (a duplicate) at 120 kg $h^{-1}$ were carried out from each batch of milk. An additional run at 150 kg $h^{-1}$ was made with each batch of milk because of milk availability. The duration of each run was up to 3 h. At the end of each experimental run, the test piece was removed for visual inspection and then reinstalled into the rig for cleaning. The equipment was cleaned using standard CIP procedures which have been outlined in Chapter 3. Visual inspection of the test piece was also carried out after each CIP to ensure the test piece was visibly clean. Care was taken not to disturb the heat flux sensors during the inspection and to reinstall the test piece in the same location and orientation after each

inspection. The run order and the composition of the whole milk used are listed in Table 5.4.

The heated milk temperature, local heat fluxes and the surface temperatures were recorded by the data logging equipment at ten second intervals during the experiment. The data were transferred to a computer for further calculation and analysis using the same procedures as described in Section 4.3.

**Table 5.4** Summary of experimental conditions and milk composition for runs 5.1 to 5.6

| **Run identifier** | **5.1** | **5.2** | **5.3** | **5.4** | **5.5** | **5.6** |
|---|---|---|---|---|---|---|
| Flow rate (kg $h^{-1}$) | 120 | 120 | 150 | 120 | 150 | 120 |
| Age of milk (day) | 2 | 4 | 5 | 1 | 1 | 2 |
| pH (at 20°C) | 6.72 | 6.67 | 6.65 | 6.71 | 6.71 | 6.69 |
| **Milk components** | **Milk A** | | | **Milk B** | | |
| Ash (% w/w) | 0.71 | | | 0.7 | | |
| Fat (% w/w) | 4.17 | | | 4.18 | | |
| Lactose (% w/w) | 4.97 | | | 4.98 | | |
| Total protein (% w/w) | 3.71 | | | 3.42 | | |
| Total solids (% w/w) | 13.56 | | | 13.28 | | |

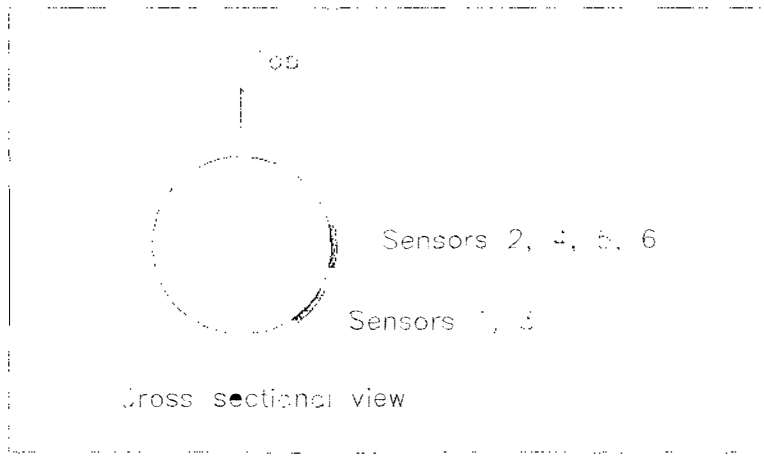


**Figure 5.8** Cross sectional view of a test piece showing locations of sensors.

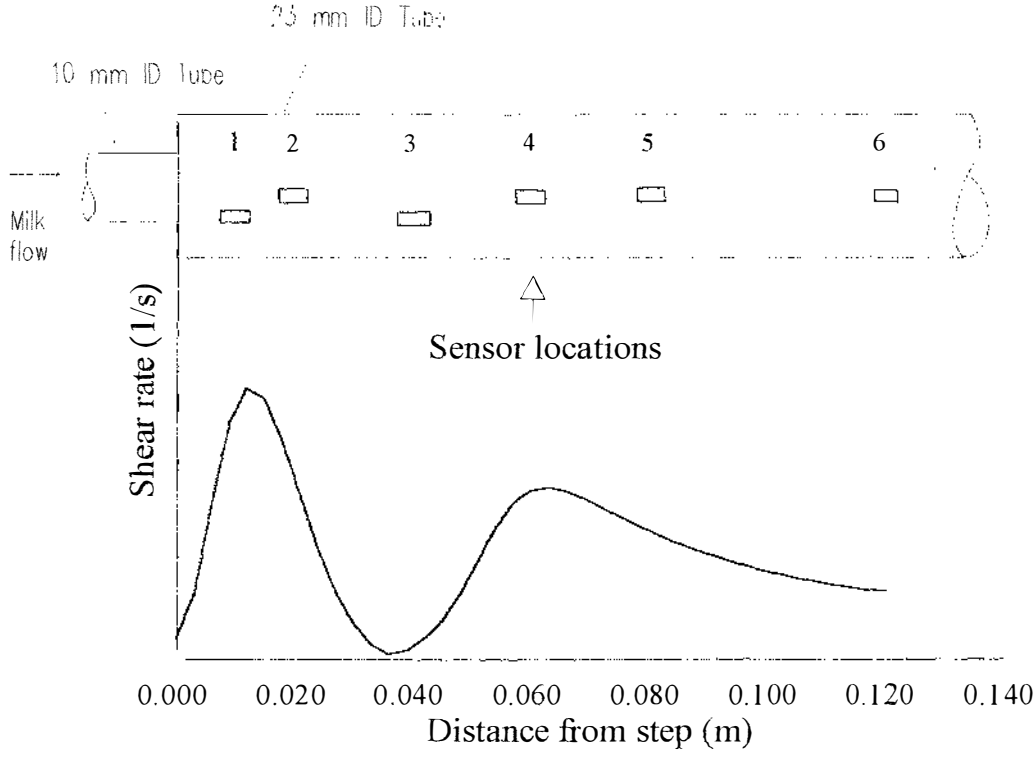


**Figure 5.9** Comparative location of heat flux sensor and CFD shear rate results at various locations downstream of sudden expansion

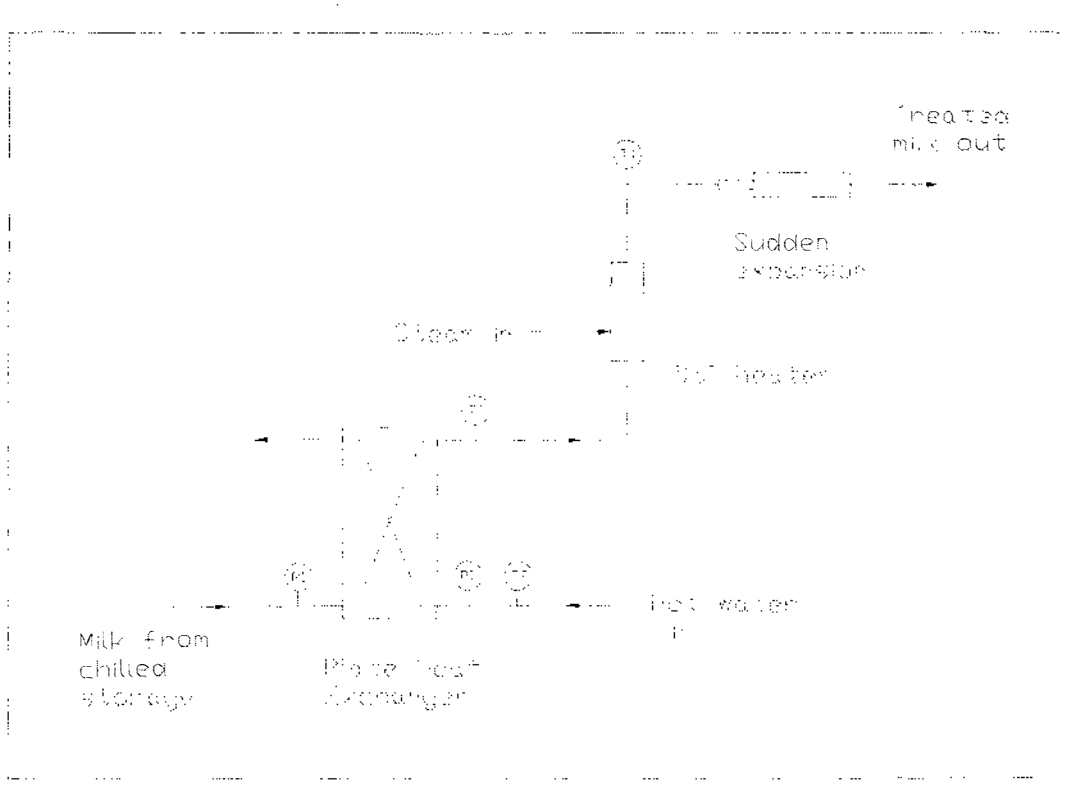


**Figure 5.10** Schematic drawing of experimental set-up.

**Notation for Figure 5.10**

PI Pressure indicator

TT Temperature transmitter

### 5.2.2.2 Results

***Local fouling curves***

Plots of $I_f$ obtained at six locations downstream of the expansion versus run time for runs 5.1 to 5.6 are given in Appendix 5.1. Only the results of a representative run, run 5.1 will be discussed. The results from this run are shown in Figure 5.11. These curves generally exhibit two periods: (a) a delay period at beginning of the run, during which $I_f$ remained relatively constant at about 1 and (b) a fouling period, during which there was a sustained decrease in $I_f$ with run time. The same pattern was found at various locations downstream of the expansion and in most experimental runs. On several occasions, a decrease in $I_f$ was not observed in the locations farthest from the step of the expansion. In these locations, the deposition was not sufficient to cause a measurable decrease in heat flux and hence $I_f$ remained about 1. In some runs, a slight increase in $I_f$ in the early stage of the fouling period was observed (*e.g.* Run 5.5). These phenomena were similar to those reported and discussed in Section 4.3.2.

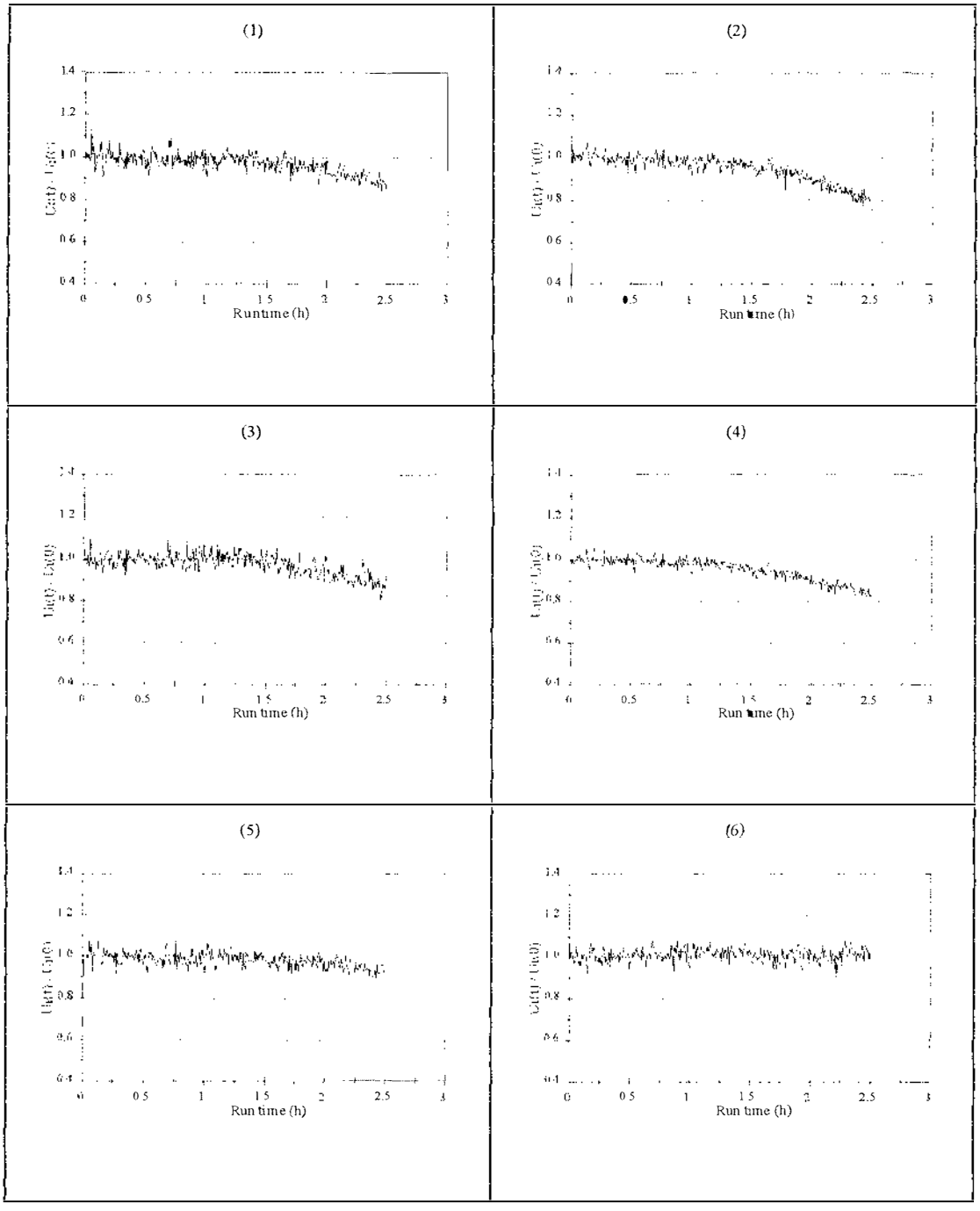


**Figure 5.11** Local fouling characteristics downstream of the expansion for Run 5.1 (milk A, day 2, 120 kg $h^{-1}$): (1) x=10 mm; (2) x=20 mm; (3) x=40 mm; (4) x=60 mm; (5) x=80 mm and (6) x=120 mm.

### *Local fouling rates*

The local fouling rates at various locations downstream of the expansion were estimated and the results are summarised in Table 5.5. The details of the analysis output are listed in Appendix 5.1. The fouling rates of run 5.5 and the average fouling rates of runs 5.1, 5.2, 5.4 and 5.6 (i.e. runs with a 120 $kgh^{-1}$ flow rate) were plotted against the distance from the step. The results are shown in Figure 5.12. A comparison between the local fouling rates and the CFD results of the sub-layer thickness was also made and the results are shown in Figure 5.13. The data for the locations at 120 mm from the step of run 5.1 and at 80 and 120 mm from the step of run 5.3 were not included in the analysis because the fouling in these locations was not observed before the end of the experimental run (when the milk supply was exhausted).

Generally, the fouling rate was at an intermediate level at the location immediately beyond the step of the expansion, increased to a higher level in the CRZ, reached a maximum level and then decreased to a minimum level at the farthest locations from the step. As depicted from these graphs, the maximum fouling rate occurred in the vicinity of the reattachment point (*i.e.* x = 40 mm) where the viscous sub-layer was thinnest. The results also showed that the fouling rates in various locations from the step expansion increased with increase in the mass flow rate.

In comparison with the sub-layer thickness profile (Figure 5.13), the measured fouling rates were found to relate consistently to the calculated thickness of the viscous sub-layer, in particular, at the locations downstream of the reattachment flow region. The results indicate that the local fouling rate is a function of the mass transfer rate. A decrease in the local mass transfer can cause a decrease in local fouling rate and vice versa.

**Table 5.5** Fouling rates at different locations downstream of the sudden expansion

| Run | Whole milk | | | Fouling rate ($10^{-5}$. $s^{-1}$) | | | | | |
|---|---|---|---|---|---|---|---|---|---|
| | Milk | Age (day) | Flow (kg $h^{-1}$) | Distance from step (mm) | | | | | |
| | | | | 10 | 20 | 40 | 60 | 80 | 120 |
| 5.1 | A | 2 | 120 | 2.5 | 4.1 | 3.0 | 3.1 | 1.3 | nd |
| 5.2 | | 4 | 120 | 4.1 | 5.0 | 4.9 | 3.1 | 2.1 | 0.7 |
| 5.3 | | 5 | 150 | 4.8 | 6.3 | 7.1 | 3.9 | nd | nd |
| 5.4 | B | 1 | 120 | 1.6 | 2.9 | 3.0 | 2.1 | 1.1 | 1.0 |
| 5.5 | | 1 | 150 | 4.2 | 3.5 | 5.0 | 5.6 | 5.2 | 2.5 |
| 5.6 | | 2 | 120 | 3.5 | 3.3 | 5.5 | 6.2 | 4.0 | 2.8 |
| **Average of all runs** | | | **120** | **2.9** | **3.8** | **4.1** | **3.6** | **2.1** | **1.5** |
| | | | **150** | **4.5** | **4.9** | **6.1** | **4.8** | **5.2** | **2.5** |

nd: not determined; (blue) 120 kg $h^{-1}$; (red) 150 kg $h^{-1}$

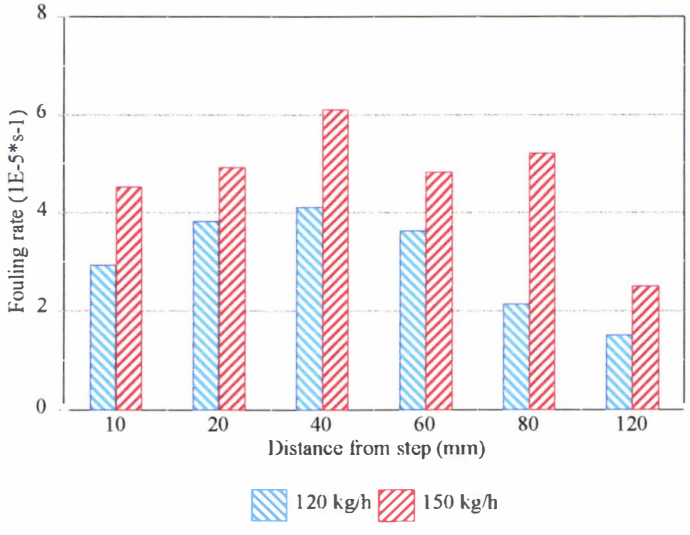


**Figure 5.12** Plots of local fouling rate versus distance from step of expansion.

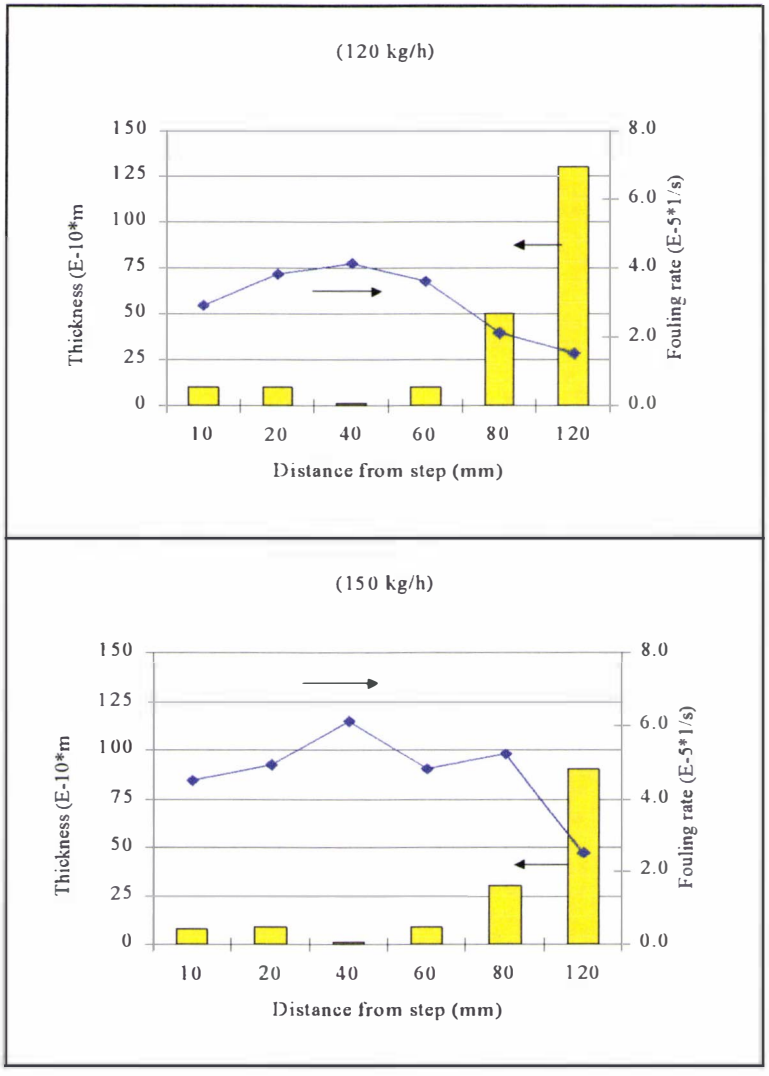


**Figure 5.13** Plots of local fouling rate (dots) and calculated sub-layer thickness (bars) versus distance from step of expansion.

### 5.2.3 Discussion

Different fouling patterns were found at different locations downstream of the expansion. The fouling process generally consisted of an initial delay period and a fouling period. The deposition patterns started at an intermediate level in the CRZ, increased to a maximum level in the reattachment flow region and then gradually decreased at locations downstream of the redeveloping flow region. Runchal (1971) who investigated the effect of sudden expansion flow on the deposition of potassium ferrocyanide also observed a similar pattern of the deposition. These results indicate that the effect of a sudden expansion flow on fouling behaviour is independent of the type of chemical reaction that occurs in the bulk fluid. In this situation, mass transfer rates of active species that can form deposits onto the solid surfaces mainly control the fouling process.

However, it should be noted that, in the experimental equipment set up, due to the physical constraints of the pipe work and the method of investigation of fouling, straightening the flow by using long sections of pipe was not feasible. The fluid flow was therefore already disturbed before entering the expansion. This flow condition would enhance the flow disturbance beyond the step. On the other hand, test pieces A, B and C were fabricated by welding of small and large diameter tubes together. Hence their edges and corners were smooth rather than sharp edged as specified in the CFD model. The effects of flow separation created by the sudden expansion would therefore be reduced. Furthermore, the flow conditions would not be strictly isothermal due to the effect of heat loss from the pipe wall. Nevertheless, the temperature variations were too small to cause any significant changes in the physical properties of the fluid along the length of the expansion. The combined effects of these departures from the assumptions (Section 5.2.1.2) were considered to be negligible in comparison to the magnitude of the effects of changes in the step height and flow rate used in the trials.

The CFD simulation was based on clean pipe conditions only and the model did not include the effect of deposition on the flow behaviour. With passage of time in a run, fouling increases the thickness of the deposit layer on the wall and hence would reduce the effective step height. Consequently, the fouling rate would decrease and the deposition pattern would change. In addition, an increase in the thickness of the deposit layer also reduces the flow passage and hence would increase the fluid velocity in the region and hence the fouling rate would increase. The relative magnitude of these two effects is not known, and would probably vary with time. But a degree of compensation, one for the other, may have contributed to the 'linear' change in heat transfer rate, implying a linear rate of fouling layer build-up. Nevertheless, modelling the effects of deposition during the run on the flow behaviour in the sudden expansion would be complex and would require further fundamental studies. Although our analysis did not allow for these effects, a comparative relationship between the calculated sub-layer thickness and the measured fouling rate could still be found. The results suggest that the present CFD model can be used to characterise, at least for a useful initial period, the local mass transfer rates in locations downstream of the sudden expansion.

For the same batch of milk, the local fouling rates increased with increases in mass flow rate and with age of milk. However, the absolute degree of fouling was not consistent if the results were compared between milk A and B. For example, the fouling rates obtained from 2-days aged milk A (Table 5.6, Run 5.1) were significantly lower than that obtained from 2-days aged milk B (Table 5.6, Run 5.6). On the other hand, at the flow rate of 150 kg $h^{-1}$, the fouling rates obtained from 2-days aged milk A (Table 5.6, Run 5.2) were almost the same with that obtained from 1-day age milk B (Table 5.6, Run 5.5). The results indicate that a quantitative fouling model to predict the absolute fouling level should be based on the evaluation of both the fluid dynamics of the system and the characteristics of the milk fluid. Further investigation is warranted, especially to identify the precise nature of the milk characteristics that influence absolute fouling

rate.

### 5.2.4 Concluding remarks

A simple tubular sudden expansion is a good model to study the effect of flow geometry on fouling of non-heated surfaces. It can provide various flow conditions such as recirculation, redeveloping and low shear force flows within a single experiment.

CFD is an useful tool for predicting local flow patterns and properties such as shear rate and apparent viscosity profiles.

The results from the fouling experiments support the proposition that deposition from heated whole milk on to a non heated surface, under a given heat treatment, is mainly affected by flow conditions that enhance mass transfer between the bulk fluid and the solid surface.

## 5.3 THE DENATURATION OF β-LACTOGLOBULIN AND ITS RELATIONSHIP TO FOULING

### 5.3.1 Introduction

Several researchers have shown that, at treatment temperatures below 100°C, the extent of β-lg denaturation correlates strongly with the rate of deposition on to heated surfaces (Lalande *et al.*, 1985; Hege & Kessler, 1986; Fryer, 1989). Recently, de Jong *et al.* (1992) developed a reaction model for fouling by skim and whole milk in plate heat exchangers and showed that the main process of fouling involves deposition of β-lg at the heat transfer surface.

We have shown in the previous section that flow geometry affected the rate of deposition from heated whole milk onto non-heated surfaces. We propose that aggregated β-lg entities ($\beta\text{-lg}_{(agg)}$) formed in the bulk fluid would not be involved in the fouling process, and that the deposition, after the surfaces have been conditioned during the delay period, would depend on the concentration of residual native β-lg ($\beta\text{-lg}_{(nat)}$), which in turn could be related to the concentration of active β-lg ($\beta\text{-lg}^*$). The proposed process is illustrated Figure 5.14.

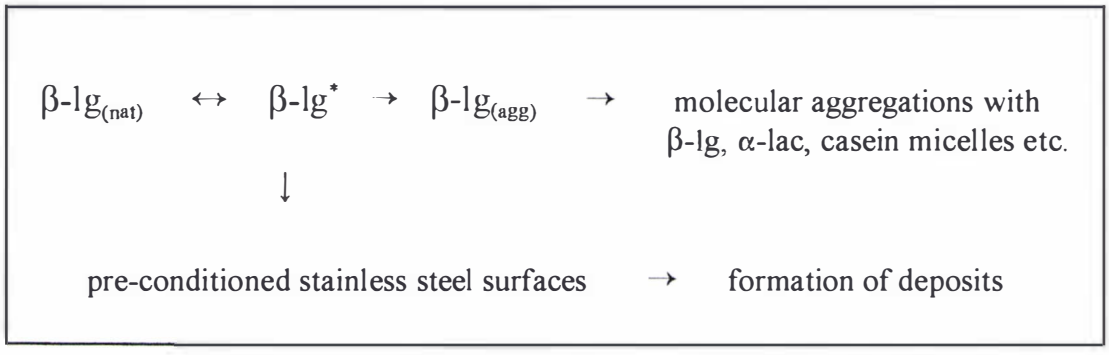


**Figure 5.14** Schematic representation of denaturation of β-lg and the consequence for deposition on non-heated stainless steel surface.

The proposition that the deposition rate would depend on the concentration of $\beta$-$lg_{(nat)}$, which in turn could be related to the concentration of active $\beta$-lg ($\beta$-$lg^*$) is explored and developed in the following sections. The model developed by Dannenberg & Kessler (1988) was used to estimate the concentration of $\beta$-$lg_{(nat)}$ from given heat treatment conditions. Experiments were then carried out to measure the local fouling rates in the sudden expansions placed at various locations, and hence different elapsed times after the start of heat treatment. The estimated amount of the local $\beta$-$lg_{(nat)}$ that was still available to be converted to $\beta$-$lg^*$ was then calculated and the two sets of data were compared.

### 5.3.2 Materials and methods

#### 5.3.2.1 Experimental materials and methods

***Determination of local fouling rate***

To measure the local fouling rate at different elapsed times, four identical sudden expansion test pieces were placed in series at positions 700, 1500, 2600 and 6200 mm downstream of the DSI heater. This arrangement resulted in four fouling zones of different mean elapsed times (Figure 5.15). The holding tubes were made of stainless steel and the inside diameter was 23 mm. Test piece B geometry, which had a d/D ratio of 0.43 or a step height of 6.4 mm (Section 3.2.3) was used in the experiments and two sets of four 'identical' test pieces were fabricated. Although these test pieces have the same dimensions, they were not precisely identically fabricated. Hence, their placement was randomised between the four fouling zones between experiments.

In order to inspect the fouling pattern and the surface structure of deposits, the axial length of each test piece was 40 mm. The local fouling rate in each zone was measured with a heat flux sensor attached at exactly 30 mm from the step. This selected location

was in the vicinity of maximum deposition area in test piece B (Table 5.6). The local fouling rate was derived from the heat flux data using the same procedure as outlined Section 4.3.1. A schematic drawing of the experimental set-up and attachment of the heat flux sensors is shown in Figure 5.15. As shown in Figure 5.15, the entire length (40 mm) downstream of the expansion step was denoted as a fouling zone.

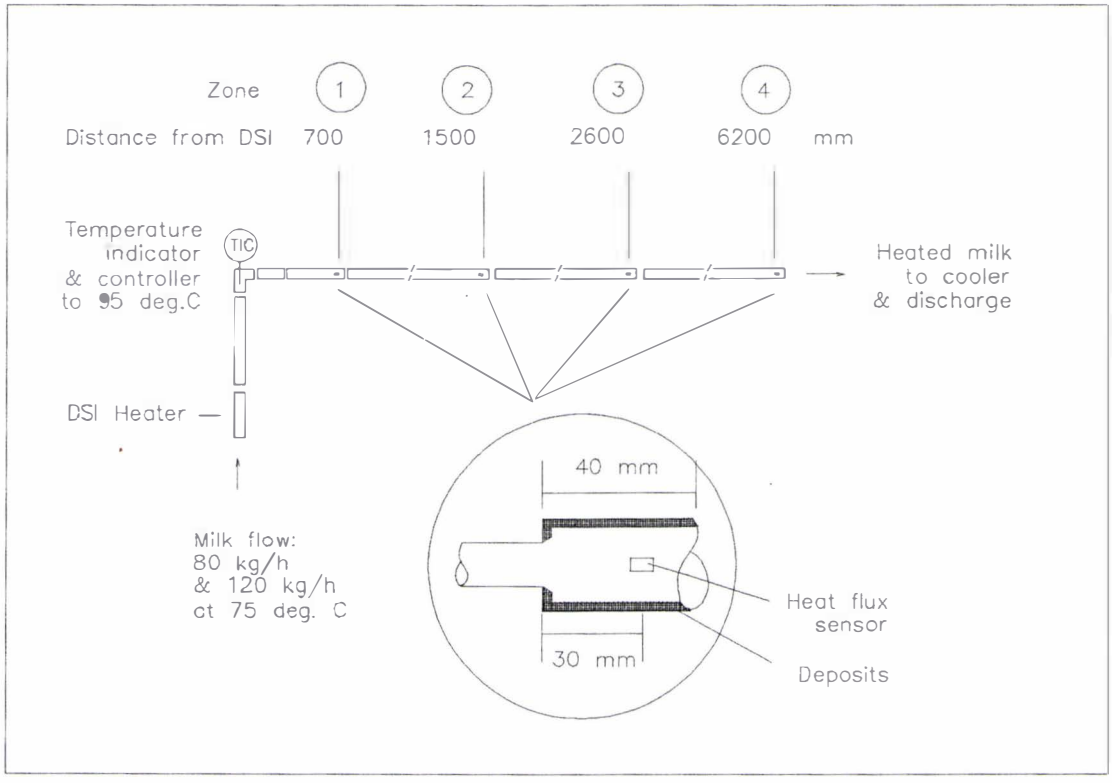


**Figure 5.15** Schematic layout of fouling zones ans heat flux sensors.

***Determination of average fouling rate***

In addition to the calculation of fouling rate at a particular location in a zone, the average fouling rate in each zone was also determined. At the completion of each run, the total dry weight, m, of deposit formed during the run in each zone surface area, A,

was measured and the average deposition rate was calculated using Equation 5.5:

$$\frac{d(W)}{dt} = \frac{m}{A\,t} \qquad (5.5)$$

The length of the selected test piece is equivalent to the length of the CRZ of the sudden expansion as shown by the results of CFD (Figure 5.5). Hence the overall hydrodynamic conditions in these test pieces is recirculating flow and its intensity is essentially the same in each fouling zone. To compare the fouling data with the concentration of $\beta$-$lg_{(nat)}$ in each fouling zone, the average fouling rate was named CRZ fouling rate.

***Experimental runs***

Four runs were carried out and three different batches of whole milk were used. The whole milks used in the experiments were obtained from Kiwi Co-operative Dairies Limited, Hawera. Milk handling and treatment used the same conditions as described in Section 5.2.2.1. The milk flow rates were 80 and 120 kg $h^{-1}$ (the Reynolds numbers in large tube ranged between 2500 and 3800). Table 5.6 shows a list of the experimental run order and the composition of the whole milk used.

At the completion of each experimental run, the test pieces were removed from the rig and rinsed with distilled water to remove any remaining milk from the deposits. The heat flux sensors were then removed from the test pieces. The fouling patterns and surface structure of deposits in each sudden expansion were observed and recorded. The whole test pieces were frozen at -18°C and then freeze dried overnight (Research Freeze Drier, Virtis Co. Inc., New York). Dried deposits were scraped from the internal surfaces of the expansion using a small sharp plate and then weighed.

A new set of test pieces was installed in the rig and the heat flux sensors were reattached to these test pieces. Care was taken to attach the sensor to each test piece in the same orientation as to the previous set. The fouling rig was cleaned using the standard CIP procedure, as outlined in Chapter 3.

**Table 5.6** Summary of experimental conditions and milk composition for runs 5.7 to 5.10

| **Run identifier** | **5.7** | **5.8** | **5.9** | **5.10** |
|---|---|---|---|---|
| Flow rate (kg $h^{-1}$) | 120 | 120 | 80 | 120 |
| Age of milk (day) | 2 | 2 | 3 | 4 |
| pH of aged milk (at 20°C) | 6.67 | 6.71 | 6.64 | 6.68 |
| **Milk components** | **Milk C** | **Milk D** | | **Milk E** |
| Ash (% w/w) | 0.75 | 0.70 | | 0.71 |
| Fat (% w/w) | 4.62 | 4.36 | | 4.22 |
| Lactose (% w/w) | 4.82 | 4.45 | | 4.58 |
| Total protein (% w/w) | 3.71 | 3.41 | | 3.27 |
| Total solids (% w/w) | 13.90 | 12.92 | | 12.78 |

### 5.3.2.2 Determination of protein composition of whole milk and deposits

Whole milk and deposits which were collected in run 5.7 were analysed for protein composition using reduced sodium dodecyl sulphate polyacrylamide gel electrophoresis (SDS-PAGE) (Anema & Klostermeyer, 1997). The protein composition of milk and deposits were further checked using a technique that involved a statistical computer program to estimate the protein composition based on their measured amino acid contents (Tsao *et al.*, 1998).

### 5.3.2.3 Calculation of concentration of denatured β-lactoglobulin

To estimate the concentration of $\beta\text{-lg}_{(nat)}$ after a given treatment temperature and elapsed time, the model developed by Dannenberg & Kessler (1988) was used. This model calculates the degree of denaturation of the β-lg A and B variants as a function of time and temperature using Equation 5.6.

$$C_{(den)}(t) = 100 \left\{ 1 - \left( 1 + 0.5\, k_o\, t \exp\left[ \frac{-E_A}{RT} \right] \right)^{-2} \right\} \qquad (5.6)$$

The reaction kinetic data for the denaturation of the A and B variants of β-lg are listed in Table 5.7. New Zealand milk contains about the same proportion of A and B variants of β-lg (Hill, 1993). Hence, the concentration of denatured β-lg was calculated as the average of that of A and B variants.

The concentration of $\beta\text{-lg}_{(nat)}$, can then be calculated from the equation

$$C_{(nat)}(t) = 100 - C_{(den)}(t) \qquad (5.7)$$

The calculated concentration of $\beta\text{-lg}_{(nat)}$ in whole milk heated and held at 95°C for different holding times are shown in Figure 5.16. Because of an average temperature drop of 2.5°C was observed between DSI and fouling zone 4 (Appendix 5.2), the concentration of $\beta\text{-lg}_{(nat)}$ at 92.5°C was estimated for comparison purposes. The results showed that the difference in the calculated concentration of $\beta\text{-lg}_{(nat)}$ between the two temperatures was about 1%. It was therefore concluded that the effect of a temperature variation of 2.5°C on the calculated $\beta\text{-lg}_{(nat)}$ is negligible.

**Table 5.7** Reaction kinetic data for the denaturation of β-lg A and B variants (from Dannenberg & Kessler, 1988)

| | n | Temperature (°C) | $E_A$ (kJ $mol^{-1}$) | $lnk_o$ |
|---|---|---|---|---|
| β-lg A | 1.5 | 70-90 | 265.21 | 84.16 |
| | | 90-150 | 54.07 | 14.41 |
| β-lg B | 1.5 | 70-90 | 279.96 | 89.43 |
| | | 90-150 | 47.75 | 12.66 |

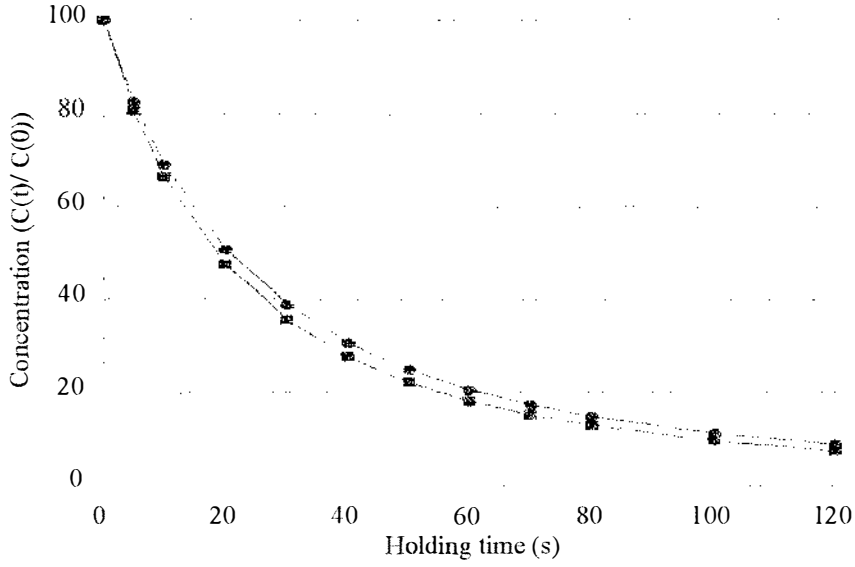


**Figure 5.16** Concentration-time curve of residual native β-lg in whole milk heated and held at (■) 95°C and (●) 92.5°C (from Dannenberg & Kessler, 1988).

Accurate estimation of the elapsed time between the DSI heater and the heat flux measurement point is important in determining the extent of β-lg denaturation. In all experiments, the average elapsed time in a given zone was calculated by the products of flow rate and the volume of the holding tube between the DSI unit and the test piece. In order to check the accuracy of the calculation method, experiments were carried out to measure the residence time distribution (RTD) of milk particles in the holding tube. The details of the experiments and the results are reported in Appendix 5.2. The average elapsed times were found to be in good agreement with the average holding times calculated using the RTD curves. It is therefore concluded that the product of flow rate and holding tube volume is a sufficiently reliable method of estimating the average elapsed time in a fouling zone without the need for RTD measurements.

### 5.3.3 Results

#### 5.3.3.1 Calculation of remaining native β-lg

To validate the assumption that denaturation of β-lg occurred to a negligible extent prior to DSI, the effect of preheating at 75 °C in the plate heat exchanger prior to the DSI heater on the denaturation of β-lg was calculated. The average holding time from the plate heat exchanger to the DSI heater was estimated at 7 s at 120 kg $h^{-1}$ and 11 s at 80 kg $h^{-1}$. Preheating whole milk in the plate heat exchanger to 75 °C prior to DSI heating was calculated to cause a reduction in native β-lg concentration of less than 1%, at both 120 and 80 kg $h^{-1}$ respectively. Therefore, it was taken that the percentage of native β-$lg_{(nat)}$ in the pre-heated whole milk prior to DSI heating was close to 100% of total β-lg.

The results of concentration-time relationship of β-$lg_{(nat)}$ listed in Table 5.8 show that at the milk flow of 120 kg $h^{-1}$, the concentration of residual native β-$lg_{(nat)}$ was about 75% in zone 1 and decreased to 15% in zone 4. At the flow rate of 80 kg/h, the concentration levels reduced to 63% and 9% in zones 1 and 4 respectively.

**Table 5.8** Summary of calculated concentration-time relationship of $\beta$-$lg_{(nat)}$.

| Parameters | Zone 1 | Zone 2 | Zone 3 | Zone 4 |
|---|---|---|---|---|
| Distance from DSI (mm) | 700 | 1500 | 2600 | 6200 |
| Milk flow rate (kg $h^{-1}$) | **120** | | | |
| **Average $\beta$-$lg_{(nat)}$ (%)** | **75** | **53** | **36** | **15** |
| Milk flow rate (kg $h^{-1}$) | **80** | | | |
| **Average $\beta$-$lg_{(nat)}$ (%)** | **63** | **40** | **25** | **9** |

### 5.3.3.2 Observations of fouling layers

Deposition occurred in all four zones. The most fouling deposit was found in zone 1 and progressively less in zones 2, 3 and 4. The fouling patterns between zones from different experimental runs were relatively similar *i.e* highest in zone 1 and lowest in zone 4. However, in run 5.10, the deposits found in zone 1 consisted of a number of large clumps of small particles and randomly distributed onto the surfaces. In particular, only a few clumps of deposits were found in the area covered by the heat flux sensor. The cause of this usual pattern of deposition is unknown. It may be related to the age of milk (4 days old), but this could not be experimentally confirmed. The unusual deposition pattern was only found in zone 1 and therefore may be due to a physical difference in this zone (*e.g.* entrapped air bubbles that could not be dislodged or change in surface characteristics of the stainless steel, such as cleanliness, that could not be visually detected).

The fouling layer in a given zone was not uniform. The deposits in the area near the step appeared less dense than that in the vicinity of the reattachment area (*i.e.* x=40 mm). The deposits were also found on the surfaces of the step.

The structure and appearance of the fouling layer between zones was different. Figure 5.17 shows an example of the structures of deposits found in zones 1, 2, 3 and 4. The deposit areas shown in the photographs were near the end of the test pieces and about 15 mm in axial length (*i.e.* between 25 and 40 mm from the step) and directly opposed to the sensors (located at 30 mm from the step). The photographs show that the deposits in zone 1 was compact, voluminous, uneven and contained high 'hills' and deep 'valleys'. In zones 2 and 3, the deposits found were more porous, less dense and consisted of individual small strands. When fouling was lowest, such as found in test pieces placed in zone 4 in runs 5.7, 5.9 and 5.10, the deposit layer consisted of discrete granules of about 20 to 1000 μm. that randomly distributed on the surface area. It should be noted that the deposits in zone 4 shown in Figure 5.17 appeared unevenly distributed. This may be because some of deposits were detached during the run or when the test piece was rinsed with water to remove any remaining milk from the deposits.

The structure and appearance of the fouling layer in different zones shown in Figure 5.17 can be used to illustrate the progressive nature of the build-up of fouling deposits, which were under the influence of similar hydrodynamic conditions. The deposits observed in zone 4 represented the early stage of fouling. They consisted of small particles of different sizes that randomly attached to the solid surfaces. As fouling build-up progressed, these particles grew in size and formed small strands (zone 3). These strands became larger (zone 2) and then linked together to create a porous network of particles (zone 4), which represented the later stage of fouling.

#### 5.3.3.3 Local fouling rate

***Fouling curve***

Plots of $I_F$ obtained at four different zones versus run duration for runs 5.7 to 5.10 are given in Appendix 5.3. Only the results of a representative run (run 5.7) are shown in

Figures 5.18 for illustration and discussion purposes. Similar to the results obtained in the previous experiments (Section 5.2.2.2), the fouling curves for runs 5.7 to 5.10 generally exhibit two periods: a delay period and a fouling period. For all runs, the deposition in zone 4 was not sufficiently large to cause a decrease in $I_f$.

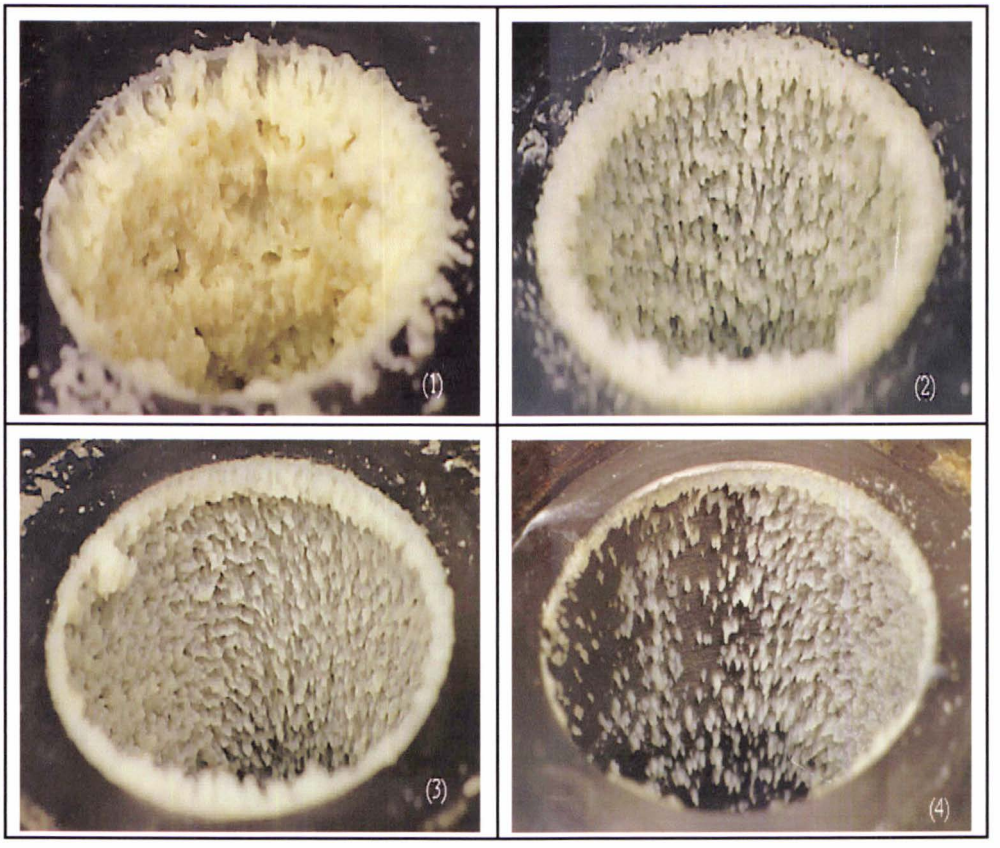


**Figure 5.17** Photographs of fouling deposits ( 3 x enlargement) in different zones: (1) zone 1; (2) zone 2; (3) zone 3 and (4) zone 4.

The duration of the experimental runs ranged between 4 and 9 h compared to about 3 h in the previous set of runs (Runs 5.1 to 5.6). This was because of the increase in the duration of the delay period. In most runs, this period lasted up to 5 h. In addition, the runs were required to continue for up to 4 hours after the delay periods to allow sufficient fouling build-up in the downstream zones, especially in zone 4 to occur.

Nevertheless, all runs had to be stopped before a reduction in the internal heat transfer coefficient, $U_i(t)$, in zone 4 was observed. It was either due to the milk supply being exhausted or $U_i(t)$ of zone 1 had reached between 50 and 60 % of its initial $U_i(0)$ and started to level out.

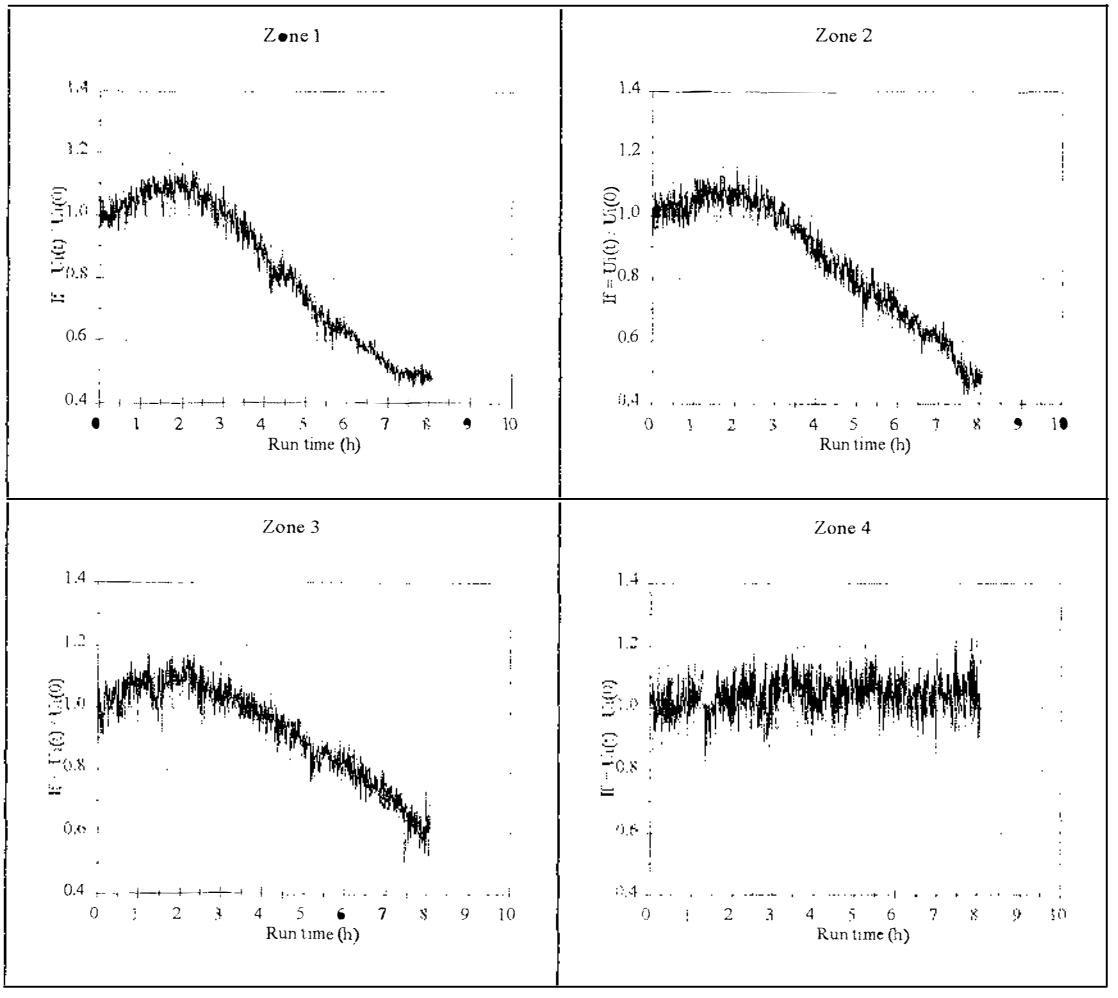


**Figure 5.18** Local fouling characteristics in four fouling zones downstream of DSI heater, Run 5.7, milk C, 120 kg $h^{-1}$.

### *Local fouling rate*

The slopes of the fouling curves were calculated, using the method described in Section 4.3.2, and a comparison of the fouling rates between different zones was undertaken. The details of the analysis output are given in Appendix 5.3. The comparative fouling rates in different zones are listed in Table 5.9.

The rates of fouling between zones were different. Generally, the highest fouling rate was observed in zone 1, and it progressively decreased in the subsequent zones and reached the lowest level in zone 4. The trends were very similar for most of the experimental runs. In run 5.10, zone 1 showed a very low fouling rate compared with the rates in zones 2 and 3. As previously reported in Section 5.3.3.2, the local fouling area in zone 1 of run 5.10, where the heat flux sensor was positioned, was found to contain only a few clumps of deposit. In contrast, a relatively higher deposition in the surrounding area was observed. It was concluded that the low local fouling rate recorded in this zone was the result of an unusual deposition pattern. Therefore, the fouling rate in zone 1 for run 5.10 was not included in the comparison of the fouling rates in different zones. In this case, a more accurate comparison would be obtained if the calculation was based on CRZ fouling rate determination method. In addition, for zone 4 of run 5.7, 5.9 and 5.10, a sustained decrease in $I_f$ with run time was not observed and hence fouling rates for zone 4 of those runs could not be calculated.

**Table 5.9** Summary of local fouling rates ($10^{-5}$ $s^{-1}$) in four fouling zones

| Run | Zone 1 | Zone 2 | Zone 3 | Zone 4 |
|---|---|---|---|---|
| 5.7 | 3.8 | 2.9 | 2.2 | - |
| 5.8 | 4.8 | 2.5 | 2.1 | 0.3 |
| 5.9 | 1.9 | 1.4 | 1.0 | - |
| 5.10 | 0.5 | 1.7 | 1.3 | - |

The local fouling rates in different zones, for the mass flow rates of 80 and 120 kg $h^{-1}$, were plotted against the elapsed times and compared to the concentration-time curve for $\beta$-$lg_{(nat)}$ (Figure 5.19). As previously discussed, the data for zone 1 of run 5.10 and zone 4 of runs 5.7, 5.9 and 5.10 were not included in the analysis. The comparison shows that curves of local fouling rates, based on heat flux measurements, versus elapsed time resemble the concentration-time curve of $\beta$-$lg_{(nat)}$.

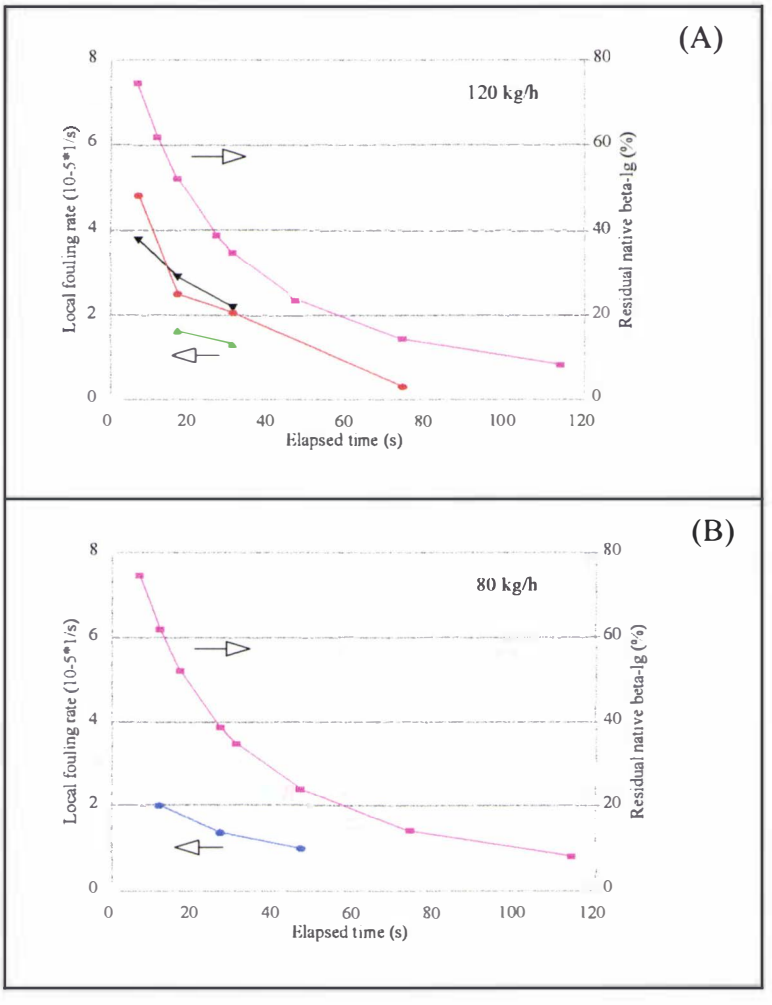


**Figure 5.19** Plots of local fouling rate and calculated concentration of $\beta$-$lg_{(nat)}$ versus elapsed time: (A) 120 kg $h^{-1}$; (B) 80 kg $h^{-1}$; (black) run 5.7; (red) run 5.8; (blue) run 5.9; (green) run 5.10; and (pink) concentration of residual native $\beta$-lg.

#### 5.3.3.4 CRZ fouling rate

In order to calculate the fouling rate in the CRZ using Equation 5.5 (Section 5.3.2.1), an estimation of the fouling time in each zone was required. It was defined as the difference between the run time and the delay time. The delay time in turn was estimated using the procedures set out in Section 4.3.2. The results are listed in Table 5.10. Generally, the delay times were found to be very similar between zones 1, 2 and 3 within a single run. The delay times however were different between runs.

Table 5.11 and 5.12 show the results dry deposit weight collected and the CRZ fouling rate in each zone. The details of the calculation are also listed in Appendix 5.3. As previously discussed, because a fouling period was not observed, the data of zone 4 for runs 5.7, 5.9 and 5.10 were not included in the calculations of CRZ fouling rate.

The highest CRZ fouling rate was found in zone 1, it was lower in zones 2 and 3 and was lowest in zone 4. This is similar to that observed for the local fouling rates (Section 5.3.3.3). The fouling pattern was also very similar in all experimental runs. In run 5.10, where the local fouling rate in zone 1 was found to be unusually low (Table 5.9), the CRZ fouling rate in zone 1 was still found to be relatively higher than the CRZ fouling rates in zones 2 and 3 (Table 5.13) for that run.

**Table 5.10** Summary of fouling time (h) in four fouling zones

| Run | Zone 1 | Zone 2 | Zone 3 | Zone 4 |
|---|---|---|---|---|
| 5.7 | 6.0 | 6.0 | 6.0 | nd |
| 5.8 | 5.5 | 5.5 | 5.5 | 6.5 |
| 5.9 | 5.0 | 5.0 | 5.0 | nd |
| 5.10 | 3.5 | 3.5 | 3.5 | nd |

**Table 5.11** Summary of dry deposit weight (g) in four fouling zones

| Run | Zone 1 | Zone 2 | Zone 3 | Zone 4 |
|---|---|---|---|---|
| 5.7 | 2.822 | 2.152 | 1.306 | 0.392 |
| 5.8 | 1.752 | 1.403 | 0.711 | 0.012 |
| 5.9 | 0.909 | 0.432 | 0.178 | nd |
| 5.10 | 0.873 | 0.865 | 0.503 | 0.248 |

**Table 5.12** Summary of CRZ fouling rate ($10^{-5}$ kg $m^{-2}$ $s^{-1}$) in four fouling zones

| Run | Zone 1 | Zone 2 | Zone 3 | Zone 4 |
|---|---|---|---|---|
| 5.7 | 4.1 | 3.1 | 1.9 | nd |
| 5.8 | 2.8 | 2.2 | 1.1 | 0.02 |
| 5.9 | 1.6 | 0.8 | 0.3 | nd |
| 5.10 | 2.2 | 2.1 | 1.2 | nd |

nd: not determined.

The CRZ fouling rates in different zones were plotted against the elapsed times and compared to the concentration-time curve for β-$lg_{(nat)}$ (Figure 5.20). The comparison shows that curves of CRZ fouling rates, based on deposit weight measurement, versus elapsed time resemble the concentration-time curve of β-$lg_{(nat)}$, *i.e.* when the concentration of β-$lg_{(nat)}$ was at the highest level, the CRZ fouling rate was highest and vice versa.

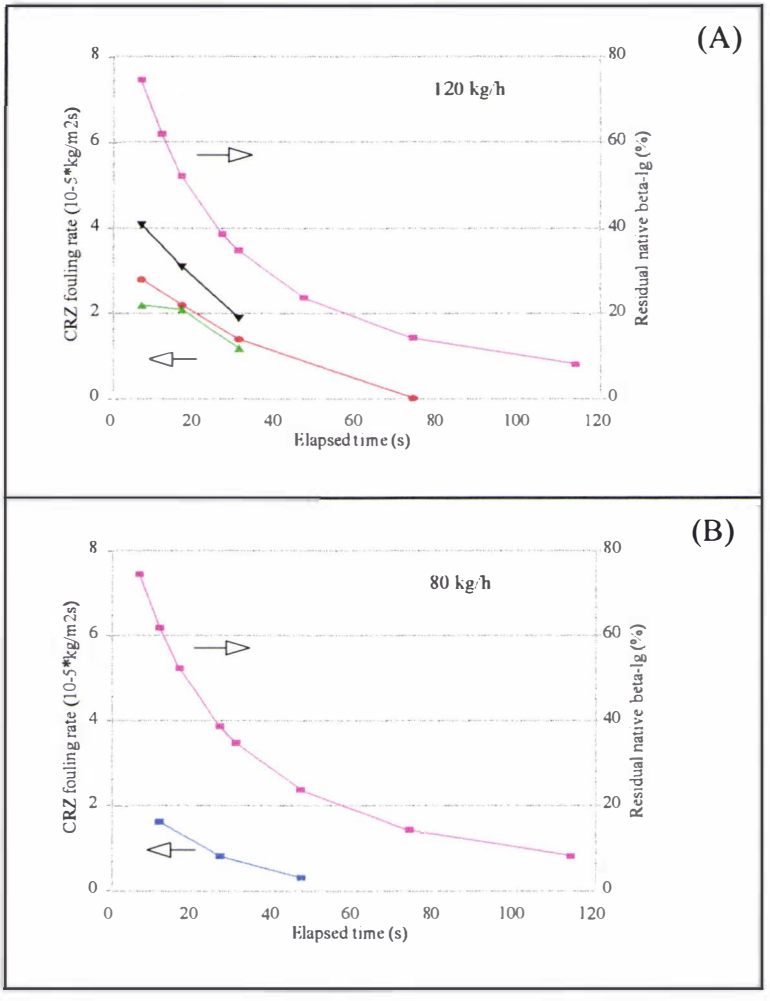


**Figure 5.20** Plots of CRZ fouling rate and calculated concentration of β-$lg_{(nat)}$ versus elapsed time: (A) 120 kg $h^{-1}$; (B) 80 kg $h^{-1}$; (black) run 5.7; (red) run 5.8; (blue) run 5.9; (green) run 5.10; and (pink) concentration of residual native β-$lg_{(nat)}$.

### 5.3.3.5 The relation between local and CRZ fouling rates

The CRZ fouling rate represents direct quantification of the accumulation of deposits on to the entire surface area and was called the overall fouling rate in the CRZ. On the other hand, the local fouling rate is measured by the interference of the deposits to the heat transfer from the small area directly opposed to the sensor. To determine whether the local fouling based on heat flux measurements (Table 5.9) can be related to the overall fouling based on deposit weight measurement (Table 5.12), the local fouling rate in each fouling zone was plotted against the CRZ fouling rate. The results are shown in Figure 5.21. There is a consistent relationship across all samples between dry weight of deposits and the effect on heat transfer rate.

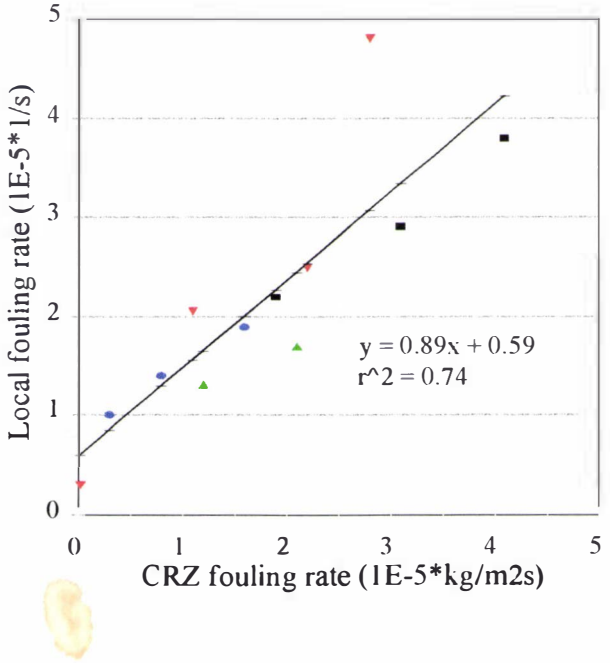


**Figure 5.21** Relation between local and CRZ fouling rates: (black) run 5.7; (red) run 5.8; (green) run 5.10 and (black line) linear fit data.

### 5.3.3.6 Composition of deposits

Figure 5.22 shows the SDS-PAGE patterns of the protein components of unheated whole milk and deposit samples in different fouling zones. Unheated whole milk had high intensities of all casein bands and relatively low intensity of the β-lg band. Milk C, D and E had the same SDS-PAGE pattern. In contrast, the SDS-PAGE patterns of the protein components of the fouling layers had high intensity of the β-lg band and very low intensities of all casein bands. The same patterns were observed in all four fouling zones.

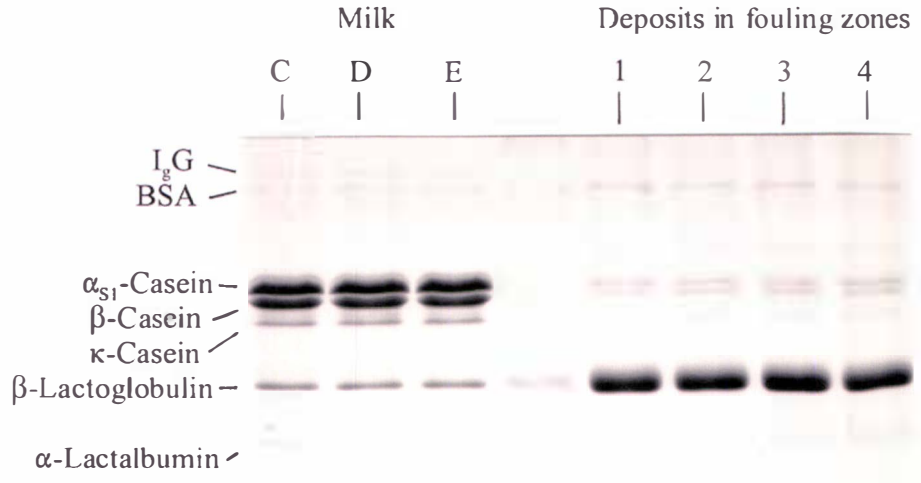


**Figure 5.22** SDS-PAGE patterns of whole milk and deposits in various fouling zones.

The comparative patterns of β-lg and caseins contents of milk and deposits were further checked using a statistical computer programme to estimate the protein composition based on their measured amino acid contents. Table 5.13 shows the quantitative data of protein compositions of milk C and deposits in different fouling zones of run 5.7. The results show that the concentration of β-lg in milk, on % dry basis, was only 2% but

but was on average 23% in the deposits. The ratios of β-lg to total caseins in milk and fouling deposits were 0.14 and 3.3 respectively. The β-lg to protein ratio in unheated milk was about 10% but it was about 62% in deposits. A similar β-lg to protein ratio in the deposit was also found in all four zones. The results confirmed the comparative patterns of concentration levels of β-lg and caseins in milk and deposits shown by the SDS-PAGE patterns.

**Table 5.13** Protein composition (% dry basis) of milk C and fouling layers in different fouling zones for run 5.7

| Protein | Milk C | Average of Four Zones | Dry Deposit in Fouling Zone | | | |
|---|---|---|---|---|---|---|
| | | | 1 | 2 | 3 | 4 |
| β-Lactoglobulin | 2.0 | 23.2 | 26.4 | 23.6 | 23.2 | 19.6 |
| Total whey protein | 4.7 | 30.5 | 33.8 | 30.5 | 30.8 | 26.8 |
| Total casein | 14.6 | 7.0 | 7.0 | 6.7 | 6.1 | 8.2 |
| Total protein | 19.3 | 37.5 | 40.8 | 37.2 | 36.9 | 35.0 |
| **β-Lg / Protein ratio** | **0.10** | **0.62** | **0.65** | **0.63** | **0.60** | **0.56** |
| **β-Lg / Casein ratio** | **0.14** | **3.31** | **3.77** | **3.52** | **3.80** | **2.39** |

### 5.3.3.7 Normalisation of fouling rate

Based on the results that deposition strongly relates to the local concentration of $\beta\text{-lg}_{(nat)}$ it was hypothesised that the fouling rate in each zone could be normalised with its concentration of $\beta\text{-lg}_{(nat)}$ to compensate for this effect.

To evaluate the hypothesis, the local fouling rates (based on heat flux measurement) and the CRZ fouling rates (based on deposit weight measurement) in the four zones were

normalised against the local concentrations of $\beta$-$lg_{(nat)}$. The dimensions of the test pieces used in these experiments were the same, hence the local hydrodynamic conditions in them could be expected to be very similar and therefore their normalised fouling rates (between the fouling zones) should also be very similar. The results of normalised local and CZR fouling rates are listed in Table 5.14. The details of the calculation are given in Appendix 5.3. As previously discussed (Section 5.3.3), the fouling data in zone 1 for run 5.10 and in zone 4 for runs 5.7, 5.8, 5.9 and 5.10 were not included in the analysis.

**Table 5.14** Summary of normalised local and CZR fouling rates

| | **Zone no.** | **Run 5.7** | **Run 5.8** | **Run 5.9** | **Run 5.10** | **Average of Four Runs** |
|---|---|---|---|---|---|---|
| Local Fouling Rate ($10^{-5}$ $s^{-1}$) | 1 | 5.1 | 6.4 | 3.0 | - | 4.8 |
| | 2 | 5.5 | 4.7 | 3.5 | 3.2 | 4.2 |
| | 3 | 6.1 | 6.0 | 4.0 | 3.6 | 4.9 |
| | 4 | - | - | - | - | - |
| CRZ Fouling Rate ($10^{-5}$ kg $m^{-1}$ $s^{-1}$) | 1 | 5.7 | 3.7 | 2.5 | 2.9 | 3.7 |
| | 2 | 5.9 | 4.1 | 2.0 | 4.0 | 4.0 |
| | 3 | 5.3 | 4.0 | 1.2 | 3.0 | 3.4 |
| | 4 | - | - | - | - | - |

The results listed in Table 5.14 show the average normalised fouling rates (for four runs), both local and CRZ fouling rates between zones 1, 2 and 3 were quite comparable.

### 5.3.4 Discussion

The fouling rates based on both heat flux and deposit weight measurements in four fouling zones were different. They were highest in zone 1, which was nearest to the expansion, and progressively lower in zones 2, 3 and 4. These fouling rate patterns were also found to resemble the concentration-time curve for residual native β-lg (β-$lg_{(nat)}$) in whole milk heated to 95 °C, which were derived from the model developed by Dannenberg & Kessler (1088).

Although the fouling rates in each zone were different, the deposits all resembled type A deposit (Burton, 1968), *i.e.* high protein and low mineral deposit. In particular, they contained similar levels of β-lg and β-lg to protein ratio (of about 23% and 62% on dry basis respectively). The results indicated that β-lg was the main protein constituent involved in the fouling process in all four zones.

Other researchers (Lalande *et al.*, 1985; Hege & Kessler, 1986; Fryer, 1989; de Jong *et al.*, 1992) who studied fouling of heat exchangers, have shown that the extent of β-lg denaturation correlated strongly with the rate of deposition on to heated surfaces *(i.e.* increasing in the extent of β-lg denaturation increases fouling). Dissimilarly, our experimental results with the fouling rig indicated that the deposition, after the surfaces have been conditioned during the delay period, would depend on the concentration of residual native β-lg (β-$lg_{(nat)}$). It is possible that native β-lg once becomes active acts as a bonding material of other species, possibly other active β-lg or denatured β-lg onto the deposit layer.

Within the variations of determining the fouling rate, the comparative results of the normalised local and CRZ fouling rates in zones 1, 2 and 3 support the proposition that the fouling rate (of whole milk heated to 95 °C) in different zones could be normalised with the concentration of β-$lg_{(nat)}$ to compensate for this effect.

However, further work is required to determine if there is to be a direct correlation between the local concentration of $\beta$-$lg_{(nat)}$ and the local fouling rate of heated milk. Milk is a complex mixture of different components and the reactions occurring after the $\beta$-lg denaturation, particularly with surfaces, is far from being completely understood. It is still not clear what the controlling reactions are, where they occur and how they affect the deposition.

Generally, the local and CRZ fouling rates are correlated. However, the results show that there was an amount of scatter of the data particularly when the deposition was relatively high (*i.e.* runs 5.7 and 5.8). It is suggested that the scatter of the data could be due to the effect of deposition on the flow pattern that in turn affected the distribution of the deposit in the fouling zone. In addition, each run was a compromise between being long enough to obtain measurable deposition in zone 4 and short enough not to stretch the criteria for normalisation of heat transfer rate in zone 1. As a result, precision correlation at high deposition rate cannot be expected.

The results also show that the line of the fitted data of the two measurement methods did not intercept either at zero or at a point on the CRZ fouling rate axis (x axis) but at a location on the local fouling rate axis (y axis). It was expected that the intercept would be on the x axis because it had been found that the fouling layer had to be sufficiently thick in order to cause a decrease in heat flux. Nevertheless, the intercept on the y axis was probably due to the inadequacies of measuring just a single location, especially at high fouling level. Only one small sensor was used to correlate to a much larger and somewhat varied landscape.

### 5.3.5 Concluding remarks

The experimental results support the hypothesis that the local fouling rate of heated whole milk at 95°C on to non-heated surfaces depends on the local concentration of remaining $\beta$-$lg_{(nat)}$, which in turn can be related to the concentration of active $\beta$-$lg^*$.

For the same operating conditions of milk flow, the local fouling rate in different locations, *i.e.* different elapsed time after the heat treatment, when normalised with its local concentration of $\beta$-$lg_{(nat)}$ shows a considerable degree of consistency in magnitude in spite of the various approximations inherent in both measuring and calculation processes.

The results also indicate that the overall fouling rate in an area can be estimated from a measurement of local fouling. However, a close analysis of the flow patterns in the area is essential for positioning of the sensor in order to capture the effects of flow geometry on the local deposition. Increasing the number of local measurements (*i.e.* heat flux sensors) would probably improve the correlation between local and overall measurements.

## 5.4 STUDY OF THE EFFECTS OF STEP HEIGHT AND MASS FLOW RATE ON FOULING

In the following section, the effects of flow rate and step height on fouling in the tubular expansion were determined. The relation between the local fouling based on heat flux measurement and the overall fouling based on deposit weight measurement was further investigated. Several sensors were used to measure fouling in various locations in a fouling zone and the results integrated to represent the overall fouling in that zone.

### 5.4.1 Materials and methods

To study the effect of step height on fouling, three test piece geometries labelled A, B, C were used. These test pieces were as previously described in Section 5.2.1. They had the same downstream diameter but different upstream diameters in order to create different step heights. In this study, the axial length of each test piece was 160 mm and the entire length of the section was denoted as a fouling zone. As shown by the CFD results (Figure 5.5), the defined fouling zone included both the CRZ and the redeveloping flow regions.

To study the effect of mass flow rate on fouling, three flow rates 80, 100 and 120 kg $h^{-1}$ were used. The geometric and flow parameters of test piece A, B and C, which have been given in Section 5.2.1 are listed in Table 5.15 for reference purposes.

A total of 9 runs would be required to complete a full set of experiments using three different step heights and mass flow rates. In order to reduce the number of runs required, test pieces A, B and C were all used in each mass flow rate condition. They were placed in series in various locations downstream of the DSI heater. Hence, the number of runs required was reduced from 9 to 3 runs. Three sets of test pieces A, B and C were fabricated and, because they could not be precisely identically made, they

were randomised between the locations for each experimental run. Two sets of three runs each were performed using two different batches of milk. The whole milks used, milk handling and treatment were the same conditions as employed in the previous experiments (Section 5.2.2). Table 5.16 shows a list of the experimental run orders and the composition of the milk used.

**Table 5.15** Geometric and flow parameters of test pieces A, B and C

| Test Piece | d (mm) | Reynolds Number, Re | | | D (mm) | d/D ratio | h (mm) |
|---|---|---|---|---|---|---|---|
| | | 80 kg $h^{-1}$ | 100 kg $h^{-1}$ | 120 kg $h^{-1}$ | | | |
| A | 16.7 | 3500 | 4300 | 5200 | 23 | 0.74 | 3.2 |
| B | 10.3 | 5600 | 6300 | 8400 | 23 | 0.43 | 6.4 |
| C | 4.6 | 12700 | 15800 | 19000 | 23 | 0.20 | 9.2 |
| **Large tube** | **23** | **2500** | **3100** | **3800** | **23** | **1** | **0** |

**Table 5.16** Summary of experimental conditions and milk composition for runs 5.11 to 5.16

| **Run identifier** | **5.11** | **5.12** | **5.13** | **5.14** | **5.15** | **5.16** |
|---|---|---|---|---|---|---|
| Flow rate (kg $h^{-1}$) | 80 | 120 | 100 | 80 | 100 | 120 |
| Age of milk (day) | 2 | 3 | 3 | 1 | 2 | 3 |
| pH of milk (at 20°C) | 6.76 | 6.7 | 6.69 | 6.71 | 6.69 | 6.68 |
| **Milk components** | **Milk F** | | | **Milk G** | | |
| Ash (% w/w) | 0.70 | | | 0.72 | | |
| Fat (% w/w) | 4.22 | | | 4.56 | | |
| Lactose (% w/w) | 4.37 | | | 4.65 | | |
| Total protein (% w/w) | 3.92 | | | 3.81 | | |
| Total solids (% w/w) | 13.21 | | | 13.74 | | |

### 5.4.2 Calculation methods

Test pieces A, B and C were located at 900, 1500 and 2000 mm (measured from the centre of each zone length) downstream of the DSI heater of the fouling rig. These selected locations were very similar to the locations of the fouling zones 1, 2 and 3 which were used in the previous experiments. There were two main factors that concurrently affected the deposition in these test pieces. They were:

(a) the local concentration $\beta$-$lg_{(nat)}$, and

(b) the local hydrodynamic conditions within a test piece.

In order to compare the fouling rates in test pieces A, B and C, the fouling rate in each of them was normalised with its concentration of $\beta$-$lg_{(nat)}$. The mathematical model which was employed to calculate the fouling rate is then given by

$$\frac{d(I_f)}{dt} = \frac{d\left(\frac{U_i(t)}{U_i(0)}\right)}{dt} = Kd_{hf}\, C_{(nat)}(t) \qquad (5.8)$$

where the model is based on heat flux measurement, and

$$\frac{d(m/A)}{dt} = Kd_{wt}\, C_{(nat)}(t) \qquad (5.9)$$

where the model is based on dry deposit weight measurement.

### 5.4.3 Measurements of fouling

#### 5.4.3.1 Deposition based on heat flux measurement

A set of five heat flux sensors each was attached at 10, 20, 40, 80 and 120 mm downstream of the step of the expansion of each of test pieces A, B and C. These locations were selected to match the shear rate profiles in test piece B only, *i.e.* two locations (or sensors) were in the CRZ, one was in the reattachment region and two were in the redeveloping region. As a result, the distribution of the sensors in relation to the shear rate profiles in test pieces A and C was different. For illustration purposes, the comparative sensor locations and the shear rate profiles in test pieces A, B and C are given in Figure 5.23.

The local fouling rates in each test piece were determined from the plots of fouling curves using the same procedures as outlined in Section 4.3.1.

The residence time in each test piece (or fouling zone) was about 2 s, hence the variation in the concentration of $\beta$-lg$_{(nat)}$ between the five sensors was small and was considered negligible. Therefore, an average $C_{(nat)}$ (referred to $\beta$-lg$_{(nat)}$ concentration) was used in the calculation of the five local $Kd_{(hf)}$ in each test piece. The procedures outlined in Section 5.3.2 was used to calculate the average $C_{(nat)}$. The local deposition coefficient, $Kd_{(hf)}$ was then calculated from the local fouling rate and the corresponding average $C_{(nat)}$ by numerical solution of Equation 5.8.

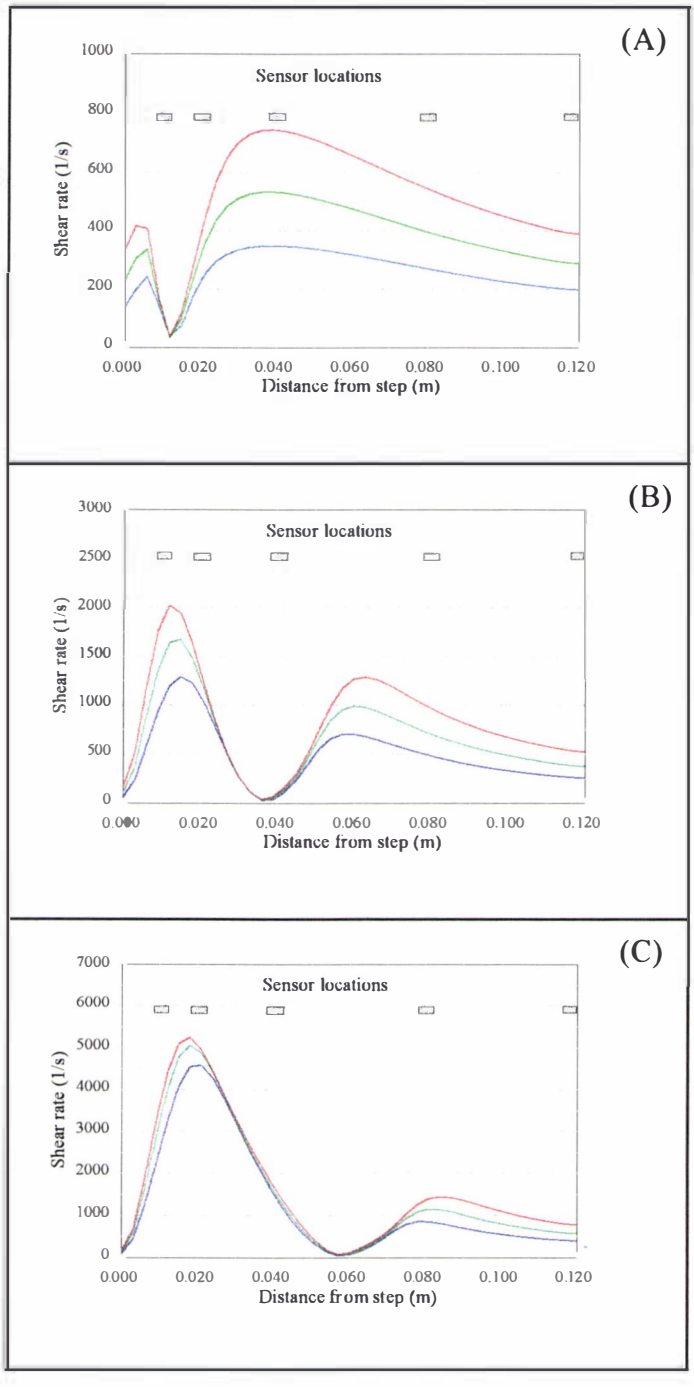


**Figure 5.23** CFD results for shear rate profiles downstream of expansions and locations of heat flux sensors: A (h=3.2 mm or d/D=0.74), B(h=6.4 mm or d/D=0.43) and C(h=9.2 mm or d/D=0.2) at 80 kg $h^{-1}$ (Blue), 100 kg $h^{-1}$ (Green) and 120 kg $h^{-1}$ (Red).

### 5.4.3.2 Deposition based on deposit weight measurements

In comparison to the deposition rate based on heat flux measurement, the deposition rate based on deposit weight measurement is an overall fouling which included the deposition both in the CRZ and the redeveloping flow regions. Similar to the calculation of the fouling rate in the CRZ (Section 5.3.2), this overall fouling rate is given by

$$\frac{d(W)}{dt} = \frac{m}{A\ t_{overall}} \qquad 5.10$$

where $t_{overall}$ is the overall fouling time which was calculated by integrating the fouling times derived from the heat flux measurements over the allocated fouled surface areas. The calculation becomes

$$t_{overall} = \frac{1}{(A_1 + \ldots + A_n)} \sum_{1}^{n} (t_1\, dA_1 + \ldots + t_n\, dA_n) \qquad 5.11$$

where n is the number of the heat flux sensors.

The fouled surface area, $A_n$, which was accounted with each heat flux sensor was determined by dividing the entire surface area of the test piece into a number of sub-areas proportional to the average distance between the adjacent sensors. Figure 5.24 shows an example of the layout of the heat flux sensors and their related sub-areas in test piece B.

The deposition coefficient, $Kd_{(wl)}$, of each fouling sub-area was then calculated from the overall fouling rate, d(W)/dt, and the average $C_{(nat)}(t)$ by numerical solution of Equation 5.9.

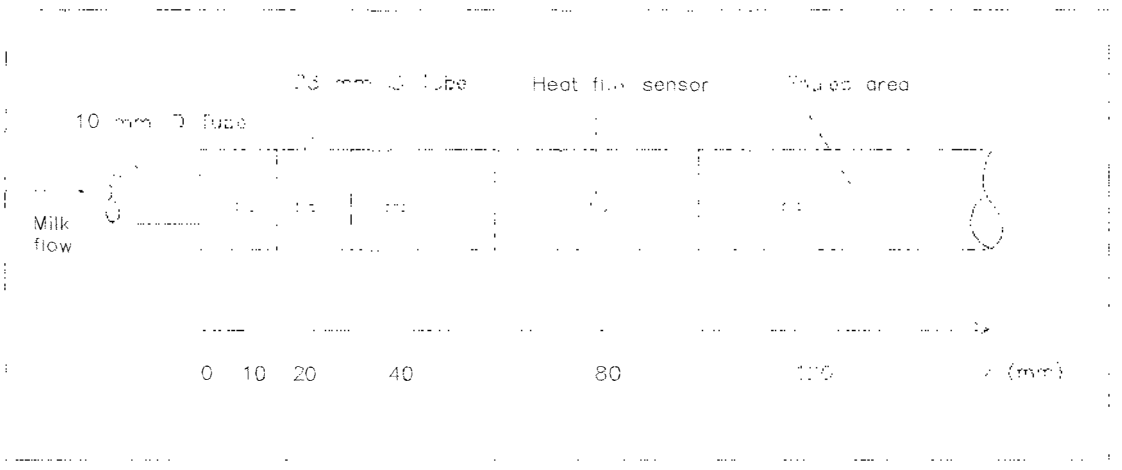


**Figure 5.24** Schematic layout of heat flux sensors and their related sub-areas.

### 5.4.3.3 The relation between $Kd_{(hf)\bullet overall}$ and $Kd_{(wt)}$

To determine whether the local depositions which were measured by the heat flux sensors could be related to the weight of deposits, the five values of local $Kd_{(hf)}$ obtained in a test piece were integrated to form an overall deposition coefficient, $Kd_{(hf)overall}$. The result was then compared to the $Kd_{(wt)}$ which was based the measurement of the deposit weight collected from the same test piece. Similar to the calculation of $t_{overall}$ (Eq. 5.11) the $Kd_{(hf)\bullet overall}$ was calculated by integrating each local $Kd_{(hf)}$ over its related sub-area. The calculation is given by

$$Kd_{(hf)overall} = \frac{1}{(A_1 + \ldots + A_n)} \sum_{1}^{n} (K_{d(hf)1}\, dA_1 + \ldots + K_{d(hf)n}\, dA_n) \quad (5.12)$$

### 5.4.4 Results and discussion

The spreadsheet calculations of the fouling rates, local and overall deposition coefficients, both based on heat flux and deposit weight measurements are listed in

Appendix 5.4. Representative results are presented and discussed below.

### 5.4.4.1 Overall fouling rates

Table 5.17 shows a summary of the results of the effects of step height and mass flow rate on the deposition coefficients $Kd_{(wt)}$ and $Kd_{(hf)overall}$ in test pieces A, B and C. The average values of $Kd_{(wt)}$ and $Kd_{(hf)overall}$ obtained from the two batches of milk were also plotted as a function of step height and mass flow rate and are shown in Figure 5.25. Generally, the results show that both $Kd_{(wt)}$ and $Kd_{(hf)overall}$, increased with increases in step height and increased with increases in mass flow rate. These results were correlated using a non-linear regression curve fitting program and the correlations are given by the following empirical equations

$$Kd_{(wt)} = 0.01\ (h)^{0.56}\ (m)^{1.18} \qquad (5.13)$$

and

$$Kd_{(hf)overall} = 0.004\ (h)^{0.74}\ (m)^{1.37} \qquad (5.14)$$

The results show that the effect on both $Kd_{(wt)}$ and $Kd_{(hf)overall}$ of the mass flow rate was about twice of the effect of the step height. This means that, for the range of conditions used in this study (*i.e.* step height was nearly tripled and but flow rate was only increased by 1.5 times), mass flow rate has a stronger effect on the fouling rate than the step height.

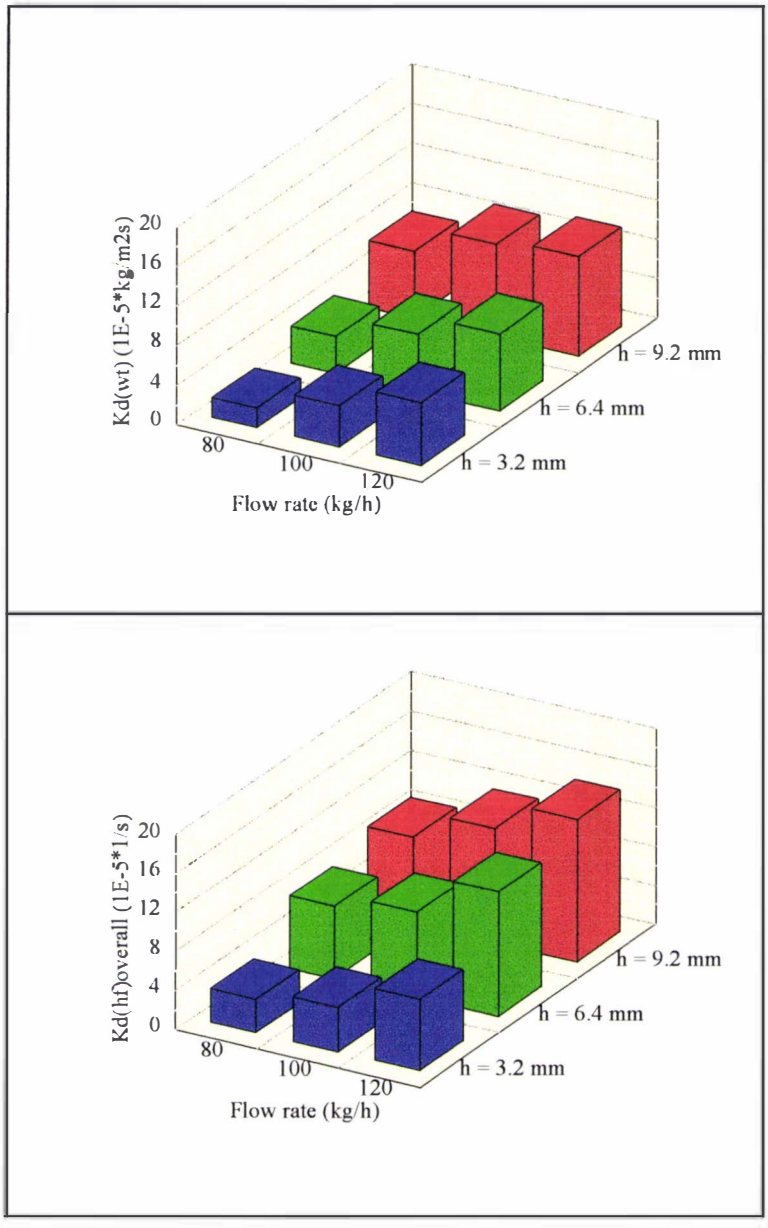


**Figure 5.25** Plots of deposition coefficients $Kd_{(wt)}$ and $Kd_{(hf)overall}$ as a function of mass flow rate and step height.

**Table 5.17** Summary of results of the effects of step height and mass flow rate on overall fouling

| | | $Kd_{(wt)}$ ($10^{-5}$*kg $m^{-2}$ $s^{-1}$) | | | $Kd_{(hf)overall}$ ($10^{-5}$ $s^{-1}$) | | |
|---|---|---|---|---|---|---|---|
| **Step height** | | **3.2 mm** | **6.4 mm** | **9.2 mm** | **3.2 mm** | **6.4 mm** | **9.2 mm** |
| **Milk F** | **80 kg $h^{-1}$** | 3.4 | 5.5 | 7.8 | 4.9 | 9.8 | 12.2 |
| | **100 kg $h^{-1}$** | 5.2 | 6.7 | 10.3 | 6.2 | 8.1 | 12.8 |
| | **120 kg $h^{-1}$** | 7.4 | 8.1 | 11.7 | 5.9 | 12.7 | 15.9 |
| **Milk G** | **80 kg $h^{-1}$** | 0.6 | 2.0 | 5.8 | 2.0 | 5.0 | 5.7 |
| | **100 kg $h^{-1}$** | 3.1 | 5.0 | 8.5 | 2.9 | 9.2 | 10.6 |
| | **120 kg $h^{-1}$** | 5.5 | 7.5 | 8.4 | 8.6 | 12.7 | 13.3 |
| **Ave-rage** | **80 kg $h^{-1}$** | 2 | 3.7 | 6.8 | 3.4 | 7.4 | 8.9 |
| | **100 kg $h^{-1}$** | 4.2 | 5.9 | 9.4 | 4.5 | 8.7 | 11.7 |
| | **120 kg $h^{-1}$** | 6.4 | 7.8 | 10 | 7.3 | 12.7 | 14.6 |

The results confirmed the findings of the previous experiments (Section 5.2.2.2) that increase in the mass flow rate increased the fouling rate. CFD modelling suggested that the influence of flow rate could be due to the enhanced mass transfer which in turn was characterised by the decrease in the thickness of the viscous sub-layer. A similar effect has also been found in a pulsatile heat exchanger, in which a high fluid velocity arose when an oscillating flow was applied (Bradley & Fryer, 1992). In the case where the bulk fluid was hot enough to denature the whey proteins (*i.e.* resemble fouling of non-heated surface) the pulsed flow enhanced mass transfer of reacted proteins to the wall and hence increased the deposition.

In contrast, it was shown, in indirect heating equipment such as tubular and plate heat exchangers, that the rate and the amount of fouling decreased with increasing fluid flow rate (or Reynolds number) (Gordon *et al.*, 1968; Belmar-Beiny *et al.*, 1993). It was

demonstrated that fouling in a tubular heat exchanger was related to the volume of a wall layer that was hot enough for protein denaturation (Gotham *et al.*, 1989). Hence, if the flow rate was increased, the volume of the 'hot wall' would decrease and so the amount of deposit would decrease. The effect of flow rate on fouling was thought to be caused by both the reduced temperature gradient at the heating surface-milk fluid interface and the increased shear stress at the interface.

In practice, to minimise fouling in heat exchangers, high flow mass rate is therefore commonly used (Bott, 1995). The results of this study suggest that to reduce deposition of heated whole milk onto non-heated surfaces, a low mass flow rate or a relatively high volume to surface area ratio should be used and flow disturbance should be minimal if they can not be avoided.

### 5.4.4.2 Local fouling rates

The calculated local deposition coefficients, $Kd_{(hf)}$, for the five locations downstream of the test pieces A, B and C at different mass flow rates are shown in Figure 5.26. Generally, the results show a similar trend compared to the deposition coefficients based on deposit weight measurements (Figure 5.25). Increase in both the step height and mass flow rate was found to increase the local fouling rate downstream of the step.

Variations of $Kd_{(hf)}$ with the distance from the step observed from different levels of step height and mass flow rate were very similar. For example, for test piece C (Figure 5.26 C), $Kd_{(hf)}$ started at an intermediate level in locations near the step, increased to a maximum level and then gradually decreased in locations downstream. Although the results obtained with test pieces B and C did not show a consistent pattern (Figures 5.26 B and C), it was thought that the difference was probably due to the effects of local deposition on the local flow pattern or the sensors were not positioned to the 'ideal' locations.

The earlier results (*e.g.* Figure 5.12) which were obtained with test piece B geometry (h=6.4 mm), showed that the maximum fouling rate occurred in the area near the end of the CRZ or in the vicinity of the reattachment point (*i.e.* at about 40 mm from the step). The results obtained with test piece B from this experiment (Figure 5.25B) support the previous findings (Figure 5.12).

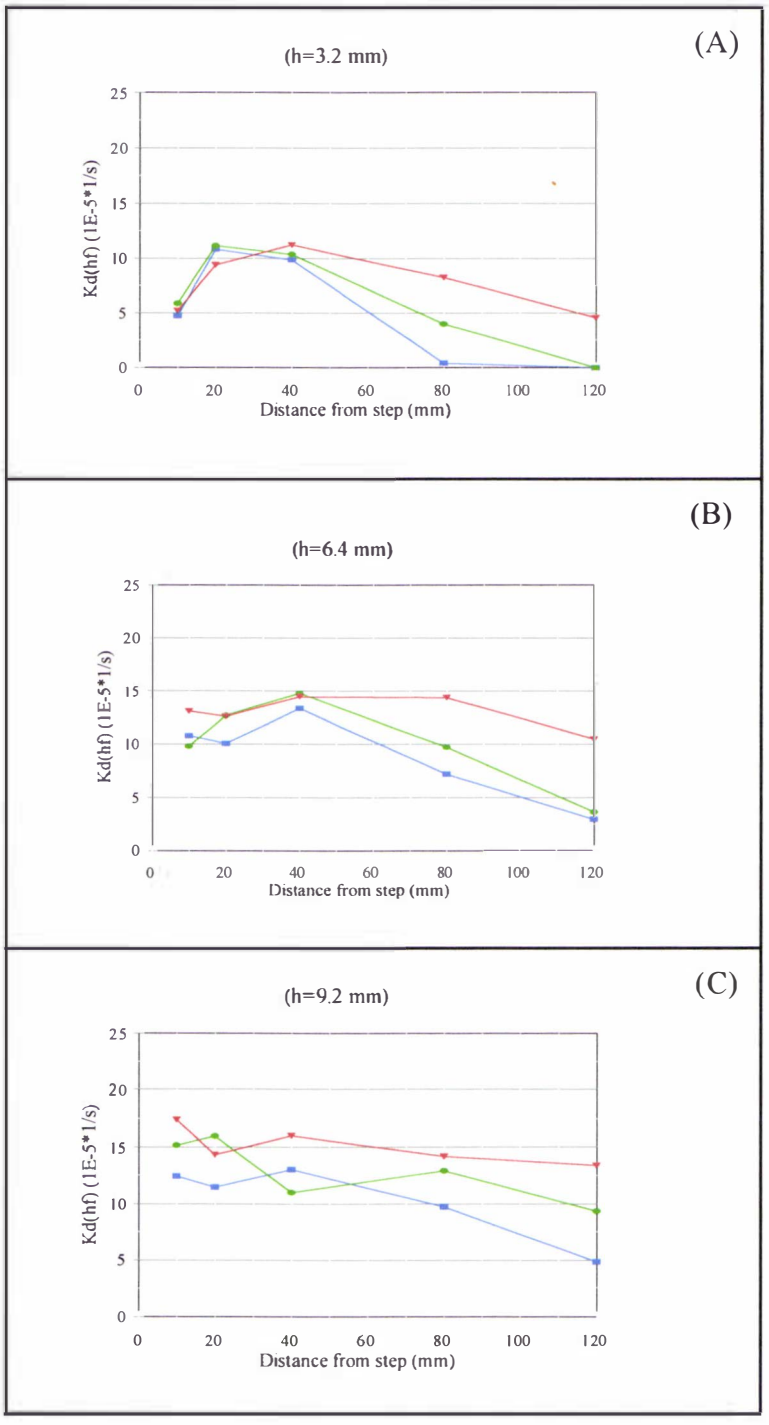


**Figure 5.26** Plots of local deposition coefficient, Kd(hf) versus distance from step for test pieces A (h=3.2 mm), B (h=6.4 mm) and C (h=9.2 mm): (Red) 120 kg $h^{-1}$, (Green) 100 kg $h^{-1}$ and (Blue) 80 kg $h^{-1}$.

### 5.4.4.3 The relation between $Kd_{(hf)\ overall}$ and $Kd_{(wt)}$

Figure 5.27 shows plots of $Kd_{(hf)\ overall}$ versus $Kd_{(wt)}$ obtained from the measurements of fouling in test pieces A, B and C. $Kd_{(hf)\ overall}$ represents the overall fouling rate derived from up to five local fouling measurements in each test piece. $Kd_{(wt)}$ represents direct quantification of the accumulation of deposits on to the surface area of each test piece. When compared with the previous results (Section 5.3.3, Figure 5.21), the line of the fitted data of the two measurement methods exhibited a similar shape and trend. It should be noted that the length of the test pieces used in this set of experiments was 160 mm, whereas test pieces of 40 mm long were used in the previous experiments. Hence, absolute fouling rates of the two series of experiments were different and therefore could not be directly compared.

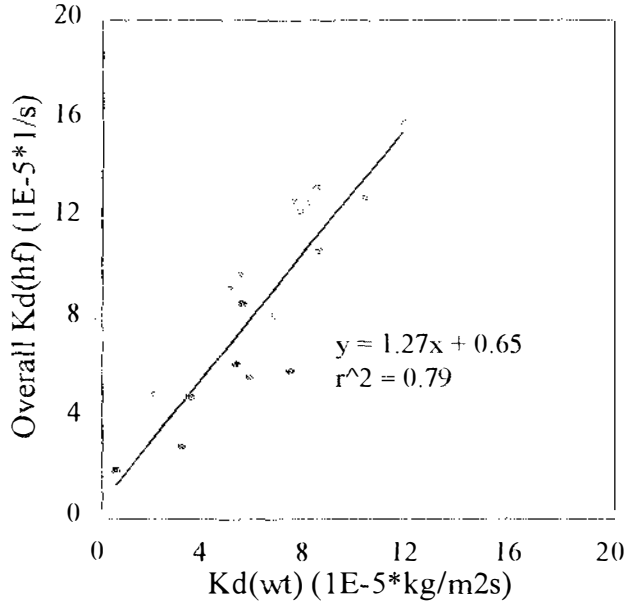


**Figure 5.27** Relation between $Kd_{(hf)\ overall}$ and $Kd_{(wt)}$: (red) h=9.2 mm; (green) h=6.4 mm, (blue) h=3.2 mm and (black line) linear fit data.

The variance value, $r^2$, of this set of data was 0.79 compared with the value of 0.74 obtained from those runs for a single sensor (Figure 5.21). The use of multiple sensors slightly reduced the amount of scatter of the data and the results exhibit a closer relation between local and overall fouling measurements. The results indicate that overall fouling in an area can be reliably estimated from local fouling measurement. Increasing the number of local measurements may slightly increase the accuracy of the estimation. However, the increased level of calculations may not make this a practical exercise.

### 5.4.5 Concluding remarks

The results obtained in this section show that:

(1) Step height and mass flow rate are both important factors affecting fouling downstream of a sudden expansion. Within the range of conditions used in this study, mass flow rate has a stronger effect on fouling than the step height.

(2) The overall fouling (*i.e.* mass deposition) in an area can be estimated from local fouling measurements using heat flux sensors. Increasing the number of local measurements slightly increases the reliability of the estimation.

## 5.5 CONCLUSIONS

The results of this study show the important aspects of local fouling of whole milk heated to 95°C on to non-heated surfaces. They are:

- The use of a simple tubular sudden expansion to study the effects of flow geometry on fouling is effective. It can provide various flow conditions such as recirculation and redeveloping flows within a single experiment. Such flow conditions enhance the mass transfer and induce increased fouling.

- CFD is an useful tool for predicting flow patterns and properties such as shear rate and apparent viscosity profiles in the sudden expansion.

- The deposition is strongly affected by flow conditions that enhance mass transfer between the bulk milk and the solid surfaces. Increasing the mass transfer rate will increase the fouling rate. This is in contrast with heated surfaces where the reverse is true.

- The local mass transfer rate is closely related to changes in the surface shear rate and the thickness of the viscous-sub-layer at the solid surface.

- A close analysis of the flow patterns in the fouling zone is useful for positioning of the local sensors in order to relate the effects of local flow geometry on local deposition.

- The overall fouling rate in a fouling zone can be estimated from a local fouling rate measured within that zone. Increasing the number of local measurements slightly increases the reliability of the estimation.

- The composition of the deposit confirms that β-lg is a major element in forming the protein content of the milk deposits.

- The β-lg content of the deposits is independent of the local absolute concentration of remaining native $\beta\text{-lg}_{(nat)}$ in the bulk milk.

- The local fouling rate depends on the local concentration of $\beta\text{-lg}_{(nat)}$, which in turn can be related to the local concentration of active $\beta\text{-lg}^{*}$.

- The local fouling rate in different locations, *i.e.* different elapsed times after the heat treatment, can be normalised with its concentration of $\beta\text{-lg}_{(nat)}$ to give a unit value of fouling consistent for a particular set of conditions.

CHAPTER 6

# MONITORING OF FOULING IN LARGE-SCALE EVAPORATOR PLANT

CONTENTS

## 6.1 INTRODUCTION

This chapter reports the measurements of local fouling in the downstream areas of the DSI heater in large-scale milk evaporators in milk powder plants. The main objectives of the study were to test the fouling monitoring system and to obtain fouling data from the commercial plants.

## 6.2 METHODS

### 6.2.1 Process plant layout

The facility used for the measurements was the Kiwi Co-operative Dairies Limited, Hawera site. This is located near the West Coast of the North Island of New Zealand. Kiwi Co-operative Dairies is the largest milk processing site in NZ and can process up to 15 million litres of milk per day.

Measurements were made in the holding tubes of four evaporators (called A, B, C and D) of the milk powder plants on the Hawera site. The evaporators are mainly four-effect falling film evaporator type. The first two effects are heated by mechanical vapour recompression (MVR) and the last two effects are heated by thermal vapour recompression (TVR). The evaporation rate is 50,000 kg $h^{-1}$ when concentrating whole milk from 12 to 50% w/w total solids except one plant has a smaller capacity of 32,000 kg $h^{-1}$ (plant D).

The milk, at about 10°C, is initially preheated in a plate heat exchanger utilising the heat of the milk condensate from the TVR. It then goes through the tubular heat exchangers where the milk condensate from the MVR heats the milk to a progressively higher temperature. On high heat treatment conditions, the milk exits the last heater at about 70°C. It then enters two steam infusion vessels which are placed in series and are

situated on the top of two flash vessels. The vapours heating the milk in the steam infusion vessels are from the flash vapours (from the flash vessels) occurring due to the milk being cooled down prior to entering the evaporator. The milk leaving the steam infusion vessels which is now at about 80°C is further heated to a higher temperature via the DSI heater. The milk then enters the holding tubes, is sequentially flash cooled in the two flash vessels and then enters the top of the first evaporator-effect to be evaporated. Figure 6.1 shows a schematic drawing of the DSI process in the industrial-scale evaporator plant.

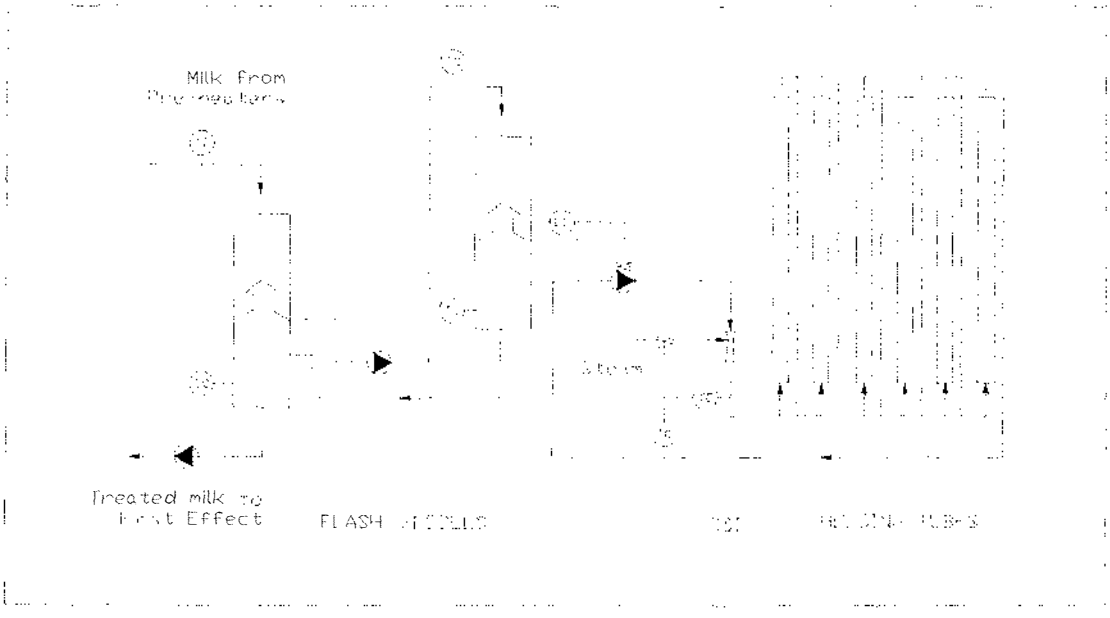


**Figure 6.1** Schematic drawing of a typical direct steam injection (DSI) process in large-scale plant: (TC) temperature control; (LC) level control.

### 6.2.2 Monitoring of fouling

Fouling in downstream areas of the DSI heater was monitored with heat flux sensors attached to the outside surface of the holding tubes. Measurements were performed on several periods during the 1997, 1998 and 1999 dairying seasons. Each measurement period included ten consecutive production runs, except for skim milk run, due to production schedule, only one measurement was made. Each production run was up to 24 h plus 3 h shut-down for cleaning. Only representative runs, in particular, those that were operated without disruption due to production problems will be reported and discussed in this chapter.

Up to four sensors were used in any single run to give an idea of the geometric distribution of fouling inside the pipe. Attachment of sensors, logging of data and calculations of heat flux, internal heat transfer coefficient and fouling rate were the same procedures set out in Chapter 4. Runs were monitored for skim milk, modified skim milk, whole milk and modified whole milk. A summary of fouling monitoring conditions is listed in Table 6.1. Figure 6.2 shows photographs of a DSI heater in plant C showing the attachment of sensors.

Because of the required production schedules, it was only possible to open plant B (run 6.3) and plant D (run 6.6) at the completion of the production runs for visual inspections. During these inspections, deposit samples were also removed from the pipes using a sharp and long plate. The thickness of the deposit samples, collected from the marked area of the heat flux sensors, was measured using a micrometer. Two measurements were made, each on the central line of the samples, in the axial direction, at 4 mm from the upstream edge and 5 mm apart. The result was taken as the average of the two measurements. The samples were then weighed , frozen at -18 °C and freeze-dried. The dried samples were weighed again and analysed for the contents of protein (as total nitrogen), fat and minerals (as dry ash). Some of the wet samples were also

buffered glutaraldehyde/formaldehyde, dehydrated using acetone and air dried. The internal structures of the dried samples were determined by cutting the samples transversally using a stainless steel razor blade. They were then gold coated and scanned in a Cambridge 250 Mark 3 scanning electron microscope (SEM).

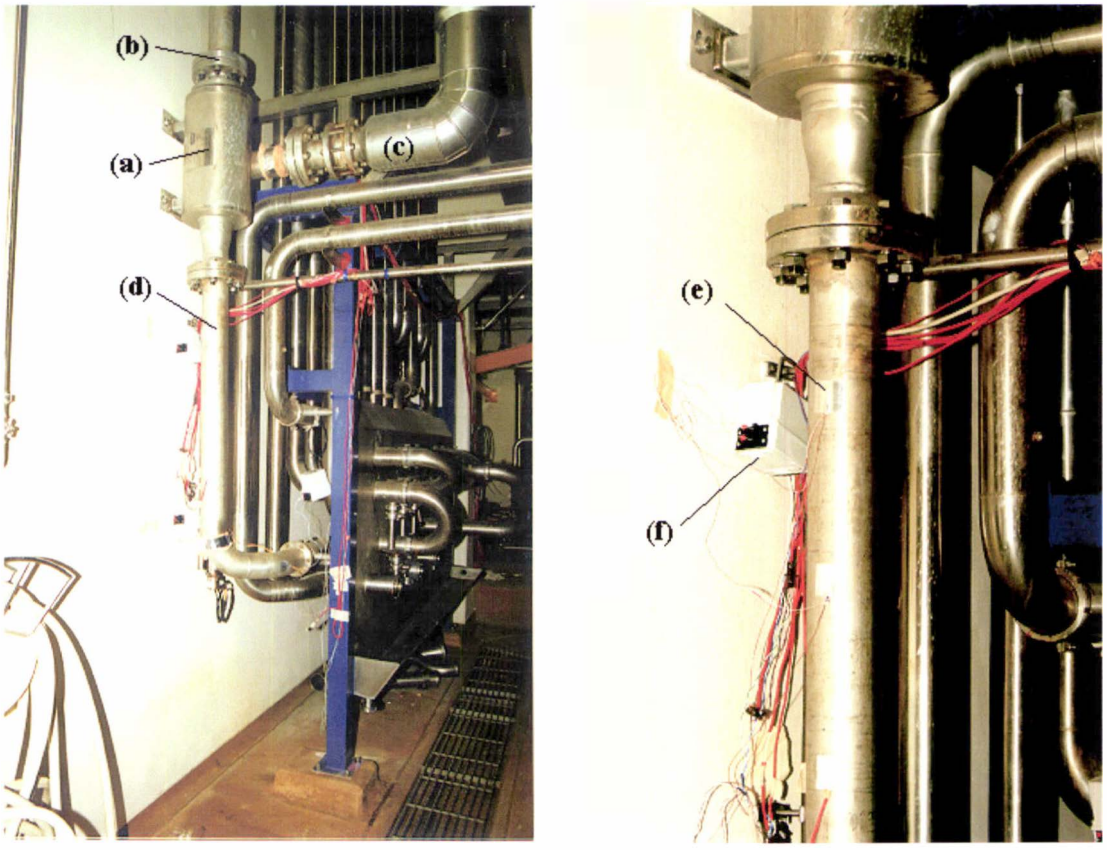


**Figure 6.2** Photographs of direct steam injection (DSI) heater and attachment of heat flux sensors in plant C: (a) DSI unit; (b) milk inlet; (c) steam inlet; (d) DSI outlet; (e) heat flux sensor; (f) transmitter.

**Table 6.1** Summary of fouling monitoring conditions in large-scale DSI heaters

| Run | Plant | Treatment Temp. (°C) | Milk Fluid | Sensor Location |
|---|---|---|---|---|
| 6.1 | A | 95 | Whole milk | One sensor on the vertical pipe section downstream of DSI outlet (distance L/D=3; D=98mm) |
| 6.2 | A | 98 | Skim milk | Same location as Run 6.1 |
| 6.3 | B | 105 | Whole milk | Two sensors on the vertical pipe downstream of DSI outlet (L/D=5, 8; D=98mm) |
| 6.4 | B | 115 | Modified whole milk | Same location as Run 6.3 |
| 6.5 | C | 95 | Whole milk | Four sensors on the vertical pipe downstream of DSI outlet (L/D=5, 8, 11, 21; D=98mm) |
| 6.6 | D | 92 | Modified skim milk | Four sensors on the vertical pipe downstream of orifice plate (L/D=1, 3, 5, 11; D=83mm) |

## 6.3 RESULTS AND DISCUSSION

### 6.3.1 Fouling curves

Comparative fouling curves obtained from four different milk fluids are shown in Figure 6.3. Due to the required production schedules, skim milk (run 6.2) and modified whole milk (run 6.4) runs were shorter than whole milk (run 6.3) and modified skim milk (run 6.6) runs. Heat flux measurements were at the same locations, which were equivalent to L/D=5 downstream of the DSI, except for run 6.2, L/D=3.

There was no detectable fouling with skim milk and modified whole milk runs, *i.e.* the normalised internal heat transfer coefficient, $I_f$, remained almost constant during the entire production periods. The fouling curves for whole milk and modified skim milk runs both exhibited, after a short delay period, a sustained decrease in $I_f$ with run time. The variations in the fouling patterns of four different milk fluids were very similar to those observed with heated whole milk in the fouling rig (Chapter 4). The differences in the fouling behaviours of skim milk (run 6.2), whole milk (run 6.3), modified whole milk (run 6.4) and modified skim milk (run 6.6) indicate, in addition to β-lg, other milk components also have a major role on the fouling process. For example, skim milk and whole milk show markedly different fouling behaviour even though their β-lg contents (on a SNF basis) are similar (Table 2.1). There may be a direct interaction between active β-lg and the fat, via the proteins of the milk fat globule membranes (*e.g.* Corredig & Dalgleish, 1996c), that enhances the interactions of fat with the fouling deposits. Further studies on the roles of milk constituents on fouling are warranted.

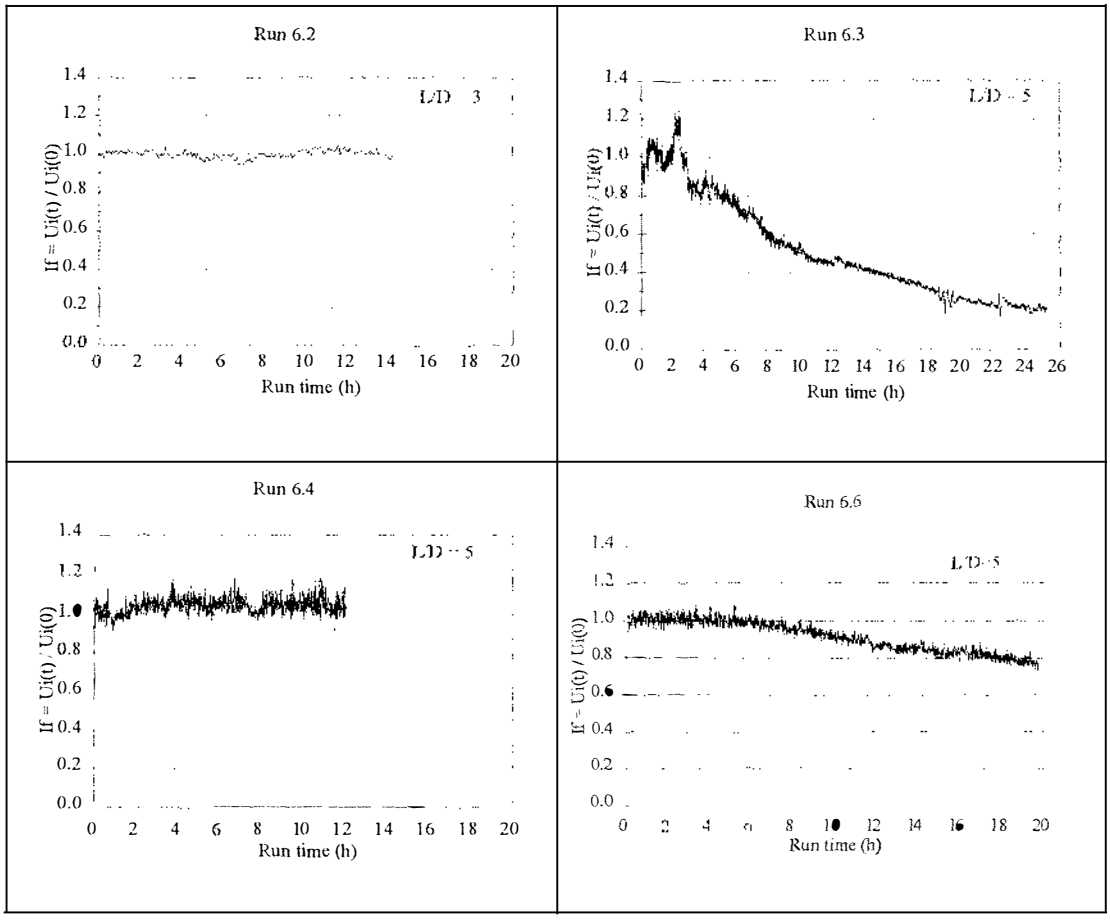


**Figure 6.3** Comparative fouling of different milk fluids:

Run 6.2: skim milk, heated to 95°C in plant A;

Run 6.3: whole milk, heated to 105°C in plant B;

Run 6.4: modified whole milk, heated to 115°C in plant B;

Run 6.6: modified skim milk, heated to 92°C in plant D.

Figure 6.4 shows the comparative fouling curves of heated whole milk obtained from evaporator plants A, B and C (*i.e.* runs 6.1, 6.3 and 6.5). The graphs show that the fouling behaviours of these runs were different. The fouling rates observed in plants A and B were about four times higher that observed in plant C (Table 6.2). Although the milk properties between runs were not the same, it was probably that the differences in the treatment temperature and configuration of the DSI heaters that affected the rate and extent of fouling in these plants.

The DSI heaters in plants A and B consist of a single unit whereas the DSI in plant C has two units connected in series. This arrangement results in a small temperature difference between milk and steam in each unit and hence over-heating of milk by steam bubbles is unlikely. Thus fouling would be reduced.

**Table 6.2** Fouling characteristics of whole milk in large-scale DSI heaters

| Run | Plant | Treatment Temp. (°C) | Milk Fluid | Deposit Thickness (mm) | $I_f$ at End of Run | Fouling Rate (1/h) |
|---|---|---|---|---|---|---|
| 6.1 | A | 95 | Whole milk | nm | 0.45 | 0.056 |
| 6.3 | B | 105 | Whole milk | 6.5 | 0.20 | 0.064 |
| 6.5 | C | 95 | Whole milk | nm | 0.85 | 0.011 |

nm: not measured

Another characteristic of the fouling curves observed from plants A and B was that they exhibited a reduced fouling rate with run time. This characteristic was similar to that observed in the fouling rig (Section 4.3.2). As previously discussed, increases in the deposit thickness could cause a decrease in $R_m$ and an increase in fluid velocity and hence $U_i(0)$ reduced. Consequently, the relative change in $U_i(t)/U_i(0)$ with run time reduced as the deposit layer continued to grow.

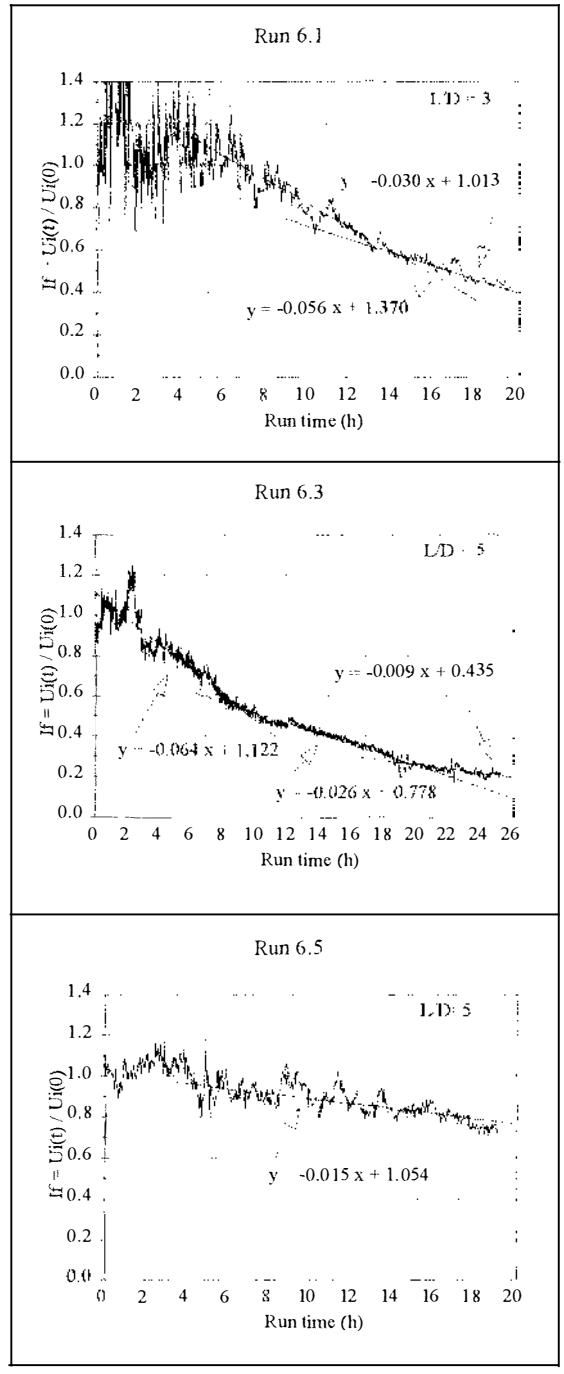


**Figure 6.4** Comparative fouling of whole milk in different evaporators:
Run 6.1: whole milk heated to 95°C in plant A;
Run 6.3: whole milk, heated to 105°C in plant B;
Run 6.5: whole milk, heated to 95°C in plant C.

The results of run 6.1 with whole milk also show that the fluctuations of $I_f$ observed in the initial stages were large then gradually decreased as $I_f$ decreased with run time. In contrast, the graph for run 6.1 with skim milk shows very small fluctuations through out the run. As previously discussed in Chapter 4, the fluctuations of $I_f$ were probably due to the induced turbulence due to variations in deposit roughness. However, the reason why large fluctuations were observed only in plant A is unknown.

A number of 'saw tooths' are observed, in particular, from the plot of run 6.5 (Figure 6.4). This was probably because some of the deposits detached from the surfaces due to turbulent flow and then later refouled (the Reynolds number in the pipe was calculated at 425 000).

### 6.3.2 Effects of local geometry on fouling

Local equipment geometry was found to have a strong effect on fouling behaviour in the large-scale plants. The results of two runs 6.5 and 6.6 (shown in Figures 6.5 and 6.6 respectively) illustrate the effect. In run 6.5, the sensors were placed at 4 different locations immediately downstream of the DSI outlet and in run 6.6, at 4 different locations downstream of an orifice plate. This orifice plate was located at 1200 mm (or L/D = 14) from the DSI outlet of that plant. Fouling was most significant at the location either close to the DSI outlet or the orifice plate. At locations further downstream, fouling was less and then became negligible at the farthest locations. The results indicate that a change either in local hydrodynamic (by steam injection) or in local geometry (by an orifice plate) can induce fouling.

The fouling patterns downstream from the DSI outlet and the orifice plate observed in plants C and D matched very well the patterns downstream from the sudden expansion observed in the fouling rig, even though the milk type, and in particular, fluid flow (*i.e.* turbulent versus laminar flow) in these plants were very different. The influence of

flow disturbance on fouling in plants C and D can therefore be considered to be due to mass transfer of 'active species' to the solid surfaces rather than shear stress effects (caused by turbulent flow).

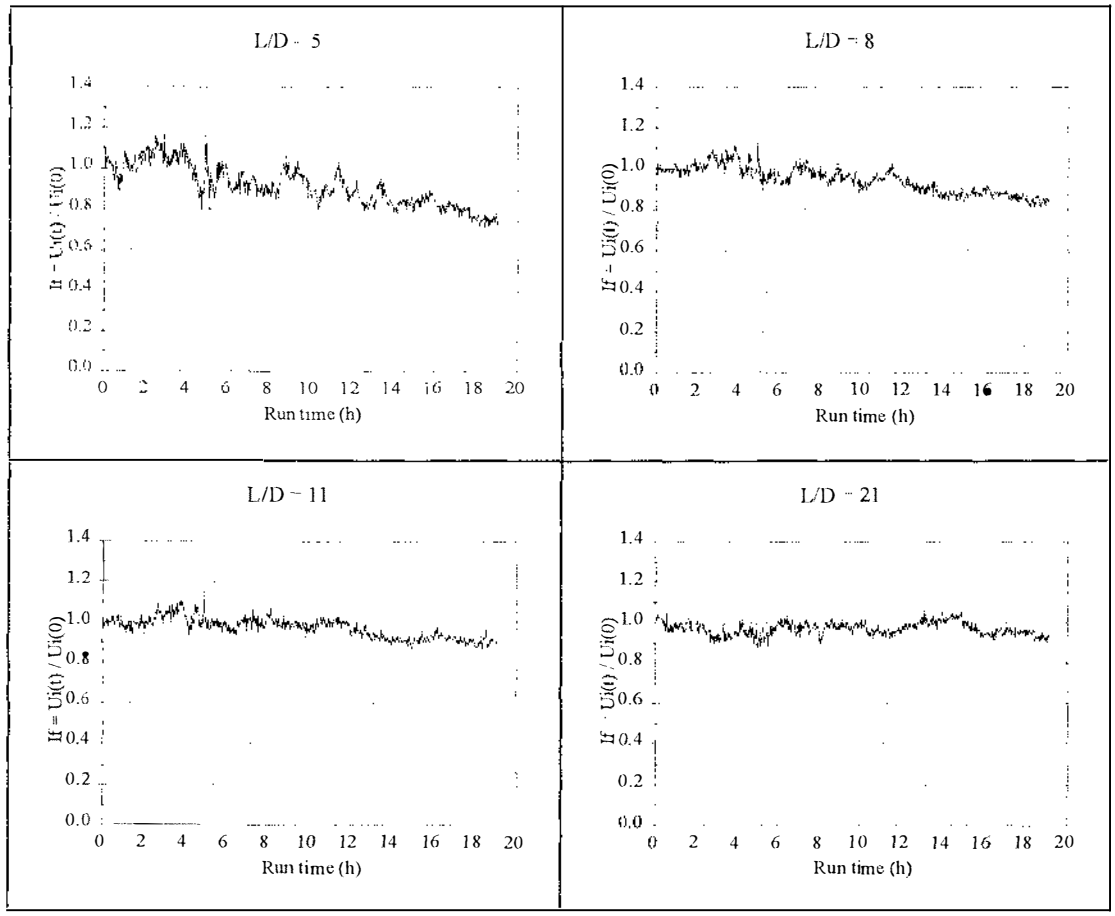


**Figure 6.5** Comparative fouling of whole milk in four locations downstream of the DSI heater in plant C (run 6.5); L/D = distance from DSI outlet to pipe diameter ratio.

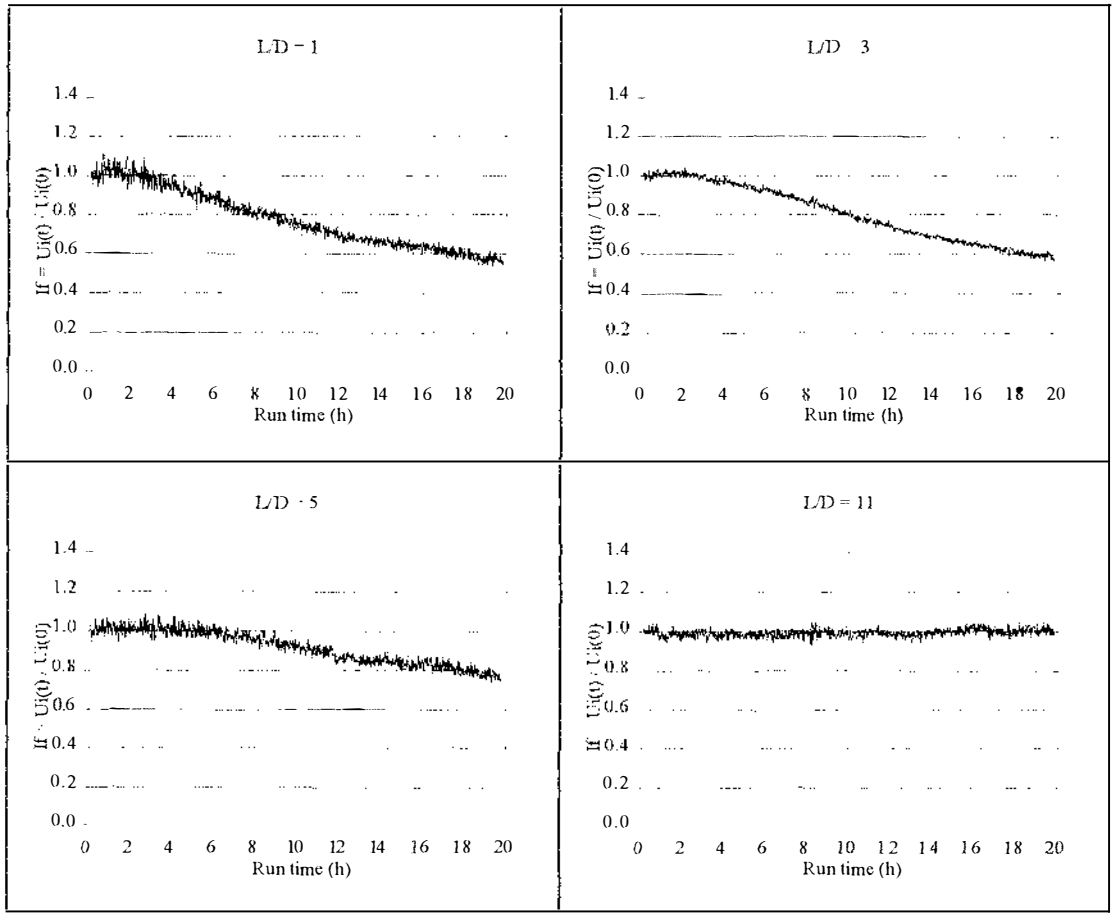


**Figure 6.6** Comparative fouling of modified skim milk in four locations downstream of the orifice plate in plant D (run 6.6); L/D = distance from orifice to pipe diameter ratio.

### 6.3.3 Characteristics of fouling deposits

The results of deposit composition and thickness obtained from plants B and D (runs 6.3 and 6.6 respectively) are listed in Table 6.3. The deposits for plant B were collected in the area located at eight pipe diameters from the DSI outlet (L/D = 8) and at a pipe diameter from the orifice plate (L/D = 1) for plant D. The composition of a deposit sample collected from run 5.13 of the fouling rig was also included for comparison and discussion purposes.

The deposits all contained mainly protein, fat (excluding modified skim milk) and minerals. The results indicate that the deposits resemble type A deposit as defined by Burton (1968), *i.e.* high protein (60%) and low mineral (30%) deposits. The sum of the fat, protein and ash contents (on a dry weight basis) of each sample was not 100%; the fouling layer might have contained other components such as lactose for which measurements were not made.

Deposits from modified skim milk contained slightly more minerals than those from whole milk. The fat content of deposits from the fouling rig (49.7%) was much higher than that observed in plant B (3.2%) (run 6.3). Storage of milk for four days before the experiment may have contributed to the result. As previously discussed, the milk fat globules may become involved in the fouling process by the interaction of the proteins of the membranes, which could have been damaged during storage, with active β-lg (*e.g.* Corredig & Dalgleish, 1996c).

**Table 6.3** Composition and chacrateristics of fouling deposits in fouling rig and large-scale DSI heaters

| Run | Milk Fluid | Deposit Thickness (mm) | $I_f$ at End of Run | Moisture (%) | Composition (% w/w, dry basis) | | |
|---|---|---|---|---|---|---|---|
| | | | | | Protein | Fat | Ash |
| 5.13 | Whole milk | nd | nd | nd | 35.3 | 49.7 | 4.3 |
| 6.3 | Whole milk | 6.5 | 0.32 | 50.2 | 63.8 | 3.2 | 20.1 |
| 6.6 | Modified skim milk | 3.1 | 0.55 | 45.2 | 57.4 | nd | 28.1 |

nd: not determined

Figure 6.7 shows photographs of deposits inside plants B and D taken at the completion of the production runs. Figure 6.8 shows the structure of these deposit samples as examined by SEM. Photographs of deposits inside test piece B geometry and SEM structure of a deposit sample collected from run 5.13 of the fouling rig (Appendix 4.3) were also included for comparison purposes.

The deposit layers observed in large-scale plants were dense, hard and compact and their surfaces were uniform. The deposit layer in the test piece appeared soft, voluminous, uneven and contained high 'hills' and deep 'valleys'. The SEM results confirmed these observations. Although the internal structures of deposits obtained in large-scale plants and in the fouling rig were very similar, *i.e.* they all composed of small particles of different sizes and were randomly linked by bridges and strands, the internal structures of deposits in plants B and D were more dense and compact than those in the fouling rig. Several dense blocks of particles were also observed within these structures. Even though higher treatment temperature or compositional

modification could have some effects on the deposit structure, it is thought that, the high prevailing fluid velocity and shear force in plants B and D (*i.e.* 1.8 m $s^{-1}$ and Reynolds number of 425000) led to formation of a compact and dense fouling layer. Whereas, in the fouling rig, in the presence of a much lower fluid velocity and shear force (0.08 m $s^{-1}$ and Reynolds number of 3800) the deposits were soft and more porous. This demonstrates a problem in comparison between the research and industrial system and it may have implication on the development of fouling models.

The results also show that the deposits collected from the large-scale plants and from the fouling rig all composed of a compact sub-layer and a porous top layer. These structures resembles those observed by previous researchers (Tissier *et al.*, 1984; Lalande *et al.*, 1985; Foster *et al.*, 1989). However, because a sub-layer was always observed in this study despite the fact that runs in the large-scale plants were much longer and the treatment temperature, milk type and hydrodynamics conditions were different from those employed in the fouling rig, it is suggested that this sub-layer developed and grew to a certain thickness (of about 20 μm) first, then 'fouling species' began to cover this surface and formed a top-layer. Further work to determine the formation of this sub-layer is recommended. For example, if the formation of this layer could be prevented or delayed, fouling could be reduced and production run could be extended.

The difference between the structures of deposits in the fouling rig and large-scale plants highlights the possibility that the $I_f$ - deposit thickness relationship obtained from the fouling rig may not represent the fouling behaviours inside large-scale plant. Hence further calibration of the monitoring device, in particular, under high prevailing fluid velocity and for different fluid compositions is needed. Similarly, makedly different treatment temperatures may produce more mineralised deposits and therefore different $I_f$ versus deposit thickness relationship (*e.g.* Figure 4.14). Hence, calibration of the device at different treatment temperatures is also needed.

(1)

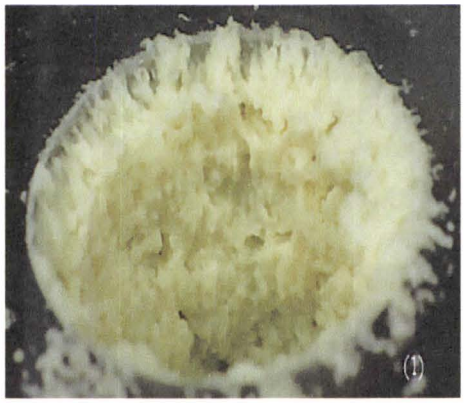

(2)

(3)

**Figure 6.7** Photographs of deposits: (1) whole milk heated to 95°C inside the test piece in fouling rig, inside pipe diameter ID=23 mm; (2) whole milk heated to 105°C in plant B, ID=98 mm; (3) modified skim milk heated to 92°C in plant D, ID=83 mm.

(1)

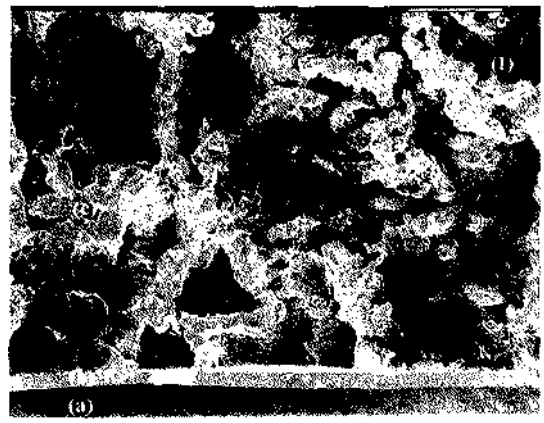


(2)

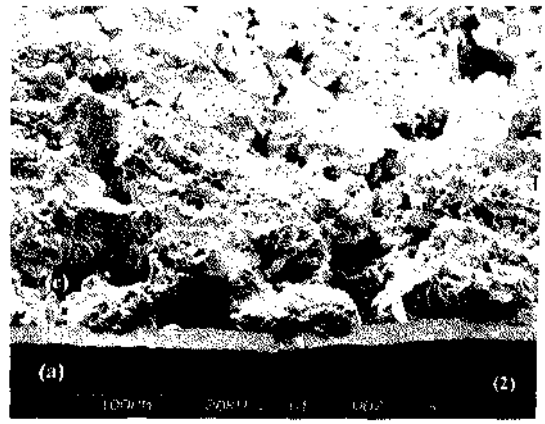


(3)

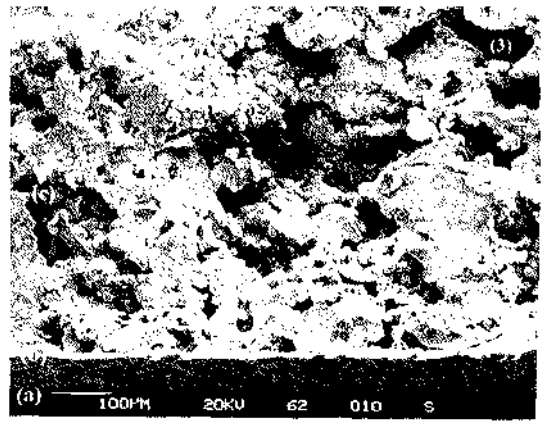


**Figure 6.8** Scanning electron micrographs of deposit structures: (1) whole milk heated to 95°C in the fouling rig; (2) whole milk heated to 105°C in plant B and (3) modified skim milk heated to 92°C in plant D. (a) stainless steel surface; (b) sub-layer and (C) top-layer.

## 6.4 CONCLUDING REMARKS

Fouling downstream of large-scale DSI heater can be monitored with heat flux sensors attached to the outside of the unheated pipes. This technique allowed attachment of fouling probes at various locations in plant without significant disturbance to the routine operations. The sensor was capable of detecting the growth and the extent of the deposit layer during processing. The rate of fouling depends on treatment temperature and milk composition. Flow irregularities caused by change in directions increases fouling.

Design of the DSI heater can be improved to include more than one heating unit to reduce fouling. Design of the holding tubes can also be improved to eliminate sudden expansion and to increase volume to surface ratio to minimise flow disturbances.

Determination of $I_f$ - deposit thickness relationship to correlate the heat flux data to the fouling behaviour occuring inside large-scale plant is needed.

CHAPTER 7

# FINAL DISCUSSION AND CONCLUSIONS

CONTENTS

## 7.1 OBJECTIVES OF THE PRESENT STUDY

This work has set out to

- have a robust and reliable system for measuring the rate and extent of fouling,
- obtain a better understanding of the fouling behaviour of heated milk fluids onto non-heated surfaces, and
- identify factors that affect the fouling deposition.

The focus has been to investigate fouling as a "local" as distinct from a "whole plant" phenomenon. Conditions such as temperature and fluid velocity can vary over the solid surfaces within a plant and result in different rates of deposition at different locations. It is important to know where the deposition occurs within the plant and what controlling processes are. The information will permit the improvement of plant design and the development of operating procedures that minimise local fouling.

Direct heating of milk fluids with steam is preferred over indirect heating in the New Zealand dairy industry, due to its rapid heating rates, which result in higher quality product. With direct heating, in particular for whole milk, deposits of insoluble materials can form over time of operation. These are observed on the solid surfaces downstream of the DSI heater even when these surfaces are not heated.

In this study the effects of mass flow rate and flow geometry of whole milk heated with steam to 95°C were investigated. Literature indicates that, at temperatures below 100°C, the proteins play a predominant role in the fouling process of heating surfaces (*i.e.* heat exchangers). At about this temperature, the proteins could also play a major role in the fouling process of heated whole milk onto non-heated surfaces.

Custom built stainless steel tubular expansion fouling test sections were developed. To measure fouling rate at various locations in these test sections, a system, which includes commercial heat flux sensors to measure local fouling, was developed. A custom built fouling rig was also developed for calibrating this monitoring system. A series of experiments that mimicked the heat treatment methods and conditions that are currently used in industrial-scale evaporator plants was carried out for this purpose.

Investigation of the fouling behaviour of heated milk fluids in industrial-scale evaporator plants was carried out to test the fouling monitoring system and to obtain real time fouling data.

## 7.2 SUMMARY OF RESULTS

This study provided new information about deposition of heated milk onto non-heated surfaces. Here is a summary of discoveries and discussions.

### 7.2.1 Fouling monitoring system

This study represented the first instance that a commercial heat flux sensor been used to measure the change in heat flux due to fouling of non-heated surfaces. The use of the heat flux sensor eliminates the need for installing a device on inner surfaces which, in some situations it is neither desirable nor possible. The sensors are small size (7 x 18 mm), thin (0.3 mm) and inexpensive (N.Z.$500 each).

The monitoring system met all the design requirements. Data collection was straightforward and was easily interfaced with computers. The system was robust and was easily disassembled after a production run and repositioned to another location. The system was un-obtrusive to routine operations and required minimal maintenance. Real

time monitoring of fouling development in plants was easily carried out either on site or several hundred kilometres away via a modem linked to the computer.

Normalisation of the calculated internal heat transfer coefficient was found to give consistent fouling patterns when applied to a fouling rig and four large-scale milk evaporator plants. The fouling behaviour observed in the large-scale plant matched the pattern obtained in the fouling rig, even though the runs in the large-scale plant were considerably longer (*i.e.* up to 24 h), under high prevailing fluid velocity and shear force (*i.e.* 1.8 m $s^{-1}$ and Reynolds number of 425000) and with different milk types (*i.e.* whole milk, skim milk, modified skim milk and modified whole milk). In contrast, runs in the fouling rig were short (*i.e.* up to 9 h), under much lower fluid velocity and shear force (*i.e.* 0.08 m $s^{-1}$ and Reynolds number of 3800) and with whole milk only. The fouling process always began with a delay period, during which there was no conclusive upward or downward trend in heat flux and was followed by a fouling period when the subsequent increase in deposition led to a linear decrease in $I_f$. These characteristics were very similar to those reported in the literature by various researchers who studied deposition of milk fluids on to heated surfaces (*e.g.* tubular and plate heat exchangers) using other methods for fouling measurements (Delsing & Hiddink, 1983; Paterson & Fryer, 1988; Changani *et al.*, 1997).

The duration of the delay time varied between the whole milk runs with the fouling rig. The delay time was not correlated with the treatment temperature, the milk flow rate conditions of the flow geometry used in the experiments. It is possible that the milk properties changed between run and this affected the initial deposition. The rate of fouling was also not consistent between runs. The results indicate that a quantitative fouling model to predict the absolute fouling level should be based on the evaluation of both the fluid dynamics of the system and the characteristics of the milk fluid.

Normalisation was also shown to be a convenient and successful method for comparing fouling behaviour of different milk types, which were heat treated to different levels under the influence of different fluid flow conditions. This method was particularly useful for comparing fouling at different locations downstream of the DSI heater. However, the use of initial internal heat transfer coefficient, $U_i(0)$, as a normalising parameter was not always perfect. As fouling progressed in extent during a run, the validity of the basic assumption that $U_i(0)$ remained constant became increasingly stretched. Increase in the deposit thickness caused an increased fluid velocity and a decreased $R_m$ and hence a decrease in $U_i(0)$. Consequently, the relative changes in $I_f$ with run time were reduced and the $I_f$ - time curve exhibited a reduced fouling rate. When this condition occurred and in order to compare the fouling behaviours between runs, the $I_f$ - time curve within the fouling period was divided into a number of linear portions and the slope of the first linear portion was taken as the fouling rate that represented the whole run.

The correlation between local fouling rate (based on wall heat flux) and the overall fouling rate (based on average deposit weight) was good. The experimental results indicated that valuable fouling data at a location could be obtained with a single sensor even though the landscape is much larger and varies in different parts of the area. The use of multiple sensors slightly increased the reliability of the data. However, a close analysis of the flow patterns in the area is essential for positioning of the sensor in order to capture the effects of flow geometry on the local deposition.

Calibration between $I_f$ and actual deposit thickness was easy with the fouling rig because the test sections could be dismantled for physical measurements. Wall heat flux was shown to correlate with the level of fouling inside the test pieces, despite the observation that milk deposits were not totally uniform in character, e.*g.* surface roughness varied from one deposit to another. The $I_f$ - deposit thickness relationship, determined at the end of the run, was not linear. The cause of this non-linear

relationship was probably similar to the effect of the use of $U_i(0)$ as a normalising parameter on the $I_f$ - run time relationship, *i.e.* $U_i(0)$ was not constant but decreased as deposits increased in thickness and hence the relative changes in $I_f$ with deposit thickness was reduced.

The deposits, which were observed in large-scale plant, were dense, hard and compact compared with the deposits in the test pieces, which appeared soft and voluminous. These differences highlighted the possibility that the deposits could have dissimilar thermal conductivity. In addition, changes in the milk type, heat treatment level and hydrodynamic conditions in the large-scale plant could also affect the physical properties of deposits (*e.g.* surface roughness) and hence the total thermal resistance. Due to the production schedule, it was not always possible to dismantle the equipment at the completion of the production run. Hence, only a couple of data points were obtained from the large-scale DSI heaters. Therefore, how well the $I_f$ - deposit thickness relationship obtained from the fouling rig represented the fouling conditions in large-scale plant requires further investigation.

### 7.2.2 Fouling of non-heated surfaces

The use of a simple tubular sudden expansion to study the effects of local transport process on fouling was found to be effective. It provided various flow conditions such as recirculation and redeveloping flows within a single experiment. Such flows can result in regions of high mass transfer rates which are several times greater than those for fully developed pipe flow at the same Reynolds numbers.

CFD was also found to be an useful tool for predicting the pattern of the local mass transfer, which were characterised by the changes in the surface shear rate and the thickness of the viscous sub-layer at various locations beyond the step of expansion.

Different fouling behaviours of whole milk heated to 95°C were found at different locations downstream of the expansion. The fouling rate was at an intermediate level in the corner recirculation zone (CRZ), which was adjacent to the expansion, increased to a maximum level in the reattachment flow region and then gradually decreased at locations downstream of the redeveloping flow region. The deposition patterns related to the patterns of mass transfer characterised by the CFD model, *i.e.* high level of fouling relates to high level of mass transfer and vice versa.

Increase in both the mass flow rates and step heights of the expansion were found to increase fouling. This contrasts with fouling of heated surfaces where increasing mass flow rate (*e.g.* Gordon *et al.*, 1968) or flow disturbance (*e.g.* Delplace & Leuliet, 1995) reduces fouling. The reason why an increase in flow rate has opposite effects on fouling rates of heated and non-heated surfaces is thought to be:

- For heated surfaces, higher flow rate reduces the concentration gradient of the 'reactive' species between the bulk milk fluid and the solid surface. The milk constituents that are hot enough and become active at the surface are replaced with the newly arrival and hence the amount of 'reacting' species at the surface is reduced. Fouling deposition rate therefore decreases with increase in flow rate.

- In contrast, for non-heated surface, higher flow rate increases the concentration gradient of the 'active' species between the milk fluid and the solid surface. The milk constituents that are hot enough and become active in the bulk fluid are transported to the solid surface to form fouling deposits. Fouling deposition therefore increases.

Flow disturbance was also found to have a strong effect on fouling in large-scale plants. The fouling patterns downstream from the DSI outlet and the orifice plate both matched

very well the patterns observed from the sudden expansion in the fouling rig. This is in spite of the fact that the mass flow rate used in the large-scale plant was much higher than that in the fouling rig and hence, deposits could be scoured from the surfaces due to high surface shear stress.

The internal structures (as examined by SEM) of deposits formed in the fouling rig and large-scale plant were very similar. They were all composed of a compact sub-layer and a porous top-layer. In the industrial plant, this top-layer was dense and compact and its surface was uniform under high prevailing fluid velocity and shear force. In contrast, in the presence of a much lower fluid velocity, as in the fouling rig, the top-layer appeared soft and voluminous and its surface contained high "hills" and deep "valleys". These differences in deposit conformation indicate that relating the pilot-scale results to the operation of the industrial-scale plant should be done with caution and it may have implications on the development of fouling models to predict fouling.

The deposits resembled type A deposits as defined by Burton (1968), *i.e.* high protein and low mineral deposits. The fat content of deposits from the fouling rig (49.7%) was much higher than those reported in the literature (*e.g.* 25%). Storage of milk for four days before the experiment may have contributed to the result. Furthermore, direct injection of steam to whole milk was found to break the milk fat globules into smaller ones. Small fat globules with damaged membranes could be involved in the fouling process. The design of the DSI heater could be improved to minimise fat globule damage.

This study also shows two important requirements for design and operation of a DSI heater to minimise fouling. They are:

- The pressure in the flow channel should be maintained at least 200 kPa absolute pressure above the boiling pressure corresponding to the treatment temperature.

- Rapid condensation of steam bubbles and minimum cavitation (hence mimimum fat globule damage) can be achieved by injecting steam via a number of injection nozzles.

### 7.2.3 The denaturation of β-lactoglobulin and its relationship to fouling

The experimental results with whole milk heated to 95°C in the fouling rig indicate that the deposition, after the surfaces have been conditioned during the delay period, related to the concentration of residual native β-lg (β-$lg_{(nat)}$). The proposed process is illustrated in the following figure.

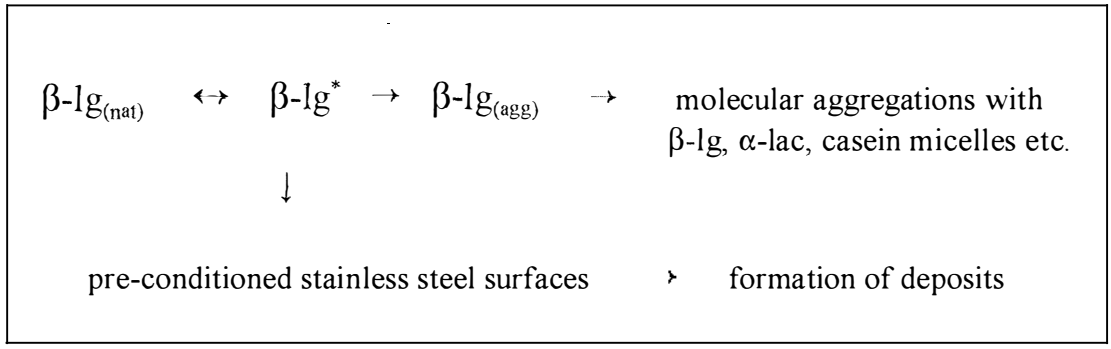


However, further work is required to determine if there is to be a direct correlation between the local concentration of β-$lg_{(nat)}$ and the local fouling rate of heated whole milk. Milk is a complex mixture of different components and the reactions occurring after the β-lg denaturation, particularly with surfaces, is certainly not completely understood. It is still not clear what are the controlling reactions, where they occur and how they affect deposition. For example, skim milk and whole milk show markedly different fouling behaviour even though their β-lg contents (on a SNF basis) are similar. There may be a direct interaction between active β-lg and the milk fat, via the proteins of the milk fat globule membranes that enhances the interactions of fat with the fouling deposits.

The structure and appearance of the deposits formed in the four fouling zones effectively illustrated the progressive nature of the build-up of fouling deposits, which were under the influence of the same hydrodynamic conditions. The deposits observed in zone 4 represented the early stages of fouling in zone 1. They consisted of discrete particle particles of different sizes (e.g. between 20 and 1000 μm) that randomly overlaid the solid surfaces. As fouling build-up progressed, these particles grew in size and formed small strands (zone 3). These strands became larger (zone 2) and then linked together to create a porous network of particles (zone 1), which represented the most fully developed fouling observed during a run.

## 7.3 CONCLUSIONS

The main objectives of the present study were achieved. Firstly, a system, which included commercial heat flux sensors to measure local fouling of non-heated surfaces was developed and effectively calibrated in the fouling rig and tested in the large-scale evaporator plants. The equipment was inexpensive, robust and required minimal maintenance. The use of the normalised internal heat transfer coefficient was a convenient and successful method for determining fouling from measured heat flux. A single sensor could monitor continuously the effect of deposit layer on the heat flux and effectively represent the fouling conditions.

Secondly, the results from the fouling rig showed that flow disturbance that enhanced the mass transfer between the bulk fluid and the solid surface strongly affected the deposition rate of whole milk heated to 95°C. Increasing the mass transfer rate increased the fouling rate. Flow disturbance was also found to have a strong effect on fouling behaviour in large-scale equipment. A change either in local hydrodynamic (by steam injection) or in local geometry (by an orifice plate) induced fouling.

Lastly, an important aspect of local fouling of whole milk heated to 95°C onto non-heated surfaces was identified. The deposition, after the surfaces had been conditioned during the delay period, was related to the concentration of residual native β-lg that had not been denatured after the start of heat treatment, *i.e.* the higher the degree of β-lg denaturation, the lower the concentration of residual native β-lg and the lower the fouling rate.

## 7.4 RECOMMENDATIONS FOR FURTHER WORK

### 7.4.1 Fundamental research

- The denaturation of β-lg in heated whole milk and its relationship to fouling of non-heated surface needs to be investigated thoroughly. The work should identify where the controlling reactions occur and how they affect deposition.

- The factors that affect the formation of a fouling sub-layer from heated milk fluids onto non-heated surfaces need to be investigated. The work should include the effects of surface material and finish on the initial stages of deposition.

- The factors that affect the delay period also need to be determined.

- Work on the role of milk constituents, in particularly, milk fat on fouling is highly recommended.

### 7.4.2 Industrial research

- Work to calibrate the heat flux sensor for monitoring of fouling in large-scale DSI heater and for different types of milk fluids is required.

- Work to improve the design and operation of the DSI heater to reduce milk fat globule damage is recommended.

# REFERENCES

Amano R. R.; Jensen M. K. & Goel P. (1983). A numerical and experimental investigation of turbulent heat transport downstream from and abrupt pipe expansion. *Journal of Heat Transfer*, Trans ASME, 105, 862-869.

Anema S. G. & Klostermeyer H. (1997). Heat-induced, pH-dependent dissociation of casein micelles on heating reconstituted skim milk at temperature below 100°C. *Journal of Agricultural and Food Chemistry*, **45**, 1108-1115.

Avalone E. A. & Baumeister III T. (1987). Marks' Standard Handbook for Mechanical Engineers, ninth edition, pp. 4-22. McGraw-Hill Book Company, New York.

AOAC International (1990). *Official Methods of Milk Analysis*, 15th edition. AOAC International.

Barton K. P.; Chapman T. W. & Lund D. (1985). Rate of precipitation of calcium phosphate on heated surfaces. *Biotechnology Progress*, **1**, 39-45.

Beek W. J. & Muttzall K. M. K. (1975). *Transport Phenomena*. John Wiley & Son, London, UK.

Bell R. W. & Sanders C. F. (1944). Prevention of milkstone formation in a high temperature short time heater by preheating milk, skim milk and whey. *Journal of Dairy Science*, **27**, 463-471.

Belmar-Beiny M. T. & Fryer P. J. (1992). Bulk and surface effects on the initial stages of fouling. *Trans IChemE*, **70**, Part C, 193-199.

Belmar-Beiny M. T. & Fryer P. J. (1993). Preliminary stages of fouling from whey protein solutions. *Journal of Dairy Research*, **60**, 467-483.

Belmar-Beiny M. T.; Gotham S. M.; Paterson W. R. & Fryer P. J. (1993). The effect of Reynolds number and fluid temperature in whey protein fouling. *Journal of Food Engineering,* **19**, 119-139.

Belmar-Beiny M. T. & Fryer P. J. (1994). Proceedings of the Fourth International Conference on *Fouling and Cleaning in Food Processing.* University of Cambridge, Cambridge, UK.

Bott T. R. (1995). Obtaining data. In *Fouling of Heat Exchanger*, pp. 492. Elsevier Applied Science, London, UK.

Bradley S. E.; Fryer P. J.; Griffin T. A. & Wilson D. I. (1989). Use of an oscillatory flow heat exchanger in food processing. In *Proceeding of the Third International Conference on Fouling and Cleaning in Food Processing* (Kessler H. G. & Lund D. B., Eds), pp. 14-24. University of Munich, Munich, Germany.

Bradley S. E. & Fryer P. J. (1992). A comparison of two fouling-resistant heat exchangers. *Biofouling*, **5**, 295-314.

Britten M.; Green M. L.; Boulet M. & Paquin P. (1988). Deposit formation on heated surface: effect of interface energetics. *Journal of Dairy Research,* **55**, 551-562.

Brooker B. E. (1991). The study of food systems using confocal laser scanning microscopy. *Microscopy and Analysis*, **26**, 13-15.

Burton H. (1966). A comparison between hot-wire laboratory apparatus ans a plate heat exchanger for determining the sensitivity of milk to deposit formation. *Journal of Dairy Research,* **33**, 317-324.

Burton H. (1967). Seasonal variation in deposit formation from whole milk on heated surface. *Journal of Dairy Research,* **34**, 137-143.

Burton H. (1968). Deposits from whole milk in heat treatment plant - a review and discussion. *Journal of Dairy Research,* **35**, 317-330.

Calvo M. & de Rafael D. (1995). Deposit formation in a plate heat exchanger during pasteurisation of carbon dioxide-acidified milk. *Journal of Dairy Research*, **62**, 641-644.

Changani S. D.; Belmar-Beiny M. T. & Fryer P. J. (1997). Engineering and chemical factors associated with fouling and cleaning in milk processing. *Experimental Thermal and Fluid Science*, **14**, 392-406.

Chieng C. C. & Launder B. E. (1980). On the calculation of turbulent heat transport downstream from an abrupt pipe expansion. *Numerical Heat Transfer*, **3**, 189-207.

Cho Y. I. & Choi B. -G. (1998). Effect of fouling on temperature measurement error and a solution. *Journal of Heat Transfer*, **120**, 525-528.

Corredig M. & Dalgleish D. G. (1996a). The binding of α-lactalbumin and β-lactoglobulin to casein micelles in milk treated by different heating systems. *Milchwissenschaft*, **51**, 123-126.

Corredig M. & Dalgleish D. G. (1996b). Effect of temperature and pH on the interactions of whey proteins with casein micelles in skim milk. *Food Research International*, **29**, 49-55.

Corredig M. & Dalgleish D. G. (1996c). Effect of different heat treatments on strong binding interactions between whey proteins and milk fat globules in whole milk. *Journal Of Dairy Research*, **63**, 441-449.

Corrieu G.; Lalande M. & Ferret R. (1986). On-line measurement of fouling and cleaning of industrial UHT heat exchanger. *Journal of Food Engineering*, **5**, 231-248.

Creamer L. K.; Berry G. P. & Matheson A. R. (1978). The effect of pH on protein aggregation in heated skim milk. *New Zealand Journal of Dairy Science and Technology*, **13**, 9-15.

Crittenden B. D. & Alderman N. J. (1992). Mechanisms by which fouling can increase overall heat transfer coefficients. *Heat Transfer Engineering*, **12**, 32-41.

Dalgleish D. G. (1990). Denaturation and aggregation of serum proteins and caseins in heated milk. *Journal of Agriculture and Food Chemistry,* **38**, 1995-1999.

Dalgleish D. G. & Banks J. M. (1991). The formation of complexes between serum proteins and fat globules during heating of whole milk. *Milchwissenschaft,* **46**, 75-78.

Dalgleish D. G. & Sharma S. K. (1992). Interactions between milk fat and milk proteins - the effect of heat on the nature of the complexes formed. In *Protein & Fat Globule Modifications by Heat Treatment, Homogenization & Other Technological Means for High Quality Dairy Products.,* pp. 7-17. IDF Special Issue No. 9303, International Dairy Federation, Brussels, Belgium.

Dannenberg F. & Kessler H. G. (1988). Application of reaction kinetics to the denaturation of the whey proteins in heated milk. *Milchwissenschaft,* **43**, 3-7.

Daufin G.; Labbe J. P.; Quemerais A.; Brule G.; Michel F.; Roignant M. & Priol M. (1987). Fouling of a heat exchange surface by whey, milk and model fluids. An analytical study. *Le Lait,* **67**, 339-364.

Davies T. J.; Henstridge S. C.; Gillham C. R. & Wilson D. I. (1997). Investigation of whey protein deposit properties using heat flux sensors. *Trans. IChemE,* **75**, 106-110.

De Jong P. (1996). *Modelling and optimisation of thermal processes in the dairy industry.* PhD Thesis, Technical University of Delft, Netherlands.

De Jong P.; Bouman S. & van der Linden H. J. L. J. (1992). Fouling of heat treatment equipment in relation to the denaturation of β-lactoglobulin. *Journal of the Society of Dairy Technology,* **45**, 3-8.

De Jong P.; Waalewijn R. & van der Linden H. J. L. J. (1993). Validity of a kinetic fouling model for heat treatment of whole milk. *Le Lait,* **73**, 293-302.

De Jong P.; Waalewijn R. & van der Linden H. J. L. J. (1994). Performance of a steam infusion plant for heating milk. *Netherlands Milk & Dairy Journal,* **48**, 181-199.

Delplace F. & Leuliet J. C. (1995). Modelling fouling of a plate heat exchanger with different flow arrangements by whey protein solutions. *Food and Bioproducts Processing,* **73**, 112-120.

Delsing B. M. A. & Hiddink J. (1983). Fouling of heat transfer surfaces by dairy liquids. *Netherlands Milk & Dairy Journal,* **37**, 139-148.

Feuerstein I. A.; Pike G. K. & Round G. F. (1975). Flow in an abrupt expansion as a model for biological mass transfer experiments. *Journal of Biomechanics*, **8**, 41-51.

Foster C. L.; Britten M. & Green M. L. (1989). A model heat-exchange apparatus for the investigation of fouling of stainless steel surfaces by milk. I. Deposit formation at 100°C. *Journal of Dairy Research,* **56**, 201-209.

Foster C. L. & Green M. L. (1990). A model heat-exchange apparatus for the investigation of fouling of stainless steel surfaces by milk. II. Deposition of fouling material at 140°C. *Journal of Dairy Research,* **57**, 339-348.

Fox P. F. (1995). *Heat-Induced Changes in Milk.* International Dairy Federation, Brussels, Belgium.

Fryer P. J. (1989). The use of a fouling models in the design of food processing plant. *Journal of the Society of Dairy Technology,* **42,** 23-29.

Fryer P. J. & Slater N. K. H. (1984). Reaction fouling from food fluids. In *Fouling of Heat Exchanger Equipment,* (Suitor J. W. & Pritchard A. M., Eds), pp. 65-72. ASME HTD-35.

Fryer P. J. & Slater N. K. H. (1987). A novel fouling monitor. *Chemical Engineering Communication,* **57,** 139-152.

Fryer P. J.; Pritchard A. M.; Slater N. K. H. & Laws J. F. (1985). A possible online fouling sensor for the food processing industry. In *Proceedings of the Second International Conference on Fouling and Cleaning in Food Processing* (Lund D. B., Plett E. & Sandu C., Eds), pp. 203-216. University of Wisconsin-Madison, Madison,

Wisconsin, USA.

Fryer P. J.; Gotham S. M. & Paterson W. R. (1992). The concentration dependence of fouling from whey protein concentrates. In *Proceedings of the Twentieth Australasian Chemical Engineering Conference.* Volume 1, pp 368-3741. Canberra, Canada.

Georgiadis M. C.; Rotstein G. E. & Machietto S. (1998). Modelling and simulation of shell and tube heat exchangers under milk fouling. *AIChE Journal*, **44**, 959-971.

Gillham C. R.; Fryer P. J.; Hasting A. P. M. & Wilson D. I. (1999). Cleaning-in-place of whey protein fouling deposits: Mechanisms controlling cleaning. *Trans. IChemE*, 77, Part C, 127-135.

Gordon K. P.; Hankinson D. J. & Carver C. E. (1968). Deposition of milk solids on heated surfaces. *Journal of Dairy Science,* **51**, 520-526.

Gotham S. M.; Fryer P. J. & Pritchard A. M. (1992). β-Lactoglobulin denaturation and aggregation reactions and fouling deposit formation: a DSC study. *International Journal of Food Science and Technology,* **27**, 313-327.

Grandison A. S. (1988). UHT processing of milk: seasonal variation in deposit formation in heat exchangers. *Journal of the Society of Dairy Technology,* **41**, 43-49.

Hall C. W. & Hendrick T. I. (1966). *Drying of milk and milk products.* AVI Publishing Company, London, UK.

Hamil N. (1996). CFD comes of age in the CPI. *Chemical Engineering*, **103** (12), 68-72.

Hasting A. P. M. & de Goederen G. (1988). The influence of process design on the fouling and cleaning of dairy process plant. In *Fouling and Cleaning in Process Plant: International Conference*, pp. 216-248. St Catherine's College, Oxford, UK.

Hege W. U. & Kessler H. G. (1986). Deposit formation of protein containing dairy liquids. *Milchwissenschaft,* **41**, 356-360.

Hiddink J., Lalande M., Maas A. J. R. & Streuper A. (1986). Heat treatment of whipping cream. I. Fouling of the pasteurization equipment. *Milchwissenchaft,* **41**, 542-546.

Hill J. P. (1993). The relationship between β-lactoglobulin phenotypes and milk composition in New Zealand dairy cattle. *Journal of Dairy Science,* **76**, 281-286.

Holt C. (1992). Structure and stability of bovine casein micelles. *Advances in Protein Chemistry,* **43**, 63-151.

Houlihan A. V., Goddard P. A., Nottingham S. M., Kitchen B. J. & Masters C. J. (1992). Interactions between the bovine milk fat globules membrane and skim milk components on heating whole milk. *Journal of Dairy Research,* **59**, 187-195.

International Dairy Federation (1985). *Surface finishes of stainless steel.* IDF Bulletin 189:1985. International Dairy Federation, Brussels, Belgium.

International Dairy Federation (1997). *Fouling and Cleaning of Heat Treatment Equipment.* IDF Bulletin 328:1997. International Dairy Federation, Brussels, Belgium.

Isermann R.; Baur, W.; Bamberger W.; Kneppo P. & Siebert H. (1974). Comparison of six on-line identification and parameter estimation methods. *Automatica,* **10**, 81-103.

Janssen P. W. M. (1994). Measurement of residence time distribution of processing plant using cross correlation technique. *Journal of Food Engineering,* **21**, 215-223.

Jeurnink Th. J. M. (1991). Effect of proteolysis in milk on fouling in heat exchangers. *Netherlands Milk and Dairy Journal,* **45**, 23-32.

Jeurnink Th. J. M. (1992). Changes in milk on mild heating: turbidity measurements. *Netherlands Milk and Dairy Journal,* **46**, 183-196.

Jeurnink Th. J. M. (1995a). Fouling of heat exchangers in relation to the serum protein concentration in milk. *Milchwissenschaft,* **50**, 257-260.

Jeurnink Th. J. M. (1995b). Fouling of heat exchangers by fresh and reconstituted milk and the influence of air bubbles. *Milchwissenschaft*, **50**, 189-192.

Jeurnink Th. J. M. & Brinkman D. W. (1994). The cleaning of heat exchangers and evaporators after processing milk or whey. *International Dairy Journal*, **4**, 347-368.

Jeurnink Th. J. M. & de Kruif C. G. (1995). Calcium concentration in milk in relation to heat stability and fouling. *Netherlands Milk & Dairy Journal*, **49**, 151-165.

Jeurnink Th. J. M., Brinkman D. W. & Stemerdink A. D. (1989). Distribution and composition of deposit in heat exchangers. In *Proceeding of the Third International Conference on Fouling and Cleaning in Food Processing* (Kessler H. G. & Lund D. B., Eds), pp. 25-36. University of Munich, Munich, Germany.

Jeurnink Th. J. M., Verheul M., Cohen Stuart M. & de Kruif, C. G. (1995). Calcium concentration in milk in relation to heat stability and fouling. *Netherlands Milk & Dairy Journal*, **49**, 151-165.

Jeurnink Th. J. M.; Walstra P. & de Kruif C. G. (1996). Mechanisms of fouling in dairy processing. *Netherlands Milk & Dairy Journal*, 50, 407-426.

Jones A. D.; Ward N. J. & Fryer P. J. (1994). The use of a heat flux sensor to monitor milk fluid fouling. In *Fouling and Cleaning in Food Processing* (Belmar-Beiny, M. T. & Fryer, P. J., Eds), pp. 199-205. University of Cambridge, Cambridge, UK.

Jones M. C. & Larner G. S. (1968). The use of steam injection as a mean of rapid heating for sterilisation of liquid foods. *The Chemical Engineer*, January, 4-9.

Kastanas P.; Lewis M. J. & Grandison A. S. (1995). Design and development of a miniature UHT plant for fouling study and its evaluation using milk adjusted to different pH values, goat milk and milk permeate. *Trans. IChemE*, **73**, Part C, 83-91.

Kessler H. G. & Lund D. B. (1989). Proceedings of the Third International Conference on *Fouling and Cleaning in Food Processing*. Prien, Bavaria, Germany.

Kessler H. G. & Beyer H. J. (1991). Thermal denaturation of whey proteins and its effect in dairy technology. *International Journal of Biological Macromolecules*, **13**, 165-173.

Lalande M.; Tissier J. P. & Corrieu G. (1985). Fouling of heat transfer surfaces related to β-lactoglobulin denaturation during heat processing of milk. *Biotechnology Progress*, **1**, 131-139.

Lalande M.; Rene F. & Tissier J. P. (1989). Fouling and its control in heat exchangers in the dairy industry. *Biofouling*, **1**, 233-250.

Levenspiel O. (1972). Nonideal flow, chapter 9. In *Chemical Reaction Engineering*, 2nd ed. John Wiley, New York, NY.

Lund D. B.; Plett E. & Sandu C. (1985). Proceeding of the Second International Conference on *Fouling and Cleaning in Food Processing*. University of Wisconsin, Madison, Wisconsin, USA.

Lyster R. L. J. (1965). The composition of milk deposits in an ultra-high-temperature plant. *Journal of Dairy Research,* **32**, 203-208.

Moon L. F. & Rudinger G. (1977). Velocity distribution in an abruptly expanding circular duct. *Journal of Heat Transfer*, Trans. ASME, **99**, 226-230.

Mottar J. & Moermans R. (1988). Optimization of the forewarming process with respect to deposit formation in indirect ultra high temperature plants and the quality of milk. *Journal of Dairy Research,* **55**, 563-568.

Mulvihill D. M. & Donovan M. (1987). Whey proteins and their thermal denaturation, a review. *Irish Journal of Food Science and Technology,* **11**, 43-75.

New Zealand Dairy Board (2000). *New Zealand Dairy Board Annual Report 2000.* New Zealand Dairy Board, Wellington, New Zealand.

Nicholas J. V. & White D. R. (1994). *Traceable Temperatures: In Introduction to Temperature Measurement and Calibration*, 2nd edition, pp 81-151. John Wiley & Son, New York, USA.

Paterson W. R. & Fryer P. J. (1988). A reaction engineering approach to the analysis of fouling. *Chemical Engineering Science,* **43**, 1714-1717

Patil G. R. & Reuter H. (1986). Deposit formation in UHT plant. I. Effect of forewarming in indirectly heated plants. *Milchwissenschaft,* **41**, 337-339.

Patil G. R. & Reuter H. (1988). Deposit formation in UHT plants. IV. Composition of milk deposits from a directly and indirectly heated plant. *Milchwissenschaft,* **43**, 430-433.

Robbins P. T.; Elliott B. L.; Fryer P. J.; Belmar M. T. & Hasting A. P. M. (1999). A comparison of milk and whey fouling in a pilot scale plate heat exchanger: Implication for modelling and mechanistic studies. *Trans. IChemE,* 77, Part C, 97-106.

Runchal A. K. (1971). Mass transfer investigation in turbulent flow down stream of sudden enlargement of a circular pipe for very high Schmidt numbers. *International Journal of Heat & Mass Transfer*, **14**, 781-792.

Sandu C. & Lund D. B. (1985). Fouling of heating surfaces - chemical reaction fouling due to milk. In *Proceedings of the Second International Conference on Fouling and Cleaning in Food Processing* (Lund D. B., Plett E. & Sandu C., Eds), pp. 122-167. University of Wisconsin-Madison, Madison, Wisconsin, USA.

Schraml J. E.; Spiegel T. & Kessler H. G. (1996). Effects of composition and concentration of dairy liquids on fouling of structure. *Milchwissenschaft,* **51**, 607-611.

Shanley A. (1996). Pushing the limits of CFD. *Chemical Engineering*, **103** (12), 66-67.

Skudder J.; Brooker B. E.; Bonsey A. D. & Alvarez-Guerrero N. R. (1986). Effect of pH on the formation of deposit from milk on heated surfaces during ultra high temperature processing. *Journal of Dairy Research,* **53**, 75-87.

Somerscales E. F. & Knudsen J. G. (1981). Fouling of Heat Transfer Equipment. Hemisphere Publishing Corporation, New York, USA.

Tavner A. C. R.; Bowen R. J. & Bishop C. W. (1996). Heat flux monitoring during cryogenic pipe freezing: a case study. *Chemical and Engineering Research and Design*, **74**, 239-241.

The Institution of Chemical Engineers (1999). *Fouling and Cleaning*. Transactions of Institution of Chemical Engineers, 77. The Institution of Chemical Engineers, Rugby, UK.

Tissier P. J. & Lalande M. (1986). Experimental device and methods for studying milk deposit formation on heat exchange surfaces. *Biotechnology Progress,* **2**, 218-229.

Tissier P. J.; Lalande M. & Corrieu G. (1984). A study of milk deposit on heat exchange surface during UHT treatment. In *Engineering and Food*, Volume 1 (McKenna B M, Ed), pp. 49-58. Elsevier Applied Science Publishers, Barking, UK.

Tong, C. H. & Sheen, S. (1992). Heat flux sensors to measure effective thermal conductivity of multi-layered plastic containers. *Journal of Food Processing and Preservation*, 16, 233-238.

Toyoda I.; Schreier P. J. R. & Fryer P. J. (1994). A computational model for reaction fouling from whey protein solutions. In *Fouling and Cleaning in Food Processing* (Belmar-Beiny M .T. & Fryer P. J., Eds), pp. 191-198. University of Cambridge, Cambridge, UK.

Tsao M.; Crawford R & Otter D. (1998). The determination of milk protein composition using amino acid analysis. *The Food Technologist*, **28**, 94-97.

Tuladhar T. R.; Paterson W. R. & Wilson, D. I. (2000). Use of dynamic gauging - a soft film thickness sensor to probe cleaning-in-place of whey protein deposits. In *Proceedings of the 28th Australian and New Zealand Chemical Engineers' Conference,* Perth, Australia.

University of Cambridge (1998). *Fouling and Cleaning in Food Processing,* Jesus College, Cambridge, 6-8 April. University of Cambridge, Cambridge, UK.

Van Dijk H. J. M. (1990). The properties of casein micelles. 3. Changes in the state of the micellar calcium phosphate and their effects on other changes in the casein micelles. *Netherlands Milk & Dairy Journal*, **44**, 125-142.

Visser J. & Jeurnink Th. J. M. (1997). Fouling in heat exchangers in the dairy industry. *Experimental Thermal and Fluid Science*, **14**. 407-424.

Visser J.; Lindell A. & Paulsson M. A. (1995). Heat-induced depositions of milk components onto a rotating disk. In *Heat treatments & Alternative Methods*, Proceedings of the IDF Symposium, Vienna, Austria, pp. 83-108. International Dairy Federation, Brussels, Belgium.

Visser H.; Jeurnink Th. J. M.; Schraml J. E.; Fryer P. & Delplace F. (1997). Fouling of heat treatment equipment. In *Fouling and Cleaning of Heat Treatment Equipment*, IDF Bulletin no. 328, pp. 7-31. International Dairy Federation, Brussels, Belgium.

Walstra P. & Jenness R. (1984). *Dairy Chemistry and Physics.* John Wiley & Son, New York, USA.

Webb B. H.; Johnson A. H. & Alford J. A. (1974). *Fundamentals of Dairy Chemis*try. AVI Publishing Company, London, UK.

Withers P. M. (1996). Ultrasonic, acoustic and optical techniques for the non-invasive detection of fouling in food processing equipment. *Trends in Food Science & Technology,* 7, 293-298.

Withers P. M., Taylor J. H., Richardson P. S. & Holah J. T. (1994). Ultrasonic detection and monitoring of fouling during UHT processing. In *Fouling and Cleaning in Food Processing* (Belmar-Beiny M. T. & Fryer P. J., Eds), pp. 181-190. University of Cambridge, Cambridge, UK.

Yoon J. & Lund D. B. (1989). Effect of operating conditions, surface coatings and pretreatment on milk fouling in a plate heat exchanger. In *Proceeding of the Third International Conference on Fouling and Cleaning in Food Processing* (Kessler H. G. & Lund D. B., Eds), pp. 59-80. University of Munich, Munich, Germany.

Zemanick P. P. & Dougall R. S. (1970). Local heat transfer downstream of abrupt circular channel expansion. *Journal of Heat Transfer*, **92**, 53-60.

# APPENDICES

CONTENTS

## Appendix 3.1

## Major Components of the Fouling Rig

| Component | Make and Model |
|---|---|
| Feed pump | Mono Pumps, Mono-SLF-5022105/C, 0.55 kW |
| Pump speed controller | PDL Electronics, PD-2.3 |
| Pressure relief valve | Swagelock, max. 9 bar |
| Plate heat exchanger | APV, U2-41-R-SS |
| Hot water pump | Salmson, SB100, single phase 220/240V, 50 Hz, 200 W |
| Steam pressure reducing valve | Spirax Sarco, BRV2, 8.6/3.5 bar gauge |
| Steam separator | Spirax Sarco, S1 |
| Steam trap | Spirax Sarco, FT14 |
| Steam filter | Ultrafilter, 5 μm |
| Steam control valve | Badger Meter, Type 807, 12.5 mm, 3-15 psi |
| Platinum resistance thermometer | Servotech, PT100, 3-wire class A |
| Temperature transmitter | Servotech, RH11 |
| Temperature controller | ABB Kent-Taylor, Commander 300 |
| Integer/Pneumatic converter | Servotech, Belloframe Type 1000 |
| Flow meter | Bailey Fischer & Porter, 10DX211-2A |
| Pressure transmitter | Rosemount, Smart Family |

## Appendix 3.2
## Design of a Direct-Steam-Injection (DSI) Heater

### 1 DSI design concepts

Although the use of direct steam injection in food processing is at least 30 years old (Jones & Larner, 1968) and a large number of DSI heaters are presently used in dairy industry for the continuous heating of various types of dairy fluids such as milk, concentrated milk, whey and concentrated whey, there are no published standard methods available for designing such steam injectors.

In general, the conventional criteria for operations of a DSI device include (Burton, 1988):

(a) Rapid condensation of steam bubbles to avoid local heating of the milk and therefore to minimise denaturation of milk proteins.

(b) Minimum cavitation, which is caused by the condensation and collapse of the steam bubbles, which in turn creates high pressure gradients of very short duration within the body of the fluid. Hence damage to milk fat globules in whole milk can be minimised.

(c) Continuous and steady flow of steam and milk fluid.

Therefore, the DSI device used in this study was designed using the following guidelines:

(1) The pressure in the flow channel is maintained well above the saturation or boiling pressure corresponding to the required treatment temperature.

This condition will result in a small temperature difference between the steam and the milk and hence steam condensation would be rapid and local over-heating of milk would be minimised. In addition, the steam volume is small thus choke flow (or water hammer flow) would be prevented. Any air dissolved in the milk (about 10 ppm air (Burton, 1968)) or non-condensable gases in the steam will not be released and form a steam-liquid-air mixture which may interfere with the steam condensation process.

(2) The steam is injected into the milk fluid via a number of small injection nozzles (about a millimetre in diameter) to produce small steam bubbles.

(3) A positive-displacement, non-pulsating type feed pump is used to maintain a continuous flow independent of the steam pressure and downstream pressure.

(4) The flow in the injector flow channel is turbulent.

## 2 Calculations of the amount of steam condensate generated by the DSI

The amount of steam condensate generated by the DSI heater can be calculated from the equation of energy balance between the milk stream and the injected steam:

$$m_l C_p ( T_2 - T_1 ) = m_v ( H_v - H_f ) \qquad \text{(A3.1)}$$

where $m_l$ and $m_v$ are the mass flow rates of the whole milk before the heater and the injected steam, $kgm^{-2}$,

$C_p$ is the specific heat of whole milk, kJ $kg^{-1}$ $°C^{-1}$,

$T_1$ and $T_2$ are the temperature of milk before and after the heater, °C and

$H_v$ and $H_f$ are the enthalpies per unit mass of steam before and after the heater, kJ $kg^{-1}$.

Rearranging the above equation to calculate the amount of steam or steam condensate gives

$$m_v = \frac{m_1 C_p (T_2 - T_1)}{H_v - H_f} \qquad \text{(A3.2)}$$

## 3 Steam injection nozzle sizing

The sizing of a steam injector was based on the thermodynamics of flow of steam through a short nozzle (Figure A3.1). For a given steam flow rate ($m_v$), steam supply pressure ($P_v$) and downstream pressure ($P_2$), the cross-sectional area (A) of a steam nozzle can be estimated using Napier's equation (Avallone & Baumeister, 1987)

$$A = \frac{m_v}{145.8\ P_v} \qquad \text{(A3.3)}$$

The steam flow rate ($m_v$), which is required for a specific heat treatment condition of the milk fluid, is calculated from equation A3.2.

$P_v$ is determined from the critical flow ratio ($r_c$) at the nozzle outlet. For dry and saturated steam, $r_c$ is given by the equation (Avallone & Baumeister, 1987)

$$r_c = \frac{P_c}{P_v} = 0.575 \qquad \text{(A3.4)}$$

where $P_c$ is the critical flow pressure at the nozzle outlet.

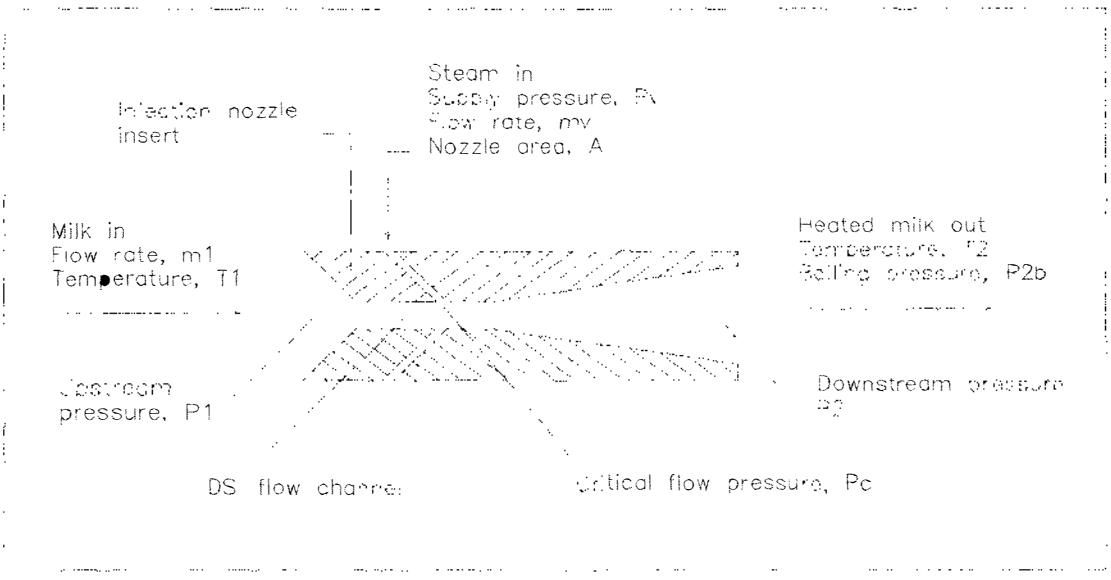


**Figure A3.1** Schematic drawing of the section view of the steam injection nozzle and flow channel.

In practice, $P_c$ is normally set at about 100 kPa (1 bar) above the boiling pressure ($P_{2b}$) of the milk, at the treatment temperature, plus a pressure drop $\Delta P_{12}$ due to the milk flow in the DSI flow channel. Thus the pressure in the flow channel is always maintained above the fluid boiling pressure. The calculation becomes

$$P_c = P_{2b} + \Delta P_{12} + 1 \qquad \text{(A3.5)}$$

## 4 Results of steam nozzle sizing

Table A3.1 shows a list of different numbers and diameters of steam injection nozzles for different heat treatment conditions of the fouling rig. The calculations were based on the heating of milk from 75 to 85, 95 and 110°C at the flow rates of 80, 120 and 160 kg/h. The diameter of the flow channel of 5 mm was selected to give a turbulent flow condition (Reynolds number of about 15000). A smaller diameter, say 2.5 mm, gave

a higher Reynolds number but was found to cause a high pressure drop across the channel and hence it was not selected. The procedures of the calculations are listed in Table A3.2 and the physical properties of milk used in the calculations are given in Table A3.3.

**Table A3.1** Summary of steam injection nozzle sizing

| **Nozzle sizing** | **Whole milk flow rate (kg $h^{-1}$)** | | | | |
|---|---|---|---|---|---|
| | **80** | **120** | **160** | **120** | **120** |
| Treatment temperature (°C) | 95 | 95 | 95 | 85 | 110 |
| Milk inlet temperature (°C) | 75 | 75 | 75 | 75 | 75 |
| Downstream pressure, $P_2$ (kPa abs) | 244 | 236 | 225 | 210 | 294 |
| Steam pressure, $P_v$ (kPa abs) | 425 | 410 | 392 | 365 | 511 |
| Steam flow rate, $m_v$ (kg $h^{-1}$) | 2.84 | 4.25 | 5.65 | 2.11 | 7.50 |
| Number of nozzles | 2 | 4 | 4 | 2 | 6 |
| Nozzle area ($10^{-6}$ $m^2$) | 0.636 | 0.493 | 0.687 | 0.552 | 0.466 |
| Nozzle diameter (mm) | 0.90 | 0.79 | 0.94 | 0.84 | 0.77 |

**Table A3.2** Spreadsheet calculations of steam nozzles

| **Process duty** | **Unit** | **1** | **2** | **3** | **4** | **5** |
|---|---|---|---|---|---|---|
| Milk fluid | Whole milk | | | | | |
| Fluid flow rate | kg $h^{-1}$ | 80 | 120 | 160 | 120 | 120 |
| Inlet temperature | 'C | 75 | 75 | 75 | 75 | 75 |
| Outlet temperature | 'C | 95 | 95 | 95 | 85 | 110 |
| Fluid density | kg $m^{-3}$ | 988 | 988 | 988 | 995 | 978 |
| Fluid specific heat (at 75 C) | kJ $kg^{-1}$ $C^{-1}$ | 3.915 | 3.915 | 3.915 | 3.915 | 3.915 |
| Fluid viscosity | Ns $m^{-1}$ | 5E-04 | 5E-04 | 5E-04 | 6E-04 | 4E-04 |
| Heating energy required | kJ $h^{-1}$ | 6,264 | 9,396 | 12,528 | 4,698 | 16,443 |
| ***Flow channel sizing:*** | | | | | | |
| Diameter | m | 0.005 | 0.006 | 0.007 | 0.006 | 0.006 |
| Length | m | 0.06 | 0.06 | 0.06 | 0.06 | 0.06 |
| Velocity | m $s^{-1}$ | 1.15 | 1.19 | 1.17 | 1.18 | 1.21 |
| Reynolds number | | 11,549 | 14,436 | 16,498 | 12,861 | 17,253 |
| Pressure drop | bar | 0.59 | 0.51 | 0.40 | 0.52 | 0.49 |
| Fluid boiling pressure | bar (abs) | 0.85 | 0.85 | 0.85 | 0.58 | 1.45 |
| **Min. back pressure (P2)** | **bar (abs)** | **2.44** | **2.36** | **2.25** | **2.10** | **2.94** |
| | **kPa (abs)** | **244** | **236** | **225** | **210** | **294** |
| ***Nozzle application:*** | | | | | | |
| (P2/Pv) critical flow | (Eq. 3.3) | 0.575 | 0.575 | 0.575 | 0.575 | 0.575 |
| **Min. steam pressure (Pv)** | **bar (abs)** | **4.2** | **4.1** | **3.9** | **3.6** | **5.1** |
| | **kPa (abs)** | **424.8** | **409.9** | **391.9** | **364.9** | **511.3** |
| Steam enthalpy, Hv (at Pv) | kJ $kg^{-1}$ | 2,741 | 2,740 | 2,738 | 2,733 | 2,750 |
| Steam enthalpy, Hf (at P2) | kJ $kg^{-1}$ | 532 | 527 | 521 | 511 | 558 |
| Steam flow rate, mv | kg $h^{-1}$ | 2.836 | 4.246 | 5.652 | 2.114 | 7.502 |
| ***Steam nozzle sizing:*** | | | | | | |
| Number of nozzle | | 2 | 4 | 4 | 2 | 6 |
| Steam flow per nozzle | kg $h^{-1}$ | 1.418 | 1.061 | 1.413 | 1.057 | 1.250 |
| Nozzle area (Eq. 3.1) | 10-6 m | 0.636 | 0.493 | 0.687 | 0.552 | 0.466 |
| **Nozzle diameter** | **mm** | **0.90** | **0.79** | **0.94** | **0.84** | **0.77** |

**Table A3.3** Physical properties of whole milk and water (reproduced from Hall & Hendrick (1966))

| Milk fluid | Physical Property | Temperature (°C) | | | |
|---|---|---|---|---|---|
| | | 75 | 85 | 95 | 110 |
| Whole milk (4% fat & 14 % total solids) | ρ (kg $m^{-3}$) | 1,004 | 995 | 988 | 978 |
| | μ (N s $m^{-2}$) | 5.9 E-4 | 5.5 E-4 | 4.9 E-4 | 4.1 E-4 |
| | k (W $m^{-1}$ $K^{-1}$) | 0.552 | 0.557 | 0.566 | 0.58 |
| | Cp (J $kg^{-1}$ $K^{-1}$) | 3,915 | 3,945 | 3,975 | 4,019 |
| Water | ρ (kg $m^{-3}$) | 975 | 969 | 962 | 958 |
| | μ (N s $m^{-2}$) | 4 E-4 | 3 E-4 | 3 E-4 | 3 E-4 |
| | k (W $m^{-1}$ $K^{-1}$) | 1 | 1 | 1 | 1 |
| | Cp (J $kg^{-1}$ $K^{-1}$) | 4,193 | 4,204 | 4,210 | 4,216 |

**Sample calculations (for process duty no. 1)**

Heating energy required:

$$m_1 C_p ( T_2 - T_1 ) = 80 \times 3.915 ( 95 - 75 ) = 6{,}264 \text{ kJ h}^{-1}$$

Flow channel pressure drop (Beek & Muttzall, 1975):

$$\frac{0.0395}{Re^{0.25}} \rho v^2 \frac{L}{D} = \frac{0.0395}{11{,}549^{0.25}} \times 988 \times 1.15^2 \times \frac{0.06}{0.005} = 59 \text{ kPa}$$

Minimum back pressure (Eq. 3.5):

$$P_2 = 59 + 85 + 100 = 244 \text{ kPa abs}$$

Minimum allowed steam pressure (Eq. 3.4):

$$P_v = \frac{P_2}{0.575} = \frac{244}{0.575} = 424.8 \text{ kPa abs}$$

Steam flow rate (Eq. 3.2):

$$m_v = \frac{Q}{H_v - H_f} = \frac{6{,}264}{2{,}741 - 532} = 2.836 \text{ kg h}^{-1}$$

If the number of nozzles is 2 then each cross-sectional area is (Eq. 3.3):

$$A = \frac{m_v}{3{,}600\ n\ (145.8\ P_v)} = \frac{3.836}{3{,}600 \times 2\ (145.8 \times 424.8)} = 0.636\ 10^{-6}\ m^2$$

and nozzle diameter

$$d = 0.9\ mm$$

## 4 Performance of the DSI heater

This section reports the performance of the DSI regarding fouling which was determined during the commissioning of the fouling rig. It includes the effect of steam injection on the milk fat globules and the effect of critical steam pressure on milk heating. Operation methods to reduce fouling in the DSI heater are also recommended.

### 4.1 Effect of direct steam injection on the milk fat globule sizes

Experiments were carried out to investigate the effect of DSI on the milk fat globules in heated whole milk. The milk was obtained from the Kiwi Co-operative Dairies Limited, Hawera, was pasteurised at 72°C for 15 s, chilled and stored at 6°C for up to six days before the experiments. The experiments were carried out using the same procedures set out in Chapter 4.

To determine the effects of steam injection on the milk fat globule size in whole milk, two techniques were used: measurement of fat globule size distribution by laser light scattering technique (Malvern Mastersizer, Model E, Malvern Instrument Ltd, Worchestershire, England) and microscopic observation using confocal laser scanning microscope (CLSM) technique (Brooker, 1991). The micrographs were taken using a Leica CLSM (Leica TCS NT, Leica Microscopy and Scientific Instruments Group, Switzerland).

Figure A3.2 shows the milk fat globule size distribution curves for non-heated whole milk and heated whole milk at 75, 85, 95 and 110°C. A summary of the results of the particle size analysis is given in Table A3.5. The results show that the particle size distribution curves for fresh milk and milk heated to 75°C in the plate heat exchanger were very similar. The average particle diameters (called Sauter Mean diameter or $D^3/D^2$) of milk fat globules for fresh milk and milk heated to 75°C were found the same at 0.96 μm. These results indicated that the size of the milk fat globules were not changed during heating in the plate heat exchanger.

The distribution curves for milk heated by the direct injection of steam tended to shift to the left (towards small particle sizes). A completely new peak showing a decrease in the volume of large particles above 1 μm and an increase in the volume of small particles below 1 μm were found for milk samples of each treatment temperature. A small increase in the volume of large particles above 10 μm for samples of milk heated to 95 and 110°C was also observed. The average particle diameters (*i.e.* Sauter Mean diameter) of milk fat globules for milk heated to 85, 95 and 110°C were 0.84, 0.78 and 0.67 μm respectively. These results indicated that increasing the DSI treatment temperature, hence the intensity of steam injection, increased the number of small particles at the expenses of the larger particles.

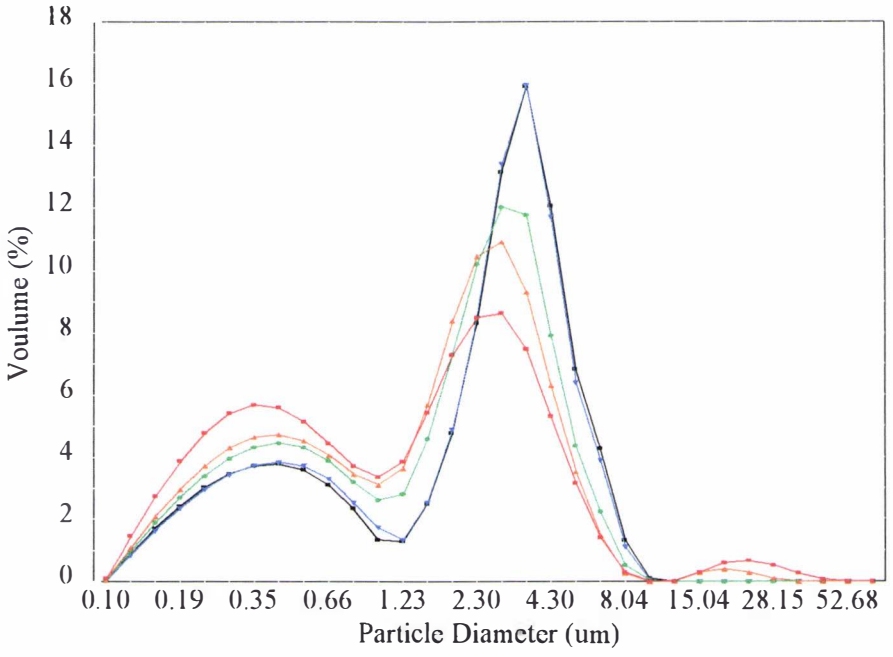


**Figure A3.2** Milk fat globule size distribution in: non-heated whole milk (black); milk heated to 72°C in plate heat exchanger (blue); milk heated to 85°C in DSI heater (green); milk heated to 95°C in DSI heater (orange); milk heated to 110°C in DSI heater (red).

Figures A3.3 (a) and (b) show confocal laser scanning micrographs of the fat globules samples from non-heated milk and milk heated to 95°C in the DSI heater. The graphs show that the number of small particles increased as the result of the DSI treatment. Some large and non-spherical particles were also observed in milk samples collected after the DSI heater (Figure A3.3b). These micrographs give a visual confirmation of the particle size analysis.

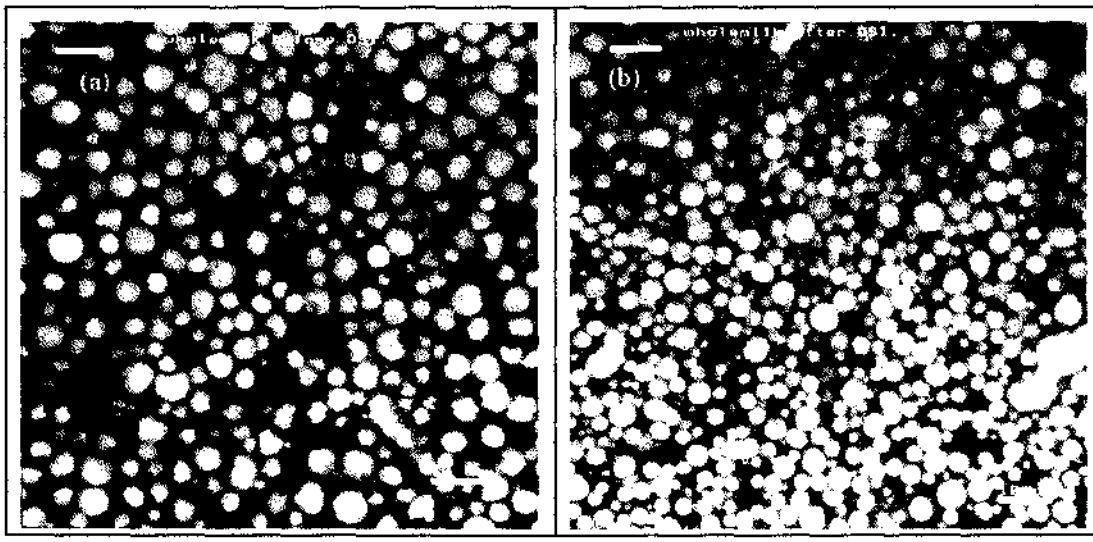


**Figure A3.3** Confocal laser scanning micrographs of the milk fat globules in (a) whole milk and (b) whole milk heated to 95°C using the DSI heater (bar=10 μm).

These results confirm the hypothesis that the DSI heater can break the fat globules into smaller ones. These small fat globules were damaged and some of them coalesced to form larger particles or aggregates. A possible explanation for the breaking up of fat globules is that injection of steam jets into the milk fluid and collapsing of steam vapour bubbles cause high pressure gradients within the body of the milk fluid. These pressure gradients impose shear forces of sufficient magnitude to deform the milk fat globule membranes and eventually rupture the membranes. Fat globules are therefore broken into many smaller ones. It was thought that small fat globules with damaged membranes were involved in the fouling process and hence the fat content of the deposits was increased. Further investigation is warranted.

**Table A3.5** Distribution of milk fat globules in fresh and heated whole milk

| Size (micron) | Volume (%) 6 C | 72 C PHE | 85 C DSI | 95 C DSI | 110 C DSI |
|---|---|---|---|---|---|
| 0.10 | 0.05 | 0.04 | 0.05 | 0.05 | 0.09 |
| 0.12 | 0.88 | 0.84 | 0.98 | 1.08 | 1.45 |
| 0.15 | 1.69 | 1.63 | 1.89 | 2.08 | 2.75 |
| 0.19 | 2.41 | 2.34 | 2.70 | 2.97 | 3.87 |
| 0.23 | 3.02 | 2.96 | 3.41 | 3.73 | 4.79 |
| 0.28 | 3.46 | 3.45 | 3.97 | 4.31 | 5.41 |
| 0.35 | 3.73 | 3.74 | 4.32 | 4.66 | 5.68 |
| 0.43 | 3.79 | 3.85 | 4.46 | 4.74 | 5.58 |
| 0.53 | 3.61 | 3.73 | 4.32 | 4.54 | 5.14 |
| 0.66 | 3.11 | 3.31 | 3.89 | 4.07 | 4.44 |
| 0.81 | 2.34 | 2.54 | 3.21 | 3.47 | 3.72 |
| 1.00 | 1.35 | 1.73 | 2.62 | 3.12 | 3.37 |
| 1.23 | 1.29 | 1.35 | 2.82 | 3.66 | 3.86 |
| 1.51 | 2.50 | 2.54 | 4.59 | 5.69 | 5.43 |
| 1.86 | 4.78 | 4.88 | 7.31 | 8.42 | 7.29 |
| 2.30 | 8.33 | 8.51 | 10.22 | 10.46 | 8.51 |
| 2.83 | 13.15 | 13.40 | 12.04 | 10.93 | 8.64 |
| 3.49 | 15.90 | 15.94 | 11.78 | 9.32 | 7.46 |
| 4.30 | 12.08 | 11.73 | 7.93 | 6.31 | 5.30 |
| 5.29 | 6.82 | 6.41 | 4.37 | 3.54 | 3.15 |
| 6.52 | 4.27 | 3.90 | 2.24 | 1.49 | 1.41 |
| 8.04 | 1.32 | 1.11 | 0.52 | 0.26 | 0.29 |
| 9.91 | 0.11 | 0.05 | 0.05 | 0.00 | 0.00 |
| 12.21 | 0.00 | 0.00 | 0.00 | 0.02 | 0.00 |
| 15.04 | 0.00 | 0.00 | 0.00 | 0.29 | 0.29 |
| 18.54 | 0.00 | 0.00 | 0.00 | 0.39 | 0.59 |
| 22.84 | 0.00 | 0.00 | 0.00 | 0.29 | 0.67 |
| 28.15 | 0.00 | 0.00 | 0.00 | 0.09 | 0.51 |
| 34.69 | 0.00 | 0.00 | 0.00 | 0.00 | 0.26 |
| 42.75 | 0.00 | 0.00 | 0.00 | 0.00 | 0.06 |
| 52.68 | 0.00 | 0.00 | 0.00 | 0.00 | 0.00 |
| 64.92 | 0.00 | 0.00 | 0.00 | 0.00 | 0.00 |
| D[3,2] | 0.96 | 0.96 | 0.84 | 0.78 | 0.67 |

## 4.3 Effects of critical flow pressure on steam condensation

To determine the effects of critical flow pressure ($P_c$) on the steam condensation, the sizes of the steam bubbles in the DSI heater was visually checked. Water was used as a test fluid and was heated to 95°C at 80 and 120 kg $h^{-1}$. A sight glass was placed immediately downstream from the DSI to allow photographs of the steam bubbles and water mixture to be taken. $P_c$ was varied using a back pressure valve (V8 in Figure 3.3), which was installed in the pipe after the sight glass. The pressure set by the back pressure valve (named $P_2$) was measured by a pressure gauge placed between the sight glass and the valve. This pressure was denoted as downstream pressure and was slightly lower than $P_c$ due to the pressure drop in the downstream area from the DSI and the sight glass. Other operation procedures of the fouling rig were similar to those set out in the previous sections.

Two runs were carried out for each flow rate (*i.e.* runs 1 and 2 for 80 kg $h^{-1}$ and runs 3 and 4 for 120 kg $h^{-1}$) and four levels of downstream pressures (called A, B, C and D) were set in each run. The downstream pressure was initially set at about the pressure required for critical flow ratio (Eq. A3.3). At this condition, $P_c$ was about 100 kPa above the boiling pressure (85 kPa) of the milk at 95°C plus the pressure drop in the DSI flow channel (condition A in Table A3.6). The downstream pressure was then increased to another three levels, at an increment of about 100 kPa each (i.e. conditions B, C and D). Consequently the steam supply pressure increased and the critical pressure ratio ($P_c / P_v$) also increased. It was observed that, for all runs, the steam bubbles were initially large, as the downstream pressures were increased the steam bubbles became smaller and then were no longer visible. These observations are also summarised in Table A3.6.

**Table A3.6** Effects of downstream pressure ($P_2$) on steam condensation

| Flow, Temperature & Initial $P_c$ | Run | Additional Pressure (kPa) | Back Pressure $P_2$ (kPa abs) | Steam Pressure $P_v$ (kPa abs) | $P_2/P_v$ Ratio | Steam Bubbles |
|---|---|---|---|---|---|---|
| 80 kg $h^{-1}$ | 1A | 91 | 235 | 490 | 0.48 | Large |
| 95°C | 1B | 236 | 380 | 520 | 0.73 | Small |
| | 1C | 296 | 440 | 580 | 0.76 | Smaller |
| 144 kPa | 1D | 356 | 500 | 610 | 0.82 | Not visible |
| 80 kg $h^{-1}$ | 2A | 136 | 280 | 510 | 0.55 | Large |
| 95°C | 2B | 196 | 340 | 570 | 0.60 | Small |
| | 2C | 296 | 440 | 620 | 0.71 | Smaller |
| 144 kPa | 2D | 356 | 500 | 660 | 0.76 | Not visible |
| 120 kg $h^{-1}$ | 3A | 89 | 225 | 375 | 0.60 | Large |
| 95°C | 3B | 179 | 315 | 430 | 0.73 | Small |
| | 3C | 314 | 450 | 530 | 0.85 | Smaller |
| 136 kPa | 3D | 414 | 550 | 620 | 0.89 | Not visible |
| 120 kg $h^{-1}$ | 4A | 124 | 260 | 400 | 0.65 | Large |
| 95°C | 4B | 229 | 365 | 460 | 0.79 | Small |
| | 4C | 294 | 430 | 520 | 0.83 | Smaller |
| 136 kPa | 4D | 364 | 500 | 600 | 0.83 | Not visible |

Figure A3.4 shows an example of the photographs of the steam bubbles and water mixture in the sight glass at various downstream pressures in run 3. Initially, large steam bubbles of about 1 - 2 mm diameter were observed at 225 kPa abs. As the pressures were increased to 285 kPa, the steam bubbles became smaller and were about 0.5 - 1 mm. The bubbles were less than 0.5 mm at 420 kPa and non were visible at 520 kPa (the steam bubbles can not be seen from the photographs at 420 kPa).

It was concluded that in order to obtain small steam bubbles for rapid steam condensation and hence reducing fouling in the DSI, $P_2$ should be set and maintained at several times higher than the fluid boiling pressure corresponding to the treatment temperature. Although any additional pressure above the initial level of 100 kPa will result in smaller steam bubbles, it also requires higher supply steam pressure and hence reduces the range of pressure that the DSI can be operated. It was therefore taken that $P_2$ (hence $P_c$) be set at 200 kPa, instead of 100 kPa, above the fluid boiling pressure corresponding to the treatment temperature. At this condition, the steam bubbles should be in the range of 0.5 - 1 mm and the steam supply pressure should be at about 400 kPa at the start of the run.

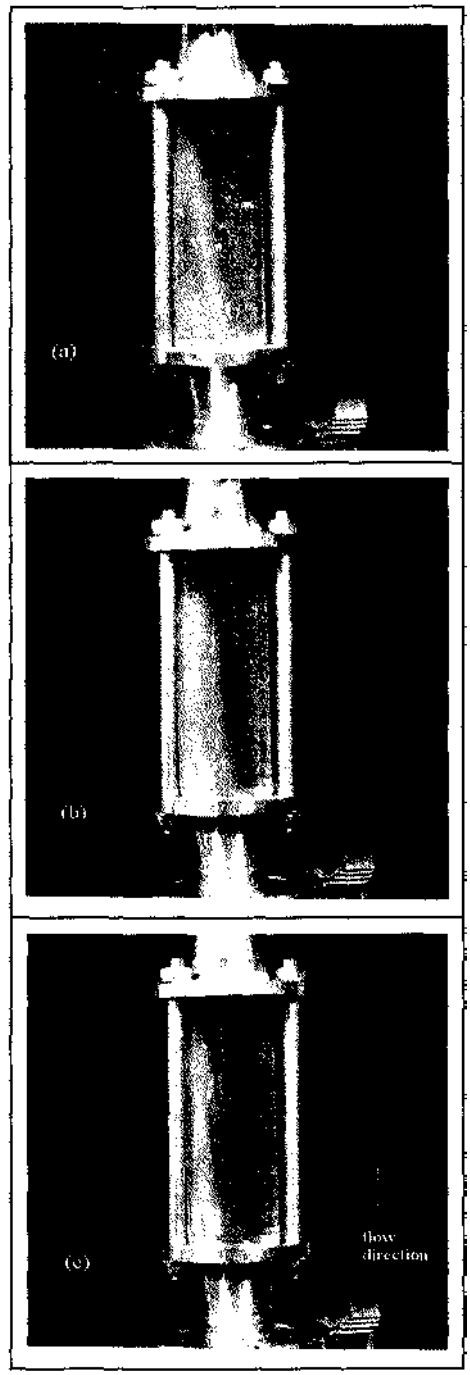


**Figure A3.4** Photographs of steam bubbles in the pipe downsteam of the DSI heater at various back pressures: (a) 125 kPa - large bubbles about 1 - 2 mm in diameter; (b) 215 kPa - small bubbles about 0.5 - 1 mm; (c ) 350 kPa - smaller bubbles (less than 0.5 mm) which can not be seen from the photograph.

To validate the new design criteria that $P_c$ should be set at about 200 kPa, above the fluid boiling pressure corresponding to the treatment temperature, a trial was carried out to determine the effects $P_c$ on fouling in the DSI heater. Whole milk was heated to 95°C at 120 kg $h^{-1}$ under two different back pressures 240 and 340 kPa (abs) (*i.e.* about 100 and 200 kPa above milk boiling pressure at 95°C). Fouling in the DSI, as indicated by the increase in the steam supply pressure, was monitored during the experimental runs. The results are shown in Figure A3.5.

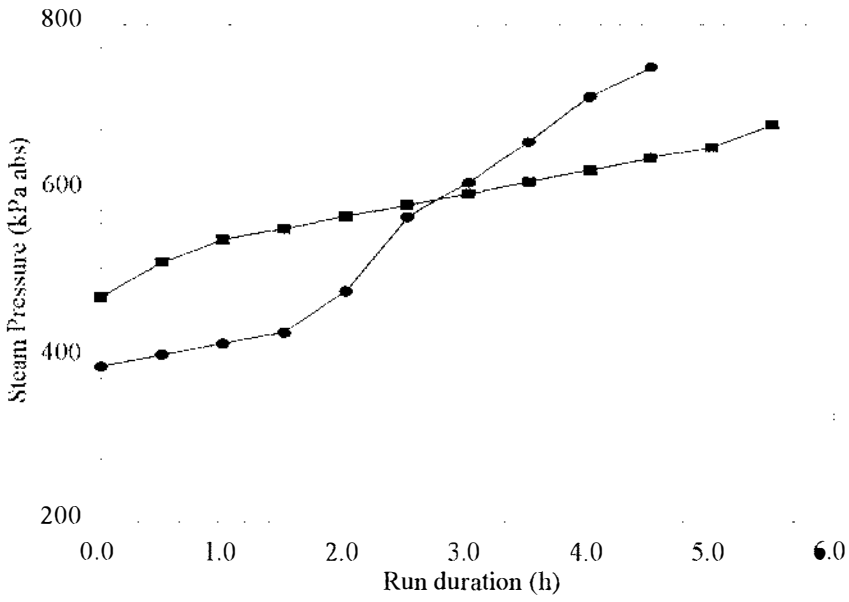


**Figure A3.5** Plots of DSI steam supply pressure versus run duration for two different downstream pressure: (●) 240 kPa; (■) 340 kPa.

At 240 kPa downstream pressure, the steam supply pressure started a low level but increased to higher levels during the run at a faster rate (88 kPa $h^{-1}$) compared with the increasing rate (33 kPa $h^{-1}$) of steam pressures with the run employed 340 kPa downstream pressure. These results support the hypothesis that the critical flow pressure at the steam nozzle should be set at 200 kPa above the fluid boiling pressure to reduce fouling in the DSI heater.

## 5 Concluding remarks

The results obtained from this investigation show the important requirements for design and operation of a DSI heater to minimise fouling. They are:

(1) The pressure in the flow channel should be maintained at least at 200 kPa absolute pressure above the boiling pressure coressponding to the treatment temperature.

(2) Rapid condensation of steam bubbles and minimum cavitation can be achieved by injecting steam via a number of small injection nozzles.

Direct injection of steam to whole milk damages the milk fat globules and brakes them into smaller ones. Some of the damaged fat globules coalesce and form larger particles or aggregates. Damaged fat globules could be involved in the fouling process. The design of the DSI heater could therefore be improved to minimise fat globule damage.

## Appendix 3.3

## Mechanical design drawing of the horizontal open test piece

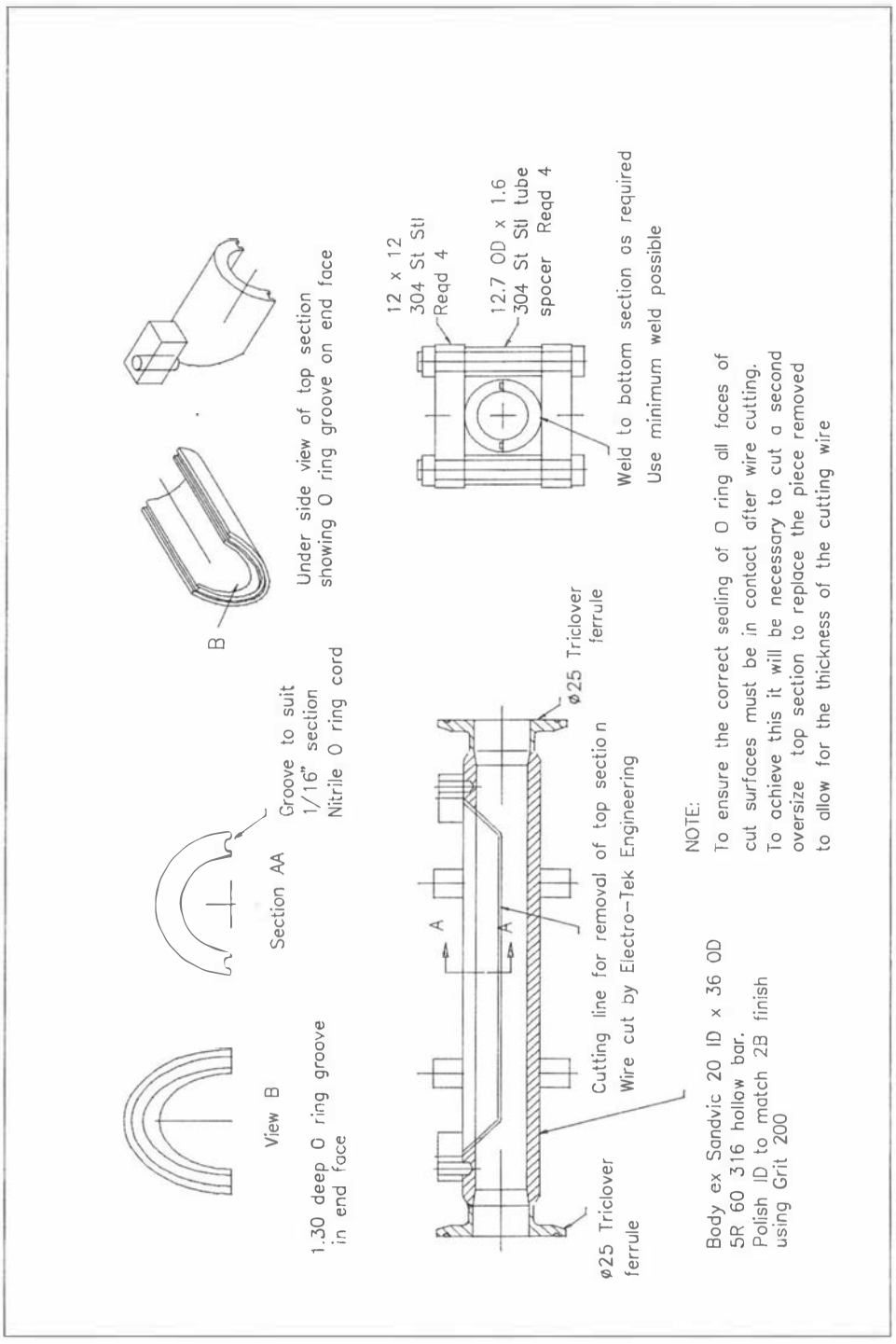

## Appendix 4.1

## Thermal properties of heat flux sensors

## (Rhopoint Ltd, Oxted, UK)

| Serial no. | Part no. | Out put At 21 C ($\mu V/Wm^{-2}$) | Multiply factor (W.m-2/mV) | Temp. correction y = a (T) + b (40 < T < 200 C) | |
|---|---|---|---|---|---|
| | | | | a | b |
| 94M-0331 | 27036-3 | 0.374 | 2,673.4 | -0.00072 | 1.0072 |
| 94M-0332 | 27036-3 | 0.371 | 2,696.2 | -0.00072 | 1.0072 |
| 96I-04530 | 27036-3 | 0.374 | 2,673.4 | -0.00072 | 1.0072 |
| 96I-04531 | 27036-3 | 0.371 | 2,696.2 | -0.00072 | 1.0072 |
| 970-68399 | 27036-3 | 0.406 | 2,464.5 | -0.00072 | 1.0072 |
| 970-68400 | 27036-3 | 0.422 | 2,371.9 | -0.00072 | 1.0072 |
| 971-22044 | 27036-3 | 0.396 | 2,523.7 | -0.00072 | 1.0072 |
| 971-22045 | 27036-3 | 0.403 | 2,483.9 | -0.00072 | 1.0072 |
| 971-22046 | 27036-3 | 0.403 | 2,483.9 | -0.00072 | 1.0072 |
| 94K-0405 | 20455-3 | 0.529 | 1,889.0 | -0.002 | 1.028 |
| 94K-0406 | 20455-3 | 0.523 | 1,911.9 | -0.002 | 1.028 |
| 94K-0407 | 20455-3 | 0.520 | 1,923.5 | -0.002 | 1.028 |
| 94K-0416 | 20455-3 | 0.526 | 1,900.4 | -0.002 | 1.028 |
| 94K-0415 | 20455-3 | 0.529 | 1,889.0 | -0.002 | 1.028 |
| 94K-0414 | 20455-3 | 0.520 | 1,923.5 | -0.002 | 1.028 |
| 94K-0413 | 20455-3 | 0.529 | 1,889.0 | -0.002 | 1.028 |
| 94K-0412 | 20455-3 | 0.533 | 1,877.7 | -0.002 | 1.028 |
| 94K-0411 | 20455-3 | 0.529 | 1,889.0 | -0.002 | 1.028 |

## Appendix 4.2

## Summary of calibration results of the fouling monitoring system

| Run | 4.1 | 4.2 | 4.3 | 3.2 | 3.3 | 4.4 | 3.4 | 3.5 | 3.6 | 4.5 |
|---|---|---|---|---|---|---|---|---|---|---|
| Date | 13/5/97 | 20/5/97 | 21/5/97 | 21/8/97 | 12/9/97 | 25/9/97 | 25/11'97 | 27/3/98 | 3/4/98 | 9/4/98 |
| Fluid | wm | wm | wm | wm | wm | wm | wm | wm | wm | wm |
| Temp. | 85 | 85 | 85 | 95 | 95 | 95 | 95 | 110 | 110 | 110 |
| $I_f$ | Deposit thickness (mm) | | | | | | | | | |
| 1.00 | | | | | | 0.50 | | | | 0.5 |
| 0.95 | | | | | | 0.50 | | 0.534 | 0.49 | 0.5 |
| 0.87 | | | | | | 0.59 | | | | |
| 0.80 | | | | | 0.50 | | 1.05 | 0.95 | | 1.05 |
| 0.70 | 2.09 | | | 1.212 | | | | | 1.51 | 1.50 |
| 0.67 | | | 2.12 | | | | | | | |
| 0.65 | | | | | 1.42 | | 1.55 | | | |
| 0.60 | | | | 2.11 | | | | | | |
| 0.52 | | | | | | | 3.03 | | | |
| 0.50 | 2.81 | | | 3.12 | 2.05 | | | | | |
| 0.45 | | 3.93 | | | | | | | | |
| 0.40 | | | 2.96 | | | | 4.05 | | | |
| 0.36 | | | | | 3.02 | | | | | |
| 0.20 | 5.93 | 6.05 | | | | | | | | |

## Appendix 4.2 (Cont.)

| Run | 4.60 | 4.70 | 5.70 | 5.80 | 5.90 | 5.10 | 4.80 | 4.90 | 4.10 | 4.11 |
|---|---|---|---|---|---|---|---|---|---|---|
| Date | 16/4/98 | 27/4/98 | 21/5/98 | 25/5/98 | 26'5'98 | 28/5/98 | 3/9/98 | 4/9/98 | 12/10/98 | 15/10/98 |
| Fluid | wm | wm | wm | wm | wm | wm | wm | wm | wm | wm |
| Temp. | 110 | 110 | 95 | 95 | 95 | 95 | 95 | 95 | 95 | 95 |
| If | Deposit thickness (mm) | | | | | | | | | |
| 1.00 | | | | | | | | | | |
| 0.95 | 0.50 | 0.50 | | 0.50 | 0.48 | 0.50 | | 0.50 | 0.50 | 0.50 |
| 0.90 | | | | 0.50 | | | 0.63 | | 0.71 | |
| 0.87 | | | | | | | | | 0.87 | 0.62 |
| 0.85 | | | | 0.59 | 0.99 | 0.83 | 1.02 | | | |
| 0.82 | | | | | | | | | 0.94 | |
| 0.80 | | | 0.93 | | | | | | | |
| 0.78 | | | | 0.99 | | | | | | |
| 0.75 | | 0.79 | | | | | | | | |
| 0.70 | 1.37 | | | 1.50 | 1.85 | | | 1.55 | | |
| 0.67 | | | | | | | | 1.95 | | |
| 0.65 | | | | 1.49 | | | | | | |
| 0.60 | | | 1.95 | | | | | | | |
| 0.55 | | 1.58 | | | | | | | | |
| 0.54 | 2.20 | | | | | | | | | |
| 0.50 | | | 2.05 | | | | | | | |
| 0.45 | | 3.02 | | | | | | | | |
| 0.40 | | 2.82 | | 2.86 | | | | | | |
| 0.30 | | 3.92 | | | | | | | | |

## Appendix 4.2 (cont.)

| Run | 4.12 | 5.11 | 5.12 | 5.13 | 4.13 | 4.14 | 5.14 | 5.15 | 5.16 |
|---|---|---|---|---|---|---|---|---|---|
| Date | 21/12/98 | 4/3/99 | 5/3/99 | 5/3/99 | 18/3/99 | 19/3/99 | 26/3/99 | 26/3/99 | 26/3/99 |
| Fluid | wm | wm | wm | wm | wm | wm | wm | wm | wm |
| Temp. | 95 | 95 | 95 | 95 | 95 | 95 | 95 | 95 | 95 |
| If | Deposit thickness (mm) | | | | | | | | |
| 0.93 | | 0.50 | | | 0.50 | 0.50 | | | |
| 0.92 | | | | | 0.50 | | | | |
| 0.90 | 0.92 | | | | | | | | |
| 0.89 | | | | | 0.50 | 0.50 | | | |
| 0.87 | | | 0.98 | | | | | | |
| 0.85 | | | | 0.85 | | 0.90 | 1.00 | | |
| 0.82 | | | | | | | 1.00 | 0.90 | |
| 0.79 | | | | | 0.85 | | | | |
| 0.78 | | | | | 1.20 | | | | |
| 0.75 | | | | | | 1.00 | | | |
| 0.72 | | | | | 1.50 | | | | |
| 0.70 | | | | | | | 2.25 | | |
| 0.65 | | | | | | | | 1.50 | |
| 0.61 | | 1.54 | | | | | | | |
| 0.60 | | | | 2.25 | | | 2.50 | | |
| 0.59 | | | | | | | | 2.00 | |
| 0.59 | | | | | | | | 1.60 | |
| 0.58 | | | | | | | | 1.90 | 2.50 |
| 0.55 | | | | 2.32 | | | | | |
| 0.54 | | | | | | 2.00 | | | |
| 0.52 | | 2.95 | | | | | | | |
| 0.49 | | | 3.45 | | | | | | |
| 0.47 | | | 3.51 | | | | | | |
| 0.43 | | | | 3.62 | | | | 3.50 | |
| 0.39 | | | 4.33 | | | | | | |
| 0.35 | | | 5.25 | | | | | | |
| 0.33 | | | | | | | | | 4.00 |
| 0.33 | | | | | | | | | 4.25 |
| 0.30 | | 4.12 | | | | | | | |
| 0.26 | | | | | | | | | 4.00 |
| 0.26 | | | | | | | | | 5.00 |
| 0.25 | | | | | | | | | 4.00 |
| 0.20 | | | | 5.70 | | | | | |
| 0.20 | | | | 5.56 | | | | | |

## Appendix 4.3
## Charactersistics of fouling deposits

This section reports the composition and structure of the fouling layer obtained from whole milk heated to 85, 95 and 110°C in the fouling rig. The details of the relevant experiments and the analytical methods have been listed elsewhere in the chapters of the thesis and hence they will not be repeated in this section.

### 1 Chemical analysis

Table A4.1 shows the compositions of fouling deposits on a dry weight basis. The sum of the fat, protein and ash contents (on a dry weight basis) of each sample was not 100%; the fouling layer might have contained other components such as lactose for which measurements were not made.

The fat content of deposits was in the range 25.8-49.7% which was higher than that observed by other workers (Jeurnink *et al.*, 1994). Although storage of milk for several days before the experiment may have contributed to this results, it was thought that the injection of steam to the milk damaged the milk fat globules and caused the fat content to increase.

The protein and mineral contents were in the range of 35.3-54.3% and 2.4-7.9% respectively. The results indicate that the deposits obtained in this study resemble type A deposit as defined by Burton (1968), *i.e.* high protein and low mineral content in the deposit. Although the protein contents were lower than the values of 50-70% commonly reported in the literature, these results were a natural consequence of the high fat contents. The results also show that increasing treatment temperatures from 85 to 110°C slightly increased the mineral content of deposits.

**Table A4.1** Compositions of fouling deposits collected from the fouling rig

| Run | DSI (°C) | Moisture (%) | Fat | Ash | Protein | SUM |
|---|---|---|---|---|---|---|
| | | | (% dry basis) | | | |
| 4.1 | 85 | na | 42.09 | 3.61 | 40.20 | 85.90 |
| 3.2 | 95 | 68.5 | 38.10 | 2.35 | 45.37 | 85.82 |
| 3.3 | 95 | 65.2 | 40.50 | 2.74 | 47.21 | 90.45 |
| 3.4 | 95 | 64.7 | 25.81 | 3.23 | 54.28 | 83.32 |
| 4.6 | 110 | 66.5 | 39.40 | 7.89 | 39.04 | 86.33 |
| 4.7 | 110 | 65.8 | 37.43 | 6.78 | 44.21 | 88.42 |
| 5.12 | 95 | na | 30.40 | 5.22 | 37.19 | 72.81 |
| 5.13 | 95 | na | 49.73 | 4.26 | 35.31 | 89.30 |
| 5.14 | 95 | na | 28.05 | 6.19 | 46.73 | 80.97 |

nd: not analysed

## 2 Observation of the structure of the fouling layer

To observe the structure of the fouling layer, some of the wet samples collected from run 5.13 were fixed with buffered glutaraldehyde/formaldehyde, dehydrated using acetone and air dried. The internal structures of the dried samples were determined by cutting the samples transversally using a stainless steel razor blade. They were then gold coated and scanned in a Cambridge 250 Mark 3 scanning electron microscope (SEM).

Figure A4.1 shows the structures of fouling deposits obtained from whole milk heated to 95°C. The deposit was a thin fouling layer of about 0.5 mm thick and consisted of a compact sub-layer of thickness of about 20 μm and a top-layer. The top-layer was composed of small strands of particles that were anchored to the sub-layer but were not linked.

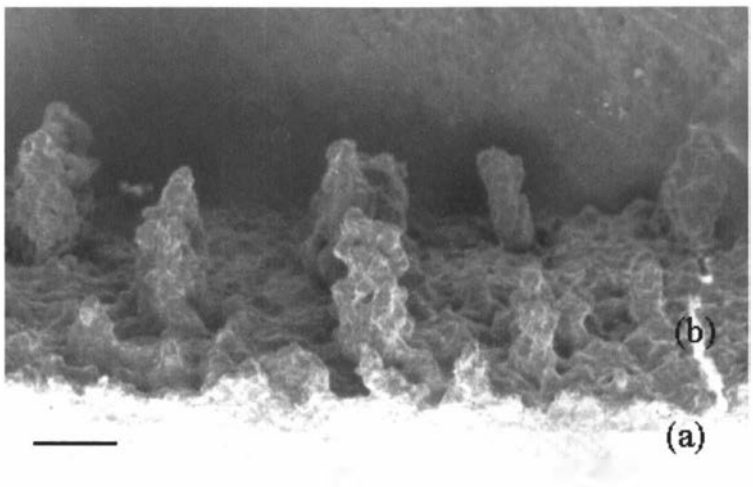


**Figure A4.1** Scanning electron micrograph of a thin fouling layer obtained from heating whole milk at 95°C, (bar=200μm): (a) fouling layer/test piece interface; (b) top-layer

Figure A4.2 shows the structure of a thick deposit layer of about 2 mm. The results show that the fouling layer consisted of a compact sub-layer of thickness of about 20μm and a porous top-layer. The top-layer was composed of small particles of different sizes, which were randomly linked by bridges and anchored to the sub-layer. Several dense blocks of particles were also obsreved. The surface of the fouling layer was irregular and contained high 'hills' and deep 'valleys'. The presence of the fouling layer composed of a sub-layer and a top-layer resembles the structure observed on heated surfaces by previous workers (Tissier & Lalande, 1986; Foster *et al.*, 1989; Foster & Green, 1990).

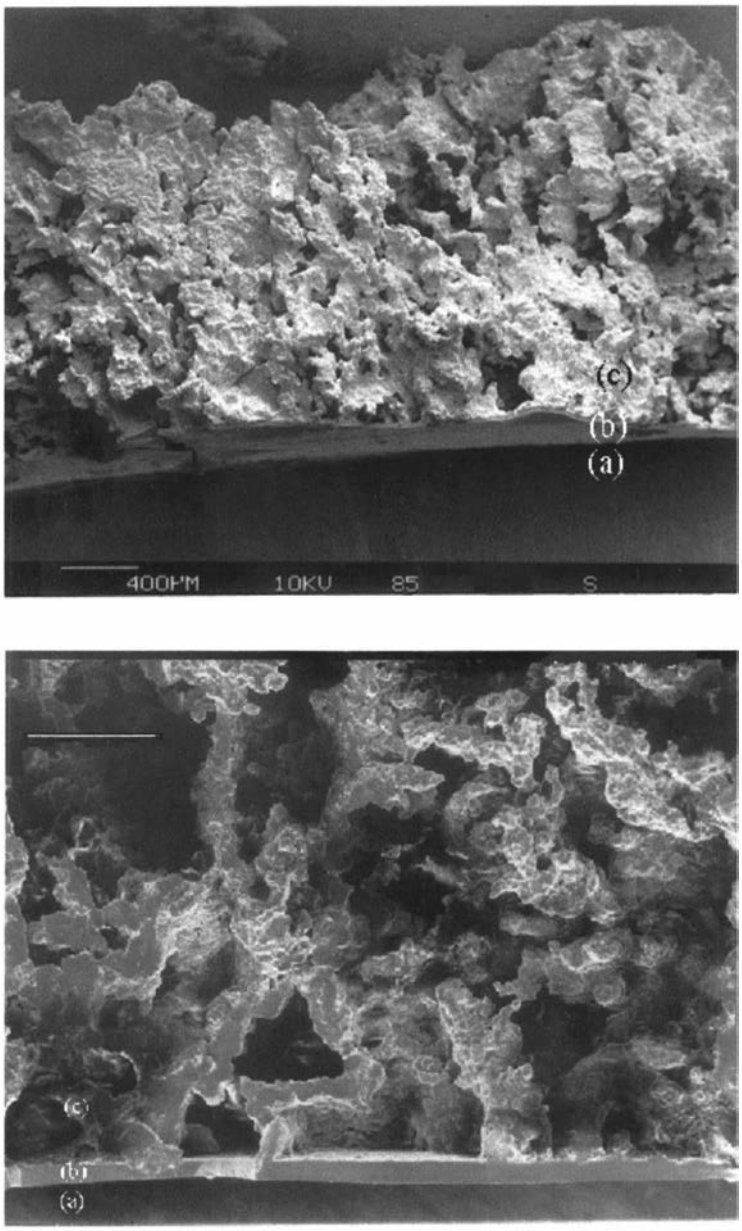


**igure A4.2** Scanning electron micrograph of a thick fouling layer obtained from heating whole milk at 95°C: (a) fouling layer/test piece interface; (b) sub-layer; (c) top-layer. The bottom picture shows the enlargement of the structure of deposit observed in the sub-layer (bar=100 μm).

## Appendix 4.4

## Normalised heat transfer coefficient of tubular heat exchanger fouled by skim milk

(Reproduced from Delsing & Hiddink, 1983)

| Time (min) | U ($W\ m^{-2}\ K^{-1}$) | 1/U ($K\ W^{-1}\ m^{-2}$) | Rf ($K\ W^{-1}\ m^{-2}$) | Ui(t)/Ui(0) |
|---|---|---|---|---|
| 0 | 670 | 0.00149 | 0.00000 | 1.00 |
| 4 | 730 | 0.00137 | -0.00012 | 1.09 |
| 8 | 770 | 0.00130 | -0.00019 | 1.15 |
| 10 | 820 | 0.00122 | -0.00027 | 1.22 |
| 12 | 830 | 0.00120 | -0.00029 | 1.24 |
| 20 | 840 | 0.00119 | -0.00030 | 1.25 |
| 26 | 840 | 0.00119 | -0.00030 | 1.25 |
| 30 | 820 | 0.00122 | -0.00027 | 1.22 |
| 36 | 800 | 0.00125 | -0.00024 | 1.19 |
| 50 | 770 | 0.00130 | -0.00019 | 1.15 |
| 60 | 750 | 0.00133 | -0.00016 | 1.12 |
| 74 | 720 | 0.00139 | -0.00010 | 1.07 |
| 86 | 700 | 0.00143 | -0.00006 | 1.04 |
| 98 | 660 | 0.00152 | 0.00002 | 0.99 |
| 110 | 650 | 0.00154 | 0.00005 | 0.97 |
| 120 | 630 | 0.00159 | 0.00009 | 0.94 |
| 132 | 620 | 0.00161 | 0.00012 | 0.93 |
| 144 | 600 | 0.00167 | 0.00017 | 0.90 |
| 156 | 590 | 0.00169 | 0.00020 | 0.88 |

## Appendix 5.1
## Summary of results of runs 5.1 to 5.6
## Section 5.2.2

Plots of normalised internal heat transfer coefficients, $I_f$, obtained at six locations downstream of the expansion (test piece B geometry) versus run duration for run 5.1 to 5.6 are shown in Figure A5.1 to A5.6.

The fouling rates for those runs were calculated using the procedures set out in Chapter 4. The results are listed in Tables A5.1 and A5.2. Generally, the $I_f$ data conform closely to the linear regression line (*i.e.* Std Err of Y Est was small) and $I_f$ strongly relates to the run duration (*i.e.* R squared is close to 1).

The absolute value of X coefficient of the regression analysis of each run was divided to 3600 seconds to yield the fouling rate (as the rate of change of $I_f$ per second). The duration of the delay period of each run, which was the period between the run starting time and the time at which $I_f$ started to decline was calculated using the procedure set out in Section 5.2.2. The results are also listed in Tables A5.1 and A5.2.

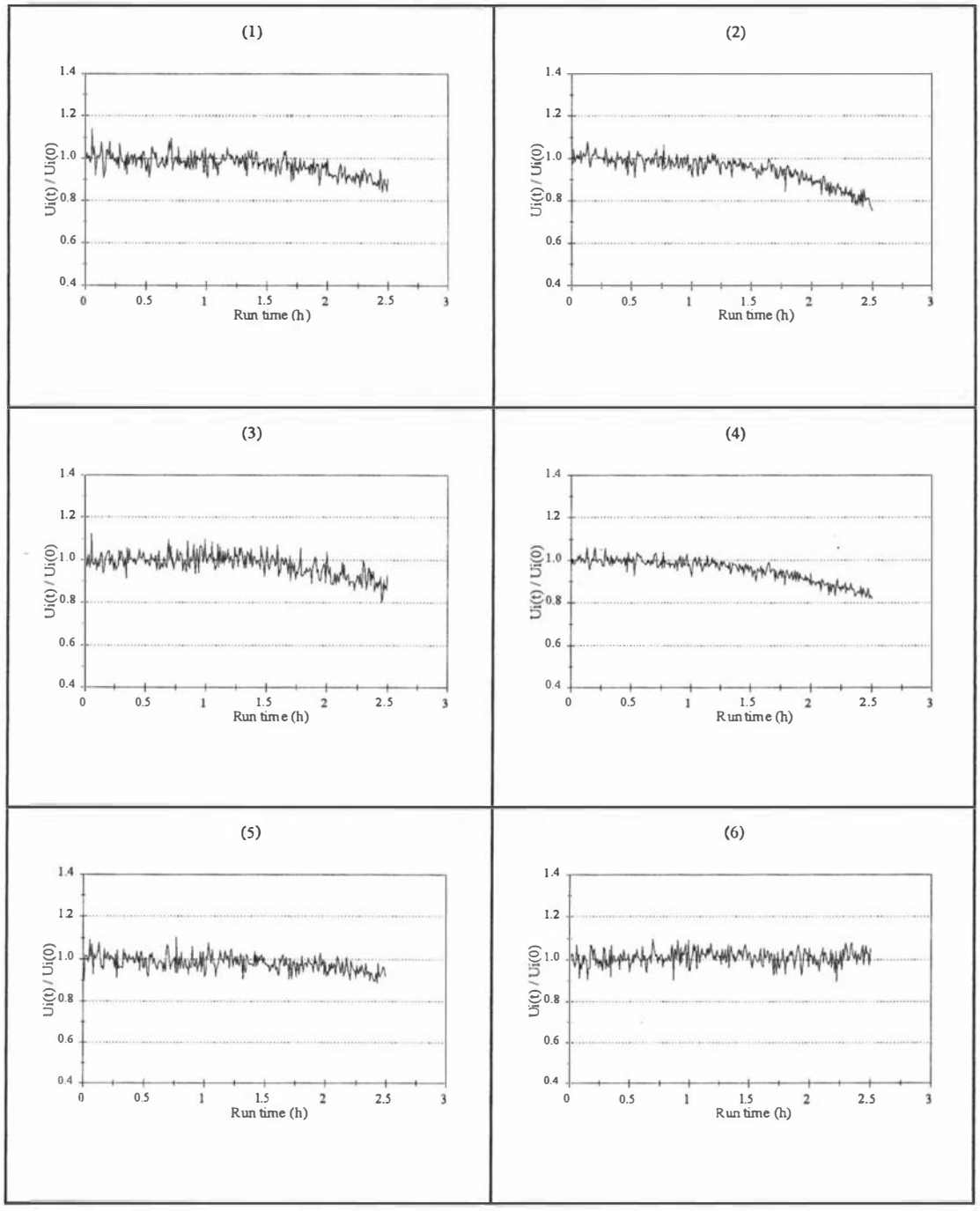


**Figure A5.1** Local fouling characteristics downstream of the step of the sudden expansion in Run 5.1 (milk A, day 2, 120 kg $h^{-1}$): (1) x=10 mm; (2) x=20 mm; (3) x=40 mm; (4) x=60 mm; (5) x=80 mm and (6) x=120 mm.

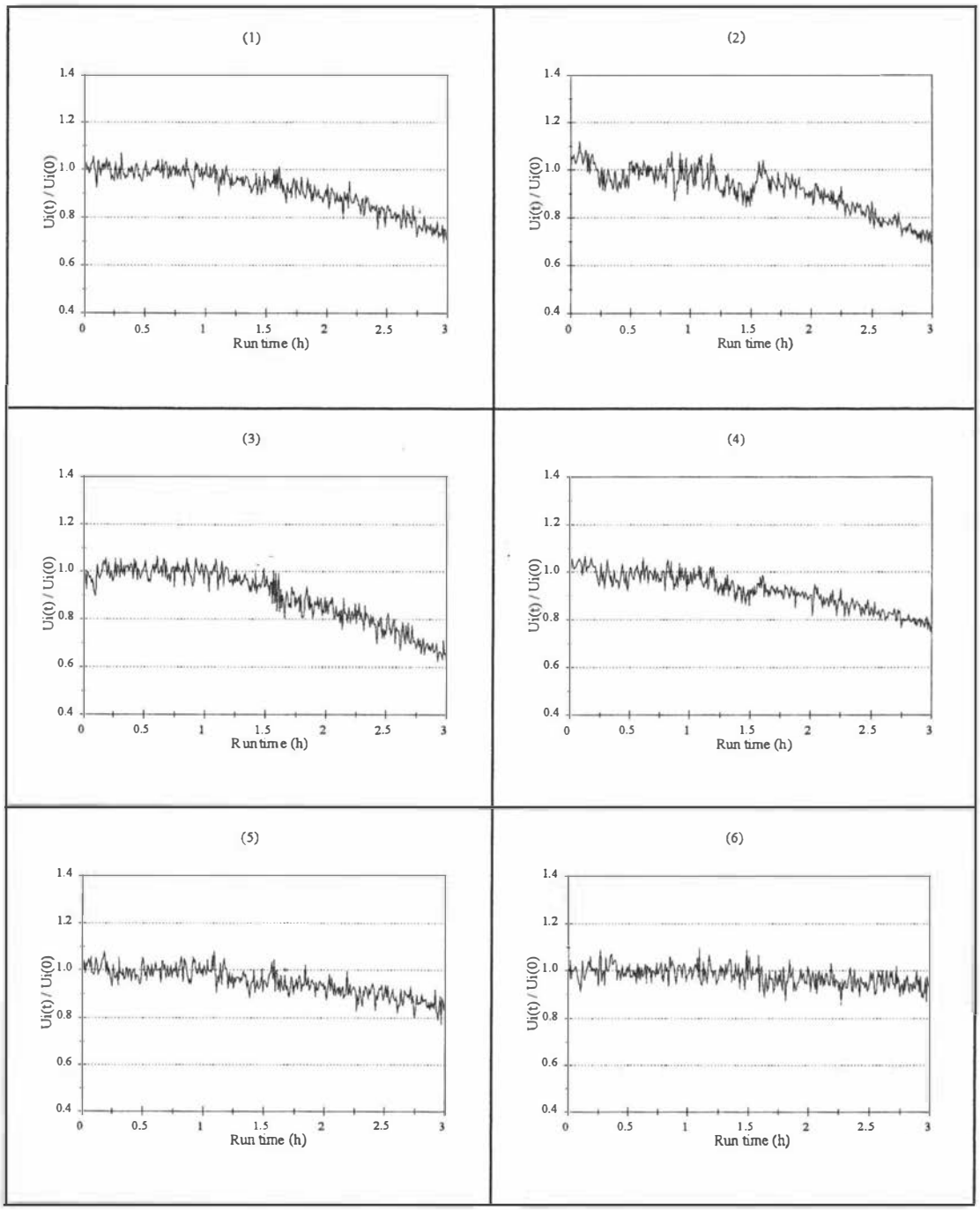


**Figure A5.2** Local fouling characteristics downstream of the step of the sudden expansion in Run 5.2 (milk A, day 4, 120 kg $h^{-1}$): (1) x=10 mm; (2) x=20 mm; (3) x=40 mm; (4) x=60 mm; (5) x=80 mm and (6) x=120 mm.

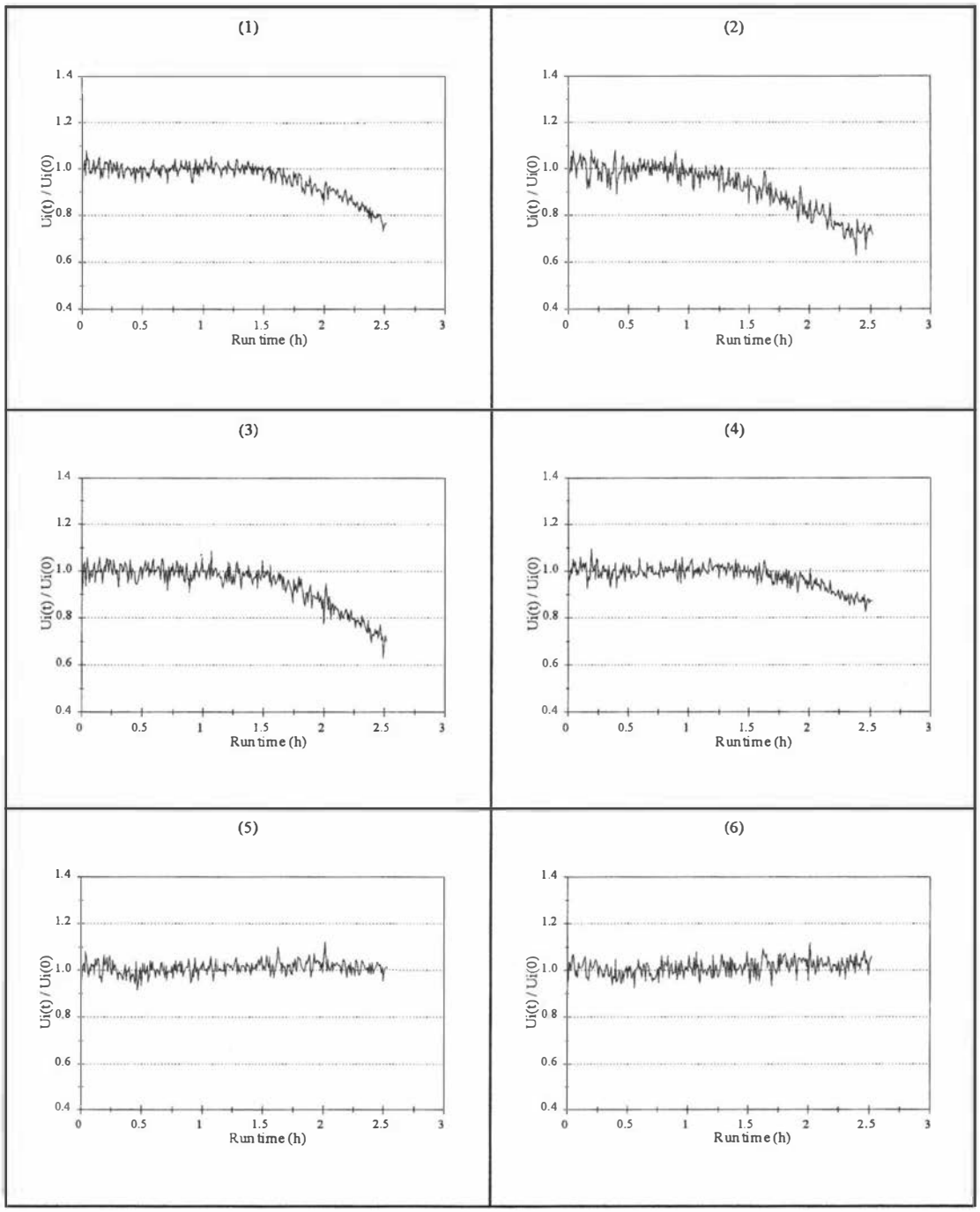


**Figure A5.3** Local fouling characteristics downstream of the step of the sudden expansion in Run 5.3 (milk A, day 5, 150 kg $h^{-1}$): (1) x=10 mm; (2) x=20 mm; (3) x=40 mm; (4) x=60 mm; (5) x=80 mm and (6) x=120 mm.

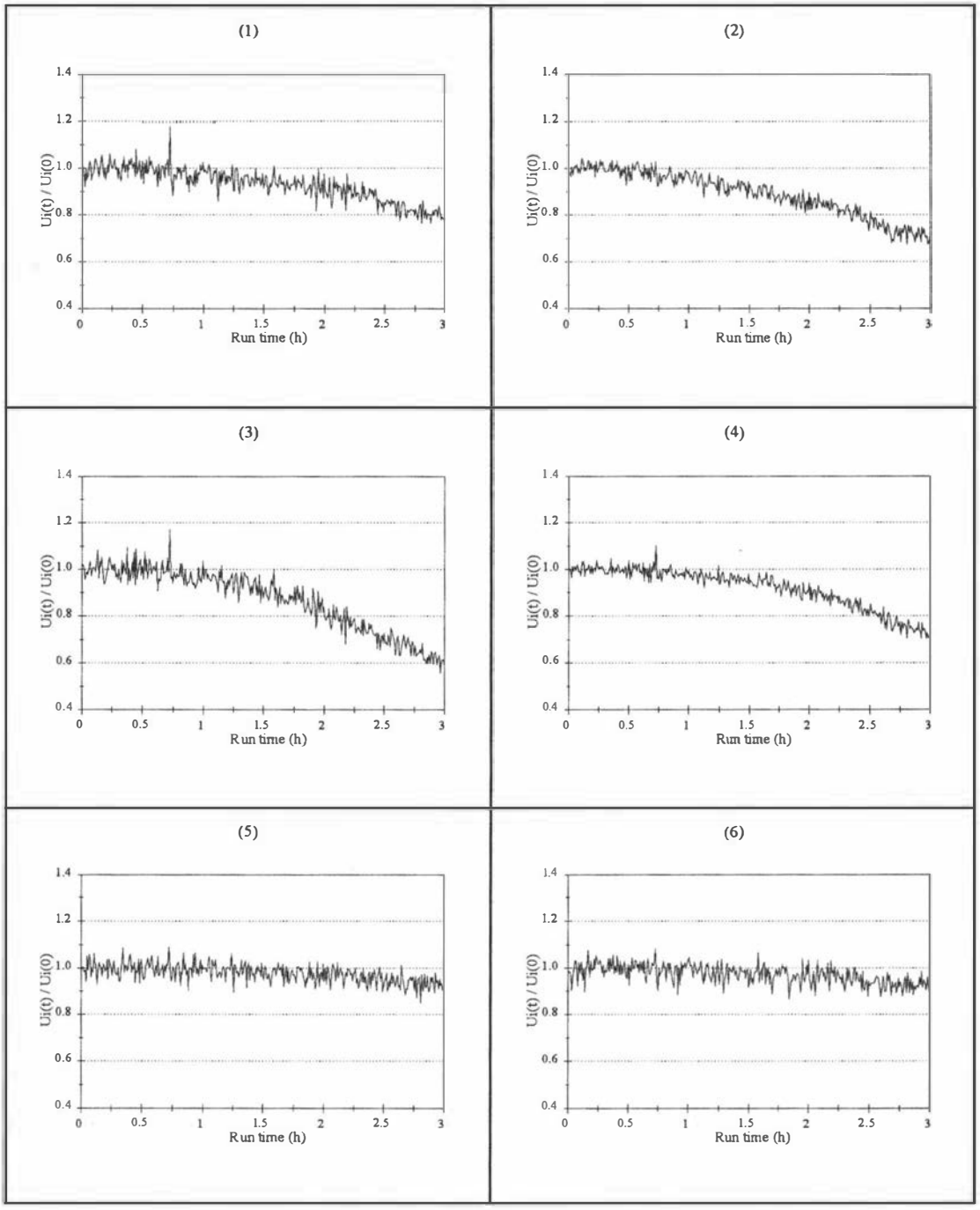


**Figure A5.4** Local fouling characteristics downstream of the step of the sudden expansion in Run 5.4 (milk B, day 1, 120 kg $h^{-1}$): (1) x=10 mm; (2) x=20 mm; (3) x=40 mm; (4) x=60 mm; (5) x=80 mm and (6) x=120 mm.

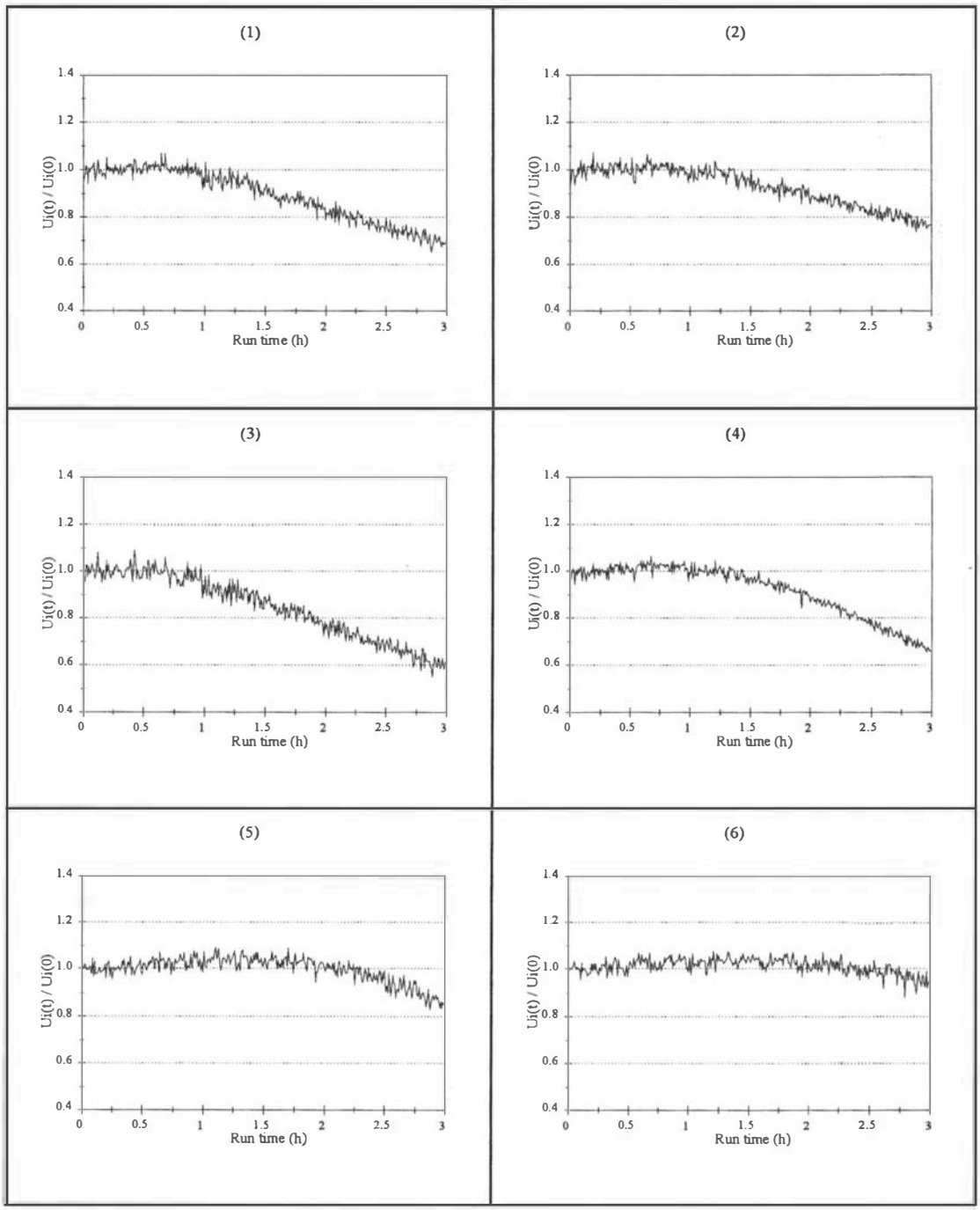


**Figure A5.5** Local fouling characteristics downstream of the step of the sudden expansion in Run 5.5 (milk B, day 1, 150 kg $h^{-1}$): (1) x=10 mm; (2) x=20 mm; (3) x=40 mm; (4) x=60 mm; (5) x=80 mm and (6) x=120 mm.

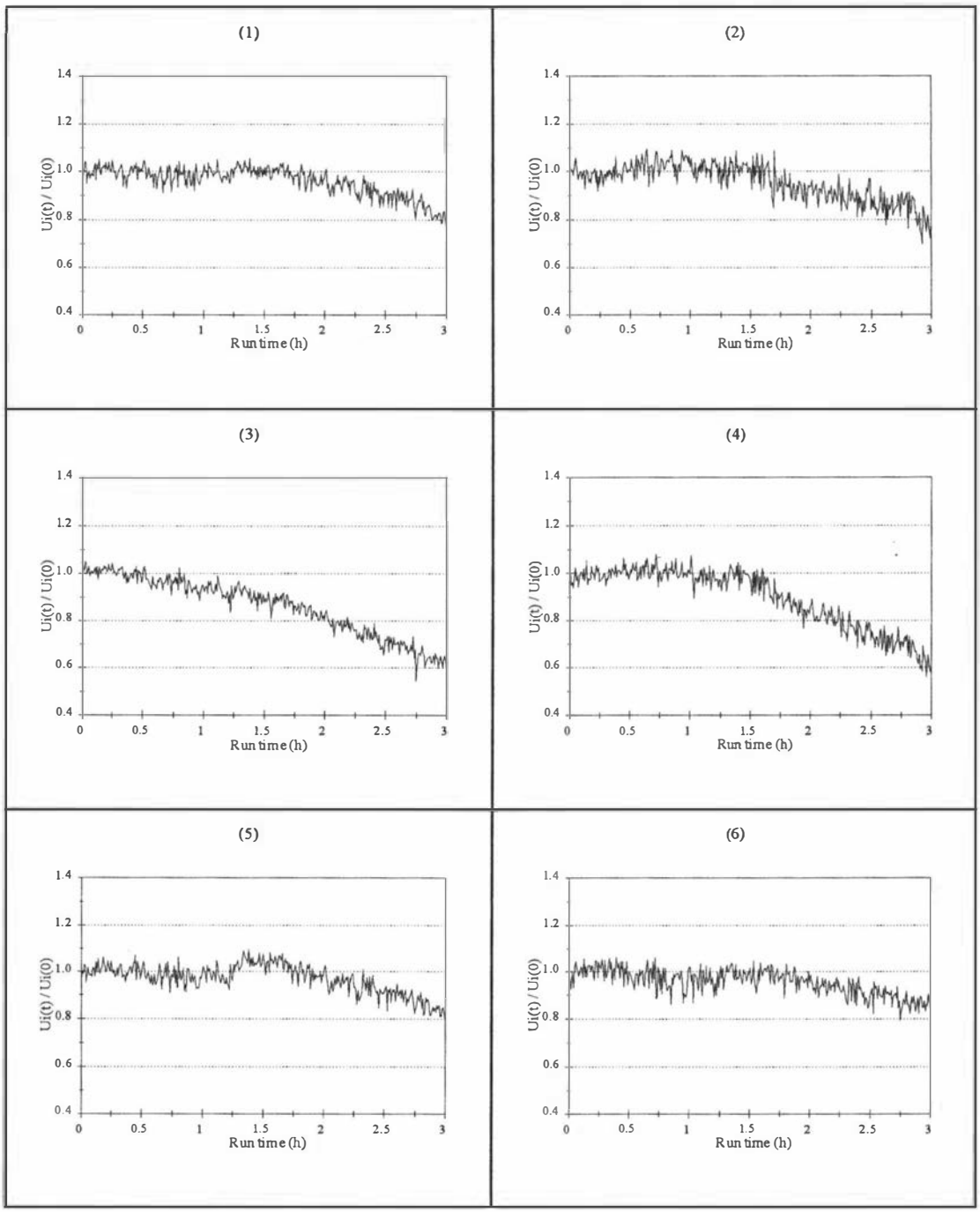


**Figure A5.6** Local fouling characteristics downstream of the step of the sudden expansion in Run 5.6 (milk B, day 2, 120 kg $h^{-1}$): (1) x=10 mm; (2) x=20 mm; (3) x=40 mm; (4) x=60 mm; (5) x=80 mm and (6) x=120 mm.

**Table A5.1** Summary of results of runs 5.1, 5.2 and 5.3

| Run | Analysis output | Distance from step (mm) | | | | | |
|---|---|---|---|---|---|---|---|
| | | **7.5** | **20** | **40** | **60** | **80** | **130** |
| **5.1** | Constant | 1.104 | 1.161 | 1.132 | 1.107 | 1.057 | 1.014 |
| | Std Err of Y Est | 0.030 | 0.027 | 0.036 | 0.019 | 0.029 | 0.034 |
| | R Squared | 0.579 | 0.823 | 0.563 | 0.842 | 0.294 | 0.001 |
| | No. of Observations | 160 | 160 | 160 | 160 | 160 | 160 |
| | Degrees of Freedom | 158 | 158 | 158 | 158 | 158 | 158 |
| | X Coefficient (h) | -0.091 | -0.148 | -0.106 | -0.113 | -0.048 | -0.003 |
| | Std Err of Coef. | 0.006 | 0.005 | 0.007 | 0.004 | 0.006 | 0.007 |
| | *Fouling rate (10-5*s-1)* | *2.5* | *4.1* | *3.0* | *3.1* | *1.3* | *0.1* |
| | *Delay time (h)* | *1.14* | *1.08* | *1.24* | *0.95* | *1.18* | *nd* |
| **5.2** | Constant | 1.188 | 1.265 | 1.197 | 1.118 | 1.081 | 1.013 |
| | Std Err of Y Est | 0.029 | 0.028 | 0.036 | 0.023 | 0.031 | 0.035 |
| | R Squared | 0.829 | 0.887 | 0.819 | 0.824 | 0.537 | 0.088 |
| | No. of Observations | 180 | 180 | 180 | 180 | 180 | 180 |
| | Degrees of Freedom | 178 | 178 | 178 | 178 | 178 | 178 |
| | X Coefficient (h) | -0.149 | -0.181 | -0.176 | -0.112 | -0.076 | -0.025 |
| | Std Err of Coef. | 0.005 | 0.005 | 0.006 | 0.004 | 0.005 | 0.006 |
| | ***Fouling rate (10-5*s-1)*** | ***4.1*** | ***5.0*** | ***4.9*** | ***3.1*** | ***2.1*** | ***0.7*** |
| | *Delay time (h)* | *1.00* | *1.20* | *1.12* | *1.06* | *1.2* | *1.5* |
| **5.3** | Constant | 1.251 | 1.273 | 1.380 | 1.220 | 1.049 | 1.011 |
| | Std Err of Y Est | 0.023 | 0.034 | 0.028 | 0.024 | 0.027 | 0.032 |
| | R Squared | 0.730 | 0.791 | 0.796 | 0.747 | 0.028 | 0.005 |
| | No. of Observations | 91 | 123 | 91 | 123 | 123 | 123 |
| | Degrees of Freedom | 89 | 121 | 89 | 121 | 121 | 121 |
| | X Coefficient (h) | -0.171 | -0.227 | -0.257 | -0.139 | -0.001 | 0.008 |
| | Std Err of Coef. | 0.011 | 0.01 | 0.013 | 0.007 | 0.008 | 0.01 |
| | ***Fouling rate (10-5*s-1)*** | ***4.8*** | ***6.3*** | ***7.1*** | ***3.9*** | ***0.0*** | ***0.0*** |
| | *Delay time (h)* | *1.47* | *1.2* | *1.48* | *1.58* | *nd* | *nd* |

nd: not determined

**Table A5.2** Summary of results of runs 5.4, 5.5 and 5.6

| Run | Analysis output | Distance from step (mm) | | | | | |
|---|---|---|---|---|---|---|---|
| | | **7.5** | **20** | **40** | **60** | **80** | **130** |
| **5.4** | Constant | 1.029 | 1.058 | 1.110 | 1.053 | 1.042 | 1.037 |
| | Std Err of Y Est | 0.035 | 0.025 | 0.039 | 0.022 | 0.030 | 0.034 |
| | R Squared | 0.381 | 0.825 | 0.702 | 0.675 | 0.258 | 0.248 |
| | No. of Observations | 202 | 214 | 178 | 178 | 194 | 218 |
| | Degrees of Freedom | 200 | 212 | 176 | 176 | 192 | 216 |
| | X Coefficient (h) | -0.057 | -0.104 | -0.141 | -0.075 | -0.038 | -0.037 |
| | Std Err of Coef. | 0.005 | 0.003 | 0.007 | 0.004 | 0.005 | 0.004 |
| | ***Fouling rate (10-5*s-1)*** | ***1.6*** | ***2.9*** | ***3.*** | ***2.1*** | ***1.1*** | ***1.0*** |
| | *Delay time (h)* | *0.52* | *0.56* | *0.75* | *0.71* | *1.09* | *1.20* |
| **5.5** | Constant | 1.134 | 1.143 | 1.132 | 1.282 | 1.412 | 1.217 |
| | Std Err of Y Est | 0.024 | 0.020 | 0.026 | 0.018 | 0.024 | 0.026 |
| | R Squared | 0.931 | 0.913 | 0.945 | 0.968 | 0.729 | 0.278 |
| | No. of Observations | 247 | 217 | 253 | 205 | 90 | 73 |
| | Degrees of Freedom | 245 | 215 | 251 | 203 | 88 | 71 |
| | X Coefficient (h) | -0.150 | -0.126 | -0.180 | -0.202 | -0.185 | -0.090 |
| | Std Err of Coef. | 0.002 | 0.002 | 0.002 | 0.002 | 0.012 | 0.017 |
| | *Fouling rate (10-5*s-1)* | *4.2* | *3.5* | *5.0* | *5.6* | *5.2* | *2.5* |
| | *Delay time (h)* | *0.89* | *1.14* | *0.74* | *1.40* | *2.22* | *2.39* |
| **5.6** | Constant | 1.212 | 1.170 | 1.205 | 1.293 | 1.265 | 1.154 |
| | Std Err of Y Est | 0.029 | 0.046 | 0.026 | 0.036 | 0.031 | 0.032 |
| | R Squared | 0.782 | 0.569 | 0.916 | 0.876 | 0.806 | 0.648 |
| | No. of Observations | 181 | 181 | 181 | 181 | 181 | 181 |
| | Degrees of Freedom | 179 | 179 | 179 | 179 | 179 | 179 |
| | X Coefficient (h) | -0.126 | -0.119 | -0.197 | -0.221 | -0.143 | -0.100 |
| | Std Err of Coef. | 0.005 | 0.008 | 0.004 | 0.006 | 0.005 | 0.005 |
| | ***Fouling rate (E-5*s-1)*** | ***3.5*** | ***3.3*** | ***5.5*** | ***6.2*** | ***4.0*** | ***2.8*** |
| | *Delay time (h)* | *1.68* | *1.52* | *0.5* | *1.32* | *1.85* | *1.85* |

## Appendix 5.2

## Determination of times and temperatures in different fouling zones

### 1 Introduction

Time and temperature combination is important in determining the extent of β-lg denaturation. When milk flows through a holding tube, not all milk particles travel at the same velocity. Those particles near the wall flow more slowly than those at the centre of the holding tube, as a result, there is a distribution of flow times. A proportion of the total milk flow will spend more or less time than the average time depending of the state of flow of the fluid. The residence time distribution (RTD) therefore shows the distribution of the residence times for milk particles in the holding tube.

RTD is normally presented by the function E(t) (Levenspiel, 1972) which can be normalised so that the area under the curve is unity. The determination of the RTD involves injecting a small volume of a high concentration tracer at the beginning of the flow system. Successive small samples of the output are quantitatively analysed for the tracer. The RTD method used here was that of Janssen (1994). He employed a cross-correlation technique (Isermann *et al.*, 1974) to measure the RTD of whole milk in a holding tube using NaCl tracer.

### 2 RTD measurement method

A solution of 20% salt concentration was injected just prior to the holding tube using a solenoid driven diaphragm pump (gamma/4 1002 ProMinent, Germany). The pump was triggered by an output signal from a personal computer. The conductivity of the mixture leaving a test piece was measured using an in line conductivity cell. The conductivity signal was recorded by a data logging and computer system for further

analysis. In-line static mixers were placed after the injector and before the conductivity probe to ensure good mixing between the salt and the milk. A schematic layout of the RTD measurement is shown in Figure A5.7

## 3 Experimental procedure

The RTD in each fouling zone was measured separately using a single batch of whole milk. The milk fluid was preheated to 75°C in the plate heat exchanger and then to 95°C by the DSI heater of the fouling rig. Once through a test piece, the fluid passed the conductivity probe and the temperature probe and was then cooled and discarded to the drain. The plant was allowed to reach a steady state (constant outlet temperature and flow) before RTD measurement began. The salt dosing pump was set at 0.3 ml per stroke and the RTD sampling interval was set at 1 s. The milk flow rates were 80 and 120 L/h. Each RTD measurement lasted for 5 minutes so that enough data could be collected to calculate the RTD.

## 4 Results and discussion

### 4.1 RTD and temperature in fouling zones

The injection volume of the salt solution was about 0.3 ml per second. The increase in the milk volume caused by the salt injection was amounted to about 1 kg/h. This level of addition and its effect on the residence time was considered insignificant compared to the milk flow rates of 80 - 120 kg $h^{-1}$.

The results of RTD in different fouling zones are listed in Table A5.3. Examples of the RTD curves are also shown in Figure A5.8. When heated whole milk passed through zone 2 at 120 kg $h^{-1}$, the calculated RTD curve had a mean residence time of 16.8 s and

a variance of 0.82 $s^2$. At lower flow rate of 80 kg $h^{-1}$, the RTD curve had a mean residence time of 27.1 s and a variance of 2.45 $s^2$. The Reynolds numbers for whole milk at 95°C with flow rates of 120 and 80 kg $h^{-1}$ were 3800 and 2500 respectively. This indicated that the flow conditions in the holding tubes were in the transitional region between laminar and turbulence. As the results show the variance of RTD of milk flows at 80 kg $h^{-1}$, being close to the laminar condition, was about 3 times that of milk flows at 120 kg $h^{-1}$. Nevertheless, the differences between the maximum and minimum residence time of milk within a fouling zone of all zones were small compared to the difference in residence times between zones. It was therefore concluded the variance in RTD within a fouling zone had no significant effect on the determination of β-lg denaturation and hence the average RTD values can be used.

The average residence times calculated by the products of flow rate and pipe volume were also determined. They were in good agreement with the average residence time calculated using the RTD curves. These results are also listed in Table A5.3. It was therefore concluded that the product of flow rate and pipe volume is a reliable method and it can be used to determine the average residence time in a tube without the need of RTD measurement.

**Table A5.3** Residence time distribution (RTD) parameters for heated whole milk in various fouling zones

| Parameter | Zone 1 | Zone 2 | Zone 3 | Zone 4 |
|---|---|---|---|---|
| Flow rate (kg $h^{-1}$) | 120 | | | |
| Calculated residence time (s) | 7.6 | 17.4 | 30.8 | 74.7 |
| Average RTD time (s) | 7.1 | 16.8 | 31.2 | 74.1 |
| Minimum RTD time (s) | 6.1 | 14.8 | 30.4 | 73.2 |
| Maximum RTD time (s) | 8.7 | 17.9 | 32.5 | 75.9 |
| RTD variance, $\delta^2$ | 0.36 | 0.82 | 1.52 | 3.60 |
| Flow rate (kg $h^{-1}$) | 80 | | | |
| Calculated residence time (s) | 11.4 | 26.3 | 46.6 | 113.1 |
| Average RTD time (s) | 12.1 | 27.1 | 47.1 | 113.7 |
| Minimum RTD time (s) | 9.9 | 25.5 | 45.1 | 112.8 |
| Maximum RTD time (s) | 14.4 | 31.3 | 51.7 | 118.5 |
| RTD variance, $\delta^2$ ($s^2$) | 1.1 | 2.45 | 4.26 | 10.3 |

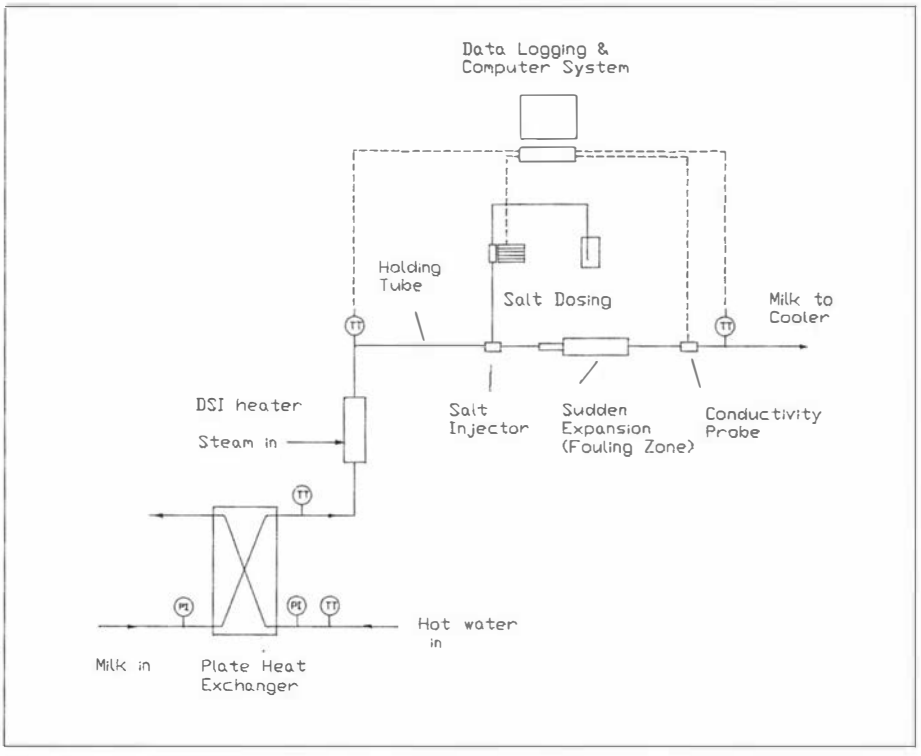


**Figure A5.7** Schematic diagram of residence time distribution (RTD) measurement.

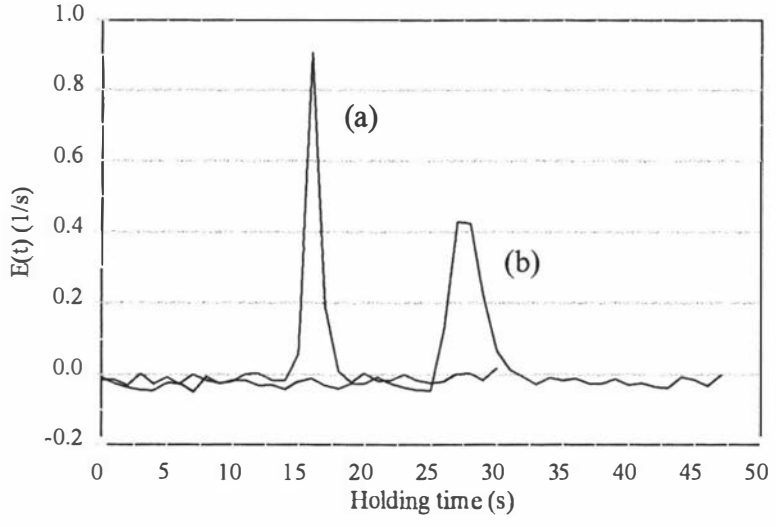


**Figure A5.8** Residence time distribution curves of heated whole milk (95°C) in fouling zone 2: (a) 120 kg $h^{-1}$ and (b) 80 kg $h^{-1}$.

## Appendix 5.3
## Summary of results of run 5.7 to 5.10
## Section 5.3.3

Plots of $I_f$ obtained at four different zones versus run time for runs 5.7 to 5.10 are shown in Figure A5.1 to A5.6. The fouling rates calculated using the procedures set out in Chapter 4. The results are listed in Tables A5.4 and A5.7.

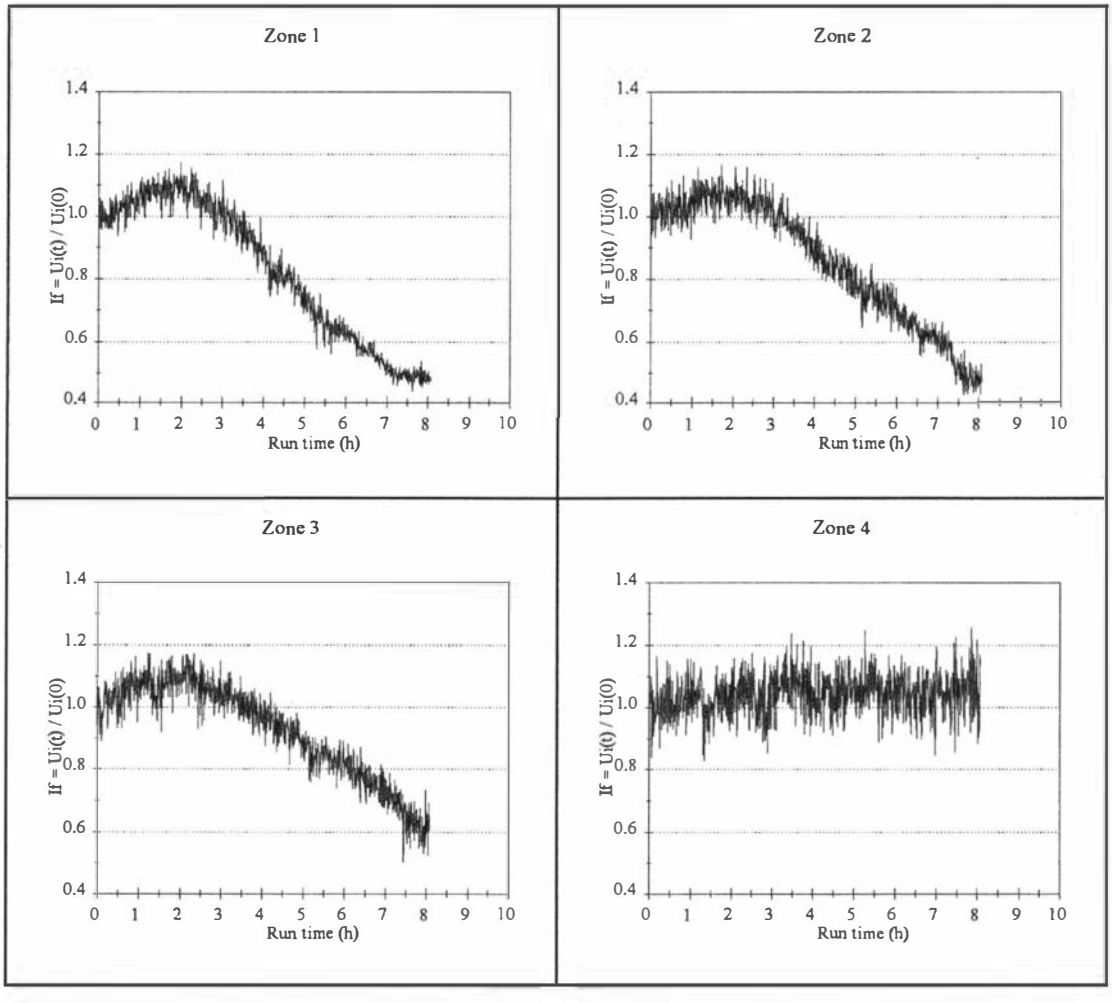


**Figure A5.9** Local fouling characteristics in four fouling zones downstream of DSI heater, Run 5.7, milk C, 120 kg $h^{-1}$.

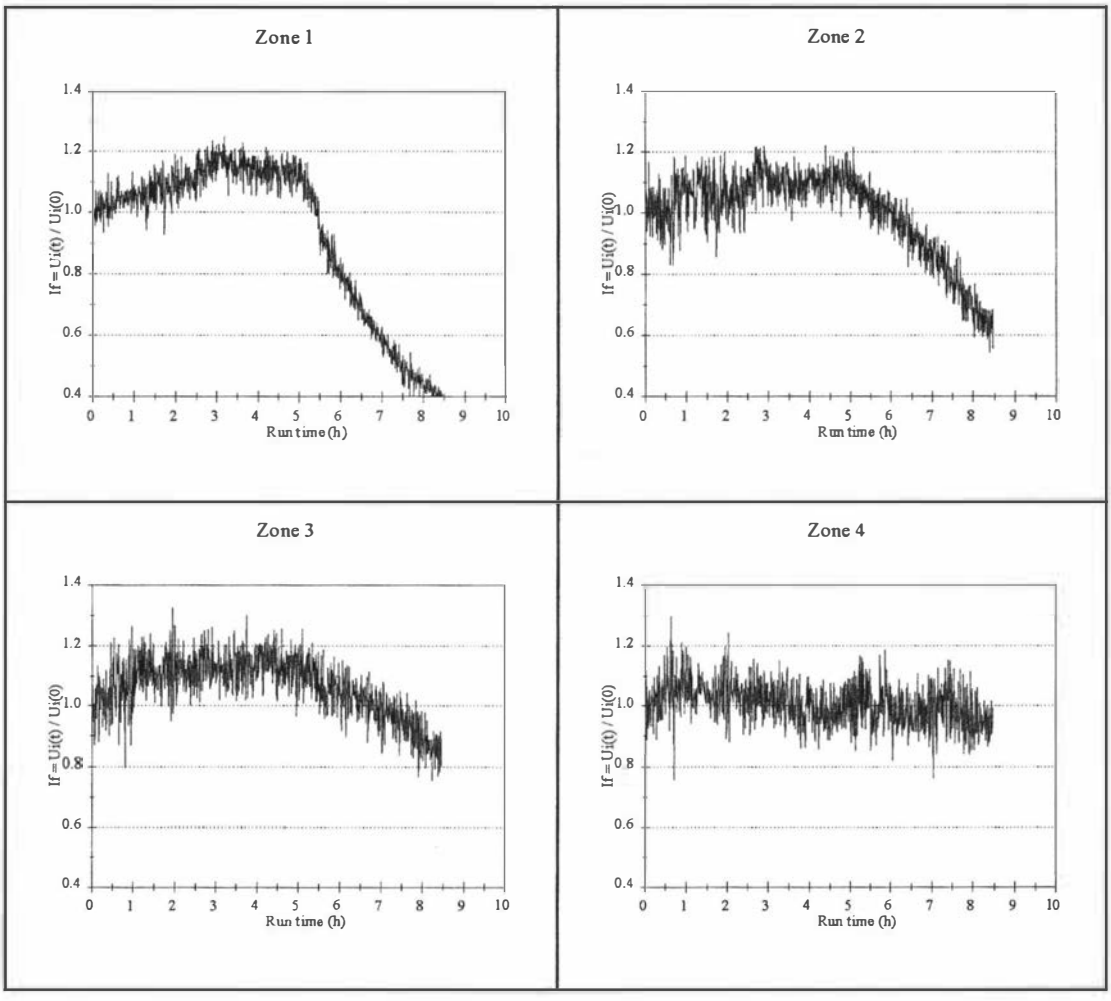


**Figure A5.10** Local fouling characteristics in four fouling zones downstream of DSI heater, Run 5.8, milk D, 120 kg $h^{-1}$.

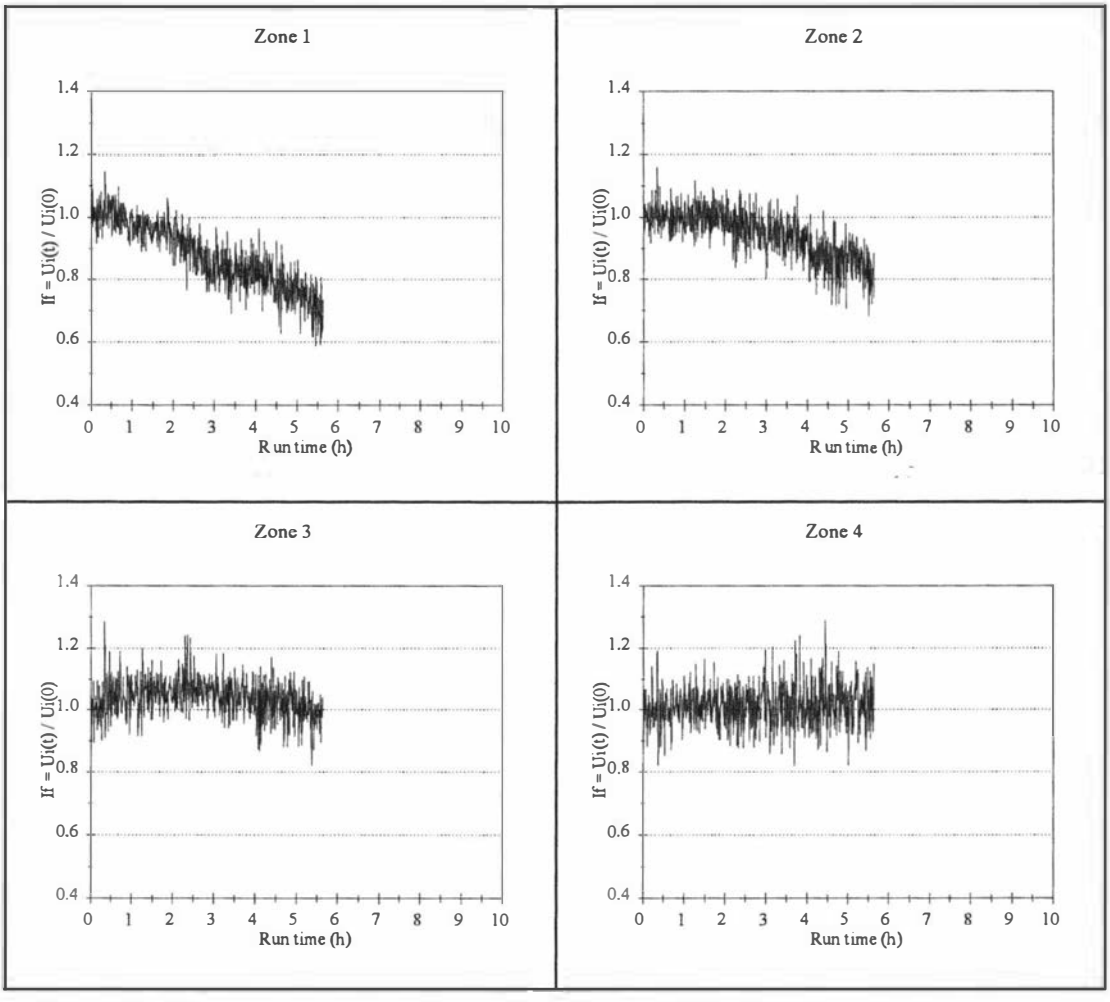


**Figure A5.11** Local fouling characteristics in four fouling zones downstream of DSI heater, Run 5.9, milk D, 80 kg $h^{-1}$.

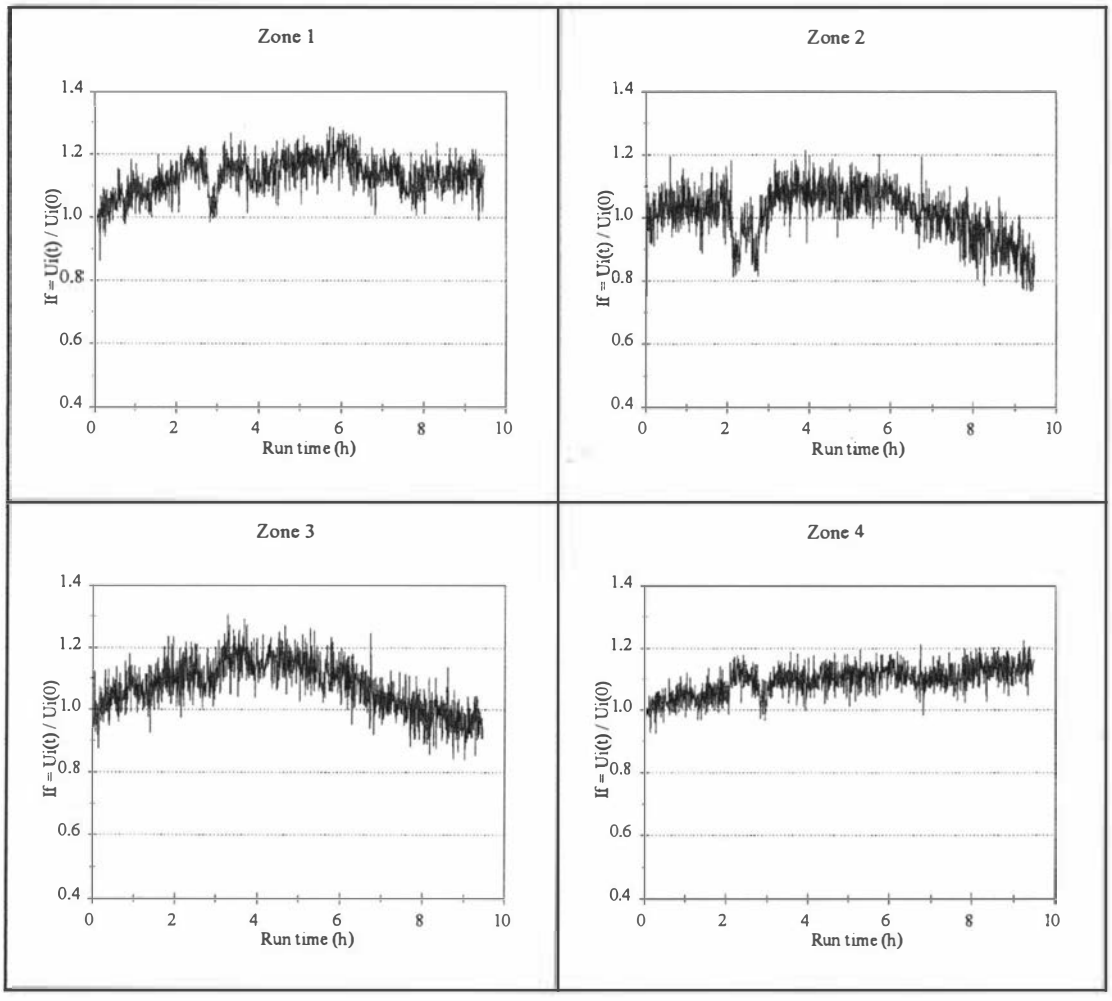


**Figure A5.12** Local fouling characteristics in four fouling zones downstream of DSI heater, Run 5.10, milk E, 120 kg $h^{-1}$.

**Table A5.4** Summary of results of run 5.7

| **Fouling zone** | **1** | **2** | **3** | **4** |
|---|---|---|---|---|
| Regression Output: | | | | |
| Constant | 1.489 | 1.378 | 1.326 | |
| Std Err of Y Est | 0.037 | 0.036 | 0.038 | |
| R Squared | 0.910 | 0.931 | 0.878 | |
| No. of Observations | 361 | 531 | 531 | |
| Degrees of Freedom | 359 | 529 | 529 | |
| X Coefficient (h) | -0.135 | -0.105 | -0.079 | |
| Std Err of Coef. | 0.0022 | 0.0012 | 0.0012 | |
| **Local fouling rate ($10^{-5}s^{-1}$)** | **3.8** | **2.9** | **2.2** | **0** |
| Run time (h) | 8 | 8 | 8 | 8 |
| Delay time (h) | 2 | 2 | 2 | 8 |
| Fouling time (h) | 6 | 6 | 6 | 0 |
| Deposit weight (g) | 2.822 | 2.152 | 1.306 | 0.392 |
| Fouled area (m2) | 0.0032 | 0.0032 | 0.0032 | 0.0032 |
| **CRZ fouling rate ($10^{-5}kgm^{-2}s^{-1}$)** | **4.1** | **3.1** | **1.9** | **0** |
| **Normalised fouling rates:** | | | | |
| Residence time (s) | 7 | 17 | 31 | 74 |
| Residual native β-lg (%) | 75 | 53 | 36 | 15 |
| ***Local fouling rate*** | ***5.1*** | ***5.5*** | ***6.1*** | ***0*** |
| ***CRZ fouling rate*** | ***5.7*** | ***5.9*** | ***5.3*** | ***0*** |

**Table A5.5** Summary of results of run 5.8

| **Fouling zone** | **1** | **2** | **3** | **4** |
|---|---|---|---|---|
| Regression Output: | | | | |
| Constant | 1.844 | 1.478 | 1.495 | 1.052 |
| Std Err of Y Est | 0.077 | 0.071 | 0.054 | 0.064 |
| R Squared | 0.927 | 0.799 | 0.713 | 0.097 |
| No. of Observations | 656 | 656 | 476 | 776 |
| Degrees of Freedom | 654 | 654 | 474 | 774 |
| X Coefficient (h) | -0.173 | -0.090 | -0.074 | -0.011 |
| Std Err of Coef. | 0.002 | 0.002 | 0.002 | 0.001 |
| **Local fouling rate ($10^{-5}s^{-1}$)** | **4.8** | **2.5** | **2.1** | **0.3** |
| Run time (h) | 8.5 | 8.5 | 8.5 | 8.5 |
| Delay time (h) | 3 | 3 | 3 | 2 |
| Fouling time (h) | 5.5 | 5.5 | 5.5 | 6.5 |
| Deposit weight (g) | 1.752 | 1.403 | 0.711 | 0.012 |
| Fouled area (m2) | 0.0032 | 0.0032 | 0.0032 | 0.0032 |
| **CRZ fouling rate ($10^{-5}kgm^{-2}s^{-1}$)** | **2.8** | **2.2** | **1.4** | **0.02** |
| **Normalised fouling rate:** | | | | |
| Residence time (s) | 7 | 17 | 31 | 74 |
| Residual native β-lg (%) | 75 | 53 | 35 | 15 |
| ***Local fouling rate*** | ***6.4*** | ***4.7*** | ***6.0*** | ***2.0*** |
| ***CRZ fouling rate*** | ***3.7*** | ***4.1*** | ***4.0*** | ***0.1*** |

**Table A5.6** Summary of results of run 5.9

| **Fouling zone** | **1** | **2** | **3** | **4** |
|---|---|---|---|---|
| Regression Output: | | | | |
| Constant | 1.092 | 1.175 | 1.112 | |
| Std Err of Y Est | 0.047 | 0.073 | 0.054 | |
| R Squared | 0.576 | 0.366 | 0.487 | |
| No. of Observations | 331 | 241 | 468 | |
| Degrees of Freedom | 329 | 239 | 466 | |
| X Coefficient (h) | -0.068 | -0.050 | -0.036 | |
| Std Err of Coef. | 0.003 | 0.008 | 0.002 | |
| **Local fouling rate ($10^{-5}s^{-1}$)** | **1.9** | **1.4** | **1.0** | **0** |
| Run time (h) | 5.5 | 5.5 | 5.5 | 5.5 |
| Delay time (h) | 0.5 | 0.5 | 0.5 | 5.5 |
| Fouling time (h) | 5 | 5 | 5 | 0 |
| Deposit weight (g) | 0.909 | 0.432 | 0.178 | 0 |
| Fouled area (m2) | 0.0032 | 0.0032 | 0.0032 | 0.0032 |
| **CRZ fouling rate ($10^{-5}kgm^{-2}s^{-1}$)** | **1.6** | **0.8** | **0.3** | **0** |
| **Normalised fouling rates:** | | | | |
| Residence time (s) | 12 | 27 | 47 | 114 |
| Residual native β-lg (%) | 63 | 40 | 25 | 9 |
| ***Local fouling rate*** | ***3.0*** | ***3.5*** | ***4.0*** | ***0*** |
| ***CRZ fouling rate*** | ***2.5*** | ***2.0*** | ***1.2*** | ***0*** |

**Table A5.7** Summary of results of run 5.10

| **Fouling zone** | **1** | **2** | **3** | **4** |
|---|---|---|---|---|
| Regression Output: | | | | |
| Constant | 1.275 | 1.428 | 1.381 | |
| Std Err of Y Est | 0.049 | 0.053 | 0.050 | |
| R Squared | 0.123 | 0.576 | 0.488 | |
| No. of Observations | 429 | 429 | 429 | |
| Degrees of Freedom | 427 | 427 | 427 | |
| X Coefficient (h) | -0.018 | -0.060 | -0.047 | |
| Std Err of Coef. | 0.002 | 0.002 | 0.002 | |
| **Local fouling rate ($10^{-5}s^{-1}$)** | **0** | **1.7** | **1.3** | **0** |
| Run time (h) | 8.5 | 8.5 | 8.5 | 8.5 |
| Delay time (h) | 5 | 5 | 5 | 8.5 |
| Fouling time (h) | 3.5 | 3.5 | 3.5 | 0 |
| Deposit weight (g) | 0.873 | 0.865 | 0.503 | 0.248 |
| Fouled area (m2) | 0.0032 | 0.0032 | 0.0032 | 0.0032 |
| **CRZ fouling rate ($10^{-5}kgm^{-2}s^{-1}$)** | **2.2** | **2.1** | **1.2** | **0** |
| Normalised fouling rates: | | | | |
| Residence time (s) | 7 | 17 | 31 | 74 |
| Residual native β-lg (%) | 75 | 53 | 40 | 15 |
| ***Local fouling rate*** | **-** | ***3.2*** | ***3.6*** | **-** |
| ***CRZ fouling rate*** | ***2.9*** | ***4.0*** | ***3.0*** | ***0*** |

## Appendix 5.4 Summary of results

## Runs 5.11

| Run | 5.11 | 80 kg/h | | | | | | | | | | | | | |
|---|---|---|---|---|---|---|---|---|---|---|---|---|---|---|---|
| Fouling zone | 1 | | | | | 2 | | | | | 3 | | | | |
| Sudden expansion | B (10/23) | | | | | A (17/23) | | | | | C (5/23) | | | | |
| Test section | 1 | | | 2 | | 1 | | | 2 | | 1 | | | 2 | |
| Sensor location | 1 | 2 | 3 | 4 | 5 | 1 | 2 | 3 | 4 | 5 | 1 | 2 | 3 | 4 | 5 |
| Distance from step of expansion (mm) | 10 | 20 | 40 | 80 | 120 | 10 | 20 | 40 | 80 | 120 | 10 | 20 | 40 | 80 | 120 |
| Fouling rate, d(If)/dt (1/h) | 0.252 | 0.302 | 0.353 | 0.189 | 0.091 | 0.147 | 0.336 | 0.152 | 0.008 | 0.000 | 0.184 | 0.237 | 0.180 | 0.152 | 0.112 |
| Constant (from regression analysis) | 1.163 | 1.166 | 1.240 | 1.160 | 1.100 | 1.091 | 1.226 | 1.092 | 0.994 | 0.000 | 1.179 | 1.156 | 1.209 | 1.146 | 1.152 |
| Deposits (g, dry basis) | 1.409 | | | 0.806 | 0.412 | 0.506 | | | 0.143 | 0.005 | 0.946 | | | 0.813 | 0.451 |
| Run duration (h) | 2.43 | | | | | 2.43 | | | | | 2.43 | | | | |
| Fouling time (h), local | 2.33 | 2.43 | 2.23 | 2.08 | 1.75 | 2.33 | 2.33 | 2.23 | 0.82 | 0.00 | 1.96 | 2.33 | 1.77 | 1.97 | 1.97 |
| Delay time (h), local | 0.10 | 0.00 | 0.20 | 0.35 | 0.68 | 0.10 | 0.10 | 0.20 | 1.61 | 2.43 | 0.47 | 0.10 | 0.66 | 0.46 | 0.46 |
| Beta-lg concentration (C/C(0)) | 0.567 | | | | | 0.432 | | | | | 0.348 | | | | |
| Sub-layer thickness (m*1E-6) | 20 | 10 | 2 | 80 | 120 | 5 | 17 | 60 | 180 | 250 | 10 | 20 | 7 | 20 | 100 |
| Area of fouling zone (m2) | 0.0043 | | | 0.0029 | 0.0043 | 0.0043 | | | 0.0029 | 0.0043 | 0.0043 | | | 0.0029 | 0.0043 |
| Area of fouling location (m2) | 0.0011 | 0.0011 | 0.0022 | 0.0029 | 0.0043 | 0.0011 | 0.0011 | 0.0022 | 0.0029 | 0.0043 | 0.0011 | 0.0011 | 0.0022 | 0.0029 | 0.0043 |
| Average fouling time (h) | 2.04 | | | | | 1.06 | | | | | 1.97 | | | | |
| Mass deposition rate (1E-5*kg/m2s) | 3.09 | | | | | 1.48 | | | | | 2.70 | | | | |
| **Kd(wt) (1E-5*kg/m2s)** | **5.46** | | | | | **3.43** | | | | | **7.76** | | | | |
| **Kd(hf) (1E-5*1/s) (local)** | **12.33** | **14.78** | **17.28** | **9.24** | **4.46** | **9.42** | **21.60** | **9.77** | **0.50** | **0.00** | **14.7** | **19.0** | **14.4** | **12.2** | **8.9** |
| **Overall Kd(hf)** | **9.76** | | | | | **4.86** | | | | | **12.24** | | | | |
| **CRZ Kd(hf)** | **13.56** | | | | | **9.42** | | | | | **15.59** | | | | |
| **Redeveloping flow Kd(hf)** | **8.89** | | | | | **4.39** | | | | | **10.23** | | | | |

## Appendix 5.4 Summary of results

## Runs 5.12

| **Run** | **5.12** | **120 kg/h** | | | | | | | | | | | | | |
|---|---|---|---|---|---|---|---|---|---|---|---|---|---|---|---|
| **Fouling zone** | **1** | | | | | **2** | | | | | **3** | | | | |
| **Sudden expansion** | **B (10/23)** | | | | | **A (17/23** | | | | | **C (5/23)** | | | | |
| **Test section** | **1** | | | **2** | | **1** | | | **2** | | **1** | | | **2** | |
| **Sensor location** | **1** | **2** | **3** | **4** | **5** | **1** | **2** | **3** | **4** | **5** | **1** | **2** | **3** | **4** | **5** |
| Distance from step of expansion (mm) | 10 | 20 | 40 | 80 | 120 | 10 | 20 | 40 | 80 | 120 | 10 | 20 | 40 | 80 | 120 |
| Fouling rate, d(If)/dt (1/h) | 0.300 | 0.352 | 0.378 | 0.377 | 0.225 | 0.155 | 0.270 | 0.263 | 0.126 | 0.000 | 0.343 | 0.238 | 0.320 | 0.252 | 0.238 |
| Constant (from regression analysis) | 1.203 | 1.118 | 1.100 | 1.385 | 1.145 | 1.094 | 1.027 | 1.109 | 1.207 | 0.000 | 1.180 | 1.084 | 1.166 | 1.176 | 1.353 |
| Deposits (g, dry basis) | 2.321 | | | 1.665 | 0.692 | 1.274 | | | 0.659 | 0.005 | 2.373 | | | 1.585 | 0.399 |
| Run duration (h) | 2.5 | | | | | 2.5 | | | | | 2.5 | | | | |
| Fouling time (h), local | 2.32 | 2.40 | 2.40 | 1.98 | 1.75 | 2.25 | 2.40 | 2.30 | 1.00 | 0 | 2.48 | 2.40 | 2.25 | 2.25 | 1.25 |
| Delay time (h), local | 0.18 | 0.10 | 0.10 | 0.52 | 0.75 | 0.25 | 0.10 | 0.20 | 1.50 | 2.50 | 0.02 | 0.10 | 0.25 | 0.25 | 1.25 |
| Beta-lg concentration (C/C(0)) | 0.681 | | | | | 0.567 | | | | | 0.467 | | | | |
| Sub-layer thickness (m*1E-6) | 10 | 10 | 2 | 50 | 130 | 2 | 12 | 40 | 100 | 150 | 7 | 9 | 10 | 17 | 70 |
| Area of fouling zone (m2) | 0.0043 | | | 0.0029 | 0.0043 | 0.0043 | | | 0.0029 | 0.0043 | 0.0043 | | | 0.0029 | 0.0043 |
| Area of fouling location (m2) | 0.0011 | 0.0011 | 0.0022 | 0.0029 | 0.0043 | 0.0011 | 0.0011 | 0.0022 | 0.0029 | 0.0043 | 0.0011 | 0.0011 | 0.0022 | 0.0029 | 0.0043 |
| Average fouling time (h) | 2.04 | | | | | 1.12 | | | | | 1.91 | | | | |
| Mass deposition rate (1E-5*kg/m2s) | 5.50 | | | | | 4.17 | | | | | 5.48 | | | | |
| **Kd(wt) (1E-5*kg/m2s)** | **8.08** | | | | | **7.35** | | | | | **11.73** | | | | |
| **Kd(hf) (1E-5*1/s) (local)** | **12.24** | **14.37** | **15.40** | **15.39** | **9.18** | **7.61** | **13.25** | **12.86** | **6.18** | **0.00** | **20.4** | **14.2** | **19.0** | **15.0** | **14.2** |
| **Overall Kd(hf)** | **12.67** | | | | | **5.91** | | | | | **15.87** | | | | |
| **CRZ Kd(hf)** | **13.30** | | | | | **7.61** | | | | | **18.16** | | | | |
| **Redeveloping flow Kd(hf)** | **12.52** | | | | | **5.74** | | | | | **14.50** | | | | |

## Appendix 5.4 Summary of results

## Runs 5.13

| **Run** | **5.13** | **100 kg/h** | | | | | | | | | | | | | |
|---|---|---|---|---|---|---|---|---|---|---|---|---|---|---|---|
| **Fouling zone** | **1** | | | | | **2** | | | | | **3** | | | | |
| **Sudden expansion** | **B (10/23)** | | | | | **A (17/23)** | | | | | **C (5/23)** | | | | |
| **Test section** | **1** | | | **2** | | **1** | | | **2** | | **1** | | | **2** | |
| **Sensor location** | **1** | **2** | **3** | **4** | **5** | **1** | **2** | **3** | **4** | **5** | **1** | **2** | **3** | **4** | **5** |
| Distance from step of expansion (mm) | 10 | 20 | 40 | 80 | 120 | 10 | 20 | 40 | 80 | 120 | 10 | 20 | 40 | 80 | 120 |
| Fouling rate, d(If)/dt (1/h) | 0.248 | 0.365 | 0.384 | 0.230 | 0.000 | 0.213 | 0.252 | 0.252 | 0.088 | 0.000 | 0.238 | 0.253 | 0.172 | 0.209 | 0.157 |
| Constant (from regression analysis) | 1.084 | 1.157 | 1.190 | 1.234 | 0.000 | 1.144 | 1.154 | 1.105 | 1.119 | 0.000 | 1.074 | 1.137 | 1.056 | 1.155 | 1.275 |
| Deposits (g, dry basis) | 2.394 | | | 1.256 | 0.277 | 0.879 | | | 0.425 | 0.007 | 1.662 | | | 1.161 | 0.301 |
| Run duration (h) | 2.5 | | | | | 2.5 | | | | | 2.5 | | | | |
| Fouling time (h), local | 2.40 | 2.30 | 2.30 | 2.30 | 2.00 | 2.00 | 2.25 | 2.00 | 1.65 | nd | 2.30 | 2.00 | 2.30 | 2.26 | 1.00 |
| Delay time (h), local | 0.10 | 0.20 | 0.20 | 0.20 | 0.50 | 0.50 | 0.25 | 0.50 | 0.85 | 2.50 | 0.20 | 0.50 | 0.20 | 0.24 | 1.50 |
| Beta-lg concentration (C/C(0)) | 0.639 | | | | | 0.507 | | | | | 0.411 | | | | |
| Sub-layer thickness (m*1E-6) | 10 | 10 | 2 | 70 | 170 | 2 | 15 | 50 | 150 | 200 | 8 | 9 | 5 | 20 | 80 |
| Area of fouling zone (m2) | 0.0043 | | | 0.0029 | 0.0043 | 0.0043 | | | 0.0029 | 0.0043 | 0.0043 | | | 0.0029 | 0.0043 |
| Area of fouling location (m2) | 0.0011 | 0.0011 | 0.0022 | 0.0029 | 0.0043 | 0.0011 | 0.0011 | 0.0022 | 0.0029 | 0.0043 | 0.0011 | 0.0011 | 0.0022 | 0.0029 | 0.0043 |
| Average fouling time (h) | 2.20 | | | | | 1.19 | | | | | 1.77 | | | | |
| Mass deposition rate (1E-5*kg/m2s) | 4.29 | | | | | 2.66 | | | | | 4.23 | | | | |
| **Kd(wt) (1E-5*kg/m2s)** | **6.72** | | | | | **5.24** | | | | | **10.29** | | | | |
| **Kd(hf) (1E-5*1/s) (local)** | **10.77** | **15.85** | **16.70** | **10.00** | **0.00** | **11.66** | **13.81** | **13.80** | **4.84** | **0.00** | **16.1** | **17.1** | **11.7** | **14.1** | **10.6** |
| **Overall Kd(hf)** | **8.13** | | | | | **6.18** | | | | | **12.81** | | | | |
| **CRZ Kd(hf)** | **13.31** | | | | | **11.66** | | | | | **14.12** | | | | |
| **Redeveloping flow Kd(hf)** | **6.93** | | | | | **5.62** | | | | | **12.03** | | | | |

## Appendix 5.4 Summary of results

## Runs 5.14

| **Run** | **5.14** | **80 kg/h** | | | | | | | | | | | | | |
|---|---|---|---|---|---|---|---|---|---|---|---|---|---|---|---|
| **Fouling zone** | **2** | | | | | **1** | | | | | **3** | | | | |
| **Sudden expansion** | **B (10/23)** | | | | | **A (17/23** | | | | | **C (5/23)** | | | | |
| **Test section** | **1** | | | **2** | | **1** | | | **2** | | **1** | | | **2** | |
| **Sensor location** | **1** | **2** | **3** | **4** | **5** | **1** | **2** | **3** | **4** | **5** | **1** | **2** | **3** | **4** | **5** |
| Distance from step of expansion (mm) | 10 | 20 | 40 | 80 | 120 | 10 | 20 | 40 | 80 | 120 | 10 | 20 | 40 | 80 | 120 |
| Fouling rate, d(If)/dt (1/h) | 0.144 | 0.083 | 0.147 | 0.080 | 0.023 | 0.001 | 0.001 | 0.203 | 0.008 | 0.000 | 0.128 | 0.050 | 0.146 | 0.092 | 0.010 |
| Constant (from regression analysis) | 1.777 | 1.191 | 1.586 | 1.450 | 1.470 | 1.000 | 1.000 | 2.036 | 0.994 | 0.000 | 1.460 | 1.067 | 1.488 | 1.231 | 1.340 |
| Deposits (g, dry basis) | 0.768 | | | 0.005 | 0.005 | 0.217 | | | 0.143 | 0.005 | 1.406 | | | 0.727 | 0.399 |
| Run duration (h) | 5.98 | | | | | 5.98 | | | | | 5.98 | | | | |
| Fouling time (h), local | 4.48 | 5.48 | 3.98 | 2.00 | 0.00 | 5.48 | 5.48 | 4.98 | 2.98 | 0.00 | 4.98 | 3.98 | 4.98 | 4.98 | 0.00 |
| Delay time (h), local | 1.50 | 0.50 | 2.00 | 3.98 | 5.98 | 0.50 | 0.50 | 1.00 | 3.00 | 5.98 | 1.00 | 2.00 | 1.00 | 1.00 | 5.98 |
| Beta-lg concentration (C/C(0)) | 0.432 | | | | | 0.567 | | | | | 0.348 | | | | |
| Sub-layer thickness (m*1E-6) | 20 | 10 | 2 | 80 | 120 | 5 | 17 | 60 | 180 | 250 | 10 | 20 | 7 | 20 | 100 |
| Area of fouling zone (m2) | 0.0043 | | | 0.0029 | 0.0043 | 0.0043 | | | 0.0029 | 0.0043 | 0.0043 | | | 0.0029 | 0.0043 |
| Area of fouling location (m2) | 0.0011 | 0.0011 | 0.0022 | 0.0029 | 0.0043 | 0.0011 | 0.0011 | 0.0022 | 0.0029 | 0.0043 | 0.0011 | 0.0011 | 0.0022 | 0.0029 | 0.0043 |
| Average fouling time (h) | 2.18 | | | | | 2.71 | | | | | 3.02 | | | | |
| Mass deposition rate (1E-5*kg/m2s) | 0.86 | | | | | 0.32 | | | | | 2.01 | | | | |
| **Kd(wt) (1E-5*kg/m2s)** | **1.99** | | | | | **0.57** | | | | | **5.79** | | | | |
| **Kd(hf) (1E-5*1/s) (local)** | **9.27** | **5.34** | **9.45** | **5.14** | **1.48** | **0.05** | **0.05** | **9.95** | **0.4** | **0.00** | **10.2** | **4.0** | **11.7** | **7.3** | **0.8** |
| **Overall Kd(hf)** | **4.98** | | | | | **1.97** | | | | | **5.65** | | | | |
| **CRZ Kd(hf)** | **7.30** | | | | | **0.05** | | | | | **9.38** | | | | |
| **Redeveloping flow Kd(hf)** | **4.45** | | | | | **2.17** | | | | | **3.42** | | | | |

## Appendix 5.4 Summary of results

## Runs 5.15

| **Run** | **5.15** | **100 kg/h** | | | | | | | | | | | | | |
|---|---|---|---|---|---|---|---|---|---|---|---|---|---|---|---|
| **Fouling zone** | **2** | | | | | **1** | | | | | **3** | | | | |
| **Sudden expansion** | **B (10/23)** | | | | | **A (17/23)** | | | | | **C (5/23)** | | | | |
| **Test section** | **1** | | | **2** | | **1** | | | **2** | | **1** | | | **2** | |
| **Sensor location** | **1** | **2** | **3** | **4** | **5** | **1** | **2** | **3** | **4** | **5** | **1** | **2** | **3** | **4** | **5** |
| Distance from step of expansion (mm) | 10 | 20 | 40 | 80 | 120 | 10 | 20 | 40 | 80 | 120 | 10 | 20 | 40 | 80 | 120 |
| Fouling rate, d(If)/dt (1/h) | 0.161 | 0.174 | 0.235 | 0.172 | 0.133 | 0.001 | 0.195 | 0.159 | 0.072 | 0.000 | 0.210 | 0.220 | 0.153 | 0.174 | 0.120 |
| Constant (from regression analysis) | 0.999 | 1.035 | 1.077 | 1.177 | 1.238 | 1.000 | 1.255 | 1.096 | 1.071 | 0.000 | 1.068 | 1.172 | 1.059 | 1.068 | 1.223 |
| Deposits (g, dry basis) | 1.861 | | | 0.613 | 0.000 | 0.842 | | | 0.222 | 0.005 | 2.037 | | | 1.085 | 0.399 |
| Run duration (h) | 2.95 | | | | | 2.95 | | | | | 2.95 | | | | |
| Fouling time (h), local | 2.70 | 2.45 | 2.45 | 1.92 | 2.45 | 2.45 | 2.20 | 1.95 | 1.96 | 0.00 | 2.45 | 2.17 | 2.45 | 2.45 | 2.45 |
| Delay time (h), local | 0.25 | 0.50 | 0.50 | 1.03 | 0.50 | 0.50 | 0.75 | 1.00 | 0.99 | 2.95 | 0.50 | 0.78 | 0.50 | 0.50 | 0.50 |
| Beta-lg concentration (C/C(0)) | 0.507 | | | | | 0.639 | | | | | 0.411 | | | | |
| Sub-layer thickness (m*1E-6) | 10 | 10 | 2 | 70 | 170 | 2 | 15 | 50 | 150 | 200 | 8 | 9 | 5 | 20 | 80 |
| Area of fouling zone (m2) | 0.0043 | | | 0.0029 | 0.0043 | 0.0043 | | | 0.0029 | 0.0043 | 0.0043 | | | 0.0029 | 0.0043 |
| Area of fouling location (m2) | 0.0011 | 0.0011 | 0.0022 | 0.0029 | 0.0043 | 0.0011 | 0.0011 | 0.0022 | 0.0029 | 0.0043 | 0.0011 | 0.0011 | 0.0022 | 0.0029 | 0.0043 |
| Average fouling time (h) | 2.34 | | | | | 1.29 | | | | | 2.42 | | | | |
| Mass deposition rate (1E-5*kg/m2s) | 2.54 | | | | | 1.99 | | | | | 3.49 | | | | |
| **Kd(wt) (1E-5*kg/m2s)** | **5.01** | | | | | **3.11** | | | | | **8.49** | | | | |
| **Kd(hf) (1E-5*1/s) (local)** | **8.81** | **9.53** | **12.88** | **9.42** | **7.29** | **0.04** | **8.48** | **6.91** | **3.13** | **0.00** | **14.2** | **14.9** | **10.3** | **11.8** | **8.1** |
| **Overall Kd(hf)** | **9.22** | | | | | **2.88** | | | | | **10.64** | | | | |
| **CRZ Kd(hf)** | **9.17** | | | | | **0.04** | | | | | **12.44** | | | | |
| **Redeveloping flow Kd(hf)** | **9.23** | | | | | **3.17** | | | | | **9.57** | | | | |

## Appendix 5.4 Summary of results

## Runs 5.16

| Run | 5.16 | 120 kg/h | | | | | | | | | | | | | |
|---|---|---|---|---|---|---|---|---|---|---|---|---|---|---|---|
| Fouling zone | 2 | | | | | 1 | | | | | 3 | | | | |
| Sudden expansion | B (10/23) | | | | | A (17/23) | | | | | C (5/23) | | | | |
| Test section | 1 | | | 2 | | 1 | | | 2 | | 1 | | | 2 | |
| Sensor location | 1 | 2 | 3 | 4 | 5 | 1 | 2 | 3 | 4 | 5 | 1 | 2 | 3 | 4 | 5 |
| Distance from step of expansion (mm) | 10 | 20 | 40 | 80 | 120 | 10 | 20 | 40 | 80 | 120 | 10 | 20 | 40 | 80 | 120 |
| Fouling rate, d(If)/dt (1/h) | 0.286 | 0.222 | 0.277 | 0.274 | 0.242 | 0.070 | 0.137 | 0.236 | 0.254 | 0.225 | 0.243 | 0.245 | 0.219 | 0.226 | 0.213 |
| Constant (from regression analysis) | 1.155 | 1.027 | 1.166 | 1.204 | 1.310 | 0.965 | 1.429 | 1.475 | 1.142 | 1.256 | 1.086 | 1.072 | 1.178 | 1.118 | 1.157 |
| Deposits (g, dry basis) | 2.516 | | | 1.708 | 1.393 | 1.328 | | | 1.035 | 1.691 | 2.396 | | | 1.878 | 1.063 |
| Run duration (h) | 3.89 | | | | | 3.89 | | | | | 3.89 | | | | |
| Fouling time (h), local | 3.39 | 3.69 | 3.39 | 3.14 | 2.89 | 2.89 | 2.89 | 2.64 | 2.39 | 2.64 | 3.39 | 3.39 | 3.14 | 3.14 | 3.39 |
| Delay time (h), local | 0.50 | 0.20 | 0.50 | 0.75 | 1.00 | 1.00 | 1.00 | 1.25 | 1.50 | 1.25 | 0.50 | 0.50 | 0.75 | 0.75 | 0.50 |
| Beta-lg concentration (C/C(0)) | 0.567 | | | | | 0.681 | | | | | 0.467 | | | | |
| Sub-layer thickness (m*1E-6) | 10 | 10 | 2 | 50 | 130 | 2 | 12 | 40 | 100 | 150 | 7 | 9 | 10 | 17 | 70 |
| Area of fouling zone (m2) | 0.0043 | | | 0.0029 | 0.0043 | 0.0043 | | | 0.0029 | 0.0043 | 0.0043 | | | 0.0029 | 0.0043 |
| Area of fouling location (m2) | 0.0011 | 0.0011 | 0.0022 | 0.0029 | 0.0043 | 0.0011 | 0.0011 | 0.0022 | 0.0029 | 0.0043 | 0.0011 | 0.0011 | 0.0022 | 0.0029 | 0.0043 |
| Average fouling time (h) | 3.17 | | | | | 2.62 | | | | | 3.28 | | | | |
| Mass deposition rate (1E-5*kg/m2s) | 4.26 | | | | | 3.71 | | | | | 3.91 | | | | |
| **Kd(wt) (1E-5*kg/m2s)** | **7.51** | | | | | **5.45** | | | | | **8.37** | | | | |
| **Kd(hf) (1E-5*1/s) (local)** | **14.01** | **10.88** | **13.57** | **13.42** | **11.86** | **2.86** | **5.59** | **9.63** | **10.36** | **9.18** | **14.5** | **14.6** | **13.0** | **13.4** | **12.7** |
| **Overall Kd(hf)** | **12.68** | | | | | **8.63** | | | | | **13.28** | | | | |
| **CRZ Kd(hf)** | **12.44** | | | | | **2.86** | | | | | **13.77** | | | | |
| **Redeveloping flow Kd(hf)** | **12.73** | | | | | **9.23** | | | | | **12.98** | | | | |